AD-A167 697 APPLICATION OF BIFURCATION AND CATASTROPHE THEORIES TO NEAR STALL FLIGHT MECHANICS(U) AIR FORCE INST OF TECH WRIGHT-PATTERSON AFB OH C A HAWKINS 1985 1/3

UNCLASSIFIED AFIT/CI/NR-86-54T F/G 12/1 NL

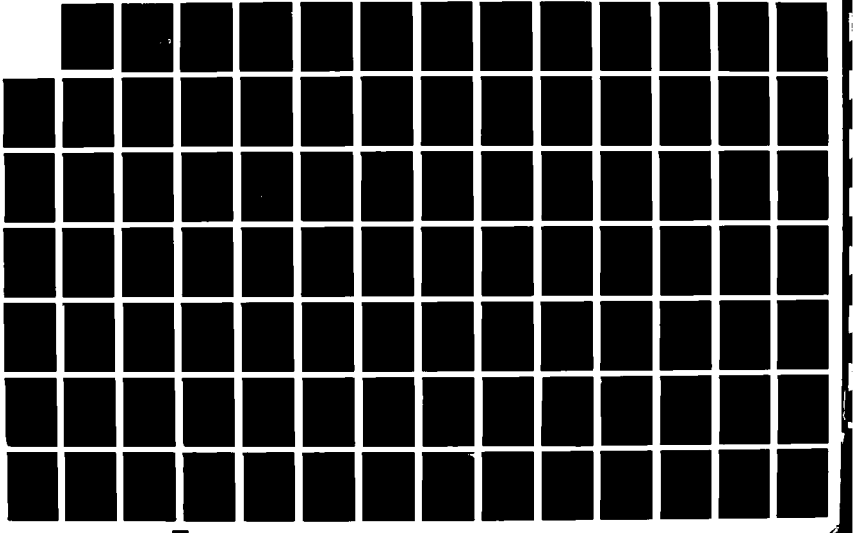

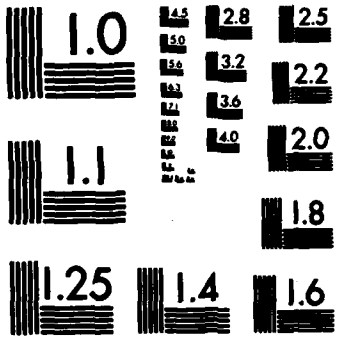

SECURITY CLASSIFICATION OF THIS PAGE (When Data Entered)

REPORT DOCUMENTATION PAGE

READ INSTRUCTIONS BEFORE COMPLETING FORM

1. REPORT NUMBER: AFIT/CI/NR 86-54T
2. GOVT ACCESSION NO.:
3. RECIPIENT'S CATALOG NUMBER:

4. TITLE (and Subtitle): Application of Bifurcation and Catastrophe Theories to Near Stall Flight Mechanics
5. TYPE OF REPORT & PERIOD COVERED: THESIS/DISSERTATION
6. PERFORMING ORG. REPORT NUMBER:

7. AUTHOR(s): Carl A. Hawkins
8. CONTRACT OR GRANT NUMBER(s):

9. PERFORMING ORGANIZATION NAME AND ADDRESS: AFIT STUDENT AT: Massachusetts Institute of Technology
10. PROGRAM ELEMENT, PROJECT, TASK AREA & WORK UNIT NUMBERS:

11. CONTROLLING OFFICE NAME AND ADDRESS: AFIT/NR, WPAFB OH 45433-6583
12. REPORT DATE: 1985
13. NUMBER OF PAGES: 247

14. MONITORING AGENCY NAME & ADDRESS (if different from Controlling Office):
15. SECURITY CLASS. (of this report): UNCLASS
15a. DECLASSIFICATION/DOWNGRADING SCHEDULE:

16. DISTRIBUTION STATEMENT (of this Report): APPROVED FOR PUBLIC RELEASE; DISTRIBUTION UNLIMITED

DTIC ELECTE S D MAY 2 1986 A

17. DISTRIBUTION STATEMENT (of the abstract entered in Block 20, if different from Report):

18. SUPPLEMENTARY NOTES: APPROVED FOR PUBLIC RELEASE: IAW AFR 190-1

LYNN E. WOLAVER 17 April 86
Dean for Research and Professional Development
AFIT/NR, WPAFB OH 45433-6583

19. KEY WORDS (Continue on reverse side if necessary and identify by block number):

20. ABSTRACT (Continue on reverse side if necessary and identify by block number):

DD FORM 1 JAN 73 1473 EDITION OF 1 NOV 65 IS OBSOLETE

A

SECURITY CLASSIFICATION OF THIS PAGE (When Data Entered)

AD-A167 697

DTIC FILE COPY

54

APPLICATION OF BIFURCATION AND CATASTROPHE THEORIES TO NEAR STALL FLIGHT MECHANICS

by

Carl A. Hawkins
Captain, USAF

B.S., United States Air Force Academy
(1979)

SUBMITTED IN PARTIAL FULFILLMENT
OF THE REQUIREMENTS OF THE
DEGREE OF

MASTER OF SCIENCE
in
AERONAUTICS AND ASTRONAUTICS

at the
Massachusetts Institute of Technology

December 1985

Signature of Author Carl A. Hawkins
Department of Aeronautics and Astronautics
December 1985

Certified by _____
Eugene E. Covert
Thesis Supervisor
Chairman, Department of Aeronautics and Astronautics

Accepted by _____
Harold Y. Wachman
Chairman, Department Graduate Committee

APPLICATION OF BIFURCATION AND CATASTROPHE THEORIES TO NEAR STALL FLIGHT MECHANICS

by

Carl A. Hawkins
Captain, USAF

Submitted the the Department of Aeronautics and Astronautics on December 19, 1985 in partial fulfillment of the requirements for the Degree of Master of Science in Aeronautics and Astronautics

This thesis sought to

ABSTRACT

A study of the flight mechanics of a three surfaced fighter aircraft was accomplished using bifurcation and catastrophe theories. The emphasis of this research was to find or develop nonlinear systems analysis techniques capable of analyzing and predicting the complex behavior found in high-angle-of-attack flight. A primary selection criteria for the method to be used in the research was that the method be more global in nature than the techniques currently in use. The technique selected was based on the concepts found in bifurcation and catastrophe theories. The primary method of research involved the calculation of equilibrium surfaces, where the time rate of change of each of the state variables is set to zero in the aircraft equations of motion, and the states that will satisfy that condition are found for various control deflections. The equilibrium surfaces were calculated numerically through use of continuation methods.

An equilibrium trajectory analysis of a fifth order model of the aircraft showed significant adverse yaw problems at high angles of attack as well as the presence of roll coupling, phenomena. Bifurcational behavior was found in the same fifth order model and verified by research previously accomplished. A mechanism for the transfer of kinetic energy during the catastrophic behavior shown is hypothesized. A spin equilibriuim surface for the aircraft was determined from an eighth order model of the aircraft, and, from that surface, possible control deflections for recovery from the spin were obtained. Numerical simulations of the model were accomplished, but few useful results were obtained due to the unstable nature of the aircraft. A number of areas for improvement of the aircraft design and methods used as well as possible areas for further research are identified.

Thesis Supervisor: Profesor Eugene E. Covert

Title: Chairman, Department of Aeronautics and Astronautics

FOREWARD

There are a number of people who have unselfishly contributed to this effort. The first such person that immediately comes to mind at this point is my wife, Chrystol. Her tremendous understanding and patience during the time that I was preparing this document was and is greatly appreciated. I am thankful to the personnel at the Air Force Wright Aeronautical Laboratory who were responsible for obtaining the F-15 STOL Demonstrator data for me. In particular, I would like to acknowledge the dedicated professionalism of Lt Daniel Young who was not only extremely helpful in answering my many questions on the material sent to me but was also very responsive to my requests for further information on the aircraft. Several people with a great deal of experience in the field related to this study took time from their busy schedules to share some of their knowledge with me. Among those people whose insight has been most helpful and whose inputs to this project have been extremely valuable are Professor Rudrapatna Ramnath, Dr. James Carroll and my thesis advisor, Professor Eugene Covert. I would especially like to thank Professor Covert for his great support and very knowledgeable advice both academically and professionally.

TABLE OF CONTENTS

LIST OF SYMBOLS AND ABBREVIATIONS

g	acceleration of gravity
aoa	angle of attack
STOL	Short Take Off and Landing
F-15S	designation given to the F-15 STOL Demonstrator
CASS	Computer Aided Stability System
BACTM	Bifurcation and Catastrophe Theory Methodology
	potential function
$\underline{x}$	aircraft state vector
$\underline{c}$	aircraft control vector
c	single, scalar aircraft control variable
$\underline{f}$	nonlinear function of the aircraft state and controls used with the time derivative of the state vector to describe the equations of motion ($d\underline{x}/dt = \underline{f}(\underline{x},\underline{c})$
k	size of the reduced order system containing the nonlinearities of the system
n	order of the system (number of state variables)
m	number of control variables
CG	center of gravity
F	system (n X n) Jacobian matrix
G	augmented system (n X n+1) Jacobian matrix
G_k	augmented system Jacobian matrix with the kth column removed
$\underline{y}$	augmented aircraft state vector, $\underline{y}=(\underline{x},c_i)$
DAI	aileron deflection
DEL	stabilator deflection
DRU	rudder deflection

$\underline{h}$	Newton-Raphson convergence step vector
Ixx	mass moment of inertia about the x-axis
Iyy	mass moment of inertia about the y-axis
Izz	mass moment of inertia about the z-axis
Ixz	xz plane product of inertia
BL	aircraft butt line
RB	rotary balance
omega	rotation rate about the aircraft spin axis
CL	coefficient of lift (stability axis)
CD	coefficient of drag (stability axis)
Cx	x direction body axis force coefficient
Cy	y direction body axis force coefficient
Cz	z direction body axis force coefficient
Cl	rolling moment coefficient
Cm	pitching moment coefficient
Cn	yawing moment coefficient
u	x direction body axis velocity
v	y direction body axis velocity
w	z direction body axis velocity
p	roll rate
q	pitch rate
r	yaw rate
V	total velocity
α	angle of attack
β	sideslip angle
θ	pitch angle

ϕ	bank angle
ψ	yaw angle (aircraft heading)
$\bar{q}$	dynamic pressure
S	wing planform surface area
b	wing span
$\bar{c}$	theoretical wing chord
TURNS	number of rotations during a spin
E	kinetic energy
$\dot{E}$	rate of change of kinetic energy
Es	kinetic energy due to spin motion alone
Iv	moment of inertia about the aircraft spin axis

CHAPTER I

INTRODUCTION

A. Historical Perspective

The prediction of an aircraft's dynamics and stability behavior has been a topic of interest since heavier than air flight was first conceived. From the very beginning, aircraft designers were at odds in their beliefs of how aircraft should be designed in terms of stability. For example, the Wright Brothers favored a slightly unstable design to increase manueverability while the European aircraft design community opted for much more stable designs [1]. The Wright Brothers insistence on maintaining the elevator forward of the wing in their early designs was motivated by both the desire to make the aircraft a servant to the controlling desires of the pilot and the desire to provide a pitch up moment following a stall to prevent the dive that typically followed stalls in aircraft of that period. It was such a stall initiated dive that caused the death in 1896 of Otto Lilienthal, the most prominent of the European airplane designers at the time [2].

Being bicycle designers and riders, the Wright Brothers' concept of controlling an aircraft in flight was much the same as that of riding a bicycle.

The bicycle is inherently unstable but the instability is easily overcome by the rider through the use of the handlebars. Unfortunately, as aircraft became more sophisticated, the large demands placed on a pilot attempting to control an aircraft with the tail forward of the wings made the design impractical and often dangerous. The tail forward design, later known as a canard due to its resemblance to a duck, was to be shunned by the worldwide aircraft design community for many years to come [2]. It was during this period that the desire for static stability became an unquestioned design feature for nearly sixty years. As will be discussed below, the Wright Brothers' understanding of the relationship between stability and manueverability was far ahead of their time. They understood that stability and manueverabilty are relative terms, and that they describe positions along the same spectrum with stability being at one end of the spectrum and manueverability at the other. Consequently, you can not enhance one without sacrificing the other. The most simple definition of stability when applied to an aircraft is: a characteristic of an aircraft in flight that causes it to return to a position of steady flight after being disturbed from that position.

Nearly all aircraft possess enough stability to recover their equilibrium after small disturbances; however, none possess the stability to recover its equilibrium under all conditions. The need to know the conditions under which an aircraft will maintain or lose its stability form the motivation for this study.

B. Aircraft Design Considerations

The capabilities of a combat aircraft are often measured in terms of performance factors such as: wing loading, maximum thrust to weight ratio, engine response time, maximum turn rate and rate of turn build up, maximum transient and sustained load factor, minimum turn radius, maximum and minumum specific excess power. In addition to these there is still one other very important measure of a combat aircraft's worth. This performance measure is aircraft agility. Agility is the ability to change the direction and magnitude of the aircraft velocity vector in three dimensional space and to accomplish this more rapidly than an opponent [3]. A measure of agility could be determined, in a sense, by a formula or set of formula that combines each of the individual factors listed above.

Aircraft performance in terms of the factors discussed above has been steadily improved with each new generation of combat aircraft so that today's modern combat aircraft are much more agile than their predecessors. This level of increased agility is a direct result of improvements in the state of the art in each of the following areas: stability augumentation, structural technology, power plant capabilities and aerodynamic design. A considerable increase in agility has been made by simply returning to the farsighted design philosophy of the Wright Brothers. For example, like the Wright Flyer, modern fighter aircraft now use statically unstable designs to enhance manueverability. This concept is demonstrated in the designs of the F-16, F-17 and F-18 fighter aircraft. These aircraft are statically unstable but are kept under control by computerized flight control systems so that the manueverability advantages of static instability can be realized without overburdening the pilot. Modern, lightweight composite materials and aircraft structural design improvements have made it possible to decrease aircraft weight while at the same time increasing structural strength. This produces relatively light weight aircraft that have load factor capabilities of up to 12 g's thereby giving the aircraft distinct increases in agility.

The powerplants of modern fighter aircraft are now powerful enough to take advantage of both the computer aided stability systems (cass) and the increased load factor capabilities of our current fighter aircraft. This makes it possible to sustain very high turn rates and to sustain flight at very high angles of attack. The modern powerplants also can achieve thrust to weight ratios in excess of one thus providing substantial advantages in air combat situations. In the area of aerodynamic design, however, progress of the same magnitude as in the three areas discussed above has not been made. Some innovative uses of the control surfaces along with increased use of some of the powerful vortex interactions around the aircraft have been accomplished, but for the most part little has been done to enhance our understanding or our ability to analyze the extremely complex aerodynamic behavior of an aircraft in air combat type situations.

A possible aircraft to fill the need mentioned above is being designed and tested by McDonnell Douglas and the Air Force Wright Aeronautical Laboratory at Wright-Patterson AFB, Ohio. The aircraft is currently known as the F-15 STOL Demonstrator. It is, basically, an F-15B aircraft with a close coupled canard mounted just forward of the wing on the engine inlet shelves.

Provisions are also being made to implement thrust vectoring engine nozzles (to enhance longitudnal control) and thrust reversal capabilities. The potential benefits of such a configuration are well documented [4,5]. A few will be briefly discussed here for the sake of completeness. The close coupled canard will improve the aircraft's lift in the high angle of attack, (aoa), range and increase stalling aoa. This is due primarily to the vortex interaction between the canard and the wing. Regarding the canard as an extra lifting surface gives the capability of direct force manuevering. Direct force manuevering allows the manuevering modes to be decoupled from each other so that turns without using bank and altitude changes without changing pitch etc. are possible. Another positive effect of the canard is that it provides the ability to decrease trim drag at all speeds. The extra lifting surface area of the canard alone offers some distinct advantages over a similar aircraft without a canard by decreasing overall wingloading. The extra control surface also increases the possibilities for control reconfiguration enabling a safe return to base following battle damage. The canard configuration also dramatically increases pitch rates and turn rates as well as the ability to obtain those high rates quickly.

The F-15 STOL Demonstrator project is still in the testing and development stage. Large amounts of wind tunnel testing (static and forced oscillation) has been accomplished. A reasonably accurate model of the aircraft has been developed through use of the data obtained from the wind tunnel testing. Full scale computerized simulations as well as 'real time' pilot in the loop simulator testing in a fully motion based simulator are also currently being accomplished. Actual test flights of the aircraft are scheduled to occur in March 1988.

C. Engineering Analysis Considerations

Originally, aircraft design and testing involved more trial and error techniques than actual engineering analysis. Experimental data was not only unreliable but was also hard to acquire. Therefore, most of the aircraft development process relied on a 'lets try it out and see what happens' attitude. As aircraft designs increased in complexity, it became not only more and more expensive to design aircraft in that manner but also quite dangerous. It was apparent that more work had to be accomplished on the ground before testing the design in flight. High aoa stability and control studies during the forties and fifties concentrated mainly on obtaining a qualitative description and understanding of the flight dynamics observed.

A lack of reliable wind tunnel and flight testing techniques, combined with little or no computational capabilities stood in the way of any major progress in the area of high aoa flight dynamics. Conventional analysis techniques based on several unrealistic assumptions and linearization were used to analytically predict aircraft behavior [6,7].

Experimental techniques and facilities as well as computational methods and capabilities have undergone major improvements in the past years. Now, quite accurate aircraft models obtained through modern testing techniques are used in full six degrees of freedom (dof) simulations with more accurate results. Additionally, a large number of advanced mathmatical techniques have been developed to deal with specific nonlinear phenomenon. These techniques when combined with information gained from various numerical simulations have given some insight to a few particular high aoa flight phenomena, but there is a conspicuous lack of global analysis techniques. The highly nonlinear and very complex behavior of an aircraft during high aoa flight coupled with poorly understood aerodynamics has created a tremendous amount of resistance to progress in the area of developing general or global analysis techniques.

The development of a global analysis technique will be of great benefit to understanding and possibly conquering high aoa flight. A global type analysis could offer specific guidance as to when use of a particular advanced mathmatical technique would be practical. A more global picture of the aircraft dynamics and behavior will enable engineers to detect areas where problems are likely to occur and study those areas more closely. The heavy use of computer simulations, while accurate within the area investigated, still tends to give a 'tunnel vision' picture of the aircraft dynamics. The possibility of missing some very dangerous or catastrophic behavior is always present in such an analysis. The more global the analysis, the less the possibility of having a very costly surprise during actual flight testing. In spite of the great difficulties discussed above, the need for a more global approach to studying high aoa flight dynamics is stronger than ever. Modern fighter aircraft currently in the inventory are able to operate routinely in areas that were once thought of as outside of the flight envelope. As the ability to generate extreme pitch rates and to sustain very high angles of attack continues to improve, we must also improve our ability to analyze and predict aircraft behavior in those areas and other areas that are considered to be at the extreme limits or actually beyond the conventional flight envelope.

Even though such high aoa manuevering capabilities exist in some of our current aircraft, flight manuals often restrict pilots from operating in this flight regime due to our inability to adequately control or even understand aircraft behavior at such high angles of attack. Such restrictions, while presently necessary for safety reasons, decrease an aircraft's capabilities in an area where an increase in capability is vitally needed to insure air superiority in air combat situations of the future.

D. Overview

In chapter two the research project will be described. This chapter will include a detailed description of the STOL aircraft, a discussion of the flight regime and types of manuevers to be studied along with a section covering problems associated with high aoa flight dynamics analysis. Chapter three will cover the preliminary research taken including a discussion of the other methods considered and the reasons for selecting bifurcation and catastrophe theory techniques. Next, the theoretical concepts will be developed and then discussed as they apply to the development of the procedure. In chapter six the specific methods and numerical techniques used in the computational application of the theroretical procedure will be outlined. A summary of the results of the study will be given next followed by a discussion of those results.

Conclusions from the study accompanied by recommendations of how to best utilize the findings of the study will comprise chapter nine and will conclude the text portion of the document. Information deemed overly detailed for the smooth flow of the text will be placed in the appendix.

CHAPTER II

PROJECT DESCRIPTION

A. Description of the Aircraft and Data

The F-15 STOL Demonstrator, (F-15S), with three major exceptions, is nearly identical in appearance and aerodynamic performance to the current inventory F-15B model. Those three exceptions are the addition of a two-dimensional thrust vectoring/reversing nozzle system, the implementation of a close-coupled-canard and the integration of flight and propulsion controls by using an aggressive computer aided stability system (CASS). The new thrust vectoring nozzle system at the time of this study has not been integrated into the aircraft, and it will not be included in this study.

The close-coupled-canard is located just forward of the wing. This creates very strong vortex coupling between the canard and the wing and explains the title given to this configuration. The vortex coupling in much the same way as leading edge flaps or wing leading edge extensions enables the aircraft to achieve much higher coefficients of lift, typically 30% to 60% higher depending on the Mach number and a stalling angle of attack that is approximately three times higher than the unmodified F-15B. When the aircraft does stall, the canard tends to stall first causing a breakup of the vortex structure across the wing.

This in turn causes the wing to stall. At this point a pitch-down moment results which is in most cases a desirable effect [8]. The canard is located on the engine inlet shelves at an average distance of approximately 2 feet forward of the root of the wing and is set at a 20 degree dihedral angle. It has a swept planform with a sweep back angle of 47 degrees and a symmetrical cross-section. The canard airfoil itself was originally the horizontal tail of an F/A-18. Apart from the canard, all other shapes and dimensions are the same as the unmodified F-15. Further details on the physical characteristics of the aircraft are contained in Appendex A.

The F-15S flight control system is hydraulically powered and fully irreversible. Each of the control surfaces have the capability to not only move symmetrically but differentially as well. This significantly enhances the aircraft's flexibility allowing it to have direct force manuevering possibilities as well as reconfigured controls capabilities. Differential control deflections also enable the aircraft to increase its capabilities in the combat performance areas discussed in chapter one. Perhaps the most important contribution of the fully differential control surfaces, however, is to give the CASS more flexibility in selecting the correct control positions to both maintain aircraft stability and follow the commands of the pilot.

The CASS is a full state feedback type control system that takes as inputs all of the state variables in addition to aircraft altitude, mach number, pilot inputs and the current positions of each of the control surfaces. From all of this information the CASS selects the control positions that will result in the performance desired by the pilot, and it updates the control positions 40 times a second. Through the use of full state feedback concepts the CASS is designed to maintain the system eigenvalues within certain boundaries selected to create the desired aircraft behavior for the various situations expected to be encountered. This means that similar to stable aircraft without stability augmentation the eigenvalues will have negative real parts or at least if the real parts are positive their magnitudes will be small. The system works quite well. In fact, without the CASS the F-15S would catastrophically diverge from straight and level, trimmed flight in less than ten seconds when left on its own. Unfortunately, the CASS is not able to completely maintain stability under all situations. We are therefore left with the typical situation of an aircraft that is stable when subjected to a large variety of disturbances from equilibrium yet unable to maintain its stability under all possible conditions. The F-16 aircraft is a good example of this situation.

It too is controlled in a similar fashion and would be unstable without its CASS. The F-16 is highly manueverable and under most conditions very stable to fly. However, at very high angles of attack during extremely transient air combat manuevering the F-16 has on several occasions departed controlled flight. This is due to the CASS's inability to deal with the conditions created by that type of high aoa manuevering, and consequently, restrictions have been placed on the F-16's flight envelope.

The F-15S is projected to be capable of some very substantial increases in performance over its conventional F-15B counterpart [9]. The takeoff distance will be 27% less while the landing distance is projected to decrease by 82%. These improvements are primarily due to the two-dimensional thrust vectoring/reversing nozzles; however, a portion of the improvement in this area is due to the decreased approach and takeoff speeds resulting from the decreased wing loading afforded by the canard. The roll rate is expected to increase by 24% while the pitch rate is projected to double. These two major increases in capability will pave the way for large increases in aircraft agility by allowing the aircraft to quickly change its attitude and flight path. The expected increases in coefficient of lift and stalling angle of attack have already been discussed above.

The addition of the canard is expected to increase the positive load factor capability to 9g. The actual role of the canard in this improvement is somewhat controversial at the present time, but it can be safely said that the decreased wing loading provided by the canard does play a role in this area of increased capability. Also, by enabling the aircraft to be trimmed to a more streamlined attitude during cruise, the canard is expected to increase the cruise range by 13%. Finally, the F-15S model should be able to decrease its deceleration time by up to 44% in certain situations giving it more flexibility in an air combat situation. The above projected increases in combat manuevering capabilities are impressive when taken into consideration that the current F-15 air combat capabilities are perhaps the best in the world.

The data available on the F-15S for this research project are wind tunnel studies accomplished at Wright-Patterson AFB, the aerodynamic model developed by McDonnell Douglas, the canard schedule, and the CASS package also developed by McDonnell Douglas. The wind tunnel studies include static and forced oscillation data. No rotary balance tests have been done yet. The wind tunnel data is in both plot form and tabular form and is very extensive. In several cases the coefficients are described as a function of four variables.

In order to keep calculation costs and time down the data set was simplified by restricting the configurations to be investigated and by decreasing the number of variables to be used in the determination of the coefficients. The aircraft configuration was restricted to gear up, flaps up and no stores. After studying the data, it was determined that the data did not vary appreciably with changes in altitude. It was also determined that the data for Mach numbers higher than .6 were not necessary since a study of high aoa flight dynamics was planned. Therefore, a data file for a Mach number of .2 and one for a Mach number of .6 were created. Both of the files were for an altitude of 20,000 feet. These two data files give the ability to accurately look at both spin type motions and wind-up turn type manuevers. These simplifications decreased the tabular data sizes so that there were no four dimensional tables and only a few three dimensional tables. In order to accurately model spin type motions the need for rotary balance data was present. This need was filled by obtaining rotary balance data for the unmodified F-15 aircraft and adjusting the data to account for the addition of the canard. The data was additionally adjusted to ensure that the system of aircraft equations of motion did not receive an impulsive input when the rotary balance correction factors were added in (aoa=55 deg.) and removed (aoa=30 deg.).

A complete discussion of the development and application of the rotary balance data is contained in appendix B. The aerodynamic model except for the addition of the rotary balance correction factors is identical to the one determined and validated in simulations by the Air Force and McDonnell Douglas. The symmetrical canard position is independent of the CASS system and inputs from the pilot; it is a function of aoa and Mach number only. The differential canard setting is controlled by the CASS and is applied to the current symmetrical canard position. When the CASS is activated, the the model used in this study for the F-15S has six independent control surfaces. The independent control surfaces are: left and right rudder, left and right stabilator, differential canard setting and the ailerons. The CASS package is implemented with no modifications to keep the aircraft model as close to the actual aircraft as possible.

B. Discussion of the Flight Regime to be Studied

Ever since the beginning of air combat manuevering, air battles would invariably progress towards higher and higher aoa manuevering in attempts to achieve a tighter turn radius than the opponent so that a favorable position for weapons delivery could be gained. Achieving higher turn rates requires in most cases that an aircraft fly at higher angles of attack.

Presently, fighter aircraft handling characteristics at very high angles of attack leave much to be desired. The problems range in severity from being unable to accurately track a target due to wing rock and other high aoa oscillations to total departure from controlled flight resulting in loss of the aircraft and possibly the pilot. Some specific high aoa flight problems are discussed below. At high aoa the rudder controls become sluggish due to the vertical tail descending into the wake of the wing and horizontal tail. This reduces weathercock stability creating a situation ripe for a nose slice type departure from controlled flight. The low aspect ratio, swept back wing design of most fighters make control with the ailerons not only ineffective at high aoa due to wing tip washout but actually dangerous in some cases where adverse yaw characteristics are severe. Additionally, swept wing aircraft experience a decrease in static longitudnal stability as a result of the wings stalling from the tips inward forcing the center of pressure location forward towards the center of gravity location. At high angles of attack the induced drag due to the slender, low aspect ratio wings becomes extremely high causing engine power to be in many cases totally inadequate to sustain manuevers or even control the aircraft.

At high angles of attack the lateral/directional and longitudnal modes experience a high degree of coupling causing an input in one mode to excite very undesirable behavior in the other. Another interesting problem peculiar to fighter aircraft results from their 'sleek' aerodynamic design which tends to concentrate the mass in the fuselage. This increases the aircraft's susceptibility to roll coupling which is a combination of the inertial and kinematic coupling that occur when rolling an aircraft. Roll coupling is aggravated by both high angles of attack and high roll rates [10] This phenomenon as well as some of the others discussed above often can occur very abruptly in a manner that can be termed as catastrophic. The above problems in addition to a few others currently make high aoa flight an undesirable flight regime to operate in.

When all of the undesirable side effects of high aoa flight discussed above are considered as a whole, the the high aoa dynamics of a fighter aircraft can be at best described as unpredictable. This is true regardless of whether or not the aircraft has been equipped with a computerized stability system. As an example, consider the F-16 and the F-5E with the shark nose modification. The F-16 as mentioned above has demonstrated a great deal of unpredictability at high angles of attack resulting in several lost aircraft.

But, the F-5E/shark aircraft has also been shown to be very unpredictable due to the complex aerodynamics brought into play by the shark nose section. It too has departed controlled flight without warning resulting in a loss of aircraft. In each of the above cases a lack of overall understanding of how each of the above high aoa phenomena might combine to make up the entire high aoa flight dynamics picture has been directly responsible for the lost aircraft. Before aircraft agility can be increased, we must remove a great deal of the unpredictability from the high aoa dynamics of our fighter aircraft.

C. High Angle of Attack Analysis Problems

The primary problem with studying high aoa flight dynamics is the nonlinear characteristics of high aoa flight. The great bulk of aircraft dynamics analysis has been based on several assumptions that become totally unrealistic when considering an aircraft flying at high aoa. The most far reaching of those assumptions was the linearization of both the equations of motion and the aerodynamics. The linearization of the equations of motion is based on the assumption of small perturbations about an operating point through the use of the Poincare/Liapunov theorem (Appendix C).

The assumption of small amplitude disturbances is a questionable one in our application but can be made to hold up given a small enough neighborhood around the point of interest. Unfortunately, the eigenstructure of the system goes through very large changes when the aoa is increased to the very large values being investigated forcing the eigenvalues to cross the imaginary axis in many cases. This partially invalidates the Poincare/Liapunov theorem forcing the use of a variation known as the Center Manifold Theorem (Chapter IV) to be used in its place. The Center Manifold theorem requires the use at least in part of the nonlinear representation of the system. Additionally, linearization of the equations of motion allows the use of stability derivatives which necessarily implies a linearization of the aerodynamic data. This is an extremely unrealistic assumption when dealing with high aoa aerodynamics. The next major assumption made to simplify the equations of motion was to assume that motions in the plane of symmetry did not create motions out of the plane of symmetry. This decoupled the equations of motion into a fourth order set of longitudnal equations and a fourth order set of lateral/directional equations [6]. For the reasons discussed above this is also an unrealistic assumption when dealing with high aoa flight. Wing rock is amoung the many examples contrary to that assumption.

The decoupled, linearised set of equations is not completely without merit though. They have and still will accurately predict aircraft behavior in low aoa small amplitude disturbance flight with excellent accuracy.

Perhaps the greatest underlying cause for the high aoa analysis problems discussed above is the highly unsteady, unpredictable, nonlinear aerodynamic flow fields that surround an aircraft at high aoa. It is those flow fields that create the nonlinearities in the data which is primarily responsible for the large variations in the location of the system eigenvalues. Consequently, it is the aerodynamic flow fields that ultimately force the governing equations for the aircraft to be nonlinear. Some specific aerodynamic flow phenomena present when flying at high aoa in the F-15S are assymetric vortex shedding, canard-wing vortex interaction and large amounts of separated and reattached flow fields [4,8,11]. These high aoa aerodynamic flow phenomenon can have both positive and negative effects on an aircraft's flight performance. Assymetric vortex shedding, for instance, is currently a problem because of its unpredictability, but should the mechanisms behind the phenomenon become better understood, the use of vortex shedding could eventually be used in a positive way to enhance aircraft manueverability.

The vortex interaction between the canard and the wing certainly has a positive effect on the aircraft's performance, but it also complicates the problem by contributing significantly to the nonlinearity of the situation as a whole. Although this study will not deal with the fluid dynamics associated with the problem, it is recognized that a better understanding of the high aoa fluid dynamics involved will pave the way for swifter progress in the understanding of the flight dynamics at high aoa.

In addition to increasing the nonlinearity and complexity of the aircraft's flight dynamics, the canard presents some other problems to be overcome in analyzing and controlling the aircraft's flight behavior. The canard by greatly increasing the aircrafts response to control inputs allows the aircraft to generate extemely high pitch rates so that the aircraft can routinely overshoot its stalling angle of attack. The higher pitch and roll rates also create increased problems due to inertial coupling. As is normally the case, the increased capabilities afforded by a design modification drastically increases the complexity of the problem for the engineer.

The single-most difficult problem in effectively studying a system as complex as this one is the lack of a practical criteria from an engineering viewpoint to discern global stability.

The great bulk of the nonlinear analysis techniques in use today are very localized, the few that are of a global nature are very difficult to apply to different or more complex systems. The specific advantages and disadvantages of the particular nonlinear analysis techniques available today will be discussed in detail in the next chapter. It can be said at this point however that the best way to handle the analysis will include a combination of linear and nonlinear methods under the general guidance of a more global method that will effectively combine several localized techniques into a complete analysis package.

CHAPTER III

PRELIMINARY RESEARCH

A. General Points

A good deal of preliminary research was necessary to not only ensure that all options were considered but also to enable me to become more familiar with the field of nonlinear analysis in general and specifically as it applies to aircraft dynamics. The types of research undertaken were quite varied. A literature search of the nonlinear analysis field including texts, papers, journals and other periodicals was accomplished; indepth discussions on the subject with several people involved in the nonlinear analysis field were held; and actual tests of the more promising techniques were made. All of the literary works studied during the reseach that had any bearing on the selection of the method of research or the method itself are cited in the references. Those individuals who gave of their time and expertise to further this project are gratefully acknowledged in the foreword. And the specific techniques tested as well as those considered are briefly discussed in the remainder of this chapter.

B. Method Selection Considerations

Most of the considerations that were taken into account in the selection of the method of analysis have already been alluded to in one manner or another. For continuity I will briefly summarize the selection criteria used. First of all, the method must be applicable to the F-15S; it must be capable of analyzing high order nonlinear systems of equations; and the method must be practical. The practicality of the method will be determined on the basis of whether it is useful from an engineering point of view, and whether the concept itself along with the difficulty of its application is within the scope of a master's thesis. A fairly important personal desire was that the concept be relatively unique. One of the most important considerations is that the method must have the potential of yielding useful and meaningful results. Specifically, the technique should be general enough to be readily applied to other systems, and to be useful to the fighter aircraft design community, it must have the capability to handle complex systems. Finally, in order to satisfy one of the primary goals of this study, the results must be of a global nature.

C. Techniques Investigated

A large number of possibilities were studied before deciding on bifurcation and catastrophe theory techniques as the best course of action to take in analyzing the high aoa flight dynamics of the F-15S. Methods from all of the general areas of engineering analysis were considered. These general areas included methods from the following fields: analytical, assymptotic, topological and numerical. Brief discussions of the techniques investigated are presented below.

1. Linearization Methods [6,7,12,13]

The major problem with all linearization schemes studied was the lack of their ability to obtain global information on the system. The very nature of the linearization process indicates that the information is valid only in a local area about a specific operating point. A major improvement over true linearization is found in quasi-linearization. In this method the small signal requirement is removed by repeatedly re-linearizing the system as the input causes changes in the nature of the system. This allows an unlimited variation of input signal, and by changing the linear characteristics of the approximation the basic nonlinearites of the system can be modeled.

Although, quasi-linearization is more global than a pure linear approximation, two major drawbacks cause this method to break down. One major problem stems from the fact that the extreme nonlinearity of high aoa flight dynamics will force quasi-linearization techniques to become impractical at some point. This is due to the inability to isolate operating areas that are large enough to be useful and still small enough to give an accurate approximation. Another severe problem stems from the inability at some operating points for linear approximations to even be valid. The theoretical basis for quasi-linearization methods is found in the Poinare/Liapunav theorem which is discussed in appendix C. As a primary analysis tool, the potential for useful results was not present in the schemes studied. However, this does not mean that all uses of linearization methods are without merit. There are a number of instances in a nonlinear problem when inexpensive, reliable results can be achieved through linearization techniques. A thorough understanding of the nonlinearities of the problem is required, however, before linearised approximations can be safely used.

2. Liapunov's Second or Direct Method [13,14,15]

This technique is certainly global in nature. Its unusual approach is to study the stability of the system in the whole without looking at the details. Without question, it does enable one to discern the stability of a complex, nonlinear system, but the method does have some serious drawbacks from a practical standpoint. One major drawback stems from the extreme difficulty in nearly all cases except relatively simple, potential governed systems of deriving a Liapunov function. Another extreme drawback to the method from an engineering point of view is the tremendous lack of generality of the Liapunov functions themselves. For instance, should a Liapunov function be found and an analysis developed for one particular system, the engineer will have made very little progress towards a solution of a similar problem since a different Liapunov function must be derived for each case. Overall, the method is very impractical for use in this particular study.

3. Phase Plane Trajectory Analysis [16,17,18,19]

This technique has some positive points to offer. Its results are easily interpreted and they are slightly more global in their nature than some of the other methods investigated.

On the other hand, due to its specific topological nature, it is difficult to apply phase plane type analysis to large scale, multi-variable systems, nor does it lend itself readily to systems that have extreme nonlinearities. The method was used with some success in the analysis of a nonlinear model of the lateral/directional mode of an F-111. As a primary analysis technique, however, phase plane analysis falls short of the selection criteria established, but it does have some promise as a technique to compliment a more global, larger scale method.

4. Assymptotic Methods [20,21,22,23,24]

Assymptotic methods have proven to be very effective in developing useful, accurate approximations to systems that are analytically very complex. These methods have been shown to be effective in analyzing both nonlinear and nonautonomous systems of equations. Multiple Scaling which is a specific assymptotic approach initially showed much promise as a technique to actually solve the nonlinear equations of motion with nonlinear coefficients in a quasi-analytical manner as opposed to numerical integration. This method is unique in that it has not yet been extensively applied to aircraft dynamics problems.

A generalized multiple scaling technique was tested on the same F-111 lateral/directional model; unfortunately, only limited success was attained during the study. I still feel that the method has the promise to make a breakthrough in this area, but at the present time the determination of the proper scaling factors is as much of an art as it is a science making the method impractical given the time constraints on the completion of this research.

5. Numerical Simulations [13]

Numerical simulations have and will continue to be used as a major flight dynamics analysis tool. Several of the techniques discussed in this chapter are made possible through numerical simulation techniques, and many other methods are validated through numerical simulations. The simulations can be quite accurate provided that the aerodynamic model correctly models the actual aircraft, and the numerical techniques are sound. There are, however, some significant problems with using numerical simulations as the primary analysis tool in a high aoa flight dynamics study. When high aoa flight is considered, the simulations become valid only in small areas around the state space point being simulated due to very complex, nonlinear aircraft behavior.

With this in mind the amount of simulations required to gain an adequate representation of the aircraft dynamics rises drastically making the method quite costly. Another serious problem arises from the fact that as the complexity of the flight dynamics increases it becomes very possible to miss critical flight behavior when studying an aircraft through numerical simulations alone. On the other hand, numerical simulations are very useful if used in conjunction with a more global approach. The more global technique should be able to locate areas where possible stability problems that require further study exist. A numerical simulation of the area in question could then be done thereby making numerical simulations more cost effective and more useful in general.

6. Describing Functions [13,25]

A quasi-linear function that describes the transfer properties of the nonlinearity is called a describing function. The major drawback to this technique is that the form of the signal must be calculated or known in advance. The form that is of most use in this research area is the sinusoidal input which is useful for determining the existence and locations of limit cycles. Another more subtle drawback of this method is that only the specific questions asked of it are answered.

This makes the method far too specific to be of great value in this study, and it is also indicates that the results will not be global in nature. Therefore, use of the method should be limited to instances where it is desired to investigate a limit cycle possibility predicted by a more global method.

D. Selection of the Actual Technique to be Used

After all of the preliminary research was completed, a technique based on bifurcation and catastrophe theories was selected as the primary research technique [26,27,28,29]. The following discussion outlines the reasons for making that particular choice. The method was very practical from several viewpoints. First of all, a great deal of information on the technique was available to me. The concept of combining bifurcation and catastrophe theories in the manner used by this method was devised by Scientific Systems Inc. which is a company located in Cambridge Ma. They were willing to share some of their knowledge and experience gained during their research. This factor contributed towards enabling me to study a realistic engineering problem within the limited time frame allotted for my master's thesis. The method is also practical from an engineering standpoint since it is readily applied to engineering type situations.

This is due to the ability to present the results in a easy to understand graphical format that relays a large amount of usable information in a short amount of time. The technique is applicable to fighter type aircraft, and has already been tested on an older current inventory fighter. The concept is quite general and can even be adapted to other uses in addition to aircraft dynamics. The concept is also very unique having been applied to just a few aircraft and none with the degree of sophistication of the F-15S aircraft. The primary advantage of the method, however, is its ability to analyze systems from a global viewpoint. One is able to get a 'picture' of the flight dynamics of an aircraft across a full spectrum of control inputs in a single gaze. Another important point is that the global nature of this method is not dimenished by the presence of nonlinearities. Overall, the general and global nature of this method make it perfect for use as a primary research technique that will promote more effective use of the techniques discussed above.

E. General Applications for the Results of the Study

A very important consequence of the results of any scientific study should be a better understanding of the phenomenon behind the driving desire for the study.

In this case the phenomenon is high aoa flight, and a better understanding of the combined effects of the many high aoa flight dynamics phenomena is expected to be gained through this area of research. A better understanding of the nature and the mechanisms behind high aoa flight could make it possible to provide early warning of impending occurences of the more undesirable consequences of high aoa flight. This concept can be likened to stall warning devices in general aviation aircraft. Another application for the method is model structure determination and validation. This particular aspect will not be treated in this study. The types of application that will be concentrated on most in this study will be the development of particular control stategies. One obvious control strategy area is to develop bifurcation free control laws for computerized flight control systems that will avoid the dangerous areas by avoiding the nonlinear jump phenomenon that normaly accompanies bifurcations. Another more immediately useful goal is to determine specific recovery techniques for certain out of control situations. And finally, after the aircraft control problems are better understood, the development of air combat tactics and techniques can be undertaken so that full advantage is taken of the newly realized high aoa manuevering capabilities of our fighter aircraft.

CHAPTER IV

THEORETICAL CONCEPTS

A. Overview

Within this chapter the theoretical basis for the method of research will be discussed in detail. This will be done by first introducing and discussing the concepts of bifurcations and catastrophes. The discussion will include a couple of simple examples that illustrate the two concepts. Next, the four major theorems that will be used to extend the concepts of bifurcations and catastrophes to 'real world' engineering applications will be discussed. For clarity and brevity the abbreviation, BACTM, which denotes Bifurcation and Catastrophe Theory Methodology will be used to refer to the general techniques used in this research. The name is adopted from the title of the research conducted in this same area by Scientific Systems Inc., Cambridge Ma.

B. Description of the Underlying Concepts

As a result of the nonlinear nature of high aoa flight, aircraft dynamics exhibit a wide variety of bifurcation and catastrophe related behavior. Bifurcations are not a new concept nor has their study been limited to recent history.

They were first studied by Poincare in the late 1800's and later by Hopf as well as others [38]. Catastrophe theory on the other hand is a relatively new topic. The earliest work published on the concept was a paper written by Rene Thom in 1968 [30,31]. The concept gained a good deal of popularity initially, but later it became overused leading to attempts to apply catastrophe theories to a large number of non-technical systems which lacked definite mathmatical structure. Examples of such subjective use of the theorem can be found in [32]. This has led to some considerable criticism of the theory itself as a result of its inability to give clear objective results in those cases [33]. This does not constitute a problem for the application proposed here since a definite physical and mathmatical model of the system exists.

1. Bifurcations

As alluded to above, bifurcations are a nonlinear phenomenon. They can occur in a number of different circumstances and in a number of different forms. Literally speaking, a bifurcation is a point where something is divided into two parts or branches. This literal definition is very close to the actual engineering application of the word. In our case, the branches are solutions to the equilibrium surface equations which will be discussed later.

A simple bifurcation occurs when a system through the variation of some independent parameter reaches a point where its behavior can assume one of two different forms for the same set of system parameters. The point where the system branches off into one of the two behavior modes is termed a simple bifurcation point. An important consequence of such a phenomenon is that the mathmatical structure of the system itself also undergoes a change at this point. This gives rise to the concept of structural stability which should not be confused with stability in terms of the aircraft motion [16].

An example of a simple bifurcation is shown below.

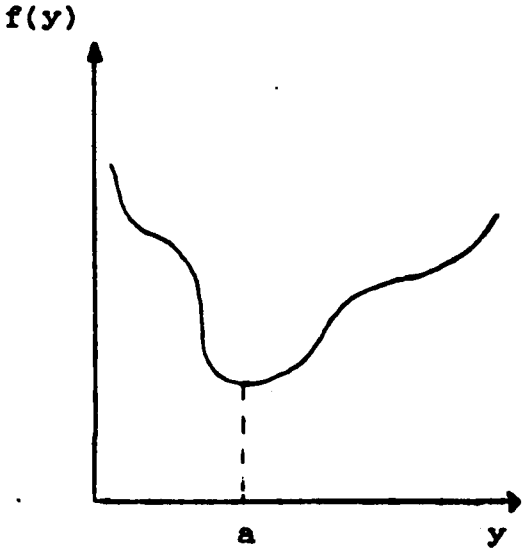

Fig. 4.1a

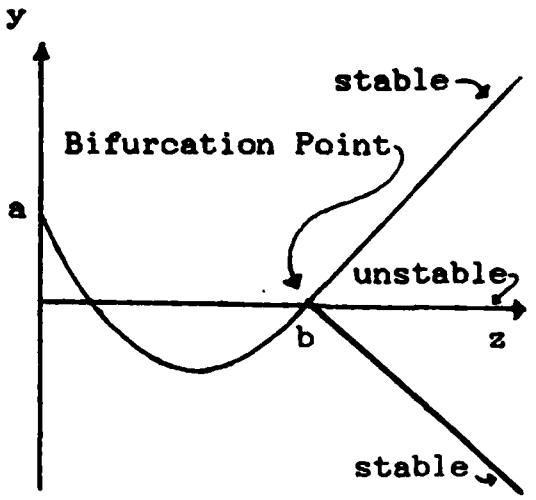

Fig. 4.1b

Figs. 4.1a and 4.1b Simple Bifurcation Example

Figure 4.1a depicts a simple y and f(y) relationship. The shape of the curve is due to the nonlinearities in the system. Let f(y) be a potential governed function such as gravity where f(y) is height at some point, y.

Therefore, the system is in equilibrium whenever df/dy=0. Potential governed systems such as gravity tend to seek minimum potential energy, and therefore, any equilibrium point that is also a local minimum will be locally stable. Point a in figure 4.1a represents a stable equilibrium since df/dy=0 and d^2f/dy^2 is positive at that point. Figure 4.1b shows the location of points of minimum potential energy in the (y,z) space where z is a variable that runs perpendicular to the paper in figure 4.1a. When the value of z is increased beyond point b, the structure of the system changes form. There are now two local minimums in the area under study and the total number of possible equilibrium positions in the area being studied has been increased to three, two stable and one unstable. The system, as it attempts to minimize potential energy, must proceed along one branch or the other as z is increased beyond point b. This is a simple bifurcation, and point b is a simple bifurcation point. Physically, this situation could represent a marble rolling along a channel towards an intersection created by a smooth ridge. The top of the ridge is a locus of unstable equilibrium points, and the bottom of the two valleys created by the ridge are loci of stable erquilibrium points. Given an exact set of circumstances the marble could roll up the divider and along the ridge; however, the most likely path would be down one of the two valleys to each side of the ridge.

This is due to the unstable nature of the equilibrium points along the ridge. The use of terms from topology is by design since the concepts of differential topology will be of great assistance in understanding and analyzing the results of a study using BACTM. If we assume that figure 4.1a is a global picture of the locations of stable equilibriums of the system for given values of z, then it can be said that the system will behave in a predetermined manner for all y and z up to z equal to b. Beyond the point where z=b the global system behavior becomes dependent on the values of y and z in addition to several other parameters. This is a common consequence of nonlinearities in a system. When z is to the left of point b in figure 4.1b, the single branch is globally stable while the two stable branches located to the right of point b are only locally stable. The domains of attraction of the two locally stable branches are very well defined. All points above the unstable equilibrium belong to the domain of attraction of the upper equilibrium branch while all points below the unstable equilibrium belong to the domain of attraction of the lower equilibrium branch.

This simple example can be successfully expanded to include large scale higher order systems. An important step to make beforehand, however, is to properly define the terms global and local.

For the purposes of this study, the term global will indicate that the full spectrum of admissible state and control variable values is to be considered. The term local will be taken to mean that the properties of the point or area being considered are valid only within some region that is smaller than the full spectrum of admissible control and state variable values.

Normally, bifurcation type behavior occurs in the manner described above. On occasion, however, the number of stable branches that intersect at one point are greater than two. This situation will be described as a general bifurcation. Another form of bifurcation that will be refered to in this study is the Hopf Bifurcation. In the context of aircraft dynamics, a Hopf Bifurcation may occur when a complex pair of eigenvalues of the linearised system cross the imaginary axis (frequency or Laplace domain description). There are two possible outcomes of this situation. If the system has the right combination of nonlinear characteristics, the behavior will grow into a stable limit cycle, or if the global system is well described by the linearised representation, it will show unstable growth as is predicted by linear analysis. Further discussion of Hopf bifurcations will be given later in this section.

2. Catastrophes

In many ways catastrophes are similar to bifurcations. They both occur in nonlinear systems and they both involve a change in the behavior of the system. Like bifurcation points, the points where catastrophes occur mark a change in the structure of the overall system, and also similar to bifurcations, catastrophes occur as a result of smoothly varying some input to the system. Unlike bifurcations, however, catastrophes result in a sudden and usually large change in the state of the system, and in most cases catastrophes also occur without warning. This explains the name given to the phenomena. Catastrophes are also described as nonlinear jump phenomena compared to a bifurcation being a smooth branching of the behavior. An example of catastrophe behavior in an aircraft would be a situation where at a certain point a smooth increase in aileron deflection causes a sudden and large increase in roll rate.

The following example will serve to give a better understanding of catastrophes and how they relate to bifurcations. This example is derived from the cusp catastrophe which is one of Thom's seven elementary catastrophes [27,30,31]. Consider the nonlinear differential equation below.

$$dx/dt = x^3 + C1x + C2 \qquad (4.1)$$

Where x denotes the state, and (C1,C2) are control variables.

Since the system is a scalar one, the system equilibrium may be represented as the minima and maxima of the potential function

$$\Phi = .25x^4 + .5C1x^2 + C2x. \qquad (4.2)$$

Equilibrium points occur whenever dx/dt=0 in equation 4.1. Let C1=-3 for this discussion. It can be shown that there is only one equilibrium point for |C2|>2 while three equilibrium points exist when |C2|<2. This is a consequence of the number of real solutions to equation 4.1 when dx/dt=0. For instance, when C2=0, the equilibrium solutions to equation 4.1 are easily shown to be $(-\sqrt{3}\ ,0,\sqrt{3}\ )$; however, when |C2|>2 there is only one real valued equilibrium solution to equation 4.1. Differentiating equation 4.1 with respect to x will result in the second derivative of the potential function and is shown below.

$$d^2\Phi/dx^2 = 3x^2 + C1 \qquad (4.3)$$

Inserting the values of x corresponding to the equilibrium positions $(-\sqrt{3}\ ,0,\sqrt{3}\ )$ into equation 4.3 show that x=0 is a local maximum and therefore, an unstable equilibrium point, and $x=\pm\ 3$ are both minima and therefore, are stable equilibrium points. This is very similar to the marble in a bifurcating channel example discussed above in that an unstable equilibrium point separates any two stable equilibrium points.

Refering back to equation 4.3 and setting $d^2\Phi/dx^2$ to 0, it can be seen that regardless of the value of C2 there will be inflection points in the potential function at $x=\pm\sqrt{-C1/3}$ when C1=-3 this corresponds to $x=\pm 1$. On the other hand, the location of the maxima and minima do vary with changes in C2. When C2 equals +2 or - 2 and C1=-3, a minimum and maximum will coalesce at one of the inflection points. When this occurs, if the system was previously at the stable equilibrium point that is now an inflection point, the system will be in unstable equilibrium and ready for a catastrophe or more simply put, a jump in its state to occur. A small variation of C2 will cause the jump. This example also shows that a stable equilibrium cannot coexist with an unstable equilibrium. The result of any such coexistance is the loss of stable equilibrium at that point. This situation is described as an unstable equilibrium annihilating a stable one [27].

The above discussion is demonstrated graphically in figure 4.2. Let X1 and X2 be the locations of the two stable equilibrium points, when they exist. The system will be a marble seeking a local minimum of its potential energy. This example varies from the preceding bifurcation example in that the behavior of this system is studied in only one variable. In Figure 4.2 the control variable, C2, is allowed to vary slowly from C2=-3 to C2=+3.

After each change in C2, the system is allowed to reach equilibrium, dx/dt=0. As discussed above, only one equilibrium point is possible when |C2|>2. This is shown in plots a and g. In plot b X2 is created when an imaginary pair of roots to equation 4.1 converge on the real axis. This occurs at the inflection point, x=-1. Plots c, d and e show the convolution of the potential function as C2 is varied from -2 to +2. Plot d depicts the C2=0 example discussed above, and therefore, $X1=-\sqrt{3}$, $X2=+\sqrt{3}$ and the unstable equibrium point is located at x=0. In plot f the local maximum and the local minimum at X1 coalesce at x=+1. As C2 is increased further, two of the three real valued solutions to equation 4.1 break away from the real axis and the equilibrium point at X1 disappears. At that point a jump in the state of the system occurs. Physically, the jump is demonstrated by the marble rolling down to X2. If C2 were now varied from +3 back to -3, the behavior would qualitatively be the same, but the jump would occur as C2 is decreased below -2 as shown in plot b revealing a definite hysteresis effect.

Figure 4.2 follows this page.

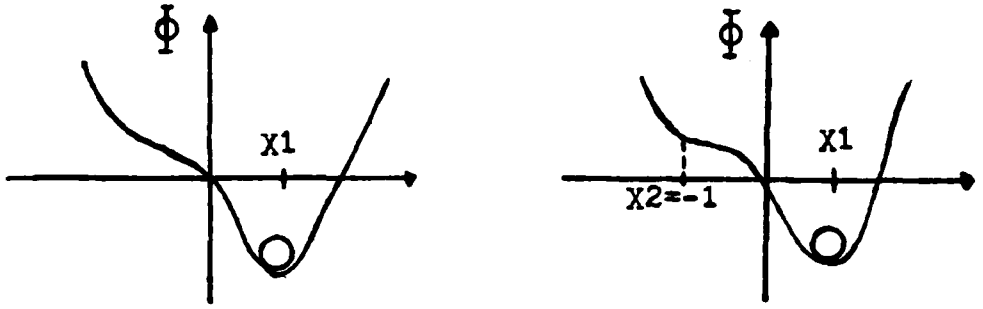

a. C2=-3

b. C2=-2

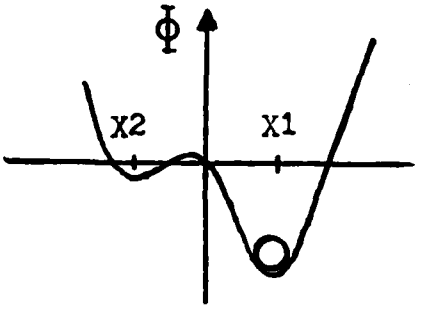

c. C2=-1

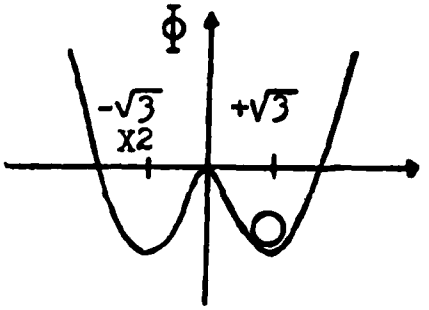

d. C2=0

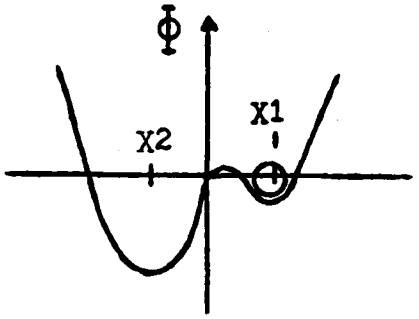

e. C2=1

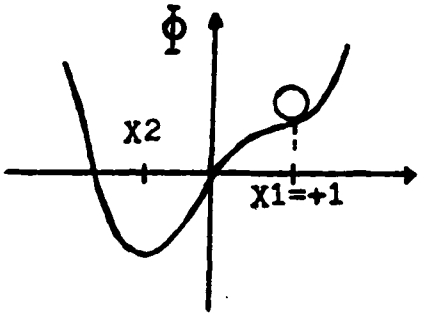

f. C2=2

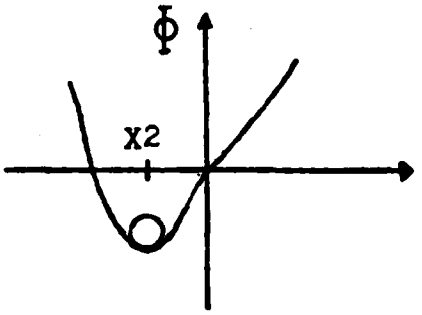

g. C2=3

Figure 4.2: Potential Function, $\Phi(x,c)$ for various values of C2 with C1=-3

Figure 4.3 brings the concepts discussed above together in a three dimensional diagram in the (x,C1,C2) space. The diagram shows a surface made up of all of the solution points satisfying equation 4.1 for various values of the control parameters, C1 and C2, when dx/dt=0. The area where three real valued solutions to equation 4.1 exist is depicted by the equilibrium surface folding over on itself. A global representation of the positions where a jump in state may occur is shown by a projection onto the control space (C1,C2) of all the locations where inflection points coincide with equilibrium points. The projection of these catastrophe point locations onto the (C1, C2) space gives a mapping of the locations where the number of equilibrium solutions change. In this example the area within the cusp show where the equilibrium surface is triple sheeted, and the area outside of the cusp show where the equilibrium solutions are single valued. The boundary between areas with different numbers of equilibrum points is called a bifurcation surface since the equilibrium solutions separate or bifurcate from each other along that surface. The combination of all the bifurcation surfaces in the control space is known as a catastrophe map since it gives the locations in the control space where catastrophes are likely to occur. Catastrophes often occur when a bifurcation surface is crossed so that the number of local equilibrium solutions decreases.

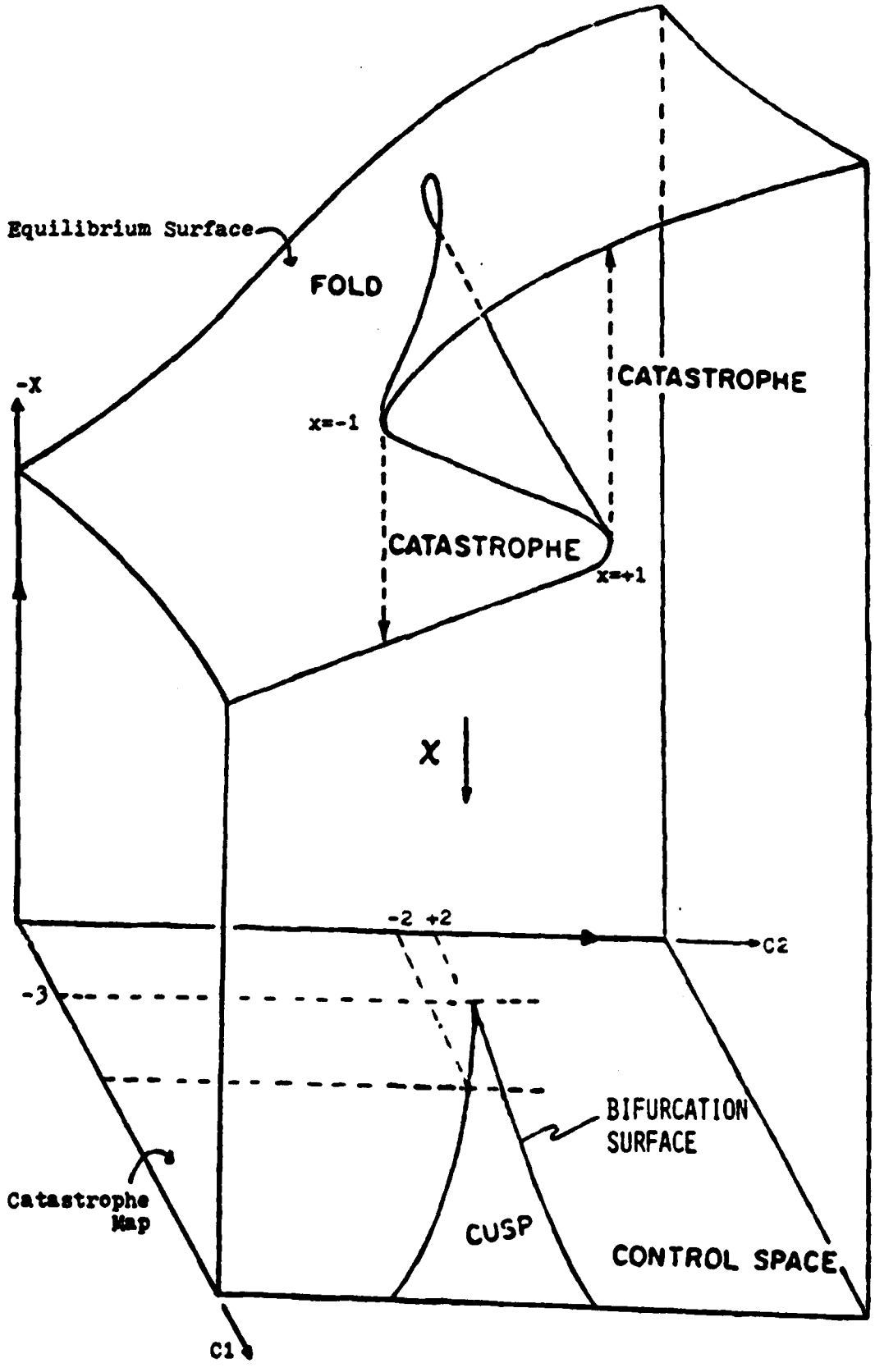

Figure 4.3: Equilibrium and Bifurcation Surfaces for $\Phi(x,c)$

The bifurcation surface shown in figure 4.3 is found by locating all of the points which are both equilibrium and inflection points. This is accomplished by solving the following pair of simultaneous equations:

$$f(x,c) = x^3 + C1x + C2 = 0 \qquad (4.5)$$

$$df/dx = 3x^2 + C1 = 0 \qquad (4.6)$$

Eliminating x from the above equations gives the equation for the bifurcation surface as

$$(1/27)C1^3 + C2((-1/3)C1)^{3/2} + 1/4C2^2 = 0 \qquad (4.7)$$

The admissible values for the control variable must be restricted real values. This requires that C1 be negative for solutions to the bifurcation equation to exist. The variable, C1 is known as a splitting factor since for C1>0 no catastrophes can occur and for C1<0 catastrophes can occur. This point is shown graphically in figures 4.4a and 4.4b which are simply two dimensional cross sections of the equilibrium surface in figure 4.3 for C1 held constant at a positive value and a negative value. Points a and b in Figure 4.4b are Bifurcation-limit points.

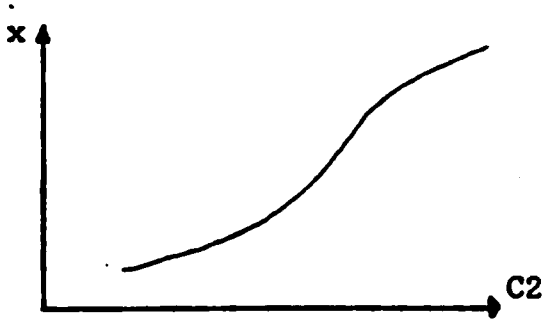

Fig. 4.4a C1>0

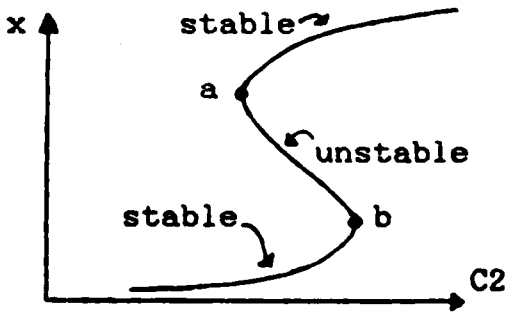

Fig. 4.4b C1<0

Figures 4.4a and 4.4b 2-D Equilibrium Plots

The simple example discussed above combines nearly all of the concepts to be used in this study. A few pivotal theorems that will be used to extend the concepts revealed in this scaler example to higher order, multi-dimensional systems will be discussed next.

C. Discussion of the Main Theorems

Currently, there are four theorems that are of primary importance in applying the concepts of BACTM to real world engineering systems. Each of those theorems will be discussed briefly here.

1. The Center Manifold Theorem [27,34,35,36]

The Center Manifold Theorem is of great use in determining the extent to which linear techniques can be applied to a nonlinear system. It is, in a sense, an extension in the application of the Poincare/Liapunov Stability theorem (appendix C). Consider a nonlinear system described by the nth order differential equation

$$d\underline{x}/dt = \underline{f}(\underline{x},\underline{c}) \qquad (4.8)$$

where $\underline{x}$ is a vector composed of n state variables and $\underline{c}$ is a vector composed of m control variables. Suppose that the eigenvalues for the system are found by using some suitable linearization technique. Let k be the number of eigenvalues of the linearised system whose real parts are zero, i be the number with positive real parts and j be the number with negative real parts.

The system can now be separated into three individual systems by use of appropriate coordinate transformations so that the original system can be represented as follows:

$$du/dt = g(u,c) \qquad (4.9)$$

$$dv/dt = A(-)v + B(-)c \qquad (4.10)$$

$$dw/dt = A(+)w + B(+)c \qquad (4.11)$$

where (-) and (+) indicate systems created from the portions of the original system whose eigenvalues have negative and positive real parts respectively. The systems represented by equations 4.10 and 4.11 are of order j and i respectively and are properly described by the linear approximations. This is a consequence of the Poincare/Liapunov theorem (Appendix C). The system described by equation 4.9 is a kth order system created from the eigenvalues with zero real parts. The essential nonlinearities of the original system are described completely by equation 4.9, and since bifurcations occur only in nonlinear systems the complete bifurcational behavior can be studied by analyzing the k dimensional u-system by itself. This greatly reduces the size of the system that must be studied. In fact Arnol'd [36,37] has shown that the maximum value of k is determined entirely by the dimension m of the control vector. This stems directly from the concept of structural stability mentioned earlier.

Arnol'd states that the number of singularities that occur in "general position" is a function of the number of independent parameters in the system. For instance, if only one control variable were available, a single eigenvalue could be placed on the imaginary axis in a structurally stable manner. There are, under some circumstances, cases where systems with only one control variable may have more than one eigenvalue on the imaginary axis at the same time; however, in these cases a small shift in the parameters within the system will cause the additional singularities to disappear. In order to maintain two eigenvalues on the imaginary axis in a structurally stable way, three independent controls must be available. When the computer aided stability system (CASS) is not operational, the F-15S will have only three independent control parameters, and therefore, k will be two or less in these situations. When the CASS is operational, however, the number of independent control parameters is increased to six, and k may now take on a maximum value of three. Systems with reduced orders greater than two have not been studied to any great extent and are not well understood. This is not necessarily a major problem since, statistically speaking, the occurances of the proper positioning of the controls to obtain singularities in "general position" become increasingly rare as k increases.

This conjecture is stated without proof by Arnol'd [37], but it does make considerable physical sense. Given that this is true, the possibility of having to deal with lesser understood reduced order systems of three may be quite small. Arnol'd also states that any information obtained on the u-system can be generalized to the original nth order system by "suspending" the linear systems having the eigenvalues with non zero real parts to the u-system. Systems with k=1,2 are reasonably well understood and well documented, and the next two theorems by Thom and Hopf define the bifurcational behavior for these systems.

2. Main Theorem of Elementary Catastrophe Theory [27,30]

This theorem by Rene Thom [30] provides classifications of the bifurcational behavior of all gradient type finite dimensional systems where $m < 6$ (a gradient type system is one in which a potential function exists). The assumption of a potential governed system means that the Jacobian matrix describing the linearized system will be symmetrical, and therefore have only real eigenvalues [27]. For systems with $m<6$, there can be no more than two zero eigenvalues. Therefore, through the Center Manifold Theorem the complete bifurcational behavior of these systems can be studied by studying either a one dimensional or two dimensional system.

The exact form of the one or two dimensional system depends on the nature of the higher order terms in the Taylor Series expansion of g(u,c) (ie. how many of the higher order terms are properly neglected). Thom has labeled the general form of the catastrophes with k=1 as cuspoids and the ones with k=2 as umbilics. The example given in the previous section falls in the general group of cuspoids since its reduced state space dimension, k, is one. The control space dimension of the example was two which further classifies the example as a member of the family of generic catastrophes known as cusps. The elementary catastrophe models developed by Thom can be of great use in understanding the behavior of nonlinear systems. Through the use of the Center Manifold Theorem and Thom's classification theorems both model identification and prediction of aircraft behavior is possible.

The above discussion has been restricted to reduced order systems made up entirely of real eigenvalues. The next theory deals with the bifurcational behavior of reduced order systems with a complex pair of eigenvalues.

3. Hopf Bifurcation Theorem [27,38]

Systems that are of the non gradient type, occasionally have equilibrium solutions which consist of closed orbits (limit cycles).

Hopf has shown that a family of limit cycles can bifurcate from an equilibrium point when a complex pair of eigenvalues of the linearized system cross the imaginary axis with non zero speed. In the study of Hopf bifurcations the maximum number of eigenvalues with zero real parts is extended to four in the $m<6$ aircraft situation. This is still considered to be a system with $k\leq 2$ since complex pairs tend to move together in the same manner as the single real valued eigenvalues discussed in the previous section [36,37]. The cases where two complex pair of eigenvalues or a complex pair and a single real valued eigenvalue cross the imaginary axis are not well understood. Consequently, in most circumstances, the number of independent control surfaces used in the study of Hopf Bifurcations are limited to two to prevent the possibility of having more than a single complex pair of eigenvalues cross the imaginary axis at once. Additionally, Hopf Bifurcations can only occur if the remaining eigenvalues with nonzero real parts are well to the left of the imaginary axis. This is not overly restrictive, since most aircraft dynamics studies are concerned with the points where stability is lost for the first time.

4. Global Implicit Function Theorem [39]

The global implicit function theorem was developed by Palias and has been successfully used to determine the uniqueness of equilibrium solutions in nonlinear networks. The applications for this theorem in nonlinear aircraft analysis are straight forward. From the discussions above, it is obvious that it is very important to know the cases where an aircraft's equilibrium solutions are not single valued. Consider the equation $\underline{f}(\underline{x},\underline{c}) = 0$. Palais' theorem states that two conditions must be satisfied for solutions of the above equation to be unique. First, the determinant of the system jacobian matrix, $F = \partial \underline{f}/\partial \underline{x}$, must be nonvanishing for all $(\underline{x},\underline{c})$ (ie. no inflexion points coincident with equilibrium points), and second, the growth condition described below must be satisfied.

$$||f(x,c)|| \rightarrow \infty \text{ as } ||x|| \rightarrow \infty$$

The importance of the first condition is clear from the above discussion of bifurcations, and if satisfied, it implies the absence of bifucations and therefore the absence of catastrophes of the types studied by Thom. The second case addresses the situations where Hopf bifurcations may be present. In general, a system that is properly described by a linearized representation should always satisfy the Global Implicit Function Theorem in the valid range of the linear approximation.

These theorems are important for a couple of reasons. First, the theoretical development of the procedure used in this study which is discussed in the next chapter is based on the concepts of bifurcations and catastrophes, and those concepts in turn are applied in the procedure through the use of these theorems. More importantly, however, they provide an excellent basis towards expanding and improving on the methods that will be brought out in this study.

CHAPTER V

THEORETICAL DEVELOPMENT

A. General Overview of the Method

The basic method to be used in this research was originally developed by Scientific Systems Inc. for use by the Navy [27,28,29]. The method, known as BACTM (Bifurcation Analysis and Catastrophe Theory Methodology), was developed primarily for use on an aerodynamic data set representing the McDonnell Douglas F-4 but was also used on several other more simple aircraft models during the early stages of its development. The remainder of this section will cover the general approach that will be taken during this study, and then the following sections will discuss each of the major steps in detail. References will be made to the theories and examples discussed in chapter 4.

As in any type of scientific research, the first major step taken during this study was the formulation of the problem in more specific terms. This included the identification of the state and control variables, the development of the aerodynamic and mathmatical models, and the selection of reasonable assumptions to simplify the problem. Several different sets of equations of motion were considered.

The ones selected as best suited for the study included a fifth order and two eighth order sets of equations. The fifth order set uses as its state variables: p (roll rate), q (pitch rate), r (yaw rate), alpha (angle of attack) and beta (sideslip angle). One eighth order set employs the wind axis variables: p, q, r, alpha, beta, theta (pitch angle), phi (bank angle) and V (velocity), while the other one uses the body axis variables: u (x-axis velocity), v (y-axis velocity), w (z-axis velocity), p, q, r, theta and phi. See Appendix D for the actual F-15S aircraft models used. The fifth order set of equations was derived by holding V constant and assuming gravity to be zero. By letting gravity be zero theta, and phi decouple from the remaining equations and thus, have no influence on the aircraft dynamics. This set of equations is most accurate in the low angle of attack, trimmed flight range and was used in the preliminary testing of the method. Mehra and Carroll [28] found that setting gravity to zero did not appreciably effect flight trajectories in the low aoa flight range but did create quantitative errors in the high aoa flight range. This problem was especially prevalent during simulations of spin motions. Surprisingly, however, the qualitative results of simulations of spin motions with and without the gravity terms did not differ greatly [27].

The eighth order, wind axis, set of equations was used for increased accuracy in the higher aoa range during BACTM computations, and the other eighth order, body axis set, of equations was used in the numerical simulations. A number of additional variables were also calculated during the simulations, and these are listed and discussed in Appendix E. For further discussion on the mathmatical models used see Appendix D. The significant simplifications made in the development of the aircraft models are listed below:

a. Altitude was held constant during the equilibrium surface calculataions.

b. The effects of spinning rotors were neglected.

c. The thrust vector was assumed to be in line with the x body axis.

d. Thrust was assumed constant during individual computer runs and was set to zero during spin type motions.

e. The configuration was restricted to gear up, flaps up and no stores.

f. The CG location was assumed to be constant during individual computer runs.

g. The data set was reduced to include only the data for 20,000 feet and Mach 0.2 or Mach 0.6.

The above simplifications were not overly restrictive in that they do not restrict the critical nonlinearities of the problem.

The above restrictions are also quite compatible with conditions normally encountered in high aoa fight.

After the problem was properly specified and the aircraft models selected, equilibrium surfaces were generated for various control inputs. This involves setting the time derivatives to zero in the equations of motion and finding the set of solutions across a spectrum of admissible control inputs. At each solution point of the equilibrium surface a local stability analysis is accomplished. The movement and location of the eigenvalues when correlated with the equilibrium surface can reveal a wealth of information on the nonlinear nature of the aircraft model in the area under study. Some of the information that can be gained is the location of possible limit cycles, hysteresis effects, domains of attraction of various stable branches, locations of bifurcations and jump phenomenon, areas that are assymptotically stable or unstable, and steady state flight trajectories. From the location of the individual bifurcation points which were the inflection points in the simple potential example in Chapter IV, bifurcation surfaces are found. These surfaces are the projections of the equilibrium surface bifurcation points onto a two dimensional control space.

These bifurcation points are also the points where the eigenvalues of the linearised system cross the imaginary axis, and it is at these points that the system either jumps to a new equilibrium position, grows to a stable limit cycle or simply becomes unstable [15]. The complete set of all bufurcation surfaces in the control space is referred to as a catastrophe map, and it depicts the locations of possible jump behavior. Once the results have been obtained, predictions of the global aircraft behavior can be made; stability criteria can be formulated; and some possible bifurcation free control laws can be developed. Each of these determinations can be tested by numerical simulation. Areas requiring further study as determined by the numerical simulation can then be studied by repeating the above process.

B. Equilibrium Surface Calculations

As mentioned above, a large amount of information can be gained from knowing the complete set of equilibrium surfaces within the admissible range of state and control variables. An equilibrium surface will not reveal information on aircraft behavior during nonlinear jumps, but it will give the general direction of the jump, the before and after steady state trajectories, and the location of the jumps.

Hysteresis effects can be found by simply reversing the movement along the equilibrium surface (in a manner similar to the minimum potential example shown in figure 4.2). Just as in the examples in Chapter IV, the domains of attraction of the stable branches are determined by the locations of the unstable equilibrium branches (see figure 4.4b). Locating the domains of attraction for a stable limit cycle is considerably more complicated, but information towards that end can be gained by superimposing maximum state variable oscillation amplitudes which are obtained by numerical simulation onto the corresponding points of an equilibrium surface. It also should be noted that there can be several different equilibrium surfaces within the admissible range of the state and control variables. This accounts for the existance of separate spin and trimmed flight equilibrium surfaces. Strictly speaking, surfaces considered separate in this application may not actually be separate since they can meet at points that are outside of the admissible control and state range.

The calculation of the equilibrium surface requires the solution of a nth order nonlinear algebriac equation for various control inputs. This can be done either by solving for the control positions given a set of state variables or vice versa.

The former of the two is, in most cases, easier due to the smaller set of equations and the fact that many aircraft models employ linear control variable coefficients. In the case of the F-15S, however, the control variable vector is not only large (6 X 1) but also has nonlinear coefficients. It is also more systematic from a research standpoint to select a control input as the independent parameter and determine the resulting state variables as the control input is varied, and therefore, that will be the approach taken here. The variation of a single parameter to generate a continuous locus of solutions from a single known solution point is known as a continuation technique. This type of technique is well suited for the computation of both the equilibrium and the bifurcation surfaces.

Using state space vector notation, the equations of motion for the aircraft can be represented as

$$d\underline{x}/dt = \underline{f}(\underline{x},\underline{c}). \qquad (5.1)$$

An equilibrium surface by definition requires that $d\underline{x}/dt = 0$, and therefore, the equation of an equilibrium surface is

$$\underline{f}(\underline{x},\underline{c}) = 0 \qquad (5.2)$$

where $\underline{x}$ is the state vector and $\underline{c}$ is the control vector. The F-15S aircraft model used in this study will require only three control inputs although the control vector may be as large as (6 X 1).

If the computer aided stability system (CASS) is operational then the three control inputs will be longitudnal stick deflection, lateral stick deflection and rudder pedal deflection as measured from within the cockpit. The CASS will take those 'pit' inputs, the current control positions and the current aircraft state and select the actual control surface deflections. The number of independent control inputs available to the CASS in this study is six. If the CASS is not operational, the number of independent control inputs will be decreased to three. In order to accomplish this, the canard will be scheduled symmetrically as a function of aoa and Mach number, the stabilator and rudders will be operated symmetrically while the aileron surface movements remain unchanged. Therefore, when computations are accomplished without the CASS, the control inputs used in the equilibrium surface calculations and the actual system control inputs will be equivalent. During the equilibrium surface calulations, two controls will be held constant while the third is varied. This makes the control vector, c, in equation 5.2 a scalar, and therefore, continuation techniques as described above are easily applied. The final form of the equilibrium surface equation is then

$$f(x,c)=0 \qquad (5.3)$$

The first step in an equilibrium surface calculation is to find a single equilibrium point satisfying equation 5.3 from which to continue the remaining solutions from. This can be done by any method which presents the least difficulty. If a 'trim' equilibrium surface is desired, then setting the control inputs as well as some of the state variables to zero will make the analytical solution of an equilibrium point feasible. For a more complicated equilibrium surface such as one involving spin type motions, a steady state spin condition that is already known to exist or that is found through simulation can be used as a starting point. Finally, once an equilibrium surface is generated, any point on that surface can be used as a starting point for another surface. This makes the method self contained from the selection of the initial equilibrium point.

There are two primary classes of continuation methods [28]. The first class is known as continuation-by-differentiation while the second class is a group of iterative continuation techniques. The continuation-by-differentiation technique solves the equation

$$d\underline{f}/dc = F(d\underline{x}/dc) + \partial \underline{f}/\partial c = 0 \qquad (5.4)$$

where as before $\underline{x}$ is the state vector, c is a scalar control parameter and $\underline{f}$ is $\underline{f}(\underline{x},c)$, the right-hand-side of equation 5.3.

F is the system Jacobian matrix

$$F \equiv (\partial f(\underline{x}, c) / \partial \underline{x}) \qquad (5.5)$$

which can be thought of as a linearized representation of the local system. Equation 5.4 indicates that c is to be varied in such a way so that equation 5.3 will always be true. The major problem with this method is the necessity of calculating both the Jacobian, F, and the vector $\partial f / \partial c$ at every point. This becomes quite time consuming when n is large. On the other hand, iterative approachs use a locally convergent, iterative method such as a Newton-Raphson technique [40,41] which requires only the computation of the Jacobian matrix at each point. The solution is converged upon by iteratively solving an equation of the following form:

$$\underline{x}(\text{new}) = \underline{x}(\text{old}) - F^{-1}\underline{x}(\text{old}) \qquad (5.6)$$

The convergence of the Newton-Raphson method is quadratic providing that the original estimate is near the root [40]. When the estimate is not 'near' the root, the method will usually fail. Iterative schemes such as the Newton-Raphson technique fall into a general class of numerical techniques known as predictor-corrector methods where the Newton-Raphson formula shown above is used as the 'corrector' step. The use of the Newton-Raphson technique alone is therefore unsuited for computation of the equilibrium surfaces.

Current continuation methods use a combination of the two classes discussed above.

As can be expected, the continuation schemes discussed above tend to break down in the neighborhood of bifurcation points. It is at these points where the slope of the equilibrium surface with respect to the control variable becomes infinite or two or more equilibrium surfaces intersect. In a multi-dimensional system these occurences are indicated by the system Jacobian matrix becoming singular. If the Jacobian is non-singular, then the point is a regular point with $f(x,c)$, and all of its first partial derivatives being continuous. The implicit function theorem (Chapter IV) ensures the existence of a unique regular solution to equation 5.3 through any regular point. Which in turn ensures the success of either class of continuation techniques at those points. Conversely though, both types of algorithms break down in the neighborhood of bifurcation points since F becomes non-invertable at those points. Before proceeding further it will be of use to define the three different types of bifurcation points found during the continuation process. The first type is called a limit point; the second type will be called a simple bifurcation point; and the third type is known as a general bifurcation point. An example of each of these is shown in figure 5.1 on the next page.

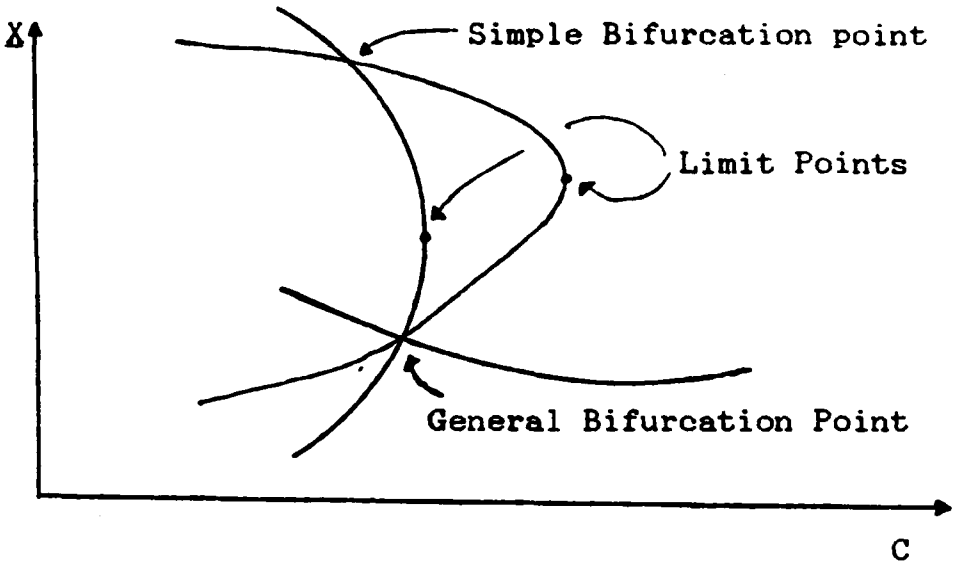

Figure 5.1 Bifurcation and Limit Points

In this study, a predictor-corrector continuation method developed by Kubicek in 1976 [28] will be employed. The Kubicek algorithm uses a combination of the continuation-by-differentiation and iterative methods discussed above. In dealing with the singular Jacobian matrix, study of the work in this area by Keller [42] gives much insight to the nature of the problem. Keller states that the types of bifurcation points that occur in the equilibrium surface are directly related to the co-rank (n-rank) of the system Jacobian. At regular points their are no bifurcations and thus, the co-rank=0. At limit points as well as bifurcation points the system Jacobian is singular, but the co-rank of the Jacobian varies between each of these cases. Limit points have a co-rank=1, and simple bifurcations have a co-rank=2, etc.

During equilibrium surface calculations, the state vector is augmented with the control vector selected to be the continuation parameter so that the state vector becomes a (n+1 X 1) vector where n is the dimension of the system. The Jacobian of the augmented system then becomes an (n X n+1) matrix. At a limit point the Jacobian of both the original and the augmented system become singular, but within the augmented system Jacobian there must be at least one nonsingular (n X n) matrix. This nonsingular matrix is found by eliminating the most singular column of the augmented system Jacobian resulting in a matrix of the form below

$$G_k = \begin{bmatrix} \partial f_1/\partial x_1, \ldots, \partial f_1/\partial x_{k-1}, \partial f_1/\partial x_{k+1}, \ldots, \partial f_1/\partial x_{n+1} \\ \vdots \\ \partial f_j/\partial x_1 \\ \vdots \\ \partial f_n/\partial x_1, \ldots, \partial f_n/\partial x_{k-1}, \partial f_n/\partial x_{k+1}, \ldots, \partial f_n/\partial x_{n+1} \end{bmatrix}$$

where $x_{n+1} = c$. There are n+1 possible (n X n) G_k matrices to choose from. The nonsingular matrix G_k is then substituted in place of the system Jacobian in the continuation scheme.

In essence, the roles of the control parameter and the kth state variable are now reversed so that the state variable corresponding to the column removed to create G_k now becomes the continuation parameter, and the control parameter, c, now acts as a state variable. This situation remains intact until the limit point is traversed and the kth column is no longer the most singular column. Where bifurcation points are encountered, as is often the case in bifurcation surface calculations (due to the compression of a three dimensional representation onto a two dimensional surface), the state variable vector must be augmented with yet another control parameter. This process can be continued until all possibilities are exhausted. From the discussion in Chapter IV, Arnold [36,37] has shown that there will always be more control variables available than bifurcation points to contend with when dealing with the number of independent control variables present in this case (up to six). Kubicek's algorithm uses a lower order continuation-by-differentiation model (a variable order Adam-Bashforth method) as a predictor step and the Newton-Raphson method as the iterative corrector step. Ferziger [40] does an excellent job in explaining these two techniques, and therefore, they will not be discussed here in any detail.

Theoretically, the concept is complete at this point. Unfortunately, there are some practical and numerical problems that still must be dealt with. First of all, the actual application of such a procedure suggested above would be very impractical when higher order bifurcations occur due to the increased size of the Jacobian that must be calculated at each step, and second, some numerical difficulties still exist in the neighborhood of bifurcation and limit points due to the behavior of $\underline{x}(c)$ near those points. This state variable behavior problem comes into play in the calculation of $\partial \underline{f} / \partial c$ in the basic continuation scheme derived from equation 5.4 and shown below

$$d\underline{x}/dc = -F^{-1}(\partial \underline{f} / \partial c) \qquad (5.7)$$

Kubicek's method handles this problem by introducing an arc length parameter, s, to evaluate the dependence of the state variable, $\underline{x}$, on the control parameter, c, [28]. By letting $(\underline{x},c)$ become $(\underline{x}(s),c(s))$ and combining this with the concept developed by Keller which was described above, the continuation scheme shown in equation 5.7 becomes

$$dx_j/ds = -G_k^{-1}(\partial \underline{f} / \partial x_k)(dx_k/ds) \quad j=k, \ 1 \leq j \leq n+1 \qquad (5.8)$$

where the kth column is the one replaced by the n+1 column containing the control parameter derivatives. A standard Euclidean arc length relationship is selected for s. This is shown in equation 5.9 on the next page.

$$(dx_1/ds)^2 + ... +(dx_n/ds)^2 + (dc/ds)^2 = 0 \quad (5.9)$$

By using equation 5.8 in equation 5.9, dx_k/ds can be found. The remaining n parametric derivatives are found by back substitution into equation 5.8. The sign ambiguity presented by the solution of $(dx_k/ds)^2$ in equation 5.9 is resolved by the orientation of the arc length parameter, s, along the solution branch. This is determined at the beginning of the algorithm when the initial continuation parameter direction is selected.

The problem of dealing with higher order bifurcation points has not specifically been addressed at this point, but the continuation method discussed so far is quite adequate for the computation of equilibrium surfaces with limit points. There are several possible means to handle the computation of the equilibrium surfaces at simple and general bifurcation points. One such method has already been alluded to. The state vector could be augumented by additional control parameters so that a non-singular Jacobian matrix can be found in the same manner described above. This method would work, but it would also be quite costly since a larger dimension system would have to be dealt with.

A more comprehensive arc length normalization scheme such as that suggested by Keller [28,42] would be better suited for the computation of equilibrium branch bifurcation points. Unfortunately, that type of arc length normalization would be overly complicated when dealing with limit points alone, and experience has shown that in the computation of equilibrium surfaces limit points occur far more frequently than bifurcation points. The approach that will be taken during this study will be to adapt the Kubicek method with minor improvements (those improvements will be discussed further in the next chapter). Bifurcation points, where two or more equilibrium branches intersect, can be stepped over by simply using a predictor-corrector technique that will converge to the other side of the bifurcation point. In the case of a simple bifurcation point the procedure for locating the second branch is discussed below. Study of the two branches eminating from the simple bifurcation point have shown that they both are tangent at the simple bifurcation point to the plane described by the two eigenvectors associated with the two zero eigenvalues of G^TG, which is a square (n+1 X n+1) matrix of co-rank=2 (G is the augmented Jacobian) [28]. The plane can be determined from those two eigenvectors and a search for all points satisfying the equilibrium equation, 5.3 can be accomplished.

Once again, it should be remembered that when the computer aided stability system is not operational, the number of zero eigenvalues is limited to two, and therefore, the equilibrium surface bifurcational behavior is restricted to simple bifurcations and limit points. When the computer aided system is operational, general bifurcations are possible but are limited to the cases where three branches intersect. As was discussed in Chapter IV, the situations where the reduced order system size, k (k=co-rank), is greater than two are not well understood. Locating the additional equilibrium branches eminating from a general bifurcation point, however, can be accomplished in the same manner described above except that it will be progressively more difficult due to the increased dimensions of the space that must be searched for the points satisfying equation 5.3. For example, one branch can always be found by the predictor-corrector technique discussed above. The second branch in the case of a simple bifurcation point is found by making a one-dimensional search in circular coordinates about the bifurcation point in the plane described by the two critical eigenvectors. In the case of three branches eminating from a bifurcation point, the eigenvectors corresponding to the three critical eigenvalues form a three dimensional space.

Therefore, a two-dimensional search in spherical coordinates must be made about the bifurcation point to find the solutions to equation 5.3.

A considerable amount of detail has been given to the calculation of equilibrium surfaces and the development of the continuation algorithm used in BACTM. This is due to the pivotal importance of the equilibrium surfaces to the method in general, and it is also due to the universal applicability of the continuation method to other areas in this study as well as possible extensions to this study. Specifically, the continuation method of Kubicek will be modified slightly and applied to the bifurcation surface calculations in section D.

C. Local Stability Calculations

At each solution point of the equilibrium surface a local stability analysis is accomplished. Since the system is an autonomous system (the coefficients are not time dependent), linearization of the system at each point is valid and will reflect the local stability behavior of each state variable provided that the restrictions of the Poincare/Liapunov theorem (Appendix C) are followed. More importantly, though, the local stability analysis will show the movement and type of eigenvalues present in the linearized system.

The importance of this information has already been discussed and will only be mentioned briefly here. The type of eigenvalues (stable or unstable) determine whether an equilibrium branch is locally stable or unstable. Eigenvalues crossing the imaginary axis constitute bifurcations and the number of those critical eigenvalues determine the size of the reduced order, nonlinear system as defined by the center manifold theorem. The reduced order nonlinear system can then be studied through the elementary catastrophe theorem or the Hopf bifurcation theorem. The location of equilibrium points that have zero eigenvalues also determine the bifurcation surfaces. The local linear analysis can also provide a direct link to phase plane analysis as well as other topological studies of the system. And finally, the local stability analysis gives insight to the possible applications and limitations of linearization and quasi-linearization schemes.

Mathmatically, the local stability analysis is accomplished by finding the characteristic roots of the Jacobian matrix, F, for each equilibrium solution point. The eigenvalues are then characterized by their location in the imaginary plane. Different designations are given to each of the different types of local instabilities.

In this manner the type and number of eigenvalues that cross the imaginary axis as the system goes unstable locally can be determined, and from this information an understanding of the systems' bifurcational behavior can be gained.

D. Bifurcation Surface Calculations

As has been thoroughly discussed earlier, the bifurcation surfaces are intimately related to the equilibrium surfaces in that they are merely a projection of the limit and bifurcation points of the equilibrium surfaces onto a two dimensional control space. It has also been brought out that the location of bifurcation points can be found in a number of ways. The method that is most consistent with the equilibrium surface calculation method discussed above is to locate the points that are both equilibrium points and have a singular Jacobian matrix. Thus, the equation of a bifurcation surface is [28]

$$g(\underline{y}, c_i) = [f(\underline{y}, c_i), \det(F)]^T = 0 \qquad (5.10)$$

where $\underline{y} = [\underline{x}, c_j]^T$ and (c_i, c_j) are two separate control inputs. Any two control inputs can be chosen to form the control space and the third is held constant. One of the selected controls is allowed to vary as a state variable while the other is varied as the continuation parameter.

The solution of equation 5.10 yields a curve $c_i(c_j)$, c_k fixed, in the control space that is a locus of the bifurcation point projections. The complete set of such bifurcation curves is known as a catastrophe map. The system described by equation 5.10 is simply the equilibrium system augmented by the constraint, det(F)=0, and therefore has the dimension of n+1 where n is the order of the system. This accounts for the addition of a control parameter as an extra dependent variable. From this point the solution of this system of equations proceeds identically to that of the equilibrium surface equations with three exceptions. First of all, the dimension of the system is increased by one, making the calculation of the surface more costly. Secondly, the nature of compressing a three dimensional locus of points into a two dimensional representation dramatically increases the possibilities of intersections occuring between the surfaces, which as discussed above, greatly increases the complexity of the continuation process. The final exception is caused by the constraint, det(F)=0. Due to the dimension of the system, it is impractical to expand the determinant of F analytically; therefore, numerical differentiation of a system with a singular or near singular matrix is required which is not only tricky but could be quite costly as well.

E. Analysis of the Results

Due to their global nature, the results of an analysis using BACTM can first be studied from a qualitative viewpoint with the purpose of better understanding the nonlinear phenomena in the area under study. Then, more quantified results can be obtained in the areas that show unusual or counter-intuitive behavior. This approach is somewhat unique in that many approaches reverse the above order of investigation. Some examples of BACTM results from two much simpler aircraft models than the F-15S are discussed below. Their coefficients are linear and their data bases are quite small when compared to the that of the F-15S. The results are therefore much clearer and more suited to a general discussion of the analysis techniques used in this study.

1. Roll Coupling Equilibrium Surface Example

One of the better known nonlinear jump phenomena is roll coupling which was first studied by William Phillips in 1948. Analytical approaches to studying roll coupling are fairly complex and cumbersome [43], and as will be shown below, the criteria obtained through those traditional techniques are not necessarily accurate [27]. Roll coupling is a phenomenon that occurs primarily in modern fighter type aircraft.

This problem stems directly from the low moment of inertia about the x axis that is characteristic of fighter aircraft. It is both a kinematic coupling (exchange of angle of attack and sideslip during roll) and inertial coupling phenomenon that occurs during high roll rates and is aggravated by high angles of attack. In order to combat this problem many fighter type aircraft have restrictions that limit the maximum stick travel and g loading during continuous aileron rolls [10].

Figures 5.2, 5.3, 5.4 and 5.5 show four different equilibrium surfaces for aircrafts A and B, the two fighter type discussed above. The figures were generated by Scientific Systems Inc. during the early development of BACTM. Figure 5.2 shows an aileron deflection equilibrium surface for aircraft A at an elevator deflection angle of -0.5 degrees and rudder deflection angle of zero. As should be expected with this simple model the progression of roll rate, p, with aileron input is very linear throughout the aileron range, and the local stability analysis shows that each point is stable. This is indicated by the S appearing above the curve. Figure 5.3 again shows aircraft A at the same conditions as Figure 5.2 except now the elevator input has been changed to 0.0 degrees.

At this point the nonlinearities of the aircraft model are evident and are indicated by the limit points present in the curve. Figure 5.3 clearly shows the presence of a jump in roll rate at DA=±8 degrees as aileron input is increased in either direction. Although the jump at DA=±8 degrees is not tremendous, the situation that has developed upon crossing that jump has the potential to become disasterous. Most aircraft are protected against this occurence by a flight manual restriction requiring that a load factor of one g be maintained during multiple aileron rolls. Unfortunately however, the difference in aircraft 'feel' between one g (Fig. 5.2) and zero g (Fig. 5.4) during continuous aileron rolls is not always obvious, yet the difference in aircraft behavior can be catastrophic. As an example, refer once again to fig. 5.3, suppose that aileron deflection is decreased from 0 to -30 degrees and back to 0 again. During that control sequence, the roll rate was increased to about 225 deg/sec, and a jump of about 60 deg/sec occured at DA=-8. As DA is decreased back to zero the roll rate will only decrease to about 130 deg/sec. In an attempt to stop the roll rate the pilot increases aileron deflection further until at about 15 degrees of aileron deflection, the roll rate undergoes a catastrophic jump to -225 deg/sec.

Closer inspection of the situation that has developed shows that the aircraft cannot return to its original starting position of zero roll rate by using aileron alone. This is due to the 'zero roll rate' equilibrium branch being embedded inside of the hysteretic loop shown in Figure 5.3. It should be noted that the other states are also undergoing similar nonlinear jumps at the jump points shown in these figures. A small elevator change to -0.5 degrees deflection will enable the aircraft state to be returned to the starting point. The much used roll coupling criteria, developed by Phillips, gives a critical aileron deflection value of $\pm$15 degrees for this situation which corresponds to the larger catastrophic jump from +225 to -225 deg/sec. The BACTM study, on the other hand, reveals a more useful critical aileron value of $\pm$8 degrees. Numerical simulations have verified the BACTM selected value of $\pm$8 degrees as the critical aileron deflection angle [27]. Figure 5.4 show the second aircraft, B, undergoing an aileron change during a pitch-up manuever. The curve has distinct linear and nonlinear regions. The limits of these regions are marked by the jumps at $\pm$34 degrees. Since the catastrophic jump occurs at the extreme limits of control deflection and at a load factor well above one, the nonlinear jump shown in Figure 5.4 is safely avoided by adhering to the flight manual restrictions listed above.

Figure 5.5 again shows aircraft B in the same flight conditions as Figure 5.4. In this case, however, the elevator deflection is held at +2 degrees and similar to Figure 5.3 the 'zero roll rate' equilibrium branch is again embedded inside of a hysteretic loop.

This example has brought to light some of the information that can be gained from the study of equilibrium surfaces. The steady-state trajectory is shown for a varying aileron input. The nonlinear jumps or catastrophes are clearly shown, and the effects of hysteresis are evident. Additional information is gained by the local stability analysis which is represented by the letters indicating the local stability of the individual solution points along the equilibrium curve. As is shown in the legend on the figures a U stands for unstable and an S indicates stable. The U designation also indicates that the local analysis is unstable as a result of a single real valued eigenvalue in the right-half-plane while the L designation indicates that the local stability analysis is unstable due to a complex pair of eigenvalues in the right-half-plane. The boundaries between two types of stability behaviors is indicated by a hash mark, |, on the curve.

AD-A167 697 APPLICATION OF BIFURCATION AND CATASTROPHE THEORIES TO NEAR STALL FLIGHT MECHANICS(U) AIR FORCE INST OF TECH WRIGHT-PATTERSON AFB OH C A HAWKINS 1985 2/3

UNCLASSIFIED AFIT/CI/NR-86-54T F/G 12/1 NL

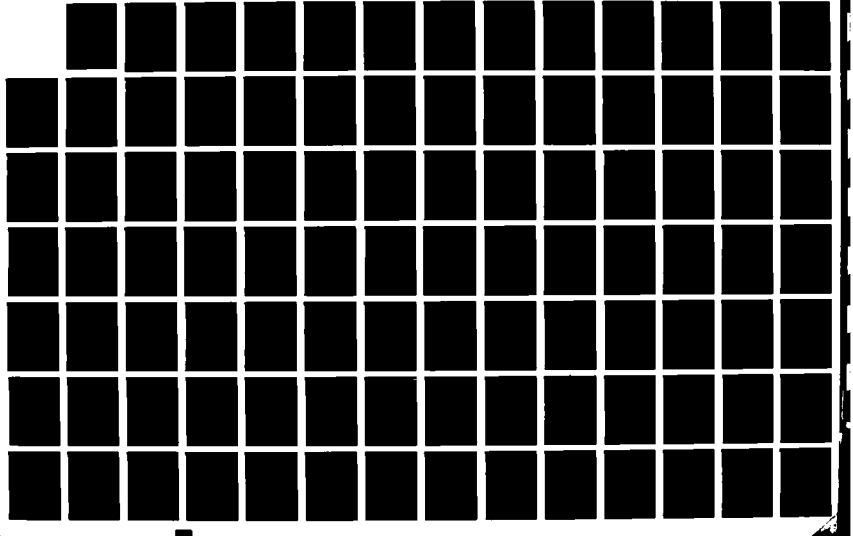

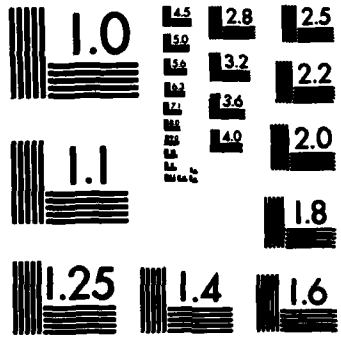

The type of local stability behavior corresponding to each section of the curve is indicated by the letter above or below that section of the curve. Refering back to Figure 5.5, the topological nature of the stable and unstable equilibriuim branches is clearly shown. Between each stable branch there is an unstable branch, and the unstable branches clearly mark the domains of attraction of the stable branches. The local stability analysis in Figure 5.5 also shows that the limit points do indeed occur when a single eigenvalue crosses the imaginary axis. Another point brought to light by the local stability study is that the bifurcational behavior of the system can be studied in terms of a single variable which is a direct result of the center manifold theorem. Wherever a transition from an S to an L designation is found, a Hopf bifurcation is present and a limit cycle may exist. The lower case letters on figures 5.4 and 5.5 correspond to points on the roll rate catastrophe map discussed in the next section.

Figures 5.2 through 5.5 follow this page.

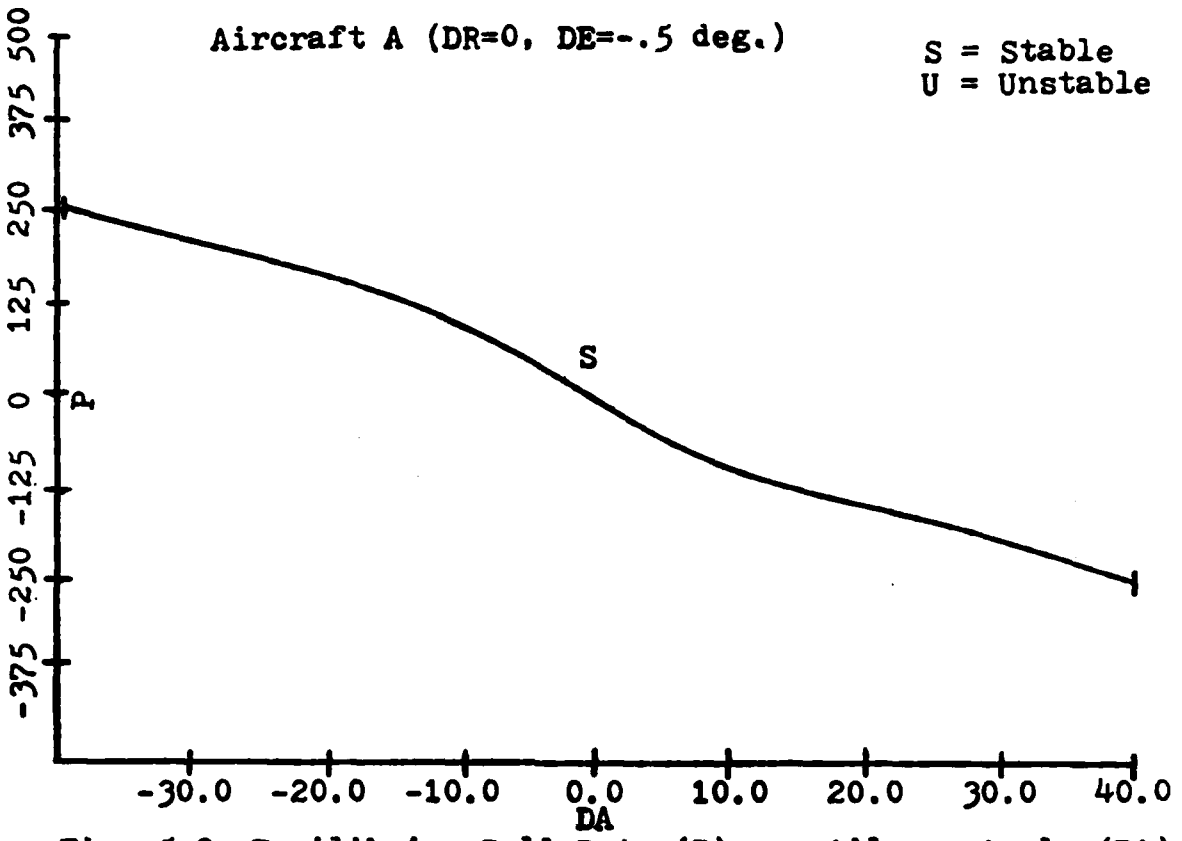

Fig. 5.2: Equilibrium Roll Rate (P) vs. Aileron Angle (DA)

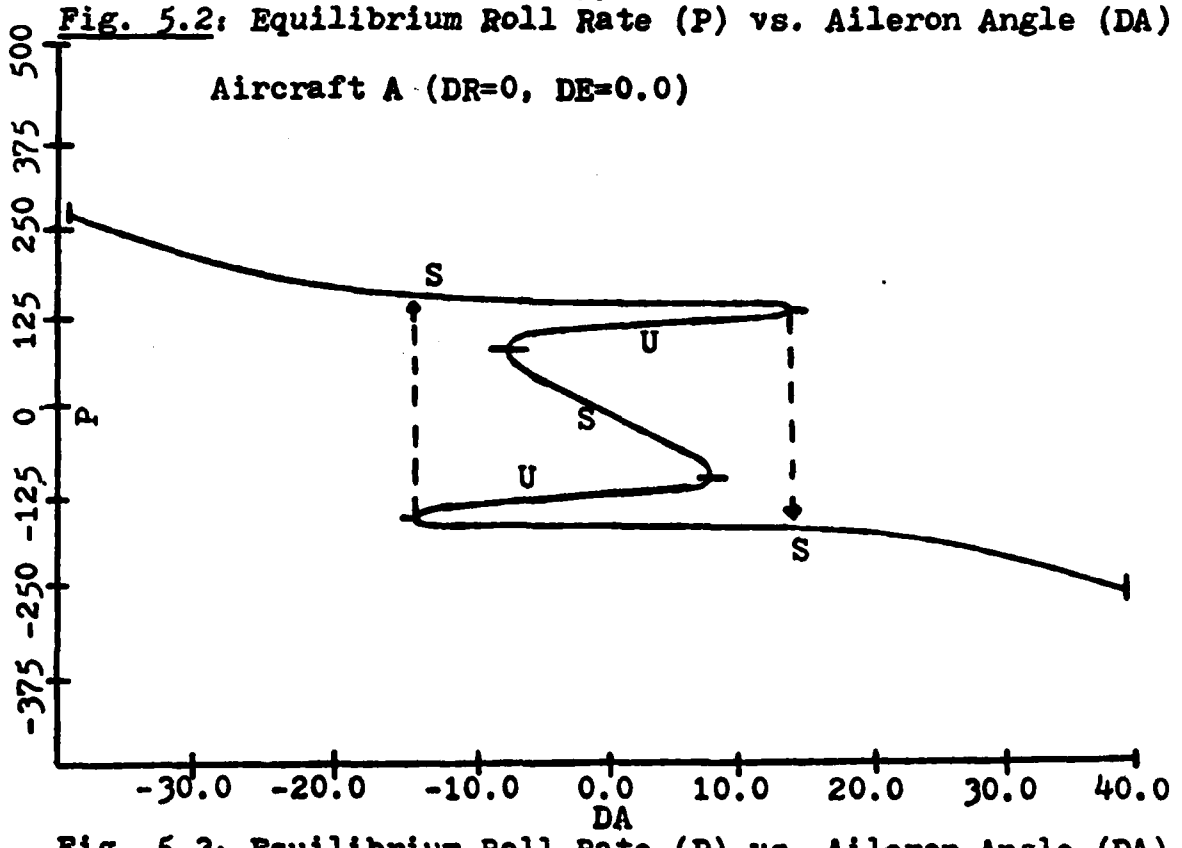

Fig. 5.3: Equilibrium Roll Rate (P) vs. Aileron Angle (DA)

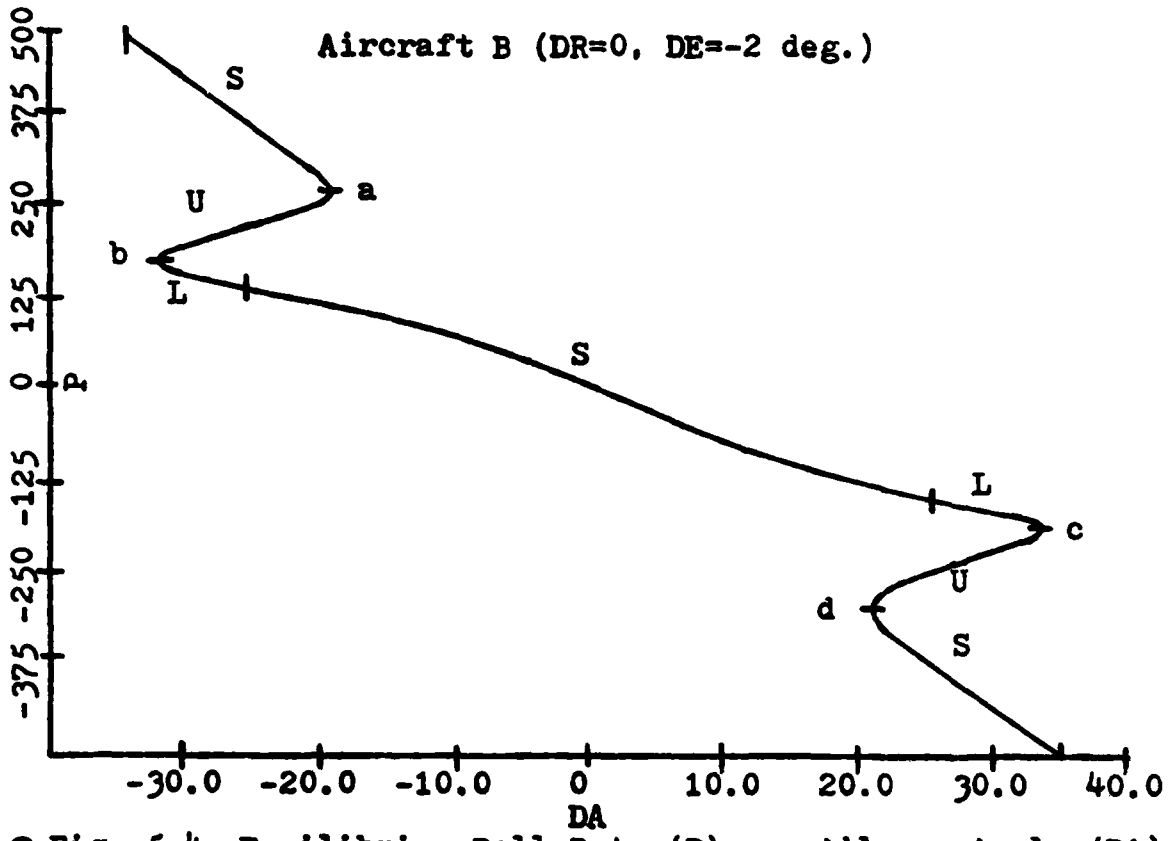

Fig. 5.4: Equilibrium Roll Rate (P) vs. Aileron Angle (DA)

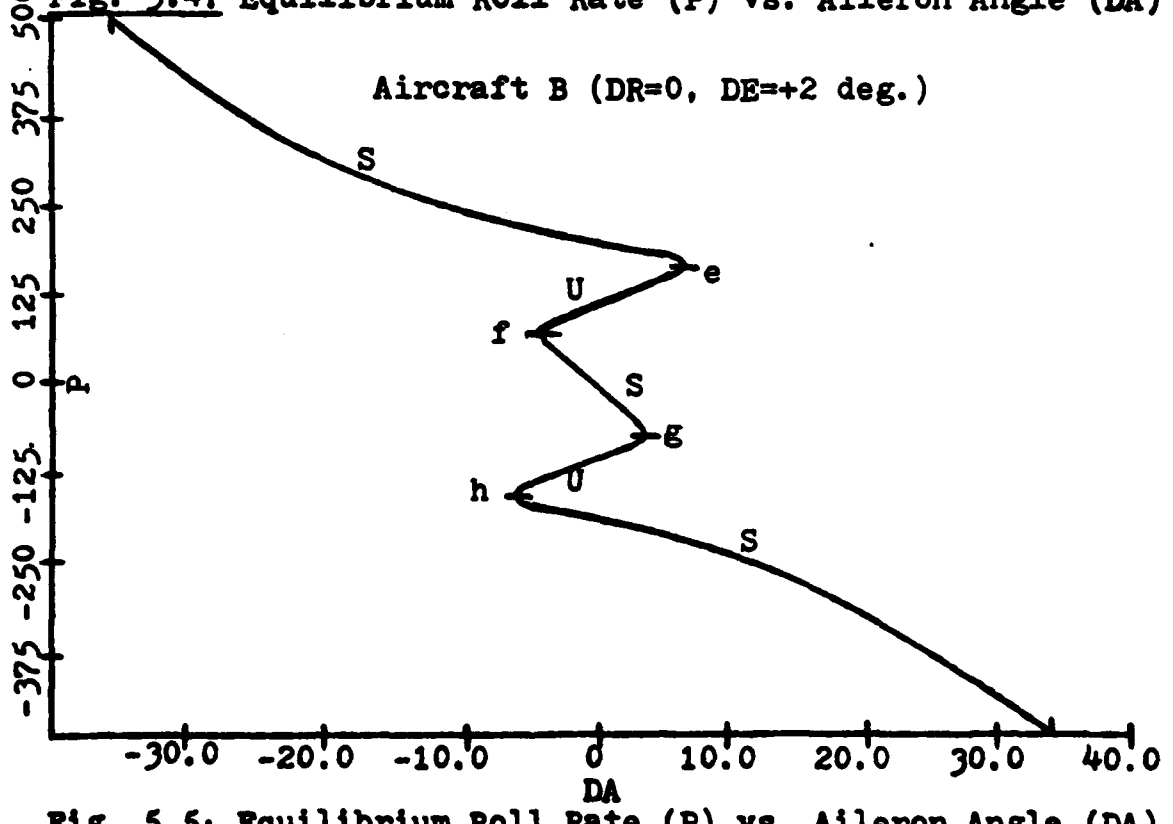

Fig. 5.5: Equilibrium Roll Rate (P) vs. Aileron Angle (DA)

2. Roll Coupling Catastrophe Map Example

Figure 5.6 shows a three-dimensional section of the roll rate equilibrium surface discussed above for DA (-35, +35), DE (-2, +2), and DR=0. The projection of the limit points from the equilibrium surface onto the elevator versus aileron control space will form a roll rate catastrophe map. This is shown in the lower portion of Figure 5.6. The shape and behavior of this particular catastrophe map is very similar to one of the elementary catastrophes attributed to Thom known as the butterfly catastrophe for its distinct shape [27,30,31]. Figure 5.7 shows a more comprehensive view of the catastrophe map. The numbers represent the number of equilibrium solutions existing at that combination of controls. The horizontal lines show the plane of figures 5.4 and 5.5. Nonlinear jump behavior may occur anytime a boundary in Figure 5.7 is crossed so that the number of equilibrium solutions decreases. High aoa catastrophes can be found by holding aileron deflection constant and increasing elevator. In this case departure may be expected at DA=0 and DE=9.3. This too was verified by simulation as being correct [27]. Finally, the area where bifurcations can not occur is shown as the region where only one equilibrium surface solution exists. Control laws can be developed to remain in this non-bifurcation region by using a combination of the control surfaces.

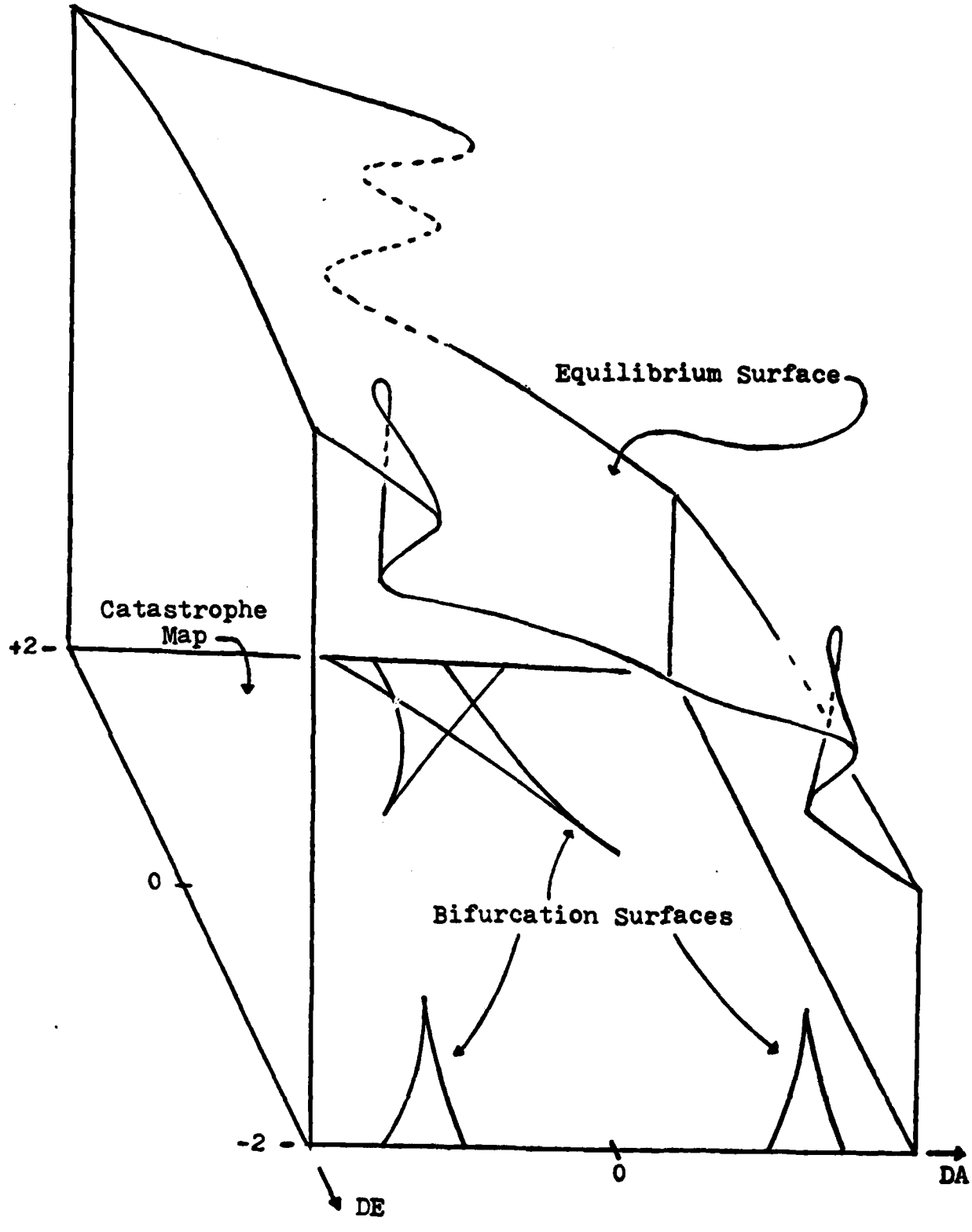

Fig. 5.6: Equilibrium Surface and Catastrophe Map for Aircraft B (DR = 0)

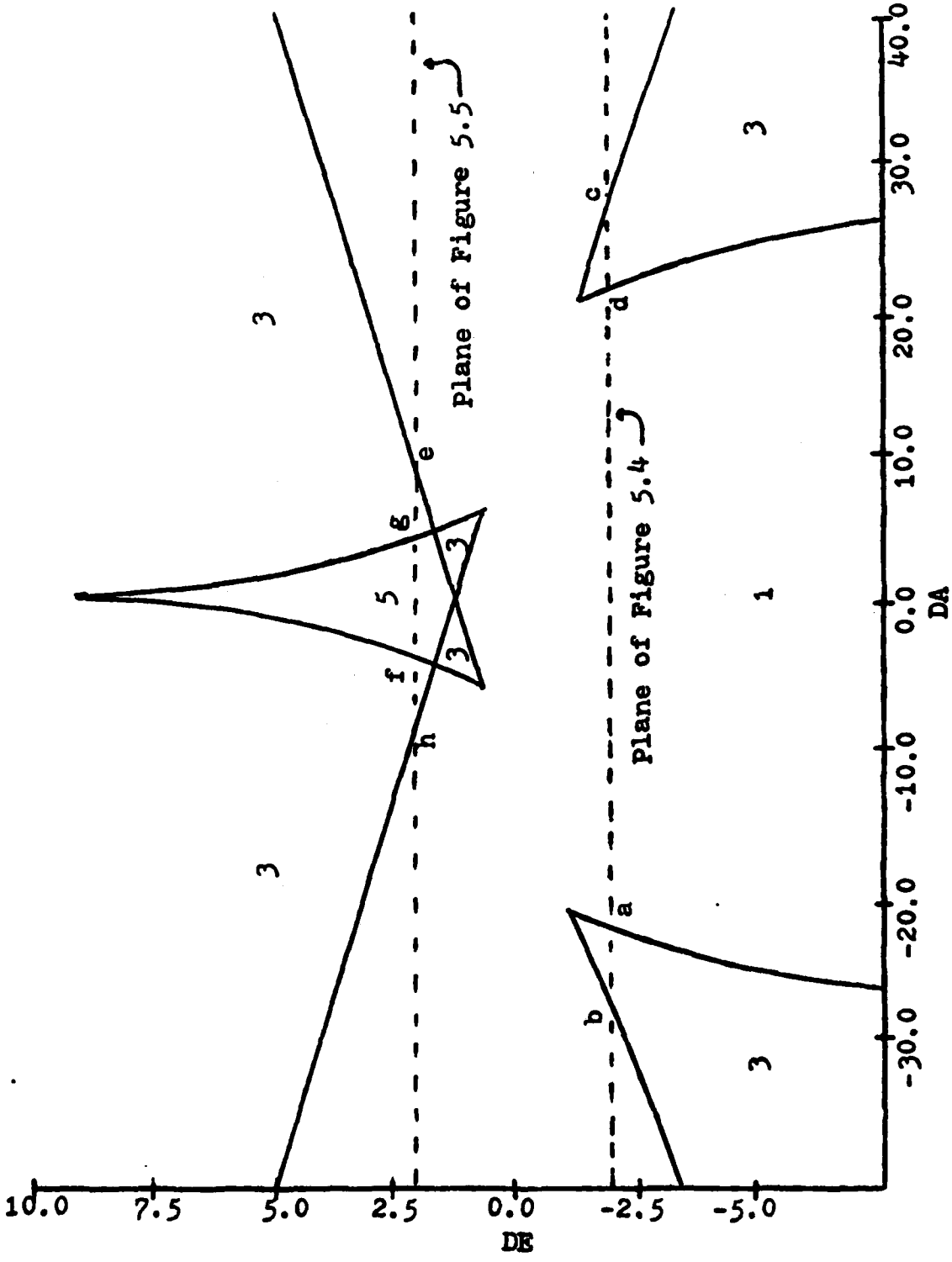

Fig. 5.7: Catastrophe Map in (DA, DE, DR = 0) plane for Aircraft B. The numbers in each region indicate the number of equilibrium solutions. The letters correspond to points shown in Figures 5.4 and 5.5.

F. Numerical Simulations

Once the results of the study have been analyzed, numerical simulations are employed to verify the predictions made and the criteria developed. The numerical simulations use the eighth order body axis model as the set of equations being actually integrated, but a number of other variables and parameters of interest are calculated as well. Among those additional values calculated are angle of attack, sideslip angle and total velocity so that the bifurcation system can be directly studied. Some additional values of interest that are monitored during the simulations are total vehicle kinetic energy and rate of change of kinetic energy. These values have shown some promise as possible quantitative indicators of impending catastrophes [28]. The complete list of the additional values monitored during the numerical simulations and their definitions is contained in Appendix E. The numerical simulation method has provisions for allowing altitude to vary and for the varying of the controls to simulate different control strategies. The numerical simulation technique also has provisions for the calculation of phase-plane trajectories as well as the standard time history plots.

CHAPTER VI

NUMERICAL APPROACH

A. Overview

The iterative nature of this method makes it a perfect candidate for evaluation by numerical methods. In fact the only way that any useful amount of information can be gained through this method is by the repeated numerical evaluation of the values discussed in the preceeding chapter. The numerical steps taken in this analysis as well as the specific numerical techniques used to accomplish those steps are discussed in this chapter. Several of the techniques used are well known and will not be covered in great detail, but the manner in which they are combined to create the complete method will be covered in sufficient detail to give an understanding of the overall process.

B. Data Preparation

As has been mentioned above, the data set for the F-15S is extensive which made it necessary to reduce the number of independent variables contained in the data. This was accomplished by restricting the altitude to 20,000 feet and the Mach number to either Mach 0.2 or Mach 0.6. After these restrictions were applied, the data set was reduced to tables that were a function of one, two and three variables.

In order to ensure a smooth variation of the aerodynamic coefficients as the aircraft state changes, a curve fit that is smooth at all points is required. Cubic spline approximations were selected as the best approach. Cubic splines represent the data by placing a third order polynomial between each data point and then matching the first and second derivatives of the adjoining curves at each data point. This ensures the smoothness of the partial derivatives of the aerodynamic coefficients with respect to the state and control variables. For the tables that were a funtion of two variables, bi-cubic spline interpolations were used. This is similar to the cubic spline method except that a cubic polynomial in two variables is fit between the four data points that represent a section of the two-dimensional data table. Bi-cubic splines have all of the properties of cubic splines. Since the nature of the first and second derivatives at the end points of the tables were not precisely known, natural cubic splines were selected. A natural cubic spline forces the second derivative to be zero at the end points thus minimizing the overall curvature of the curve. The spline coefficients which represent the coefficients of the cubic polynomial between each data point were calculated separately.

Since the values of the spline coefficients will remain unchanged so long as the data remains unchanged, the spline coefficients only need to be evaluated once. The spline curves are then evaluated each time a variable that is a function of the table approximated by the spline changes. During a dynamic simulation, all of the values are evaluated on each call to the aerodynamic coefficient subroutine, but during the determination of the partial derivatives for the Jacobian matrix, only values that are varied during that call to the subroutine need be calculated. This is discussed in more detail below. The cubic and bicubic spline curves are generated and evaluated by International Mathmatics and Science Library (IMSL) routines. The remaining tables that are functions of three variables were interpolated by linear interpolation. The difficulty and expense of applying a spline curve fit in three variables out weighed the possible curve continuity problems that could arise. Additionally, the number of tables requiring linear interpolation and their overall effect as compared to the other tables on the aerodynamic coefficients was small. All of the interpolation methods maintain the values at the boundary of the table when an independent variable exceeds the bounds of the table (ie. no extrapolation was accomplished).

Ferziger [40] discusses the origin and application of splines as well as a possible computer algorithm for their implementation.

C. Details of the Major Steps

1. Outline of the Algorithm

In this section, I will briefly describe the basic flow of the algorithm to give some order to the description of the specific techniques that follow. The first major step after the initialization of a number of quantities necessary for the control of the routine and the calculation of the equations of motion is to read in the spline fit data and parameters for the specific Mach number of interest (Mach=0.2 or Mach=0.6). The system Jacobian is then calculated and the Newton-Raphson technique is used to converge on the initial point from the given initial conditions. Then the Adams-Bashforth method is used to predict the next point. The Newton-Raphson technique is then used again to converge to the next solution point. During the Newton-Raphson process, the augmented system Jacobian is calculated and Gaussian elimination with controlled pivoting is used to select the continuation parameter and solve for F^{-1}. This step is repeated until convergence occurs. Once convergence is achieved within a given criteria, the Adams-Bashforth method is again used to predict the next point.

This process is continued until a state or control parameter exceeds the limits set prior to the start of the program. Then, if desired, the routine returns to the original starting point and generates a branch in the opposite direction. The computation of a complete branch is rarely required in the case of the F-15S model due to the symmetric nature of its lateral/directional data.

2. Jacobian Calculation

The calculation of the augmented system Jacobian is accomplished by finding the partial derivative of $\underline{f}$ with respect to each state variable and the control parameter, c. Due to the complexities of the data, numerical techniques were used to evaluate the partial derivatives. This task is accomplished by first evaluating the aerodynamic coefficients at the initial state and control value, $(\underline{x}, c)$, and then using them in the equations of motion to find $\underline{f}(\underline{x}, c)$. In the same manner, the value of $\underline{f}$ is found at four additional points by varying a state variable twice in each direction from its original value and then evaluating $\underline{f}$ at each of those points. A cubic spline curve fit is then made to each of the resulting five point curves (there is one curve for each of the n components of $\underline{f}$). This passes a set of n smooth curves through the original component values of $\underline{f}$.

Each curve shows the variation of $\underline{f}$ as a function of the state variable that was varied to generate that curve. The derivatives of each of the n curves with respect to the state variable varied to generate them are then easily found. This process is repeated for each of the n state variables and the one control parameter resulting in the (n X n+1) augmented Jacobian matrix shown in chapter 5. Some checks are made to ensure that the steps made to each side of the state variables create a meaningful change in $\underline{f}$ so that an accurate partial derivative can be found. The change in $\underline{f}$ must be large enough to be representative but not so large as to lose accuracy.

3. Corrector Phase

As has been mentioned above, the corrector step used in this algorithm employs the Newton-Raphson method shown below.

$$\underline{h} = -G_k^{-1}\underline{f} \qquad (6.1)$$

where $\underline{h}$ is an (n X 1) vector of corrector steps and G_k is the Jacobian matrix of the augmented system with the kth column removed. The kth column represents the most singular column in the augmented Jacobian matrix. This is selected by Gaussian elimination with controlled pivoting.

This process involves selecting a pivot element that has the largest magnitude of all candidate elements. Then, all elements that share the same row or column as the pivot element are reduced to zero by matrix row operations. The above process is repeated until n rows and columns have only one element. No pivot element may be used more than once in this process. The remaining column is the kth column that is removed as the most singular one. If n non-zero elements cannot be found in this manner, then the rank of the augmented Jacobian is less than n and G_k is non-invertable. The pivoting is controlled in the Kubicek algorithm by selectively scaling the variables [28]. This is accomplished by weighting each of the n+1 columns in the augmented Jacobian matrix. The column associated with the variable selected as the continuation parameter is given the smallest weighting factor. In this way the variable selected as the continuation parameter is ensured to remain as the continuation parameter unless an actual singularity is encountered. When G is reduced to cannonical form by the above process, it is easily inverted, and then equation 6.1 is solved for the Newton-Raphson corrector step. The Jacobian for the new values of $\underline{x}$ found through the corrector step is then calculated. The above process is repeated until a solution point satisfying a preset precision criteria is found.

In order to increase efficiency, an option has been included in the routine to avoid the recalculation of the Jacobian on each step as the method approaches the solution point. The logic behind this option stems from the fact that the steps made in the Newton-Raphson method become very small when the solution point is approached, and therefore, the Jacobian will not vary much between those steps. Since the Jacobian matrix is totally a function of the state variables and the controls, the Jacobian is calculated only when $\underline{x}$ varies a predetermined amount from the point where the Jacobian was last calculated. The Jacobian is also always calculated at the beginning of the search for a new solution point. Not calculating the Jacobian at each step tends to increase the total number of iterations required to reach the solution point but at the same time decreases the overall time to reach the solution point [40]. The Gaussian elimination technique described above is well known. Further information on the subject can be found in [40,41].

4. Local Stability Analysis

Once convergence to a solution point has been accomplished, the system Jacobian and state variables at that point are retained. Through the use of an IMSL subroutine the eigenvalues and, if desired, eigenvectors are calculated.

The eigenvalues are classified by the type and number of unstable eigenvalues. The eigenvectors can be of use when the rank of G is less than n. This occurs in the higher order bifurcation situations discussed in chapter 5. Consequently, the eigenvector calculation option is usually put into effect during the bifurcation surface calculations.

5. Predictor Step

The inverse of the Jacobian matrix, G, is also saved from the last iteration of the Newton-Raphson corrector method. It is then used in equations 5.8 and 5.9 to solve for the n+1 parametric derivatives, dx_i/ds. After this information is obtained, the variable corresponding to the kth column is stepped a predetermined amount. The remaining n parametric derivatives are then used in an Adams-Bashforth method to predict the next point on the curve. Adams-Bashforth methods are implicit, multi-step methods whose order can be varied to achieve the desired accuracy. The particular method used in this approach is a variable order algorithm with a maximum order of four. The use of the Adams-Bashforth method over the simpler Adams-Moulton, or any other explicit method, ensures that stability can be unconditionally guaranteed for whatever order is selected by the routine.

Due to the popularity of the Adams methods in general, a good deal of information on them can be found in the literature [40,41].

The new predicted solution point, found through use of the Adams integration step, where all n+1 values have been changed is the next starting point for the Newton-Raphson iterations. The complete process is repeated until the control surface deflection or one of the state variables exceeds a preset limit. The routine will then generate another branch from the starting point in the opposite direction if desired. As was mentioned above, this is not usually necessary due to the symmetrical nature of the F-15S lateral/directional aerodynamic model.

The bifurcation surface routine is handled in exactly the same manner except for the addition of the constraint that the Jacobian be singular at each solution point. During the computation of the bifurcation surfaces, the eigenvectors are usually calculated as well as the eigenvalues. As was discussed in Chapter 5, the eigenvectors can be used as an aid in the location of the additional branches emanating from simple and general bifurcation points.

D. Evaluation and Validation of the Results

The procedure described above will yield a locus of points that describe the variation of the equilibrium solutions of each of the state variables as a single control is varied. In order to get a more complete picture of a particular flight regime several equilibrium branches must be created by varying the other controls also. The results of these runs are best understood when placed in graphical form. Three-dimensional plotting routines would present the most information in a single plot but have the draw backs of being more complicated to generate and more difficult to obtain specific quantitative information from. Therefore, the results of this study will be represented in a series of two-dimensional plots that are linked together by indicating common points between certain plots. Local stability information and in some cases maximum oscillation amplitudes are also contained in these plots.

The numerical simulations are accomplished by integrating the equations of motion through use of a fourth order Runge-Kutta method. A fourth order Runge-Kutta method is a predictor-corrector method that employs an explicit method as the primary predictor step followed by two implicit corrector steps and one implicit predictor step.

The method is applied through the use of an algorithm known as DYSYS which stands for DYnamic SYstem Simulation. The numerical form used by DYSYS to integrate the equations of motion is shown below:

$$Y(t_0 + dt) = Y_0 + 1/6\ (K_0 + 2K_1 + 2K_2 + K_3) \quad (6.2)$$

where Y_0 is a vector of the initial conditions for Y, dt is the time step and the K's are defined below:

$$K_0 = F(t_0, Y_0) * dt$$

$$K_1 = F(t_0 + dt/2,\ Y_0 + 1/2(K_0)) * dt$$

$$K_2 = F(t_0 + dt/2,\ Y_0 + 1/2(K_1)) * dt$$

$$K_3 = F(t_0 + dt,\ Y_0 + K_2) * dt$$

where F is a vector of the first order time derivatives of Y. The use of implicit corrector steps gives the method stability, and the order of the method gives the accuracy acceptable for this type of engineering application. Much has been written about Runge-Kutta methods, and therefore, I am not going to discuss the method further here. More information on the subject can be found in [40,41].

The complete package of numerical techniques used in this study has been made as efficient and universal as possible. Most of the subroutines are shared by the different programs, and little would be required to expand on the methods currently developed or apply them to a different aircraft model.

CHAPTER VII

PRESENTATION AND DISCUSSION OF THE RESULTS

A. Outline of Work Accomplished

A large number of equilibrium surface calculations and numerical simulations were attempted. As a result of the numerical and aircraft stability problems encountered during the course of this investigation only a small portion of those computer runs yielded meaningful results. The numerical difficulties encountered, among other things, resulted in no equilibrium surfaces being successfully computed with thrust while the unstable nature of the eighth order aircraft model reduced the number of meaningful numerical simulations to a small number. Due to the complexity of the aircraft model and the method itself, the equilibrium surface calculations were initially, quite costly. A number of improvements on the numerical efficiency of the technique have been made during the course of the study so that the computer time expended during the equilibrium surface computer runs has been reduced to a reasonable level. Some logistical problems as well as certain time constraints set on the completion of this project resulted in little being accomplished in the area of studying the aircraft with an operational computer augmented stability system.

The work that was accomplished in this area was limited to setting the system up for operation on our computer facilities and developing the means for its integration into the existing algorithms. Therefore, all of the results reported here are for the aircraft without the computer aided stability system operational. Given the high computer run times experienced at the beginning of this investigation as well as the lack of substantial bifurcational behavior in the equilibrium surfaces, it was felt that calculation of bifuracation surfaces were not warranted, and therefore, no bifurcation surface runs were attempted. From a computational point of view, the greatest amount of success was found during the calculation of the fifth order equilibrium surfaces. Consequently, seven fifth order equilibrium surfaces were successfully computed while only two eighth order equilibrium surfaces were successfully computed. This disparity is a direct result of the numerical difficulties presented by the eighth order model. One of the eighth order equilibrium surfaces generated was a spin surface, and one of the fifth order equilibrium surfaces showed distinct bifurcational behavior. These two particular surfaces combined with one of the other fifth order equilibrium surfaces where roll coupling effects were noted contain the most interesting findings of the study.

The next section describes and discusses the individual results in detail.

B. Equilibrium Surface Results

In each of the plots presented in this section the following symbols are used to annotate the local stability behavior:

S = all eigenvalues are stable

U = a single real valued eigenvalue is unstable

L = a single complex pair of eigenvalues are unstable.

Combinations of the letters shown above simply indicate additional unstable roots in the form indicated. The plotting routine used to display the results is a simple 'connect the dots with straight lines' type of routine, and therefore, some roughness in the curves may be noted. This can easily be corrected by decreasing the continuation step size in the equilibrium surface algorithm. In some cases erratic behavior of the curves may result from the equilibrium surface convergence criteria. On the other hand, however, some discontinuous behavior in the curves can be attributed to the type of nonlinear jump behavior sought after in this investigation. The subtle differences in these cases will be pointed out below.

1. Fifth Order Equilibrium Surfaces

During the fifth order investigation, all of the equilibrium surfaces were generated with the velocity set to 500 f/s, altitude set to 10,000 ft and thrust set to zero. Additionally, the data set for Mach=0.6 was used for each of the fifth order equilibrium surface calculations. With the exception of the first and seventh fifth order cases the results are presented in a series of six figures contained on three pages. The first page shows the pitch rate and angle of attack plots versus the appropriate control variable; the second page shows the roll rate and yaw rate plots; and the third page shows the sideslip angle plot and the yaw rate plot again. The repeated presentation of the yaw rate plot here as well as the repeated presentation of a few plots during the discussion of the eighth order equilibrium surface results is done to enable easy comparisons to be made between related plots. Plots that are repeated are given the same title to avoid confusion.

a. Case Number One (DAI=DRU=0, DEL=+8 to -30)

The first fifth order equilibrium surface generated was a pitch up and pitch down manuever from DEL=-5 degrees.

During this run, both the aileron and rudder deflections were held to zero while the stabilator deflection angle, DEL, was varied from -5 to +8 and then again varied from -5 to -30 degrees. The results of this computation are shown in figures 7.1a and 7.1b. Due to the symmetrical nature of the fifth order model at relatively low angles of attack the variables p, r and beta were essentially zero for the entire run and therefore are not presented. The plots in Figure 7.1 show that angle of attack and pitch rate are very closely related, and this point is confirmed by inspecting the mathmatical model used. The model (Appendix D) shows that pitch rate should have the dominant effect on the rate of change of angle of attack during low angle of attack flight conditions. This is confirmed by Figures 7.1a and 7.1b. The local stability analysis shows a transition to an 'L' instability in the -15 to -20 degrees stabilator deflection range. This corresponds to an angle of attack just below the stalling angle of attack and quite possibly indicates a Hopf Bifurcation to wing rock or some other type of high aoa oscillatory phenomenon. This could be confirmed by numerical simulation; however, a fifth order simulation package was not developed. The somewhat discontinuous increase in both aoa and pitch rate at DEL=-22 could be a small catastrophe whose limit points were stepped over by the algorithm.

In terms of comparison to expected aircraft behavior, it is interesting to note that an aoa of 10 degrees is generated at 0 degrees stabilator deflection. This result was not confirmed one way or the other due to the lack of available data of this type. Three of the fifth order equilibrium surface calculations reported below share points from this run as their initial starting point.

b. Case Number Two (DRU=0, DEL=-10.2, DAI=0 to -30)

The second surface calculated was an aileron roll to the left at approximately 24 degrees angle of attack. Note that the aileron deflection sign convention for the F-15S is unconventional with negative aileron deflection generating a left rolling moment. In this set of figures rudder deflection is held to zero and stabilator deflection is held to -10.2 degrees. Figures 7.2a and 7.2b show that at these conditions angle of attack and pitch rate are not effected by aileron control input. Figures 7.2c and 7.2d show that a significant amount of adverse yaw is created by the aileron input. This is demonstrated by the right yaw rate that is generated by left aileron input. At this angle of attack the loss of aileron roll control authority is evident and is demonstrated by a right roll rate being generated by a left aileron deflection.

This effect is present to a certain degree in all high performance aircraft due to their sweptback, low aspect ratio wings. The requirement for an aileron rudder interconnect that blends in pro-rudder as a function of angle of attack when aileron input is commanded is verified in Figures 7.2c and 7.2d. During a similar equilibrium surface calculation at a low angle of attack, a pro yaw situation was noted during aileron input, and this was confirmed as being one of the aerodynamic design stategies employed by McDonnell Douglas to minimize the effects of adverse yaw. On the next page Figures 7.2e and 7.2d show that yaw rate and sideslip angle are related in a manner typical of uncoordinated flight conditions in that a positive yaw rate creates a negative sideslip angle. The local stability analysis showed all points to be stable during this run. This is partially substantiated by the linearity of the curves shown in Figures 7.2a through 7.2e.

c. Case Number Three (DAI=0, DEL=-19.6, DRU=0 to -30)

Figures 7.3a through 7.3e show the effects of a high angle of attack (approximately 30 degrees) right rudder roll. In this set of figures, aileron deflection is held at zero and stabilator deflection is held to -19.6.

The initial point of this run corresponds to a stable point very near the L/S stability boundary shown in case number two. As can be seen in the figures, the solution points throughout the rudder deflection range remained locally stable. Figures 7.3a and 7.3b indicate that at these conditions angle of attack and pitch rate are not effected by rudder control input. Figures 7.3c and 7.3d reveal a very linear increase in yaw rate and roll rate with rudder input. Figures 7.3e and 7.3d on the next page show that the rudder roll at these conditions is a coordinated manuever with zero sideslip angle throughout the rudder control input. This is an indication that the rolling moment is generated by the velocity differential seen by the left versus the right wing due to the yaw rate. This is somewhat unusual in that sideslip is usually the mechanism responsible for the rolling moment during a rudder roll. This set of results confirm that rudder should be the primary control surface for generating rolling moment in the angle of attack range shown.

d. Case Number Four (DEL=5.3,DRU=0,DAI=0 to -30)

This equilibrium surface is also derived from the first equilibrium surface, and it is a surface for left aileron roll at a negative angle of attack. In this set of figures rudder deflection is held to zero while the stabilator deflection is constant at 5.3 degrees.

During this aileron roll manuever, the adverse yaw effects present in case number two are not present but evidence of roll coupling is present. This is shown by the increase in negative pitch rate and negative angle of attack with aileron input in Figures 7.4a and 7.4b. This type of behavior is caused by the high roll rate generated by the aileron deflection combined with the aircraft inertial axis being offset from the axis that the aircraft is attempting to roll about. Figure 7.4c shows that the roll response to the ailerons is good throughout the aileron deflection range. Figures 7.4d and 7.4e further confirm the existence of inertial roll coupling type motion depicting a build up of a positive yaw rate while sideslip angle remains slightly greater than zero throughout the manuever. This indicates that the yaw rate component is about the aircraft velocity vector. Physically, the situation is very similar to a spin type motion. This can best be understood by considering each of the three rotational components as a single angular velocity vector. At zero angle of attack and zero sideslip angle (assuming Ixz=0) the aircraft inertial axis is coincident with the flight path of the aircraft. The angular velocity vector of a roll about the flight path would, in this case, be composed entirely of p, the aircraft x-body axis roll rate.

At angles of attack or sideslip angles other than zero, however, an attempted roll about the aircraft x-body axis using the ailerons will result in a combination of rolls about each of the body axis with the overall angular velocity vector still aligned with the flight path vector. Rotating bodies tend to seek a mass distribution that is symmetric with respect to its axis of rotation. Therefore, the heavy mass concentration in the fuselage of modern fighter aircraft results in the tendency for the x-body axis to become perpendicular to the axis of rotation. If this is allowed to happen, a transformation will occur where the angular velocity vector is changed from consisting entirely of the body axis roll rate to consisting entirely of the body axis yaw rate which, of course, is a flat spin. The direction of the yaw build up is a function of both the direction of the roll and whether positive or negative angle of attack flight conditions are present. Experience has shown that the transformation will not occur smoothly, and at some point when the build up of yaw rate exceeds the amount that can be offset by the inherent directional stability of the aircraft, the aircraft will become unstable, and a departure from controlled flight will result. This is a physical explanation for departures from controlled flight as a result of inertial roll coupling.

The amount of roll coupling shown in Figure 7.4 is not large, however, and no serious roll coupling problems should be experienced at those particular flight conditions.

e. Case Number Five (DAI=-29.2, DEL=-10.2, DRU=0,-30)

The initial starting point in Figures 7.5a through 7.5e is the full scale aileron deflection position from case number two. A cross control input of right rudder against full left aileron deflection with stabilator deflection held at -10.2 degrees was accomplished. This was an attempt to further aggravate the adverse yaw problem noted in Figure 7.2. The eigenvalues of the individual solution points were once again all stable. A slight increase in angle of attack is noted in Figure 7.5b, and this can be attributed to the roll coupling phenomena discussed above. Figures 7.5c and 7.5d show the direct relationship between yaw rate and roll rate, and that the effects of a full scale aileron deflection against the rudder movement appear to have little effect on the roll authority of the rudder at these flight conditions. The sideslip angle and yaw rate plots on the next page once again show the tendency for the aircraft to rotate about the flight path vector with sideslip remaining near zero.

f. Case Number Six (DAI=-29.2, DEL=5.3 DRU=-30 to 18)

In an attempt to further investigate the roll coupling phenomenon noted in case number four, an equilibrium surface for rudder deflection angles of 0 to -30 and 0 to 18 degrees was generated. The DRU=0 position in Figures 7.6a through 7.6e corresponds to the full scale aileron deflection point in case number four. Unlike the positive angle of attack cross control equilibrium surface discussed in case number five, the steady state flight trajectories shown in Figure 7.6 are far more complicated. This is due primarily to the combined effects of the inertial roll coupling already present at the starting flight condition and the somewhat counterintuitive behavior created by rudder deflections when flying at negative angles of attack. Before presenting Figures 7.6a through 7.6e, the reader is once again reminded that the aircraft is already under the effects of inertial coupling, and therefore, the body axis rotation rates (p, q, and r) should be considered as components of angular rotation about the flight path. A consequence of neglecting gravity effects in this model allows the flight path to be considered level at all times without any loss of generality. During moderate to high angle of attack flight, the blockage effects created by the horizontal tail make the pitching moment, the rolling moment and the roll damping due to rudder surface deflection negligible.

However, at negative angles attack these effects are not negligible, and they play an important roll in the results shown in Figure 7.6. When the rudder is deflected during negative angle of attack flight, several interrelated inputs to the aircraft dynamical situation are made. Given a right rudder deflection (DRU=0 to DRU=-30), the following inputs to the system occur:

a. right yawing moment

b. positive pitching moment (independent of rudder deflection direction)

c. left rolling moment (considering the tail as a wing and the rudder as an aileron)

d. left sideslip angle

e. alteration of the flow fields around the tail section resulting in increased roll damping during left rolls.

With the rudder deflection inputs discussed above in mind, refer to Figure 7.6. Figure 7.6c depicts the most counterintuitive results of this particular run and will be discussed first. At a negative angle of attack (provided that C_L is also negative), a right rudder deflection should result in a left rolling moment. This is due to the rolling moment due to yaw rate, sideslip and rudder deflection all having the same algebraic sign as the rudder deflection when flying at negative angles of attack. This clearly is not the situation indicated in Figure 7.6c.

The roll rate magnitude is sharply decreased initially when the rudder is moved from 0 to -30 degrees. This occurance can best be explained by the change in the air flow about the tail that occurs when the rudder is deflected. During a roll, the horizontal tail provides some damping effect but it is usually minimized by the blockage of airflow due to the vertical tail. When a right rudder deflection is made, the roll damping due the stabilator is enhanced for rolls to the left only. The mechanism responsible for this phenomenon is high energy airflow directed by the rudders onto the right upper stabilator surface. This dramatically increases the damping capabilities of the horizontal tail and is responsible for the counterintuitive behavior seen in Figure 7.6c. During rudder roll manuevers at positive angles of attack, however, this is not a problem since a right rudder deflection will increase the damping of left rolls only thereby improving the capability of the rudder to check roll rates while at the same time not decreasing the roll rate generated by the rudder itself. Figure 7.6e shows that the sideslip angle changes sign at a rudder deflection of approximately -8 degrees. This corresponds to the inflection point seen in the roll rate curve.

Ultimately, the negative sideslip angle is responsible for producing a left rolling moment strong enough to overcome the increased roll damping due to rudder deflection. When considering the left rudder input in this situation, the damping effect will not be present since the aircraft is rolling to the left in this equilibrium branch. The remaining results are relatively straight forward. In Figure 7.6a the right rudder deflection (DEL=0 to DEL=-30) clearly shows a smooth increase in pitch rate. This is due to both the pitching moment created by the rudder deflection and the decreased roll rate seen in Figure 7.6c which causes a reduction in the negative pitching moment due to inertial coupling. During a left rudder deflection, Figure 7.6c shows the roll rate to eventually decrease as the rudder deflection exceeds 10 degrees. The increasing sideslip angle shown in Figure 7.6e is the driving force behind that behavior. In Figure 7.6d the yaw rate decreases when rudder is deflected in either direction. This phenomenon is more easily understood by breaking the yaw rate up into two separate components, one component is due to rudder deflection and the other component is due to inertial coupling. At the point where DRU=0, the yaw rate shown is made up primarily of yaw rate due to inertial coupling. A left rudder deflection naturally tends to decrease the yaw rate.

In the case of the right rudder deflection, the decrease in yaw rate due to inertial coupling is greater than the increase in yaw rate due to rudder input thus, an overall decrease in yaw rate is demonstrated initially. The two yaw rate components appear to balance each other out as the rudder deflection is decreased below -20 degrees.

The changes in stability noted in the DRU=7 to DRU=18 degrees range shows the possibility for a Hopf Bifurcation to a limit cycle as DRU is increase past 7 degrees and the possibility of a small nonlinear jump at DRU=16 degrees. The numerical convergence was excellent throughout this particular run including at the point in question. This fact as well as the positions of the eigenvalue in question before and after the unstable point indicate that a very small bifurcation whose limit points were stepped over by the computer algorithm may exist in that area of the curve.

g. Case Number Seven (DAI=-29.2, DRU=-29.2, DEL=-10.2 to DEL=-30)

The starting point for this equilibrium surface comes from case number five and is a pitch up manuever with full cross controls. The aileron is held at -29.2 degrees and the rudder is held at -29.2 corresponding to full left aileron and full right rudder.

The results indicate a distinct bifurcation in the equilibrium surface in the -15 to -20 degrees stabilator range. In this case the figures are shown one per page to provide a better view of the results. Some step size and convergence difficulties were encountered in the computation of the portion of the curve connecting the two limit points. The curves were generated by initially varying the stabilator deflection from -10.2 to -30. The run went very well numerically but a jump in both the equilibrium surface and the locations of the eigenvalues was noted at approximately -17 degrees stabilator deflection. The run was repeated with a smaller step size and another equilibrium surface was generated in the other direction by varying stabilator deflection from -20 degrees to -10 degrees. The repeat of the original run continued to a slightly lower stabilator setting before making a similar jump and then following the same trajectory as the original run. The reverse direction run followed the same trajectory as the original run except that the jump was made at a significantly higher stabilator deflection than the point where a jump was made during the first run thus showing a definite hysteretic pattern. These results were confirmed by subsequent runs, all of which showed good numerical convergence, but the proper step size to continue around the limit points was not found.

This indicates that some problems may exist with the continuation algorithm. Although an actual calculation of the eigenvalues of the branch connecting the two limit points was not computed, the behavior of the trajectory along that branch indicates that it is probably an unstable branch. A smooth curve was fit between the last confirmed point on the upper and lower branches to give a more realistic view of the equilibrium surface in that region. The hash marks just proir to the limit points show the location of the last confirmed solution points prior to the jump.

Figure 7.7a shows the equilibriuim pitch rate versus stabilator deflection for the conditions given above. The pitch rate shows little change up to the limit point where at that point a small but sharp drop in pitch rate is predicted. The point dropped to is right on the S/L stability boundary and further movement of the stabilator places the aircraft in a Hopf Bifurcation region where limit cycle motion may be experienced. Given the type of manuever and the large jump in roll rate that occurs during the catastrophe (shown in figure 7.7c), a wing rock type motion is a solid possibility. Comparison of Figure 7.7a with Figure 7.7b shows that contrary to the other fifth order surfaces the angle of attack behavior at the bifurcation point is opposite of the pitch rate behavior.

A small but sharp increase in angle of attack is predicted at DEL=-16.5. Figures 7.7c through 7.7e all show similar nonlinear jumps with the largest one occuring in the roll rate equilibrium surface. The sharp jump in sideslip angle from slightly less than zero to approximately -4 degrees corresponds closely to the large increase in roll and raw rates shown in Figures 7.7c and 7.7d. In each of the plots except for the angle of attack equilibriuim surface, the location of the L instability corresponds to an area where the state variable shown is changing sharply with stabilator deflection. Since the catastropic changes shown in the aircraft states must be accompanied by a similar change in kinetic energy, I believe that a limit cycle does exist in the region where the L instability occurs, and it is through the limit cycle oscillations that the kinetic energy is built up or released prior to or after the nonlinear jump. Whether the energy is increased or decreased during the limit cycle motion is dependent on the direction from which the bifurcation region is approached. As an example, consider the case of increasing stabilator deflection from DEL=-25 to DEL=-10. In this situation the equilibrium roll rate is shown to begin to increase significantly with increasing stabilator deflection at DEL=-20 which is also the point where the L instability is encountered.

As the aircraft state crosses the stability boundary, a limit cycle is born. The limit cycle behavior during this phase imparts energy to the system and roll rate is increase until the eigenvalues are again all stable. This corresponds to the level portion of the upper roll rate branch where the increase in roll rate stops. The system is now ripe for a catastrophe which does indeed occur at DEL=-15 The energy previously gained is then released from the system during the catastrophe so that the energy level is once again at the level prior to entering the limit cycle phase. The aircraft behavior during the catastrophe cannot be predicted by the equilibrium surface, but it is clear that it will involve the dissapation of the energy built up as the catastrophe was approached. A definite hysteresis effect can be seen in this hypothesis as well as in all of the equilibrium surface trajectories for this case. If the bifurcation is approached from the other direction, the energy increase occurs suddenly in a manner very similar to a departure from controlled flight. The energy gained during the catastrophic jump at DEL=-16.5 is dissipated gradually by the limit cycle motion as the stabilator deflection angle is decreased until the kinetic energy is returned to a level approximately equal to the level of kinetic energy prior to the catastrophe.

The information contained in these equilibrium surface plots is physically substantiated in the results reported in a NASA Technical Memorandum by Grafton, et al. [8]. In the document the results of a stability study on a wind tunnel model very similar to the F-15S are reported. In that report the canard stalling angle of attack is shown to be approximately 30 degrees. This corresponds to the angle of attack where the bifurcational behavior occurs. At that angle of attack a sharp stabilizing break in the C_m versus angle of attack curve as well as a very sharp peak in the C_L versus angle of attack curve occurs. This explains in part the behavior of the angle of attack and pitch rate curves. The change in sign of the pitching moment stability derivative at that point can account for the sharp decrease in pitch rate that is seen across the catastrophe. The angle of attack in the fifth order model is a function of both pitch rate and C_z. The sharp loss of lift that occurs as the slope of the lift curve changes signs will create a plunging effect along the z-body axis which tends to increase angle of attack and is most likely responsible for the catastrophe seen in the angle of attack equilibrium surface. The report also states that at an angle of attack of 30 degrees the aircraft "exhibits highly nonlinear characteristics with a very abrupt unstable variation in rolling moment over a small sideslip range near 0 sideslip angle."

These instabilities were found to be a direct result of the canard configuration and disappeared when the canard was removed. Additionally, the report states that this configuration exhibits its minimum yaw damping at an angle of attack of 30 degrees and that around 35 degrees angle of attack there is "an abrupt decrease in roll damping to very low values." This is precisely the type of behavior predicted in the yaw and roll rate equilibrium surface plots, and the sideslip plot does confirm that the aircraft is near zero sideslip angle. And finally, the report also indicates that this configuration can be expected to be susceptible to wing rock motion in the angle of attack range corresponding to the L instability region which adds some credence to the energy transfer hypothesis stated above. These findings correlate very closely with the predictions made by the bifurcation and catastrophe analysis shown in Figures 7.7a through 7.7e. No known simulations of this type of configuration in this or any other similar high angle of attack flight regime have been accomplished. Therefore, the existence of the limit cycle energy transfer model hypothesized above can not readily be established. But there is clear evidence that the bifurcational behavior exhibited in Figures 7.7a through 7.7b does exist, and the behavior predicted through their study is correct.

2. Eighth Order Equilibrium Surfaces

As was discussed above only two eighth order equilibrium surfaces were calculated. The increased degrees of freedom offered by the eighth order model not only increased the complexity of the results but tremendously increased the numerical difficulty of the problem. The major factor contributing to the bulk of the numerical problems appeared to be the extra degree of freedom allowing velocity to vary. This caused the equilibrium surface calculations with thrust to be very difficult since velocity tended towards either zero or a very small value as the routine searched for the initial equilibriuim points. The larger the thrust the faster velocity would tend to zero. This behavior indicated conditions typical of operating an aircraft 'behind the power curve'. Therefore, initial conditions of level flight, thrust equal to drag and velocity equal to a value well above that for minimum drag were selected. The results were the same and study of the system with thrust was discontinued. This presented no major problems since the study of spin type motions was the main goal of the eighth order investigation.

Velocity variations did continue to cause some problems, and although the problems were not as severe as those present with thrust, the large velocity variations during the iterations to initial solution points as well as new points during the continuation process ultimately resulted in only one non-spin equilibrium surface being computed. The one that was found could not be continued to a stabilator deflection greater than -5 degrees. This corresponded to an angle of attack of approximately 29 degrees. Grafton et al [8] reports that the canard had serious detrimental effects on pitch damping at angles of attack above 25 degrees and this may partially explain the problems encountered in this area. Another intersting aspect is that while the fifth order system was mostly stable, the eighth order system was rarely stable. This will be discussed more thoroughly in the next section.

a. Case Number One (DAI=0, DRU=0, DEL=-5 to -30)

Case one was a pitch up manuever with aileron and rudder deflections held to zero. The results of this run are presented in Figures 7.8a through 7.8p. Several plots are duplicated for comparison purposes and those that are duplicated are given the same title. Some plots are repeated in an amplified scale to see the small order variations that occur in the equilibrium surface.

Figures 7.8a and 7.8b show the pitch angle and angle of attack equilibrium surfaces. These plots indicate that the aircraft has a descent angle that varies from approximately 2 degrees at DEL=-5 to a descent angle of 6 degrees at DEL=-30. The shape of the two curves is nearly identical and comparison with the pitch rate plot in Figure 7.8c on the next page show that including the gravity coupling terms has decoupled the pitch rate behavior from the angle of attack behavior and at the same time has apparently coupled the pitch angle behavior to the angle of attack. A zero pitch rate is realistic given the high angle of attack conditions and zero thrust. Figure 7.8d shows an amplified version of the pitch rate equilibrium surface which reveals a sharp change in behavior as DEL is decreased below -25 degrees. This point corresponds to an angle of attack of 40 degrees and it is at this point where the aerodynamic model removes the drag input due to ailerons by setting K2 to zero (see Appendix D). Additionally, two other impulsive type changes are made to the system. One is made at 32 degrees angle of attack which corresponds to the point where the UUU instability transitions to the UUL instabilty and the other is at an angle of attack of 35 degrees which corresponds to the point where the UUL instability transtions to an L instability.

Also, the first impulsive change, discussed above, occurs at the point where transition from the L instability to the LL instability occurs. Study of the actual aerodynamic data shows that the terms involved in the impulsive changes were decreased to zero or near zero values prior to the angles of attack given above to create a smooth transition; however, it is hard to believe that these occurances are unrelated, and there may be a problem with the rate of change of those values not also being zero at the point where they are included or removed from the aerodynamic data. Figure 7.8e shows the aircraft velocity equilibrium surface, and the behavior of the curve is what should be expected given the flight conditions. Figures 7.8f and 7.8g show the roll and yaw rate equilibrium surfaces, and these confirm the symetrical nature of the aerodynamic model. Amplified versions of the roll and yaw surfaces are shown on the next page, and they reveal the same type of behavior seen in the previous amplified plot as well as a definite coupling between the two states. The next two pages show the sideslip angle and yaw rate plots together in both the non-amplified and the amplified versions. The amplified versions, Figures 7.8k and 7.8l show nearly identical behavior between yaw rate and sideslip.

The fact that the sideslip angle and yaw rate share the same algebraic sign is an indication of the increased complexity introduced in the model by removing the restriction that gravity be equal to zero. In this particular case a very slight "dutch roll" type behavior is noted which is a type of motion suppressed in the fifth order system. Figures 7.8n, f, o and p show the relationship between roll rate and bank angle.

b. Case Number Two (DEL=-21, DRU=-24.5, DAI=-29.2)

This equilibrium surface is the spin surface discussed earlier. It was found by simply trying various estimated spin conditions until the Newton-Raphson method was able to converge to an equlibrium solution. As has been mentioned before, no spin studies have been done on this configuration. The trajectory given by the equilibrium surface routine is quite reasonable and indicates a strong possibility for recovery at full high performance aircraft anti-spin controls. In the case of this particular spin which is a left spin, the anti-spin controls are full deflection of left aileron, right rudder and negative stabilator where the aileron is usually considered the primary spin recovery control surface. The type of spin trajectory indicated is a flat spin with very little variation in each of the state variables except yaw rate with the movement of aileron deflection.

The scales used for the Y axis in the plots vary from plot to plot to provide the 'best' view of the individual surfaces. Figures 7.9a and 7.9b show the relationship between pitch angle and angle of attack as aileron is varied. The curves are nearly identical and the sum of their angles as measured from the vertical is 90 degrees indicating a vertical descent condition. As the aileron deflection nears -30 degrees both of the curves drop off sharply indicating a possibility for recovery. Figure 7.9c shows the variation of yaw rate with aileron and a very large increase in spin rate is seen as the left aileron input is decreased. Figure 7.9d shows the velocity equilibrium surface and that is compared to the angle of attack surface. The velocity shows little variation except when near DAI=-30. Figure 7.9e shows the sideslip angle equilibrium surface and that too shows evidence for recovery at full anti-spin aileron input. The greatest evidence of possible spin recovery is indicated in Figure 7.9g on the next page. In this figure the pitch rate curve actually undergoes a large change in slope as the anti-spin aileron input is increased. Figures 7.9i and 7.9j show an enlarged view of the pitch rate and velocity surfaces taken from an equilibrium surface run accomplished in an attempt to obtain a surface for the full left aileron deflection.

Evidence of numerical difficulties is shown by the poor convergence of a couple of the points near the end of the run.

Ideally, obtaining a surface that extends all the way to DAI=-30 degrees as well as increasing the other two controls to full anti-spin deflections would help verify the proper recovery control strategy, but serious numerical difficulties were encountered when this was attempted. This problem stems from the same situation found during the generation of the fifth order equilibrium surface in the neighborhood of limit points for case number seven. Unfortunately, in the case of the spin surface the jump that probably occurs at approximately DAI=-29.5 degrees is quite large and the algorithm is unable to converge to this new point. Overall, the equilibrium spin trajectory depicted in this case appears to be correct with one exception that will be discussed below. The plots clearly indicate the possibility of a limit point ocurring between DAI=-29 and DAI=-30 degrees. If that is the case, then the standard anti-spin controls should create a jump from the spin equilibrium surface shown to some other surface that is at least a lower energy spin surface or quite possibly a full recovery to controlled flight.

A noteworthy point indicating that this surface may not predict an actual stabilized spin condition for the aircraft is given by the local stability analysis being unstable throughout. This indicates that the surface is an unstable equilibrium branch, and the likelihood of a similar stable equilibrium branch that exists nearby is present. A few solution points were found during the study indicating that a lower energy stable spin surface may indeed exist, but numerical problems once again prevented the complete computation of the branch associated with those few points.

It should be remembered at this time that the rotary balance data used may not be as accurate as is necessary to give the proper stability indications. The data was good enough however to allow the calculation of a reasonable spin equilibrium trajectory. An analysis of spin data for the F-15 [45] showed that the F-15 should have stabilized spin rates in the 150 to 170 deg/sec range, an angle of attack in the 80 to 85 degree range and velocity in the 230 to 250 f/s range. These values are reasonably close to those given by the spin equilibrim surface in this study. The addition of the canard can account for a good deal of the difference in the stabilized spin modes of the two aircraft.

During high angle of attack spin conditions, the canard will provide a destabilizing pitch up increment since it is above its stalling angle of attack and therefore is operating in the region of negative lift curve slope. This fact when combined with the fact that the canard adds additional planform area forward of the center of gravity indicates that the F-15S should have a flatter stabilized spin mode when compared to the original F-15. An aircraft experiencing a relatively flatter spin tends to have a higher yaw rate since the aircraft center of gravity is closer to the spin axis and the other rotation rates are decreased to near zero values. Therefore, as a result of conservation of angular momentum, the yaw rate component is increased.

C. Numerical Simulations

The numerical simulation portion of the study did not yield a great deal of useful information. The model simulated was an eighth order model which was shown in the local stability analysis to be unstable, and it was indeed shown to be unstable during the simulations that will be presented in this section.

The instability of the model was not considered to be a great draw back initially since it was intended to use the computer aided stability system during the bulk of the numerical simulations. Two sets of two different but related simulations will be presented here. The first set is at a relatively high angle of attack without thrust, and the second set is at a lower angle of attack. One of the two runs in the second set is with thrust. The scales on the plots are not constant.

1. Cases One and Two (DRU=0, DAI=0, DEL=-5 to -27 and DEL=-5 to +.1)

During these two simulations, the initial conditions were identical and they were taken from the conditions in the eighth order non-spin equilibrium branch for DEL=-8.7 except that the stabilator was set at -5.0 as the initial condition for the simulation. In Figure 7.10 the results of a smooth decrease in stabilator deflection angle is shown and in Figure 7.11 a smooth increase in stabilator deflection is shown up to where DEL=+.1 and then held constant. Initially, a decrease in angle of attack is expected due to the pitch up stabilator setting being less than that required for equilibrium conditions and that is shown to be the case in both of the runs.

However, from that point stabilator deflection seems to have no effect on the aircraft. The control inputs were double checked and appeared to be correct. The subroutine that generates the aerodynamic coefficients as a function of the control surface deflections as well as a number of other variables is the same one used successfully in the fifth and eighth order equilibrium surface calculations. This pointed to the possibility that the aircraft may actually have very limited stabilator control authority in the situation shown. The next obvious step was to determine the canard behavior during this simulation. The canard is scheduled as a function of angle of attack alone and the schedule is shown below:

$$DC = 2.0 - 1.25 * \alpha \qquad (7.1)$$

The canard deflection range is -36 to +18 degrees with positive deflection being trailing edge down. The canard schedule is designed to unload the canard at high angles of attack to delay the adverse effects created by the canard stall and thus extend the usable angle of attack range. Therefore, at 25 degrees angle of attack the canard is at -29.25 degrees deflection and increases to -10.5 at an angle of attack of 10 degrees. As a result of this, the effects of the canard in the case shown in Figure 7.10a tend to work against the stabilator deflection.

The nearly identical angle of attack curves indicate that the canard may have more control authority than the stabilator in the situation shown in the two figures. Figures 7.10b and 7.11b show identical, near zero behavior for roll rate, sideslip angle and pitch rate. This verifies the symmetric trajectory behavior predicted by the non-spin eighth order equilibrium surface. Figure 7.10c shows an enlarged plot of the decrease in angle of attack plotted against stabilator deflection.

2. Cases Three and Four (DAI=0, DEL=-1, DRU=0)

Figures 7.12a through 7.12d show the results of a five second simulation where the initial state was taken from the DEL=-5 degrees non-spin equilibrium branch. The actual stabilator deflection used in this run as well as case four was DEL=-1. In these plots a large decrease in velocity with the increase in angle of attack is shown up to the point where the angle of attack reaches approximately 70 degrees. At this point it is apparent that the aircraft is developing a 'sink rate' as the velocity is again increased due to the increasing component in the z-body axis direction. Figures 7.12c and 7.12d show a slow but definite instability in pitch rate and roll rate.

The sideslip angle (not shown) showed a smooth increase from 0 up to +.77 degrees at 56 degrees angle of attack and then a smooth decrease at nearly the same rate to -.22 degrees where the simulation aborted at 90 degrees angle of attack. An interesting point to note at this time is that 55 degrees is the angle of attack where the rotary balance data is included in the aerodynamic model, and this may account for the decrease in sideslip angle seen past that point. The final simulation was similar to case three except an initial value for velocity that should have placed the aircraft on the 'front side' of the power curve was chosen. The initial velocity was 640 f/s, and the data for Mach=0.6 was used. Roll rate, yaw rate, pitch rate and sideslip angle were all set to zero and remained there throughout the simulation. Additionally, thrust was set to 8500 lbs in this case. Figures 7.12a and 7.12b show the velocity and angle of attack versus time curves. The curves shown in these figures are very similar to the ones in Figures 7.12a and 7.12b with the two exceptions that a longer period of time was required in case four to reach 90 degrees angle of attack and the velocity range traversed in case four was higher than case three.

In the simulations described above, the eighth order model is shown to be definitely unstable as is predicted by the local stability analysis in eighth order case number one. The lack of significant lateral motion predicted by the equilibrium surface when the rudder and ailerons are held at zero degrees deflection is also verified. The addition of thrust appears to change the time scale of the instability but not the qualitative nature of the unstable trajectory. Little more than this can be said concerning the numerical simulations themselves or their comparison to the equilibrium surfaces. As a result of the obvious limits to the usefulness of numerical simulations without the computer aided stability system, the time spent on the numerical simulations during this study was less than the other areas discussed in this chapter.

D. Comparison of the Fifth and Eighth Order Models

In this section the significant differences and similarities between the two equilibrium surface models will be discussed. The main areas of interest in this portion of the discussion involve comparisons of the model trajectories, stability and numerical behavior.

A significant difference between the conditions that the two investigations were accomplished under involves the thrust being zero in the case of the eighth order calculations and the velocity being held constant in the case of the fifth order calculations. Holding velocity constant gives the fifth order trajectory a certain amount of 'implied thrust'. This is seen in the angle of attack versus stabilator deflection equilibrium surface plots of the two models shown in Figures 7.1b and 7.8b. Both of the models show a maximum angle of attack near 40 degrees at full scale stabilator deflection, but the angle of attack range hat the fifth order equilibrium surface shows is much larger than the eighth order plot. For instance, the equilibrium angle of attack at DEL=-5 degrees is nearly 10 degrees higher in the eighth order system than the fifth order system. This is a direct effect of allowing velocity to vary in the eighth order model. As discussed above the pitch rate and angle of attack are decoupled in the eighth order model while on the other hand, the pitch angle and angle of attack appear to be coupled in the eighth order model. In both of the models the lack of lateral motions during a pitch up manuever is shown, and this was confirmed to a certain extent in the numerical simulations discussed above.

The increased degrees of freedom allowed in the eighth order model create a more subtle coupling between the lateral terms. This is seen in the amplified plots shown in Figure 7.8 while that type of behavior was not present in the fifth order pitch up equilibrium surface.

In terms of local stability behavior the differences are quite significant. The fifth order equilibrium points tended to be locally stable during most of the investigation while just the opposite was noted in the eighth order equilibrium points. The numerical simulations that were accomplished combined with discussions with personnel involved with the F-15S project at Wright-Patterson AFB, Ohio support the eighth order system as having the correct stability information. The behavior of both the fifth order model and the equilibrium curves indicate that the fifth order stability calculations are correct for the model used (additionally, the same routine was used to calculate the eigenvalues for both of the equilibrium surface routines), but it is apparent that the released degrees of freedom in the eighth order model contain the critical destabilizing components found in the actual aircraft. Consequently, it is believed that the fifth order model is inadequate to make stability predictions on the F-15S.

On the other hand, however, the equilibrium trajectories revealed by the fifth order model seems to be at least qualitatively correct, and the bifurcational behavior found in case number seven does explain the existence of stability problems revealed during earlier research on the configuration. These seemingly contradictory results can be reconciled by refering to the theoretical discussion on the concepts of bifurcations and catastrophes in Chapter 4. Applying the concept proposed by the center manifold theorem to the local stability analysis of the eighth order system shows that there is a group of three to five eigenvalues that remain in the neighborhood of the imaginary axis with the other eigenvalues far removed either to the right or left of the imaginary axis. Comparison of these eigenvalues with the ones present in the fifth order case show those three to five eigenvalues also to be present in the fifth order system. Therefore, it appears that the reduced order system as determined by the center manifold theorem is contained within the fifth order system used in this investigation, and thus, the complete bifurcational behavior of the aircraft should be revealed in the behavior of the fifth order model. The added degrees of freedom in the eighth order model do tend to make the aircraft unstable, but this behavior is linear in nature and is therefore irrelevant to the bifurcational behavior of the system.

The complete behavior of the system, according to Arnol'd [37] can be found from the fifth order system by 'suspending' the linear unstable and stable parts present only in the eighth order system to the nonlinear fifth order system. The resulting system will be identical to the eighth order system in this study except the bifurcational behivior will have been found by studying the much simpler fifth order system. This accounts for the differences in local stability behavior of the two systems, and at the same time shows the close relationship between the two models from a bifurcational behavior point of view. It is clear now that, contrary to initial indications, the fifth order system can indeed reveal accurate information regarding the behavior of the complete aircraft model, and provides a means to at least partially sidestep the numerical problems encounted in the eighth order system by studying the bifurcational behavior of the fifth order system and then generalizing the results to the eighth order system. This would reduce the number of eighth order equilibrium surface runs which as will be shown in the next section could provide a significant improvement in the efficiency and success of similar studies.

Numerically speaking, the differences between the two models is very large.

After fine tuning the algorithm and including a number of computer time saving steps, some of which are discussed in chapter six, the fifth order equlibrium surface calculation routine was working quite well. By the end of the study, none of the partial differentiation or convergence problems found in the eighth order routine were present in the fifth order routine, and the computer time per solution point was reduced to under 30 seconds during some of the fifth order runs. The eighth order system, on the other hand, was not nearly so easy to work with. The difficulties were isolated for the most part to the large variation caused in each of the states by small changes in velocity. In an attempt to solve this problem weighting factors that weighted the relative importance of having the time derivatives of each of the state variables be zero at the solution point were used. Both a relatively small value and a relatively large value for the velocity time derivative weighting factor were attempted with no real success. Problems were even encountered during attempts to converge to a previously established equilibrium point. Finally, both of the routines appeared to have difficulties continuing the equilibrium surface around limit points. This problem may be a result of either improper continuation step size or improper weighting of the columns in the augmented system Jacobian matrix (see Chapter 5);

however, a number of runs were attempted where these factors were varied and still little success was found. This tends to indicate that the method used may need to be improved to be useful on a more complex or unstable aerodynamic model.

CHAPTER VIII

SUMMARY OF SIGNIFICANT FINDINGS

In this chapter the more significant results discovered during the course of this study are summarized. The order in which they are presented here is the same relative order in which they were originally presented in the above discussion to aid the reader in locating the more indepth discussions on these findings located in Chapter 7.

During the fifth order equilibrium surface investigation, three of the surfaces yielded behavior that predict notable problem areas for the F-15S. The first of these findings is that the aircraft is susceptible to severe adverse yaw problems in the 25 degree angle of attack range, and this results in rolling moments being produced that are opposite of the aileron control deflection direction. This phenomenon is demonstrated in Figures 7.2a and 7.2d where a left aileron input is shown to generate a smooth yawing motion to the right which in turn results in a smooth rolling motion to the right at a stabilator deflection of -10.2 degrees.

The second area of interest stems from the roll coupling behavior seen at an angle of attack of approximately -5 degrees.

The inertial roll coupling forces on the aircraft when combined with additional control inputs create highly nonlinear, counter-intuitive behavior in the equilibrium trajectories. The first evidence of roll coupling behavior is shown in Figure 7.4 where pitch rate and angle of attack are seen to decrease with increasing roll rate to the left while the yaw rate smoothly increases. The unusual behavior described above occurs when a rudder control movement is made after reaching an aileron deflection of -29.2 degrees (full left position) in Figure 7.4. The -29.2 degrees aileron position in figure 7.4 and the 0 degrees rudder position in figure 7.6 correspond to the same point on an aileron versus rudder equilibrium surface. The highly nonlinear, counterintuitive behavior mentioned above occurs as a result of an interaction between the inertial roll coupling forces present prior to the rudder input, the forces that are a direct result of the control deflections and the forces created as a result of a variation in the flow fields about the aircraft. In the case shown in Figure 7.6 a rudder deflection to the right is seen to decrease the left roll rate by causing a variation of the flow field about the aircraft tail section which in turn causes a large increase in roll damping. The lower roll rate decreases the effects of roll coupling which when combined with the other forces create the nonlinearities seen as well as aircraft state changes that are opposite of the expected behavior.

These interactions and the mechanisms causing them are more completely discussed in Chapter 7. The discovery of this unusual behavior does underscore the usefulness of the equilibrium surfaces in studying aircraft behavior during unusual control sequences. By studying aircraft trajectories from an equilibriuim surface, the complex transient behavior that would normally accompany these flight conditions is removed so that the underlying causes of the behavior can be studied in a more direct manner.

The third and most important finding during the fifth order equilibrium surface investigation is the discovery of an area with dictinct bifurcational behavior. Figures 7.7a through 7.7e show the evidence of catastrophic behavior in the aircraft states during stabilator movements in the -20 to -15 degrees stabilator deflection range while holding full left aileron and full right rudder. The nonlinear jump behavior predicted by this finding is substantiated in a NASA Technical Memorandum by Grafton et al. [8] in which the stability of an aircraft very similar to the F-15S is studied through wind tunnel tests. In the NASA document the existence of abrupt changes in the aircraft stability derivatives at the angle of attack where the bifurcational behavior is seen to occur in Figure 7.7 is reported but not explained. The occurance of the behavior reported in the NASA document is accurately predicted by catastrophe theory.

Additionally, a mechanism based on a Hopf Bifurcation to limit cycle motion is proposed to explain the physical transfer of kinetic energy that must occur during the nonlinear jumps. The basis for this mechanism is partially supported by one of the predictions made in the NASA Technical Memorandum. According to that document, the origin of the nonlinear behavior is traced to the addition of the canard to the original F-15 configuration.

During the eighth order equilibrium surface investigation a spin trajectory equilibrium surface was discovered for variations in aileron deflection. The values of the state variables correspond reasonably close to known stabilized spin modes for the original F-15 configuration. The spin mode found for the F-15S is flatter and has a higher rotation rate than that typical of the F-15, but these differences in spin behavior can be attributed to the addition of the canard to the basic F-15 configuration. Additionally, the spin equilibrium surface indicates a significant possibility for a jump from the spin surface shown to either a lower energy spin or possibly to non-spin flight conditions by using a full anti-spin aileron deflection. One significant detraction from the reliability of this spin mode prediction is the locally unstable eigenvalues present at each of the equilibrium points indicating that the spin surface shown is a series of unstable equilibrium points. For a more detailed discussion on this point see Chapter 7.

Due to the unstable nature of the aircraft without an operational computer aided stability system, very little useful information was gained from the numerical simulations. One significant point that was noted, however, was that during a power off stall, stabilator deflection appeared to have little bearing on the aircraft behavior. This effect is shown in Figures 7.10 and 7.11. The canard behavior was determined to have an input that opposes pitch up stabilator deflections at the conditions simulated, and that may explain the behavior noted.

The comparisons between the eighth and fifth order local stability results show a large disparity. The evidence indicates that the fifth order model does not accurately predict the local stability behavior of the actual aircraft, but the trajectory and bifurcation information gained during the fifth order equilibrium surface investigation was shown to be useful in predicting aircraft behavior. The discussion on this topic explains that the large difference in the local stability of the two models is not necessarily significant in terms of studying the bifurcational behavior of the aircraft since the additional three roots in the eighth order model tended to be far removed either to the left or to the right of the imaginary axis.

Refering to the center manifold theorem (Chapter 4) showed that the reduced order system for the F-15S is, for the most part, contained within the fifth order system, and therefore, the bifurcational complete behavior of the aircraft could be studied by studying the fifth order system. The complete aircraft behavior is then recovered by generalizing the fifth order nonlinear behavior to the eighth order system in the manner discussed by Arnol'd [37]. Once this is done, the complete behavior of the aircraft including the linear instabilities seen in the eighth order model as well as the nonlinear bifurcational behavior found in the fifth order model will be seen, and of course, the end result will be locally unstable wherever either model predicts local instabilities.

In some cases the findings reported above are primarily of a qualatative nature, however, each of these as well as those findings based on more quantitative results are shown to be valid based on the documentation available and the evidence presented in the results of this study. Further investigation of the areas listed above through the use of more specific techniques such as those discussed in Chapter 3 is warranted, and additionally, the application of this technique to this area of flight mechanics research should be continued so that a better understanding of this and other high angle of attack flight phenomena can be gained.

CHAPTER IX

CONCLUSIONS AND RECOMMENDATAIONS

A. Summary

During this research, a method for studying aircraft flight mechanics through the use of bifurcation and catastrophe theories was studied and implemented into the computer facilities available at the Massachussetts Institute of Technology. The study was based primarily on the generation of equilibrium surfaces for a fifth and an eighth order aircraft model. The aircraft configuration studied was an F-15 with a canard mounted on the engine inlet shelves. The aircraft is known as the F-15 STOL Demonstrator and is currently being developed and studied by McDonnell Douglas and the Air Force Wright Aeronautical Laboratory at Wright-Patterson AFB. The aircraft is inherently unstable and requires a computer aided stability system for normal operation. The results in this study are for the aircraft without the computer aided stability system. Seven fifth order and two eighth order equilibrium surfaces were successfully computed, and those results are all reported in this document. Numerical simulations were attempted, but due to the unstable nature of the aircraft little information was gained from them.

A summary of the significant findings of this research is contained in Chapter 8, and a more indepth discussion of all of the results as well as those significant findings discussed in Chapter 8 are found in Chapter 7.

Overall, the research was a successful effort, a good deal of the objectives set were to at least some degree realized. One major shortcoming of the research was the inability to determine more tangible results based on the bifurcational behavior of the aircraft. Time and logistical limitations were directly responsible for the second major limitation which was the failure to make any studies of the aircraft with its computer aided stability system intact. The amount of work required to make the software package compatible with the computer facilities available and to implement it into the software already developed was much greater than anticipated. At this point, I would like to thank Julie Wolf for the time and effort she expended working on the implementation of the flight control system. It was not by any means an easy task.

B. Recommendations

There are a number of areas in which this research has led to the identification of suggestions for possible improvements and further research. A few of these areas are aircraft design improvements, improvements in the numerical methods used and areas where further study may be beneficial. These points, of course, are listed next.

1. Suggestions for General Aircraft Modifications

The adverse yaw problem noted in the fifth order case number two is not an uncommon occurence, and I am sure that this aspect of the aircraft behavior has been taken into account in the aircraft's flight control system. If this problem has not been taken into account, then as a minimum, an aileron rudder interconnect system that is scheduled as a function of angle of attack should be implemented. The lack of stabilator authority during the power off post stall situation discussed in the numerical simulation section of Chapter 7 indicates that scheduling the symmetrical deflection of the canard as a function of angle of attack and Mach number alone may be a bit restrictive in post stall situations. Finally, since the possibility for spin recovery shown in Figure 7.9 does not occur until near the full scale aileron deflection, extra aileron control deflection capability may be a possible means for insuring the control authority to recover from spin situations.

This extra capability could be included whenever the computer aided stability system senses spin type conditions.

2. Suggestions for Improvement of the Numerical Method

The efficiency of the continuation routines was a major problem during a good deal of the research. Improvements were made in the algorithms and those are discussed in the text, but overall the method is still somewhat time consuming. The key to faster operation is to decrease the number of derivatives that must be calculated. This means reducing the Jacobian calculations or ideally eliminating them altogether. The technique of only calculating the Jacobian when the aircraft state travels a specified distance form the last time the Jacobian was calculated worked very well for the fifth order system and made some substantial improvements in the run time of the routine. No real improvement was noted in the efficiency of the eighth order routine. Another helpful technique used was to ensure that when the aerodynamic coefficients are computed during the Jacobian calculation phase, only the terms that are varied during that specific call to the aerodynamic coefficient routine are recalculated. This too was helpful in decreasing run time.

These points, however, are merely fine tuning the efficiency of a method whose cost will eventually become prohibitive as the order and complexity of the system is increased. Ultimately, a derivative free algorithm would give the greatest margin of improvement in this area.

The numerical problems noted in the neighborhood of the limit points during the study indicates that some improvement is needed in either the implementation of the continuation method used or the actual method itself.

C. Suggestions for Further Research

The most obvious research step to take next is to continue the research on the F-15S with the computer aided stability system operational. This would undoubtedly improve the usefulness of the numerical simulations, but more importantly, the model being studied will then closely resemble the actual aircraft being developed and thus the information revealed can be directly used to further the development of the aircraft. Another very interesting area to study will be the role that the computer aided stability system will play in the generation of the equilibrium surfaces. It is not clear whether or not the flight control system will make changes in either the local stability behavior of the solution points or the bifurcational behavior of the aircraft.

On the other hand, it can be said with some confidence that since the flight control system is a linear full state feedback type control system it should not be able to effectively deal with most of the types of nonlinear instabilities that occur as a result of bifurcational behavior. The comparison of a computer simulated trajectory where the flight control positions are updated 40 times a second and a similar equilibrium surface where the flight control system is only updated on each iteration to a new solution point would be most interesting. The freedom that the flight control system has to vary the controls between iterations may make convergence to an equilbrium solution point very difficult, or it may actually accelerate the convergence since it too is seeking an equilibrium for the cockpit control setting given to it. The soil for research in this area is quite fertile and is virtually unbroken.

The Hopf Bifurcation energy transfer model hypothesized in the discussion of case number seven has the potential to warrant further study by continued equilibrium surface calculations and numerical simulations. The end result of this type of research would be the development of ways to monitor energy build ups of the type discussed in case number seven so that impending catastrophes could be predicted and eventually prevented.

Refering to the center manifold theorem (Chapter 4) showed that the reduced order system for the F-15S is, for the most part, contained within the fifth order system, and therefore, the bifurcational complete behavior of the aircraft could be studied by studying the fifth order system. The complete aircraft behavior is then recovered by generalizing the fifth order nonlinear behavior to the eighth order system in the manner discussed by Arnol'd [37]. Once this is done, the complete behavior of the aircraft including the linear instabilities seen in the eighth order model as well as the nonlinear bifurcational behavior found in the fifth order model will be seen, and of course, the end result will be locally unstable wherever either model predicts local instabilities.

In some cases the findings reported above are primarily of a qualatative nature, however, each of these as well as those findings based on more quantitative results are shown to be valid based on the documentation available and the evidence presented in the results of this study. Further investigation of the areas listed above through the use of more specific techniques such as those discussed in Chapter 3 is warranted, and additionally, the application of this technique to this area of flight mechanics research should be continued so that a better understanding of this and other high angle of attack flight phenomena can be gained.

REFERENCES

1. Anderson, J.D., Introduction to Flight, McGraw-Hill, 1978.

2. Hooven, F.J., "The Wright Brothers' Flight-Control System", Scientific American, November 1978.

3. F-5E Combat Tactics Manual, Part 3, Air-To-Air Combat Effectiveness, Northrop Coorperation, Aircraft Division, Hawthorne, Ca., 1977.

4. Agnew, J.W., Lyerla, G.W. and Grafton, S.B., "The Linear and Nonlineear Aerodynamics of Three Surface Aircraft Concepts", Journal of Aircraft, vol. 18, no. 11, November 1981, pp. 956-962.

5. Agnew, J.W. and Hess, J.R., Jr., "Benefits of Aerodynamic Interaction to the Three Surface Configuration", AIAA Paper 79-1830, August 1979.

6. Etkin, B., Dynamics of Flight Stability and Control, 2nd ed., Wiley, 1982.

7. Kolk, W.R., Modern Flight Dynamics, Prentice Hall, 1961.

8. Grafton, S.B., Croom, M.A. and Nguyen, L.T., "High-Angle-of-Attack Stability Characteristics of a Three-Surfact fighter Configuration", NASA TM-84584, 1983.

9. Ropelewski, R.R., "Modified F-15 Will Investigate Advanced Control Concepts", Aviation Week & Space Technology, Feb. 11, 1985, pp. 51-53.

10. Stability and Control Flight Test Theory, vol. 1, Chapter 8, USAF Test Pilot School, Edwards AFB, Ca., 1977.

11. Henderson, W.P. and Leavitt, L.D., "Stability and Control Characteristics of a Three Surfaced Advanced Fighter Configuratio at Angles of Attack up to 45 Degrees", NASA TM-83171, 1981.

12. Kalaba, J., "Some Aspects of Quasi-Linearization", Nonlinear Differential Equations and Nonlinear Mechanics, Eds: J.P. Lasalle and S. Lefschetz, Academic Press, 1963.

13. Gelb, A. and Van der Velde, W.E., Multiple-Input Describing Functions and Nonlinear System Design, McGraw-Hill, 1968.

14. D'Azzo, J.D., and Houpis, C.H., Linear Control System Analysis and Design, McGraw-Hill, 1981.

15. Lasalle, J. and Lefchetz, S., Stability By Liapunov's Direct Method, Academic Press, 1961.

16. Andronov, A.A. and Chaikin, C.E., Theory of Oscillations, trans. G. Natasha, ed. S. Lefschetz, Princeton University Press, 1949.

17. Minorski, N., Introduction to Nonlinear Mechanics, Edwards, 1947.

18. Minorski, N., Nonlinear Oscillations, Van Nostrand, Princeton, 1962 (Reprinted, R.E. Krieger, Huntington, New York, 1974).

19. Nayfeh, A.H., and Mook, D.T., Nonlinear Oscillations, Wiley, 1979.

20. Ramnath, R.V. and Sinha, P., "Dynamics of the Space Shuttle During Entry into the Earth's Atmosphere", AIAA Journal, vol. 13, no. 3, March 1975, pp. 625-631.

21. Ramnath, R.V., "Scaling Transformations in Nonlinear Systems", in Nonliner Systems Analysis and Synthesis, vol. 2, Techniques and Application, ASME Monograph, 1981, Eds: R.V. Ramnath, et al.

22. Cole, J.D., Perturbation Methods in Applied Mathmatics, Blaisdell, 1968.

23. Nayfeh, A.H., Perturbation Methods, Wiley, 1973.

24. Padfield, G.D., "Nonlinear Oscillations at High Incidence", Dynamic Stability Parameters, AGARD CP-235, paper #31.

25. Taylor, J.H., "Applications of a General Limit Cycle Analysis Method for Multivariable Systems", in Nonlinear Systems Analysis and Synthesis, vol. 2, Techniques and Application, ASME Monograph, 1981, Eds: R.V. Ramnath et al.

26. Carroll, J.V. and Mehra, R.K., "Bifurcation Analysis of Nonlinear Aircraft Dynamics", Journal of Guidance and Control, vol. 5, no. 5, 1982, pp.529-536.

27. Mehra, R.K., Kessel, W.C. and Carroll, J.V., "Global Stability and Control Analysis of Aircraft at High Angles-of-Attack", Report ONR-CR215-248-1, 1977.

28. Mehra, R.K. and Carroll, J.V., "Global Stability and Control Analysis of Aircraft at High Angles-of-Attack", Report ONR-CR215-248-2 1978.

29. Mehra, R.K. and Carroll, J.V., "Global Stability and Control Analysis of Aircraft at High Angles-of-Attack", Report ONR-CR215-248-3, 1979.

30. Thom, R., Structural Stability and Morphogenisis, Addison Wesley, 1974.

31. Zeeman, E.C., "Catastrophe Theory", Scientific American, April, 1976.

32. Casti, J.L., Connectivity, Complexity and Catastrophe in Large Scale Systems, Wiley, 1979.

33. Amson, J.C., "Catastrophe Theory: A Contribution to the Study of Urban Systems?", Environment and Planning B, vol. 2, 1975.

34. Kelly, A., "The Stable, Centre-Stable, Centre, Centre-Unstable, Unstable Manifolds", Journal of Differential Equations 3, 1967.

35. Carr, J., Application of Centre Manifold Theory, Springer Verlag, 1979.

36. Arnold, V.I., "Singularities of Smooth Mappings", Russian Maths. Surveys 23:1, 1968.

37. Arnold, V.I., "Lectures on Bifurcations in Versal Families", Russian Maths. Surveys, 27, 1972.

38. Marsden, J.E. and McCracken, M., The Hopf Bifurcation and Its Applications, Springer Verlag, 1976.

39. Palais, R.S., "Natural Operations on Differential Forms", Trans. Amer. Math. Soc., vol. 92, July 1959.

40. Ferziger, J.H., Numerical Methods for Engineering Application, Wiley, 1981.

41. James, M.L., Smith, G.M. and Wolford, J.C., Applied Numerical Methods for Digital Computation, Harper and Row, 1977.

42. Keller, H.B., "Numerical Solution of Bifurcation and Nonlinear Eigenvalue Problems", in Applications of Bifurcation Theory, Ed: P.H. Rabinowitz, Academic Press, 1977.

43. Schy, A.A. and Hannah, M.E., "Prediction of Jump Phenomenon in Rolling Coupled Manuevers of Airplanes", AIAA third Atmospheric Flight Mechanics Conference, Arlington, Tx., 1976.

44. Barnhart, B., "F-15 Rotary Balance Data for an Angle of Attack Range of 8 to 90 Degrees", NASA CR-3478, 1982.

45. Barnhart, B., "Analysis of Rotary Balance Data for the F-15 Airplane Including the Effect of Conformal Fuel Tanks", NASA CR-3479, 1982.

References Found Useful but not Cited

Cochran, J.E., and Ho, C.S., "Stability of Aircarft Motion in Critical Cases", AIAA Flight Mechanics Conference, 1981, pp. 1-9.

Jones, B.M., "Dynamics of the Airplane", in Aerodynamic Theory, vol. 5, section N, Springer Verlag, 1934, ed: W.F. Durand.

Ross, A.J., "Investigation of Nonlinear Motion Experienced on a Slender-Wing Aircraft", Journal of Aircraft, vol. 9, September 1972, pp. 625-631.

Schoenstadt, A.L., "Nonlinear Relay Model for Post Stall Oscillations", Jornal of Aircraft, vol. 11, July 1974, pp. 407-413.

APPENDIX A
F-15S PHYSICAL CHARACTERISTICS

As was explained in chapter two, the F-15S is, in nearly all aspects, physically identical to the F-15B. It is an F-15B (serial number 71-0290) modified to include the canards and the two-dimensional thrust vectoring nozzles. A comprehensive diagram of the planview of the aircraft is shown in figure A.1. The following table lists the precise physical characteristics of the aircraft.

TABLE A.1

Takeoff gross weight (clean configuration, 5718 lbs of internal fuel)		37,794 lbs
Ixx		25,938 slug-ft^2
Iyy		185,287 slug-ft^2
Izz		206,359 slug-ft^2
Ixz		-2,543 slug-ft^2
Wing		
Area (reference)		608.00 sq ft
Area (actual)		599.39 sq ft
Span		42.808 ft
Aspect Ratio		3.01
Taper Ratio		0.25
Sweep (leading edge)		45 degrees
Dihedral		-1 degree
Airfoil & Chord		
Root (BL 0)	NACA 64A006.6	301.5 in actual
BL 77.0	NACA 64Ax05.9	226.0 in actual
BL 155.0	NACA 64Ax04.6	149.6 in actual
BL 224.73	NACA 64A203.5	94.0 in actual
Tip	NACA 64A203.0	68.3 in actual
Incidence		None
Twist		None
Modified Conical Camber		CL/D=0.3
Aileron Area		26.48 sq ft
Aileron Travel		±30 degrees
Flaperon Area (not used)		35.84 sq ft
Flaperon Travel (not used)		0 to 30 deg. down

Stabilator		
Area (reference)		120.00 sq ft total
Area (actual)		111.36 sq ft total
Aspect Ratio		2.05
Taper Ratio		0.34
Sweep (leading edge)		50 degrees
Dihedral		0
Airfoil & Chord		
Root (BL 0)	NACA 0005.5-64	137.2 in reference
BL 90.0	NACA 0003.5-64	117.9 in reference
Tip	NACA 0002.5-64	46.5 in reference
Stabilator Travel		+20 to -30 degrees
Vertical Tails		
Effective Area		125.2 sq ft total
Aspect Ratio		1.7
Taper Ratio		0.27
Sweep (leading edge)		47.16 degrees
Airfoil & Chord		
Root	NACA 0005.0-64	115.0 in actual
Tip	NACA 0003.5-64	30.6 in actual
Rudder Area		19.94 sq ft total
Rudder Travel		±30 degrees
Canard		
Area		88.1 sq ft
Aspect Ratio		2.44
Taper Ratio		0.46
Span (exposed)		14.67 ft
Sweep (leading edge)		47.16 degrees
Dihedral		+20 degrees
Airfoil & Chord		
Root	NACA 65A w/sharp LE 6%	98.70 in
Tip	NACA 65A w/sharp LE 2%	45.45 in
Canard Travel (Trailing edge)		30 up, 20 dn (deg)

Since nozzle effects and configurations other than clean were not considered in this study, details pertaining to those areas have been omitted from table A.1 and from figure A.1 (shown on the next page).

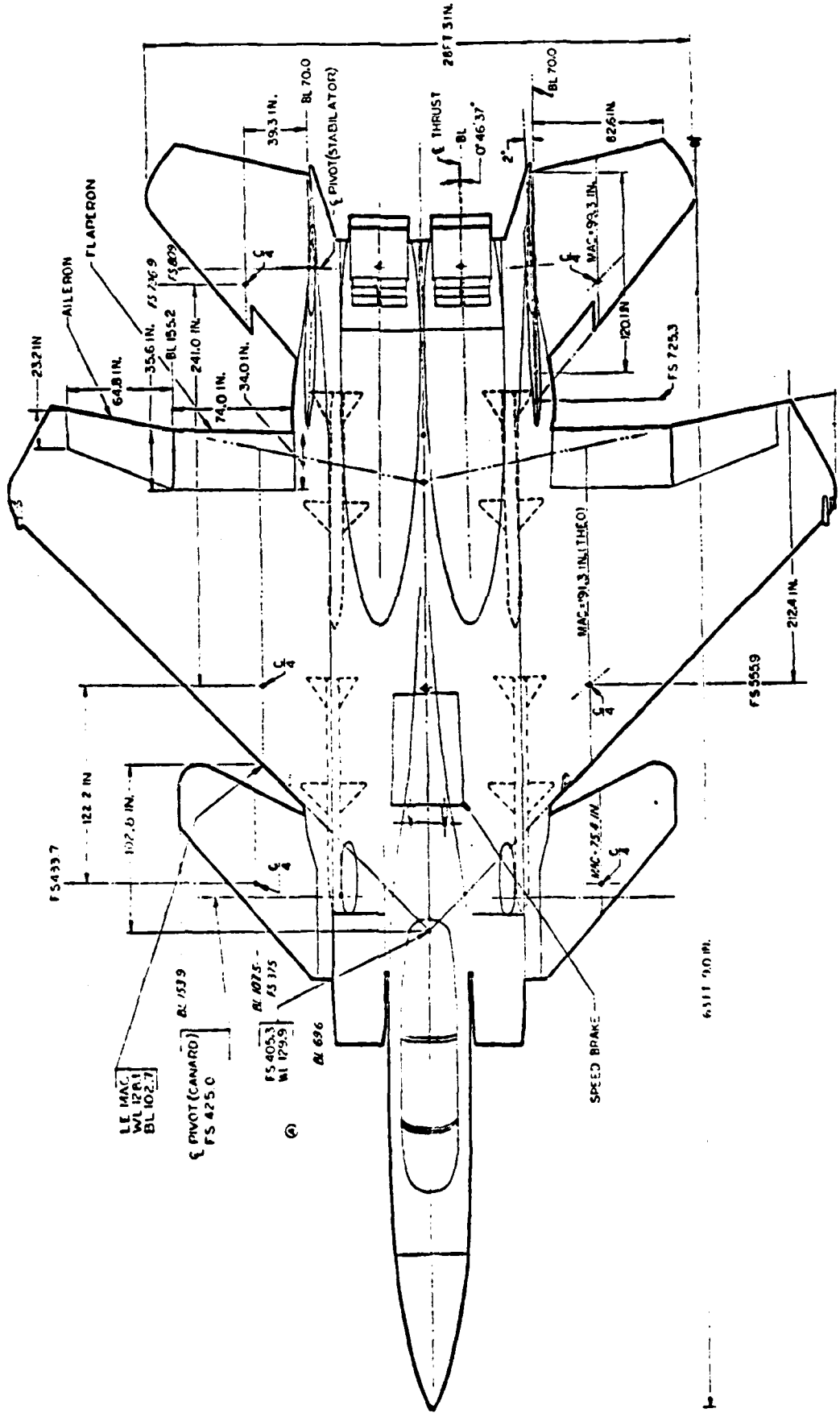

Fig. A.1 F-15S Planform

APPENDIX B

ROTARY BALANCE DATA

B.1 General Remarks

Standard wind tunnel aerodynamic coefficient data is normally composed of two different types of data, static data and forced oscillation data. The fact that these types of data neglect the complex rotational flows that develop around an aircraft in spin type motion was not a factor in the earlier days of aircraft development. Those earlier combat aircraft, in the same manner as most general aviation aircraft today, could rapidly enter and recover from a spin with use of standard aerosurface controls. This fact when combined with the fact that the rotary balance, (RB), data for those earlier aircraft showed little variation with changes in omega, the RB parameter (to be discussed in detail later), allowed the earlier fighter aircraft to be successfully modeled throughout their flight envelope without using rotary balance data [29]. This is not the case with modern fighter aircraft. Due to their slender bodies and low aspect ratio wings, modern fighter aircraft are not easily recovered from spin type situations, and the variation of their RB data is much higher than their predecessors.

Although currently there is still much debate over the proper implementation of RB data into the aerodynamic model, it is clear that high aoa spin type conditions can not be properly modeled without RB data.

B.2 Implementation of the RB Data

Rotary Balance wind tunnel tests are conducted by rotating the wind tunnel model about the relative wind with the axis of rotation being through the CG. There are two major points of contention in the RB data debate. The first is when to include the RB data in the aerodynamic model and the second is how the RB parameter, omega, should be modelled. A consensus has been found, more or less on the first point by the physical limitations of the current testing apparatus and procedures. Due to the nature of the wind tunnel test setup for rotary balance testing, data is not usually taken at angles of attack below 55 degrees. This limit arises from the fact that the sting is connected to the center of gravity through the top of the aircraft. Therefore, rotating the aircraft at lower angles of attack becomes impossible due to geometric and aerodynamic interference between the tail and the sting.

Sideslip angles greater than ±10 degrees are also not normally attempted due to the large hole that must be made in the top of the aircraft to allow for that particular degree of freedom and still have the sting connected to the CG. The size of the hole necesary for testing at sideslip angles greater than ±10 would distort the flow fields to the point of destroying the accuracy of the results. A combination of these circumstances and observations of actual aircraft spin behavior make an aoa of 55 degrees the usual RB data input aoa. The RB data is usually retained in the aerodynamic coefficient models until the aoa drops below 30 degrees. The removal of the RB data at an aoa of 30 degrees is somewhat arbitrary, but it is based on the fact that the aoa threshold for spin entry is normally higher than the aoa at which rotational motion still occurs during a recovery from a spin. Additionally, some spin test setups allow the gathering of data at angles of attack as low as 30 degrees by off-setting the aircraft from the axis of rotation. If this type of data is unavailable, then the data for aoa=55 degrees is used when the aoa drops below 55 degrees.

The second problem area, selecting the correct definition for omega, is a much more difficult task. It is possible to choose several definitions that have merit at one particular condition but fail at others.

For instance, $omega^2 = p^2 + q^2 + r^2$ or even omega=r would adequately describe the stabilized flat spin condition since p,q<<r during a flat spin, but neither definition is very adequate in oscillatory type spin conditions. This is a major drawback of most of the models considered and arises from the fact that the RB data is composed of much of the same components as the forced oscillation data. Therefore, considerable redundancy is introduced into the aerodynamic coefficients by this method. This problem is normally dealt with by using adjusted values for p, q, and r when the RB data is in use. The RB data also has a static component that is evident by the non-zero value of the RB coefficients when omega=0. This is removed by simply subtracting that value from each of the RB coefficients calculated so that RB=0 when omega=0.

B.3 Development of RB data for the F-15S

Since no RB data on the F-15S has been collected at the present time, a set of RB data for the F-15S was approximated by adjusting F-15 RB data to account for the addition of the canard. The F-15 RB data used was presented in a series of component build-up plots that represented the various changes the addition of specific components had on the rotary balance parameter, (omega*b)/(2*V) (non-dimensional form) [44,45].

This type of data presentation made it possible to estimate the effects that an addition of the canard would have on the RB data by comparison of the F-15 aerodynamic RB data for omega=0 to the F-15S static aerodynamic data and using some simple calculations to find the relative effect the addition of the canard would have on the data based on the effect created by the addition of the other aerodynamic surfaces. Due to the complex nature of the flows, no estimations were made for data other than zero sideslip. A discussion of the process used to develop the F-15S RB data is given below.

The Rotary Balance data can be thought of as a combination of static and forced oscillation data with the exception that rotational flow fields are allowed to develop. As a first cut approximation the values for the changes in static forces are added in as a constant bias. These are found by comparison of the omega=0 RB data for the F-15 to the corresponding static coefficient values for the F-15S. The difference is the static bias. This is a relatively unimportant point for our application, however, since the static values are removed from the RB data to avoid duplication of the static force coefficients.

In each of the following cases where adjustments beyond the changes in the static forces are required, the adjustment is found by using the points discussed below to determine the relative effectiveness of the canard as compared to the appropriate tail section surface. The RB data is then adjusted accordingly based on that particular tail section's build-up plot. These are plots that show the effect that the addition of that particular control surface alone has on the RB data. In the cases involving the longitudnal coefficients (Cm, Cx and Cz) few additional adjustments were required. Since the canard's stalling aoa is equal to approximately 32 degrees, the corrections involved only simple calculations of the canard volume versus the horizontal tail volume in the case of the Cm and Cz, and a comparison of the exposed frontal surface area of the canard versus the horizontal tail in the case of Cx (taking into account the blockage and downwash effects of the wing on the horizontal tail). In the calculation of Cn the 20 degree dihedral angle of the canard made it necessary to make some adjustments beyond the simple static force changes discussed above. These amounted to recognition of the destabilizing contribution of the increased vertical surface area forward of the CG due to the canard, and a comparison of the yawing moment forces created by the canard with those that would be created by the vertical tails without the stabilator.

The canard tends to be destabilizing in yaw at zero to low rotation rates but has a stabilizing influence at higher rotation rates while the vertical tail is stabilizing at both zero and high rotation rates. This points towards the probability of easier spin entries but lower stabilized spin rates for the F-15S when compared to the original F-15. In both the yawing moment and the sideforce coefficient calculations consideration was given to the effects of blockage due to the fuselage on the canard's ability to influence of those coefficients. Finally, although the canard has some significant influences on Cl, it loses its effectiveness in this area when placed beyond its stalling angle of attack, and therefore, only small adjustments to Cl are necessary. These are due to the increased stability and roll damping offered by the dihedral angle and the horizontal surface area of the canard.

Although the above adjustments may appear crude on the surface, it should be remembered that any data is better than no data at all when attempting to model high aoa spin type motions. This data is a first approximation to the actual RB data and is therefore qualitatively accurate in that the shift of the data is in the correct direction, but the amount of the shift may not be correct.

B.4 Application of the RB Data to the F-15S

As discussed above the static components have been removed from the data that the RB coefficient is zero when omega=0. The data has also been adjusted so that the first derivative of each RB coefficient with respect to alpha and omega is 0 when aoa=55 and 30 degrees. This prevents an impulsive input to the system at the points where the data is to be included and removed from the system of aerodynamic coefficient equations. Since sideslip effects are not in the data, a rotational parameter was selected that described the aircraft rotation as a projection of the total aircraft angular velocity vector onto the XZ plane. Thus,

$$\text{omega} = p*\cos(\text{aoa}) + r*\sin(\text{aoa}), \qquad \text{(B.4.1)}$$

and in order to prevent redundancies between the forced oscillation terms and the RB data the following substitutions are made while the RB data is being used:

$$p = p*\sin(\text{aoa}) \qquad \text{(B.4.2)}$$

$$r = r*\cos(\text{aoa}) \qquad \text{(B.4.3)}$$

APPENDIX C

POINCARE-LIAPUNOV STABILITY THEOREM

The Poincare-Liapunov Stability Theorem is a very simple but powerful theorem. It has been the basis for the successful linearization of nonlinear systems for many years, and it is also gives major support to the nonlinear analysis theorems discussed in chapter 4. In fact, the Center Manifold Theorem is merely an extension of the Pioncare-Liapunav Theorem. The Pioncare-Liapunov Theorem is stated below without proof.

"The <u>local</u> stability of a nonlinear system at a particular operating point can always be characterized in the same way as the equivalent linear system that is valid in the neighborhood of that operating point except in those cases where the linearised system has eigenvalues with zero real parts."

APPENDIX D

F-15S AIRCRAFT MODELS

This appendix contains the two aircraft models used in the BACTM software and the model used in the numerical simulations. The BACTM models consist of a fifth and an eighth order model used in equilibrium surface calculations. A separate eighth order model is used in the numerical simulation phase.

D.1 Aerodynamic Force Representation

All of the equations of motion use six main aerodynamic coefficients that are calculated in the exact same manner. This is true for cases when the computer aided stability system is operational and when it is not operational. The F-15S data is represented in terms of CL, CD, Cy, Cl, Cm and Cn. The lift and drag coefficients are in stability axis coordinates while the remaining coefficients are in fixed body axis coordinates. The lift and drag coefficients are transformed into body axis coordinates, Cx and Cz, for use in the equations of motion. For clarity, the actual fortran code for those equations is used in the descriptions shown here.

```
CL  = CLO + .5*(CLCANL+CLCANR) + CLFLX +
      .5*FLX1*(CLSTBL+CLSTBR) + DCLBET                (D.1.1)

CD  = CDO + .5*(CDCANL+CDCANR) + .5*(CDSTBL+CDSTBR) +
      K2*DCDAIL*AVDA + CDRUD + DCDPCF                 (D.1.2)
```

```
CY1 = CYO*FLXNY*SBE + (1.-FLXNY)*FLXCYO*BE +
        DCYAIL*FLXAI*DA + CYDSTB*DHD*FLX6 +
        .5*(CYRUDL*DRL+CYRUDR*DRR)*FLX5 + CYCAN*SBE +
        DCYDC*DCD + CYFLX + K7*DCYASY                    (D.1.3)

CLL1= CLLO*FLXRM*SBE + DCLLP*P*B2V + DCLLR*R*B2V +
        DCLLAI*FLXAI*DA + CLLDST*FLX2*DHD +
        .5*(CLLRDL*DRL + CLLRDR*DRR)*FLX4 + CLLCAN*SBE
        + DCLLDC*DCD + CLLFLX                            (D.1.4)

CM1=CMO + .5*(CMCANL+CMCANR) + CMFLX + .5*FLX1*(CMSTBL
        +CMSTBR) + DCMAIL*AVDA + CMRUD + RAMP3*DCMDS2
        + DCMQ*Q*C2V + .5*(CMSDCL+CMSDCR)*FLX1 +
        AVDHD*CMCF                                       (D.1.5)

CN1= CNO*FLXNY*SBE + (1.0-FLXNY)*FLXYM*BE + DCNP*P*B2V +
        DDCNP*K6*P*B2V + DCNR*R*B2V + DCNAIL*FLXAI*DA +
        CNDSTB*FLX2*DHD + .5*(CNRUDR*DRR+CNRUDL*DRL)*FLX3
        + CNCAN*SBE + DCNDC*DCD + CNFLX + DCNASY*K7      (D.1.6)
```

The terms used in the above set of equations are defined as follows:

P, Q and R are roll, pitch and yaw rates respectively.
BE is the sideslip angle, beta.
B2V and C2V are span/(2*VT) and chord/(2*VT) respectively
VT stands for true airspeed
DA is the aileron surface deflection.
DCL and DCR are left and right canard surface deflections.
DHL and DHR are left and right stabilator surface deflections.
DRL and DRR are left and right rudder surface deflections.
DCD and DHD are differential canard and rudder surface deflections and are defined as:

DCD=DCL-DCR and
DHD=DHR-DHL.

DC, DH and DR are the symmetrical canard, stabilator and rudder deflections, respectively and are defined as:

DC=(DCL + DCR)/2
DH=(DHL + DHR)/2
DR=(DRL + DRR)/2.

A prefix of AV found in terms such as AVDA indicates absolute value of the term following the AV.
SBE is +1 whenever beta is 0 or positive and -1 when beta is negative.

The individual components from the above coefficient equations are grouped together below into terms as they appear in the equations and the overall effect of each term is defined.

LIFT TERMS

CLO	Basic lift
.5*(CLCANL+CLCANR)	Lift due to canard
CLFLX	Canard flexibility effects
.5*FLX1*(CLSTBL+CLSTBR)	Lift due to stabilator
DCLBET	Lift due to beta

DRAG TERMS

CDO	Basic drag
.5*(CDCANL+CDCANR)	Drag due to canards
.5*(CDSTBL+CDSTBR)	Drag due to stabilator
K2*DCDAIL*AVDA	Drag due to ailerons
CDRUD	Drag due to rudder
DCDPCF	Performance corr. factor

SIDE FORCE TERMS

CYO*FLXNY*SBE	Side force due to beta
(1.-FLXNY)*FLXCYO*BE	Flexibility effects
DCYAIL*FLXAI*DA	Side force due to ailerons
CYDSTB*DHD*FLX6	Side force due to stab.
.5*(CYRUDL*DRL+CYRUDR*DRR)*FLX5	Side force due to rudder
CYCAN*SBE	Side force due to sym. can.
DCYDC*DCD	Side force due to dif. can.
CYFLX	Canard flexibility effects
K7*DCYASY	High alpha asymmetry effects

ROLLING MOMENT TERMS

CLLO*FLXRM*SBE	Rolling mom. due to beta
DCLLP*P*B2V	Rolling mom. due to P
DCLLR*R*B2V	Rolling mom. due to R
DCLLAI*FLXAI*DA	Rolling mom. due to aileron
CLLDST*FLX2*DHD	Rolling mom. due to stab.
.5*(CLLRDL*DRL+CLLRDR*DRR)*FLX4	Rolling mom. due to rudder
CLLCAN*SBE	Rolling mom. due to sym. can.
DCLLDC*DCD	Rolling mom. due to dif. can.
CLLFLX	Canard flexibility effects

PITCHING MOMENT TERMS

CMO	Basic pitching mom.
.5*(CMCANL+CMCANR)	Pitching mom. due to canard
CMFLX	Canard flexibility effects
.5*FLX1*(CMSTBL+CMSTBR)	Pitching mom. due to stab.
DCMAIL*AVDA	Pitching mom. due to ailerons
CMRUD	Pitching mom. due to rudder
RAMP3*DCMDS2	High alpha effects
DCMQ*Q*C2V	Pitching mom. due to Q
.5*(CMSDCL+CMSDCR)*FLX1	Effect of canards on stab.
AVDHD*CMCF	Pitching mom. due to dif. stab.

YAWING MOMENT TERMS

CNO*FLXNY*SBE	Yawing mom. due to beta
(1.0-FLXNY)*FLXYM*BE	Flexibility effects
(DCNP*P+DDCNP*K6)*P*B2V	Yawing mom. due to P
DCNR*R*B2V	Yawing mom. due to R
DCNAIL*FLXAI*DA	Yawing mom. due to aileron
CNDSTB*FLX2*DHD	Yawing mom. due to stab.
.5*(CNRUDR*DRR+CNRUDL*DRL)*FLX3	Yawing mom. due to rudder
CNCAN*SBE	Yawing mom. due to sym. can.
DCNDC*DCD	Yawing mom. due to dif. can.
CNFLX	Canard flexibility effects
DCNASY*K7	High alpha asymmetry effects

The following equations show the transformations made to convert the above stability/body axis set of equations into a body axis only set of equations.

CX= CL*Sin(Alpha) - CD*Cos(alpha) + IROTGP*DCXRB (D.1.7)

CY= CY1 + IROTGP*DCYRB (D.1.8)

CZ= -CD*Sin(alpha) - CL*Cos(Alpha) + IROTGP*DCZRB (D.1.9)

CLL=-CY1*(WLCG-WLREFCL)/(Span*12.) + CLL1 + IROTGP*DCLLRB (D.1.10)

CM= CX*(WLCG-WLREFCM)/(Chord*12.) - CZ*(CG-CMCGR) + CM1 + IROTGP*DCMRB (D.1.11)

CN= CY1*(CG-CNCGR)*CBAR/BB + CN1 + IROTGP*DCNRB (D.1.12)

In the above equations, (D.1.7)-(D.1.12), CG is the Center of Gravity (measured horizontally in % of chord). WLCG is the Water Line Center of Gravity (measured vertically in inches). The values, WLREFCM, WLREFCL, CMCGR AND CNCGR, describe the location of the origin of the original axis system which causes moments about the CG in the new body axis system. The values, DCXRB, DCYRB, DCZRB, DCLLRB, DCMRB AND DCNRB, are the rotary balance data additions for the indicated coefficients.

The term, IROTGP, is a switching parameter that is 0 whenever alpha is below 30 degrees. It is switched to 1 when alpha increases above 55 degrees and then is returned to 0 when alpha decreases below 30 degrees. See appendix B for complete details on the rotary balance data.

Finally, one last adjustment is made before the above coefficients are ready to be used in the equations of motion. If thrust is to be included, then CX is adjusted as shown below

$$CX = CX + Thrust/(.5*rho*VT**2*S) \qquad (D.1.13)$$

where rho is the atmospheric density and S is the wing planform surface area. Figure D.1 shows the sign convention used in the aerodynamic model. Note that the aileron deflection sign convention is non-standard.

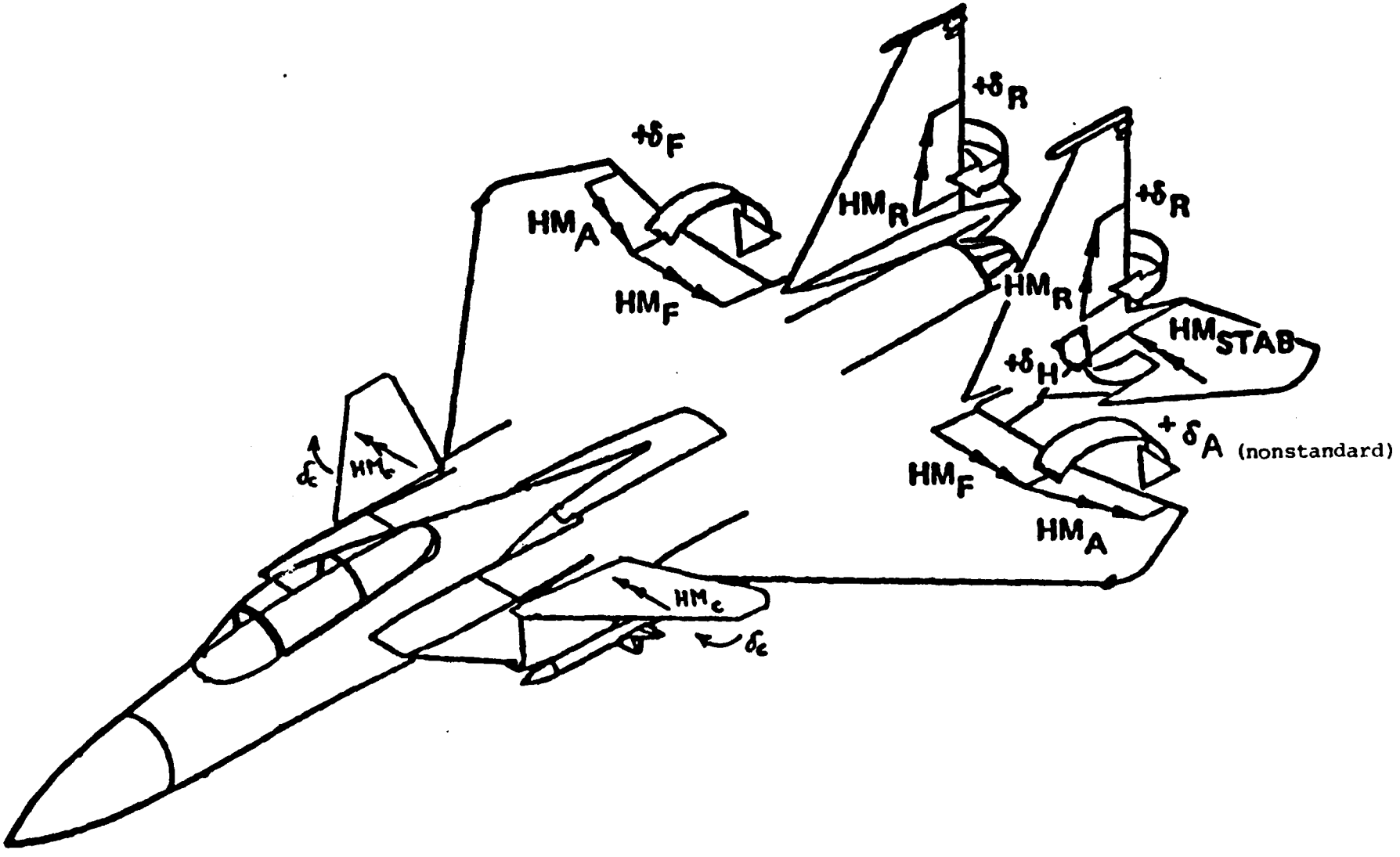

Fig. D.1 F-15S Sign Conventions

AD-A167 697 APPLICATION OF BIFURCATION AND CATASTROPHE THEORIES TO NEAR STALL FLIGHT MECHANICS(U) AIR FORCE INST OF TECH WRIGHT-PATTERSON AFB OH C A HAWKINS 1985 3/3

UNCLASSIFIED AFIT/CI/NR-86-54T F/G 12/1 NL

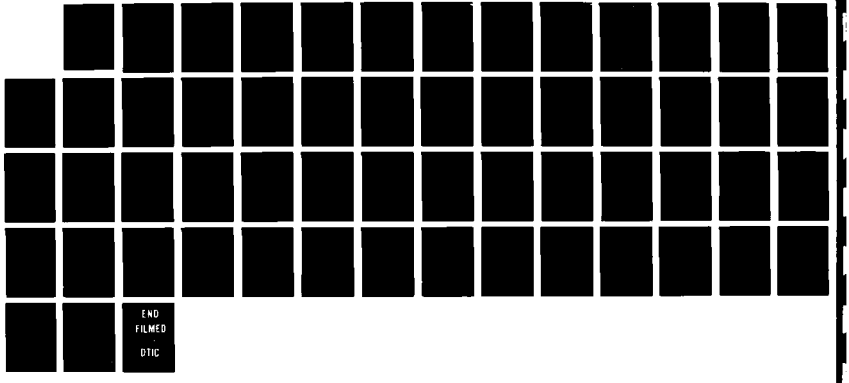

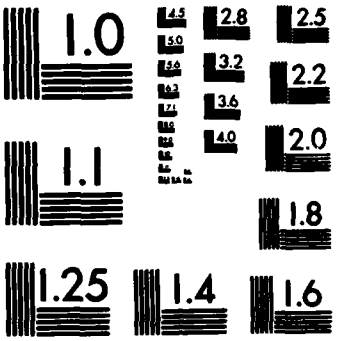

D.2 Equations of Motion

As discussed above, there are three major versions of the equations of motion used in this study. The first of these to be discussed here is the fifth order set used for equilibrium surface calculations. This set is most accurate in the non-spin flight regime, and it is derived by setting gravity to zero and holding velocity constant. These simplifications reduce the order of the system by three. Letting gravity be zero decouples the bank angle and pitch angle variables from the remaining equations of motion, and therefore, those terms do not contribute to the dynamics of the system. It has been shown that neglecting gravity does not seriously effect the modelling of the flight dynamics in the low aoa flight regime, but the assumption of $g=0$ does deteriorate the accuracy when modelling high aoa spin type behavior [28,29]. Letting velocity be constant implies that the thrust available is always equal to the thrust required which is, of course, unrealistic at high angles of attack. The restriction of velocity to a constant value also has the effect of suppressing oscillations in the other varibles. This is confirmed by the fact that wing rock and other oscillatory type motions are not readily found in simulations where velocity is not allowed to vary [28,29].

Below is the fifth order set of equations used in this study [28].

$$\dot{p} = \left[-\left(\frac{I_z - I_y}{I_x} + \frac{I_{xz}^2}{I_x I_z} \right) qr + \left(1 - \frac{I_y - I_x}{I_z} \right) \frac{I_{xz}}{I_x} pq + \frac{\bar{q}Sb}{I_x} \left(C_\ell + \frac{I_{xz}}{I_z} C_n \right) \right] \Bigg/ \left[1 - \frac{I_{xz}^2}{I_x I_z} \right] \tag{D.2.1}$$

$$\dot{q} = \frac{\bar{q}S\bar{c}}{I_y} C_m + \frac{I_z - I_x}{I_y} pr + \frac{I_{xz}}{I_y} \left(r^2 - p^2 \right) \tag{D.2.2}$$

$$\dot{r} = \left[\left(\frac{I_{xz}^2}{I_x I_z} - \frac{I_y - I_x}{I_z} \right) pq - \left(1 + \frac{I_z - I_y}{I_x} \right) \frac{I_{xz}}{I_z} qr + \frac{\bar{q}Sb}{I_z} \left(\frac{I_{xz}}{I_x} C_\ell + C_n \right) \right] \Bigg/ \left[1 - \frac{I_{xz}^2}{I_x I_z} \right] \tag{D.2.3}$$

$$\dot{\alpha} = q + \left[-\left(\frac{\bar{q}S}{mV} C_x + r \sin\beta \right) \sin\alpha + \left(\frac{\bar{q}S}{mV} C_z - p \sin\beta \right) \cos\alpha \right] \sec\beta \tag{D.2.4}$$

$$\dot{\beta} = -\left[\left(\frac{\bar{q}S}{mV} C_x \sin\beta + r \right) \cos\alpha + \frac{\bar{q}S}{mV} C_y \cos\beta - \left[\frac{\bar{q}S}{mV} C_z \sin\beta - p \right] \sin\alpha \right] \tag{D.2.5}$$

The other equilibrium surface set of equations also uses the wind axis variables, alpha and beta, but it also includes the velocity, pitch angle and roll angle equations that were removed to create the fifth order set of equations.

It is one of several sets of equations that can fully describe six degrees of freedom aircraft motion. Using the wind axis variables does result in relatively complicated equations for alpha and beta, but these variables are necessary since they contain the most meaningful information when studying high aoa spin type motion. By calculating them directly the time and effort of repeatedly recalculating their values as auxilliary equations is saved. The eighth order equilibrium surface set of equations is shown below [6,28].

$$\dot{p} = \left[-\left(\frac{I_z - I_y}{I_x} + \frac{I_{xz}^2}{I_x I_z} \right) qr + \left(1 - \frac{I_y - I_x}{I_z} \right) \frac{I_{xz}}{I_x} pq + \frac{\bar{q}Sb}{I_x} \left(C_\ell + \frac{I_{xz}}{I_z} C_n \right) \right] \Bigg/ \left[1 - \frac{I_{xz}^2}{I_x I_z} \right] \tag{D.2.6}$$

$$\dot{q} = \frac{\bar{q}S\bar{c}}{I_y} C_m + \frac{I_z - I_x}{I_y} pr + \frac{I_{xz}}{I_y} \left(r^2 - p^2 \right) \tag{D.2.7}$$

$$\dot{r} = \left[\left(\frac{I_{xz}^2}{I_x I_z} - \frac{I_y - I_x}{I_z} \right) pq - \left(1 + \frac{I_z - I_y}{I_x} \right) \frac{I_{xz}}{I_z} qr + \frac{\bar{q}Sb}{I_z} \left(\frac{I_{xz}}{I_x} C_\ell + C_n \right) \right] \Bigg/ \left[1 - \frac{I_{xz}^2}{I_x I_z} \right] \tag{D.2.8}$$

$$\dot{\alpha} = q + \left[-\left(\frac{\bar{q}S}{mV} C_x - \frac{g}{V} \sin\theta + r \sin\beta \right) \sin\alpha + \left(\frac{\bar{q}S}{mV} C_z + \frac{g}{V} \cos\theta \cos\phi - p \sin\beta \right) \cos\alpha \right] \sec\beta \tag{D.2.9}$$

$$\dot{\beta} = -\left[\left(\frac{\bar{q}S}{mV} C_x - \frac{g}{V}\sin\theta\right)\sin\beta + r\right]\cos\alpha + \left(\frac{\bar{q}S}{mV} C_y + \frac{g}{V}\cos\theta\sin\phi\right)\cos\beta - \left[\left(\frac{\bar{q}S}{mV} C_z + \frac{g}{V}\cos\theta\cos\phi\right)\sin\beta - p\right]\sin\alpha \qquad \text{(D.2.10)}$$

$$\left(\frac{\dot{V}}{V}\right) = \left(\frac{\bar{q}S}{mV} C_x - \frac{g}{V}\sin\theta\right)\cos\alpha\cos\beta + \left(\frac{\bar{q}S}{mV} C_y + \frac{g}{V}\cos\theta\sin\phi\right)\sin\beta + \left(\frac{\bar{q}S}{mV} C_z + \frac{g}{V}\cos\theta\cos\phi\right)\sin\alpha\cos\beta \qquad \text{(D.2.11)}$$

$$\dot{\theta} = q\cos\phi - r\sin\phi \qquad \text{(D.2.12)}$$

$$\dot{\phi} = p + q\tan\theta\sin\phi + r\tan\theta\cos\phi \qquad \text{(D.2.13)}$$

The set of equations of motion selected for the numerical simulations is also an eighth order set, but in this case the fixed body axis variables (u, v and w) were chosen over their wind axis counterparts (alpha, beta and velocity). This sel-ection was motivated by the clean and simple form of the body axis set of equations. It was felt that these equations would make the simulation package more readily adaptable to other uses in addition to verifi-cation of BACTM results. Since, regardless of the particular model used, a number of auxiliary variables were to be calculated during the simulation, the additional calculation of alpha and beta presented no increase in effort or computation time.

See appendix E for the particular auxiliary variables calculated during the simulations and their definitions. Below is the eighth order set of equations of motion used in the numerical simulation phase [7].

$$\dot{u} = -g \sin\theta + vr - wq + \frac{\bar{q}S}{m} C_x \tag{D.2.14}$$

$$\dot{v} = g \cos\theta \sin\phi + wp - ur + \frac{\bar{q}S}{m} C_y \tag{D.2.15}$$

$$\dot{w} = g \cos\theta \cos\phi + uq - vp + \frac{\bar{q}S}{m} C_z \tag{D.2.16}$$

$$\dot{p} = \left[-\left(\frac{I_z - I_y}{I_x} + \frac{I_{xz}^2}{I_x I_z} \right) qr + \left(1 - \frac{I_y - I_x}{I_z} \right) \frac{I_{xz}}{I_x} pq + \frac{\bar{q}Sb}{I_x} \left(C_\ell + \frac{I_{xz}}{I_z} C_n \right) \right] \Bigg/ \left[1 - \frac{I_{xz}^2}{I_x I_z} \right]. \tag{D.2.17}$$

$$\dot{q} = \frac{\bar{q}S\bar{c}}{I_y} C_m + \frac{I_z - I_x}{I_y} pr + \frac{I_{xz}}{I_y} \left(r^2 - p^2 \right) \tag{D.2.18}$$

$$\dot{r} = \left[\left(\frac{I_{xz}^2}{I_x I_z} - \frac{I_y - I_x}{I_z} \right) pq - \left(1 + \frac{I_z - I_y}{I_x} \right) \frac{I_{xz}}{I_z} qr + \frac{\bar{q}Sb}{I_z} \left(\frac{I_{xz}}{I_x} C_\ell + C_n \right) \right] \Bigg/ \left[1 - \frac{I_{xz}^2}{I_x I_z} \right] \tag{D.2.19}$$

$$\dot{\theta} = q \cos\phi - r \sin\phi \tag{D.2.20}$$

$$\dot{\phi} = p + q \tan\theta \sin\phi + r \tan\theta \cos\phi \tag{D.2.21}$$

APPENDIX E

AUXILIARY VARIBLES

In order to fully utilize the computational effort expended during the numerical simulations, a number of auxiliary variables were calculated in addition to the trajectories of the state variables. Through these variables a better understanding of the behavior of the aircraft can be obtained as well as the chance to monitor and verify some possible departure or jump prediction parameters. Table E.1 shows the variables calculated as auxiliary variables and the formulae used to calculate the variables. A discussion of the significance of each of the variables follows table E.1.

TABLE E.1

$$\alpha = \tan^{-1}(w/u) \tag{E.1}$$

$$\beta = \sin^{-1}(v/V) \tag{E.2}$$

$$V = \sqrt{u^2 + v^2 + w^2} \tag{E.3}$$

$$\dot{\psi} = q \sin\phi\sec\theta + r \cos\phi\sec\theta \tag{E.4}$$

$$\text{TURNS} = \frac{1}{2\pi}\int_{t_0}^{t_f} \dot{\psi}\, dt \tag{E.5}$$

$$\psi = \psi_0 + \text{TURNS}(2\pi) \tag{E.6}$$

$$VVI = u \sin\theta - (v \sin\phi + w \cos\phi)\cos\theta, \tag{E.7}$$

$$h = h_0 - \int_{t_j}^{t_f} VVI \, dt \tag{E.8}$$

$$E = \tfrac{1}{2} mV^2 + \tfrac{1}{2} \underline{\omega} \cdot \underline{I} \cdot \underline{\omega} \tag{E.9}$$

$$\dot{E} = mV\dot{V} + I_x p\dot{p} + I_y q\dot{q} + I_z r\dot{r} + (r\dot{p} + p\dot{r})I_{xz} \tag{E.10}$$

where

$$\dot{V} = (u\dot{u} + v\dot{v} + w\dot{w})/V \tag{E.11}$$

if the body-axis velocity set is used

$$\omega = \sqrt{p^2 + q^2 + r^2} \tag{E.12}$$

$$D_{SPIN} = \left[\sum_{i=1}^{n} \left[\frac{x_i - x_{s_i}}{} \right]^2 \right]^{\frac{1}{2}} \tag{E.13}$$

$$E_s = \tfrac{1}{2} I_v \dot{\psi}^2/(\bar{q}Sb) \tag{E.14}$$

where

$$I_v = \sin^2\theta I_x + (\sin^2\phi I_y + \cos^2\phi I_z)\cos^2\theta + I_{xz}\cos\phi\sin 2\theta \tag{E.15}$$

when Ixy=Iyz=0

The wind axis variables (alpha, beta and total velocity) are calculated to provide direct verification of the results of BACTM computer runs. The heading variable, , is calculated so that an aircraft's horizontal trajectory during a spin can be calculated.

It is also used in the calculation of the variable, Turns, which is the number of rotations that have occurred during a spin. This value is of interest since spin recovery techniques are often evaluated by the number of turns that occur between the setting of the spin recovery controls and the actual recovery from the spin. Aircraft vertical velocity, VVI, and altitude, h, are calculated to allow altitude to vary during the simulation if desired and to determine sink rates during stalled and near stall flight. Vehicle kinetic energy, E, and rate of change of kinetic energy, $\dot{E}$, are calculated to help develop possible techniques to monitor and predict nonlinear jump behavior. Dspin is a measurement of the distance that the current state is from a known spin condition, and spin energy, Es, is a measurement of the kinetic energy due to the spin motion of the aircraft alone. These last two terms are used to measure the relative effectiveness of different spin recovery control strategies.

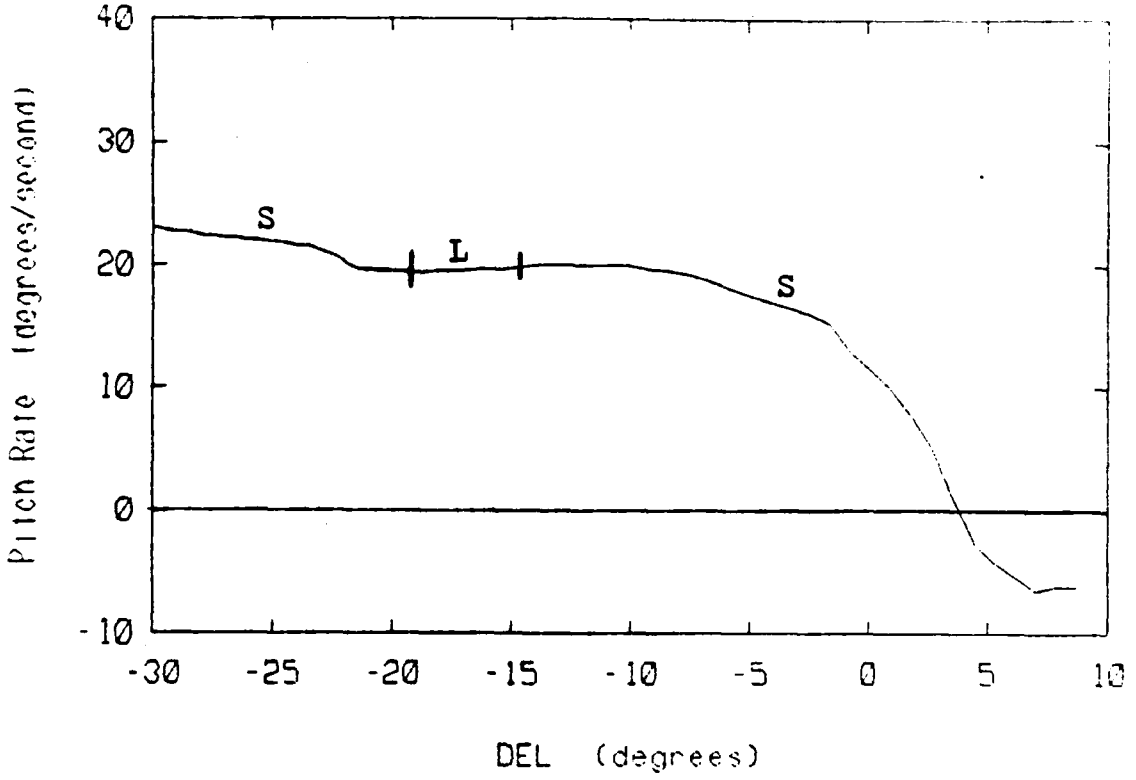

Fig. 7.1a: Pitch Rate vs. Stabilator

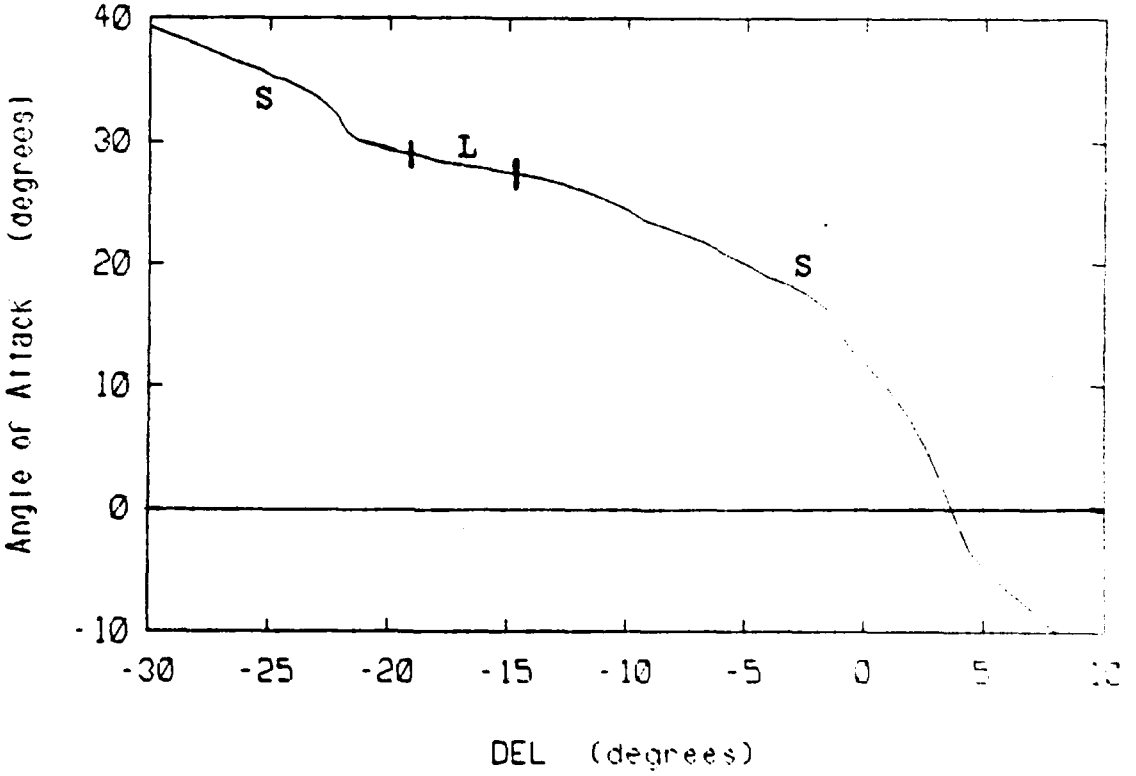

Fig. 7.1b: Angle of Attack vs. Stabilator
V=500 f/s; g=0; DAI=DRU=0

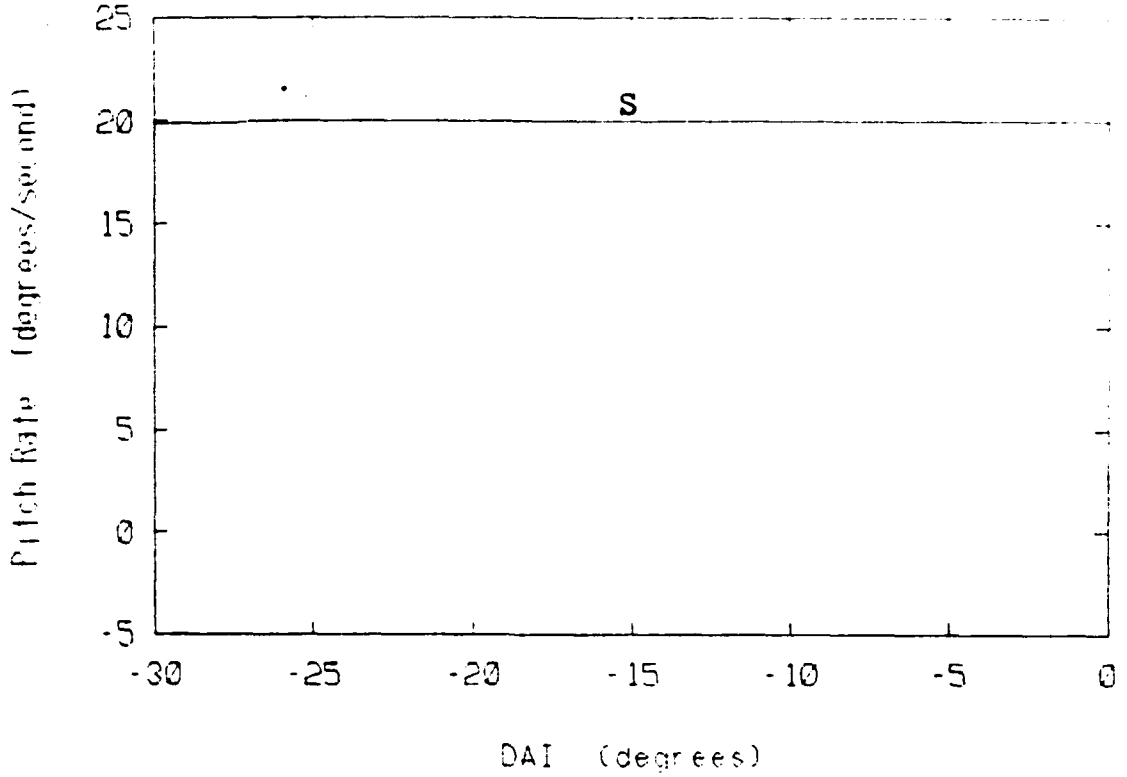

Fig. 7.2a: Pitch Rate vs. Aileron

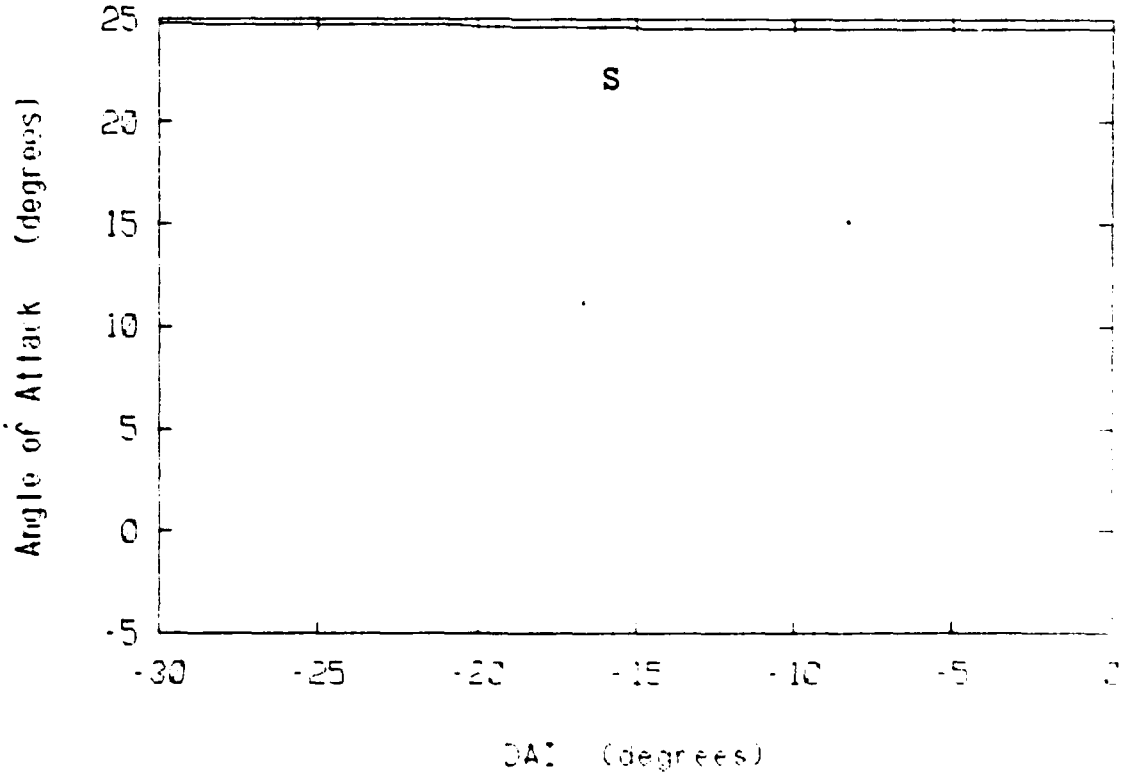

Fig. 7.2b: Angle of Attack vs. Aileron
V=500 f/s; g=0; DEL=-10.16; DRU=0

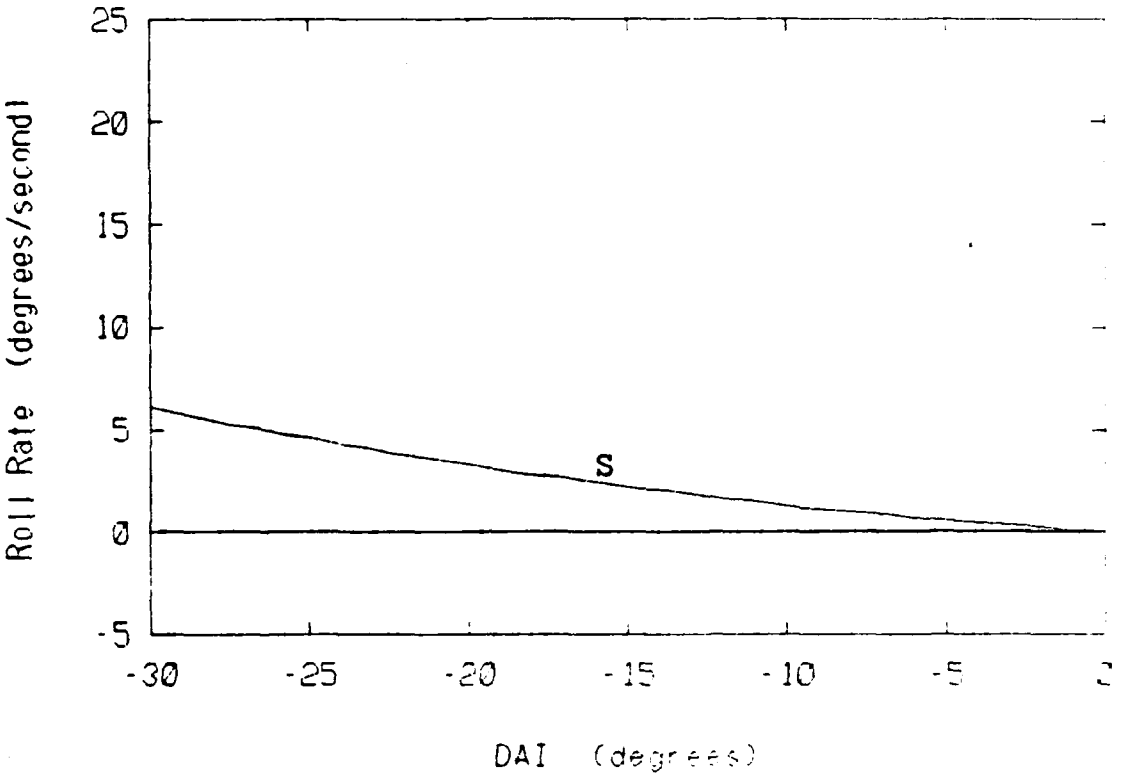

Fig. 7.2c: Roll Rate vs. Aileron

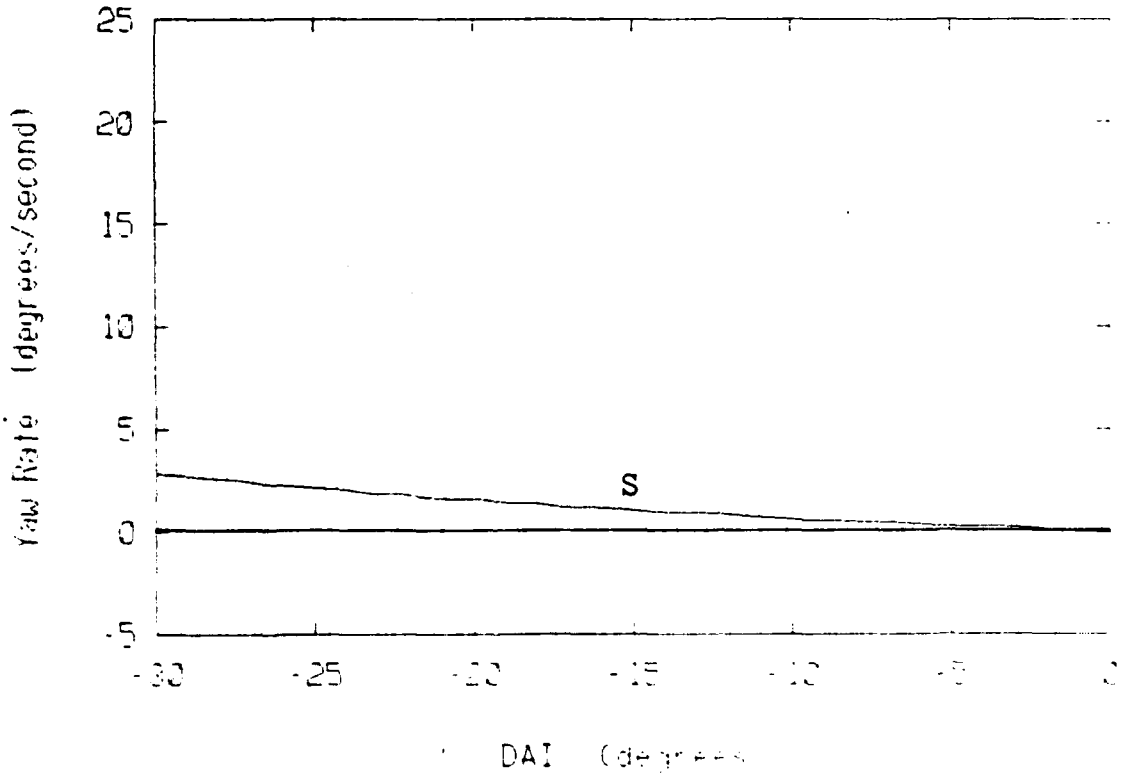

Fig. 7.2d: Yaw Rate vs. Aileron
V=500 f/s; g=0; DEL=-10.16; DRU=0

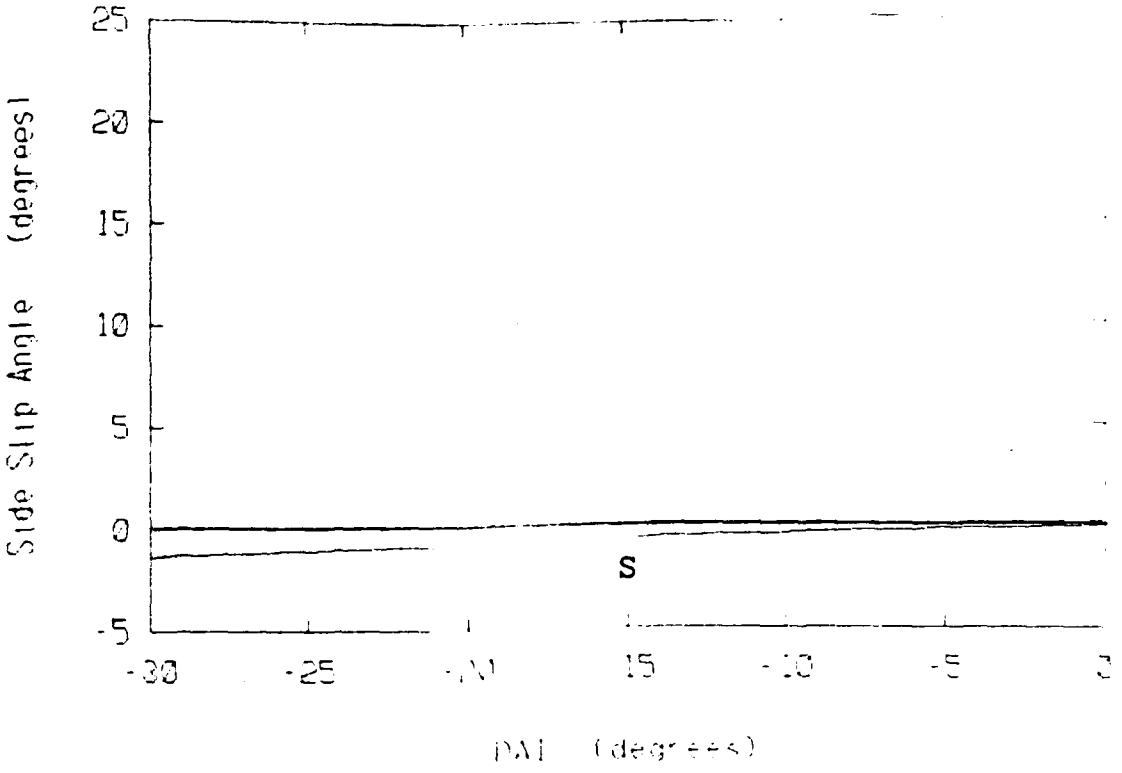

Fig. 7.2e: Side Slip Angle vs. Aileron

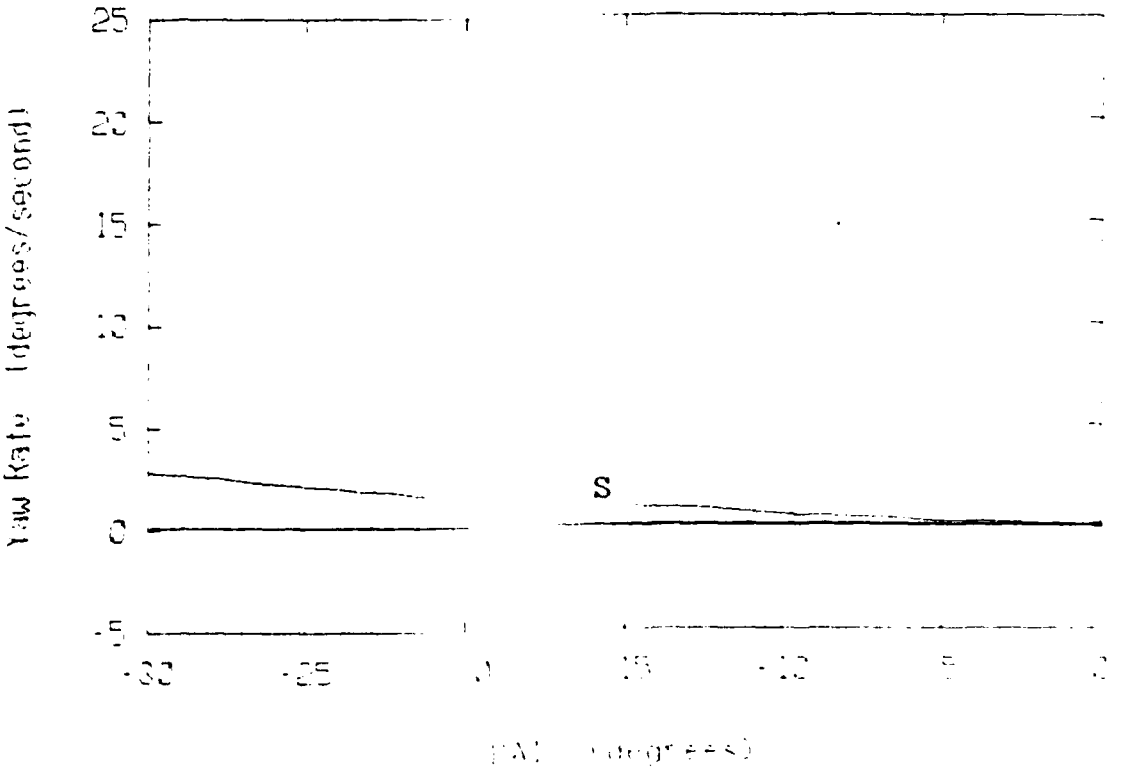

Fig. 7.2d: Yaw Rate vs. Aileron
V=500 f/s; [illegible]=0; DEL=-10.16; DRU=0

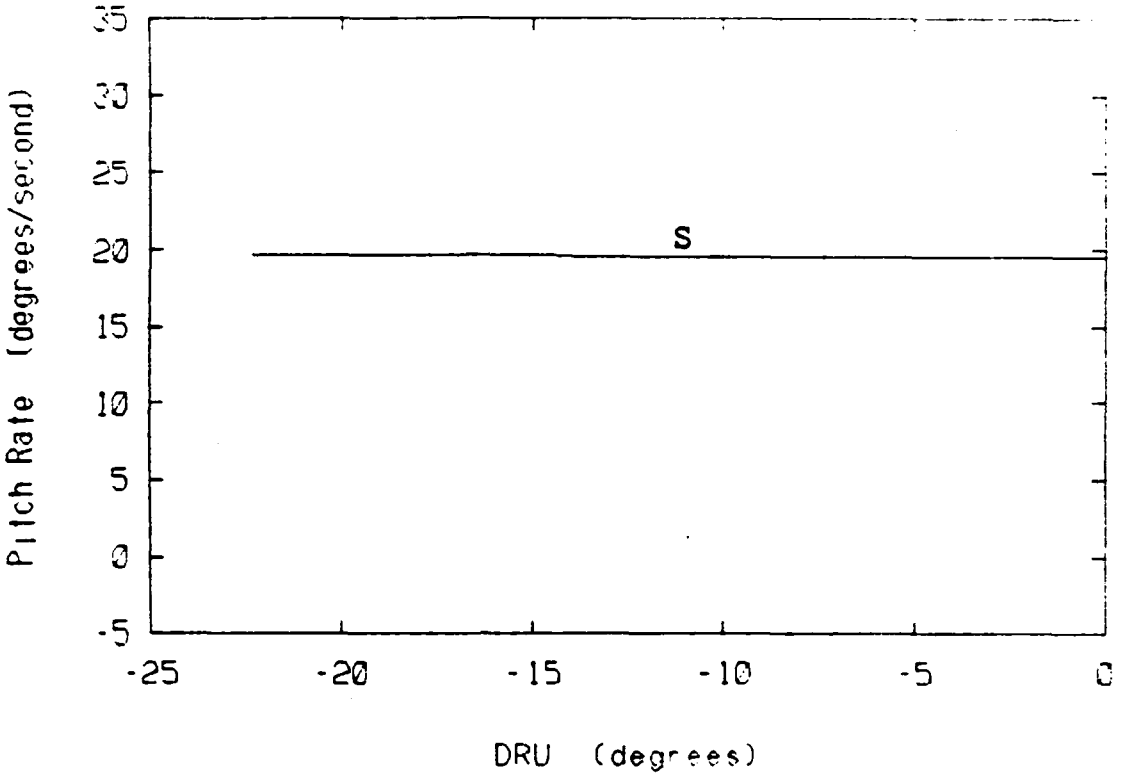

Fig. 7.3a: Pitch Rate vs. Rudder

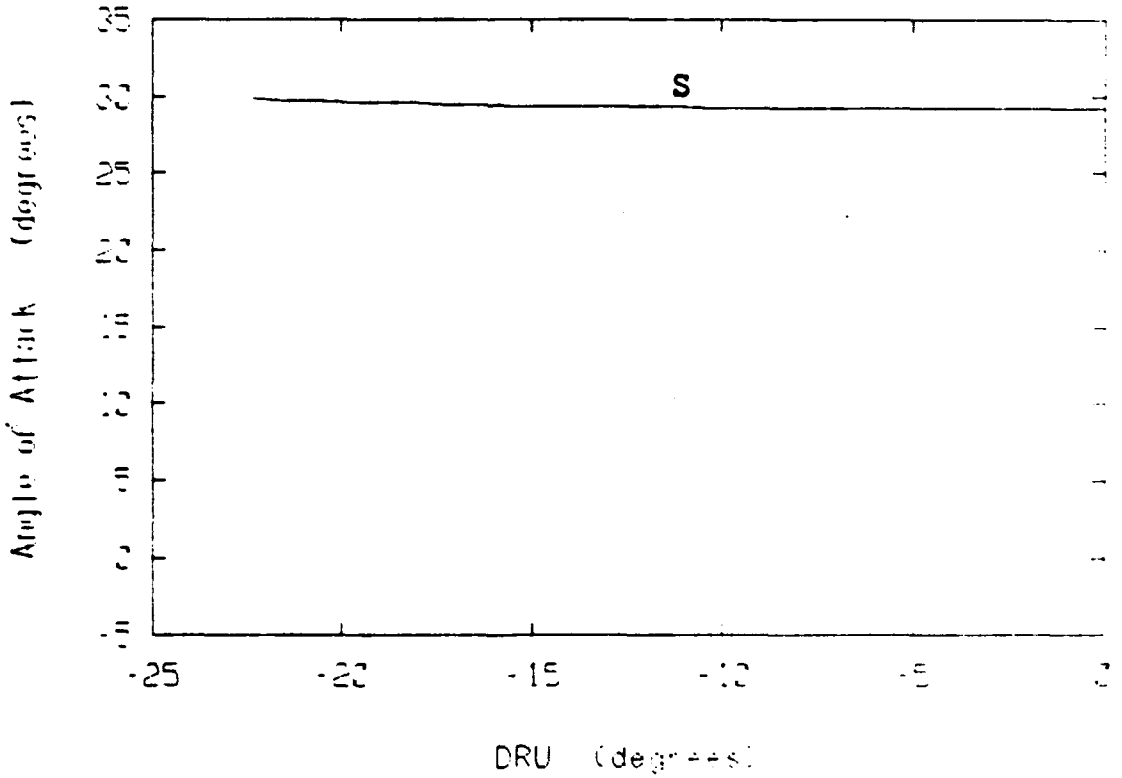

Fig. 7.3b: Angle of Attack vs. Rudder
V=500 f/s; g=0; DAI=0; DEL=-19.61

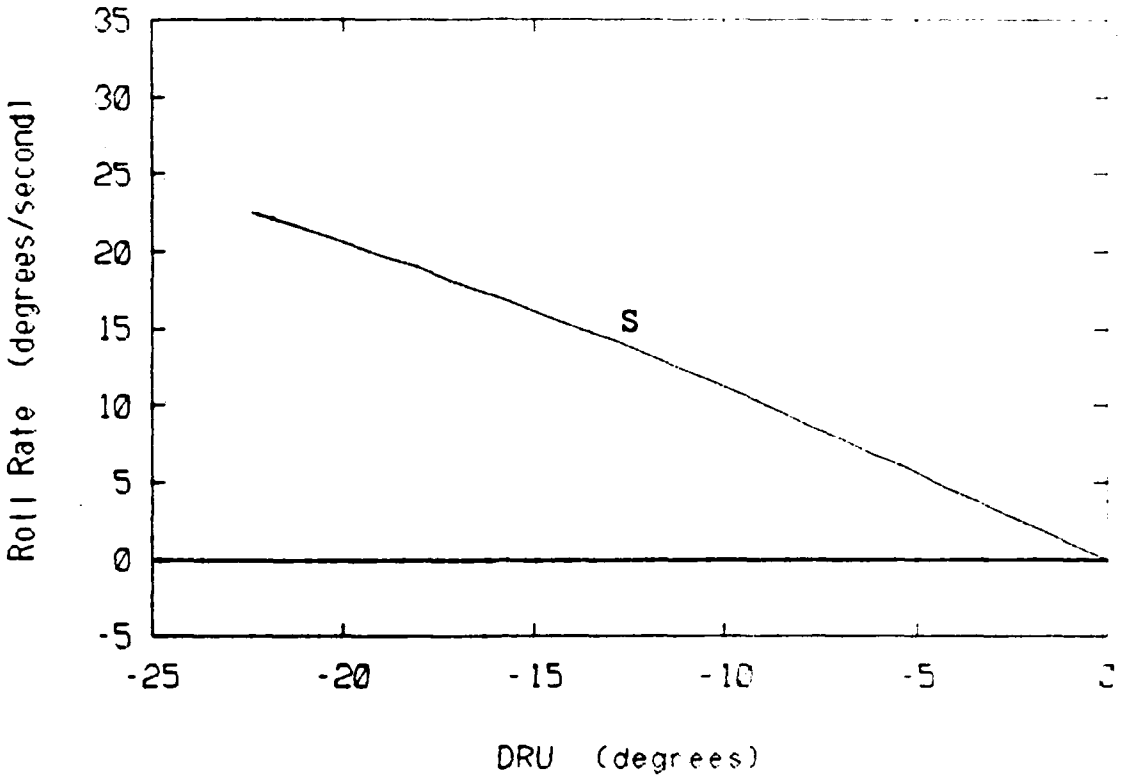

Fig. 7.3c: Roll Rate vs. Rudder

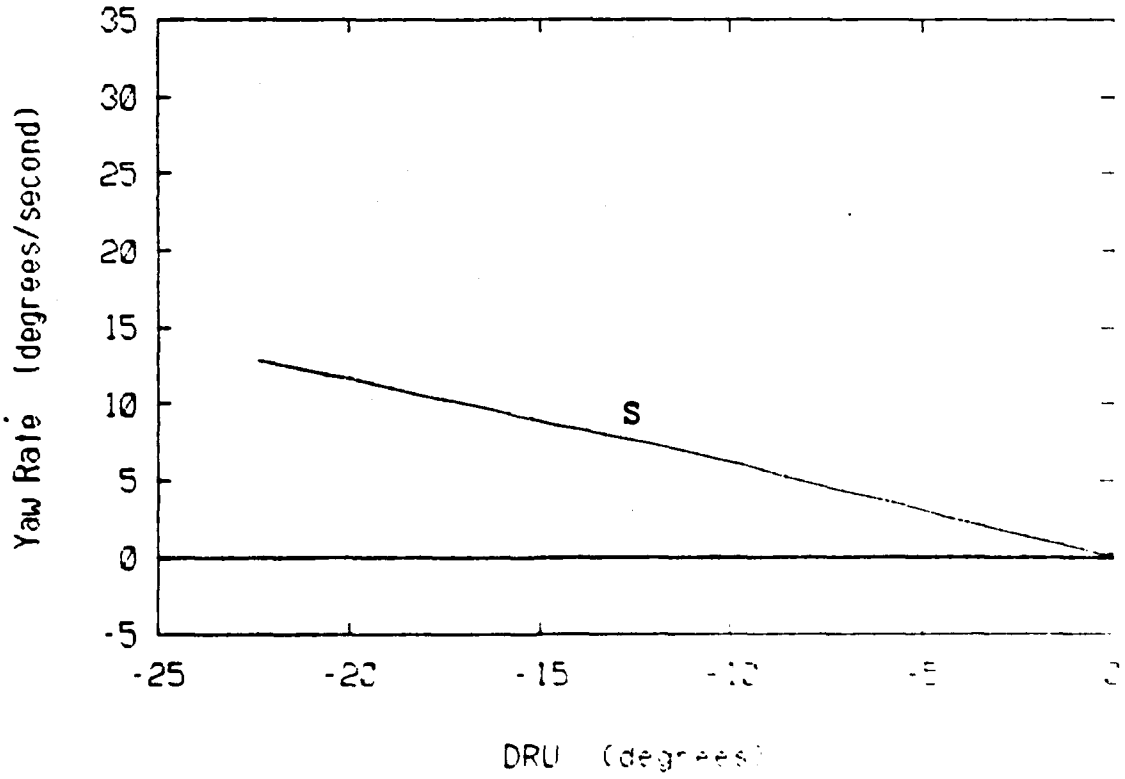

Fig. 7.3d: Yaw Rate vs. Rudder
V=500 f/s; g=0; DAI=0; DEL=-19.61

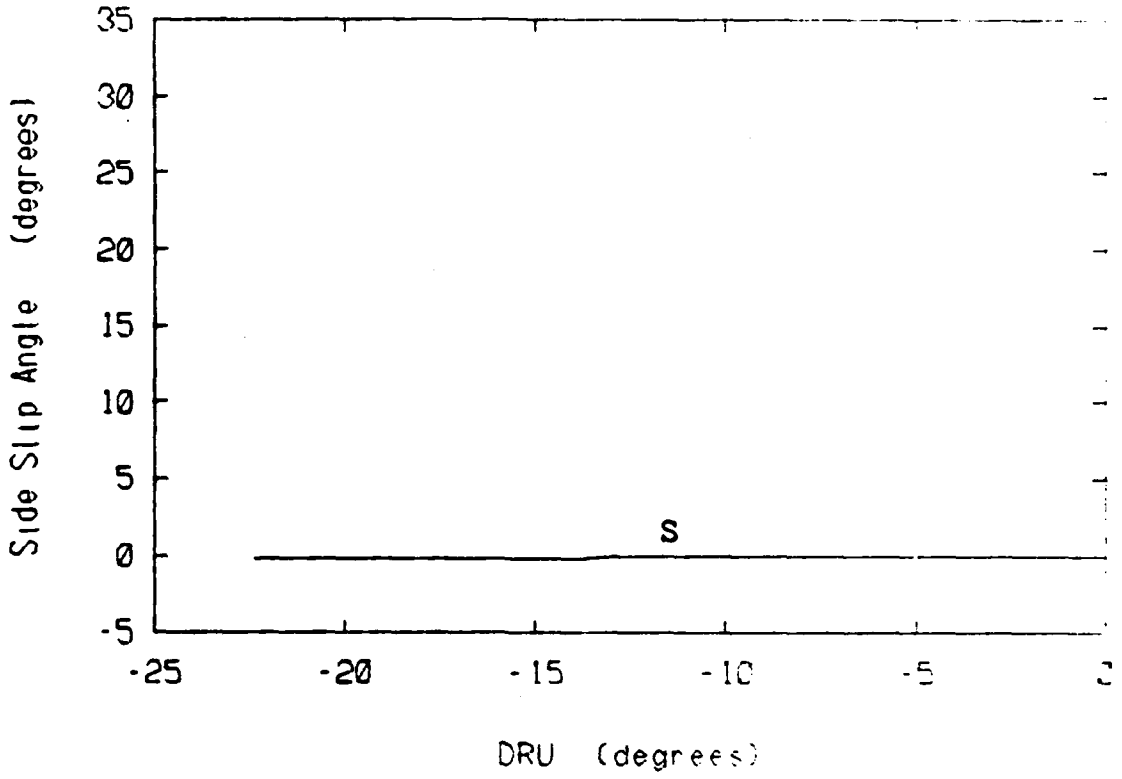

Fig. 7.3e: Side Slip Angle vs. Rudder

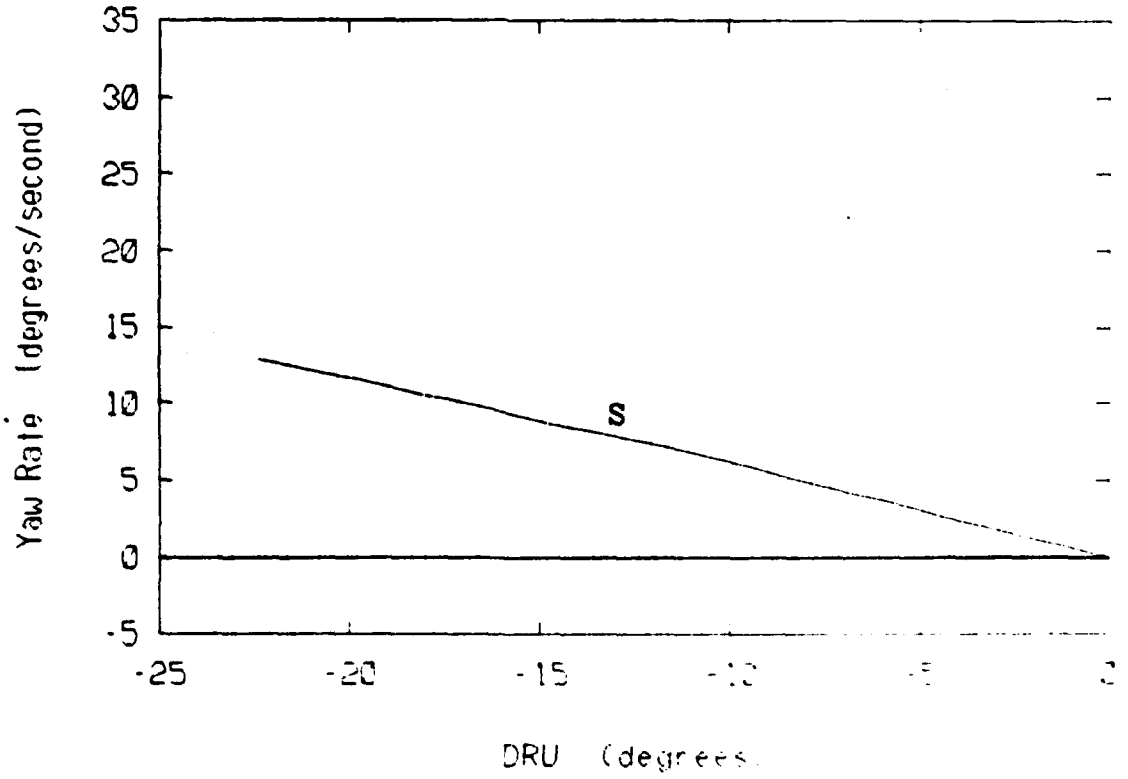

Fig. 7.3d: Yaw Rate vs. Rudder
V=500 f/s; g=0; DAI=0; DEL=-19.61

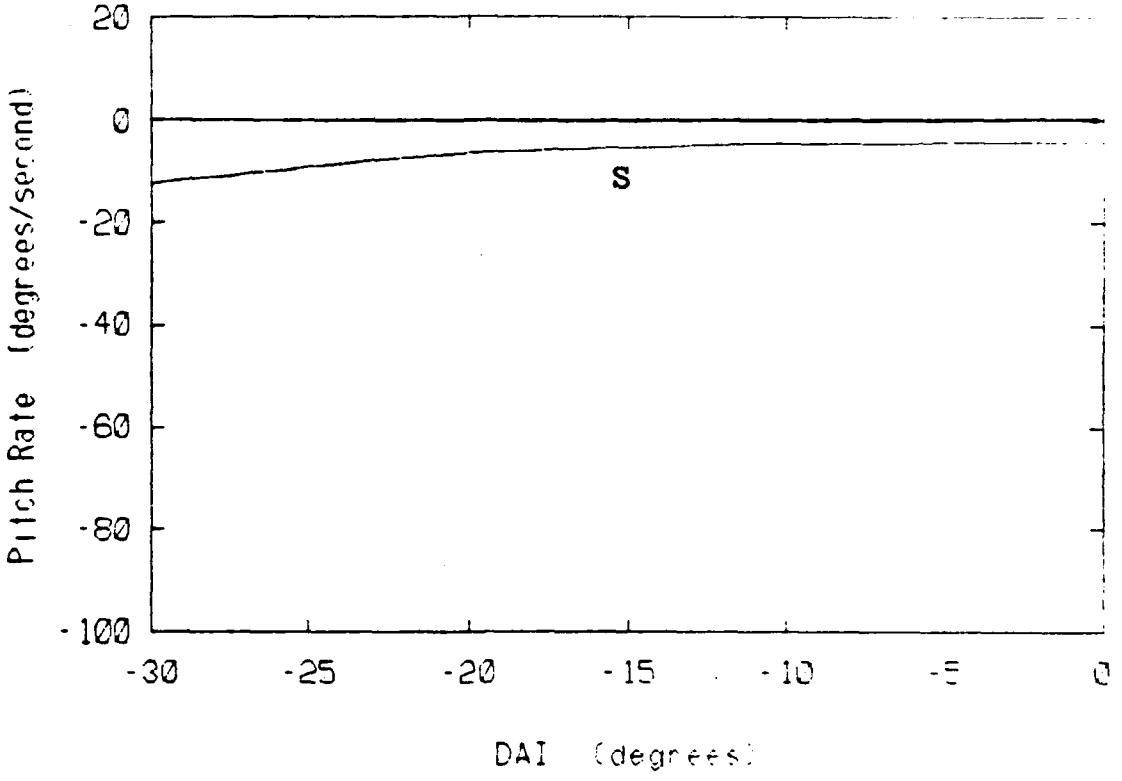

Fig. 7.4a: Pitch Rate vs. Aileron

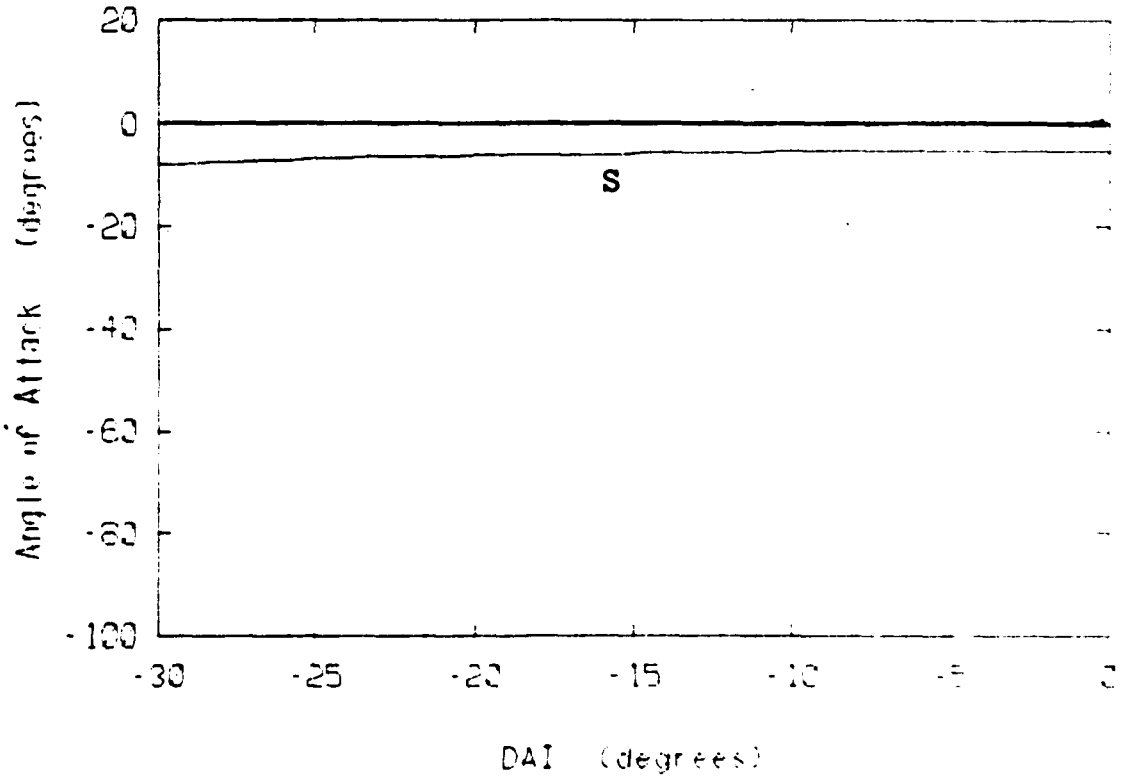

Fig. 7.4b: Angle of Attack vs. Aileron
V=500 f/s; g=0; DEL=5.31; DRU=0

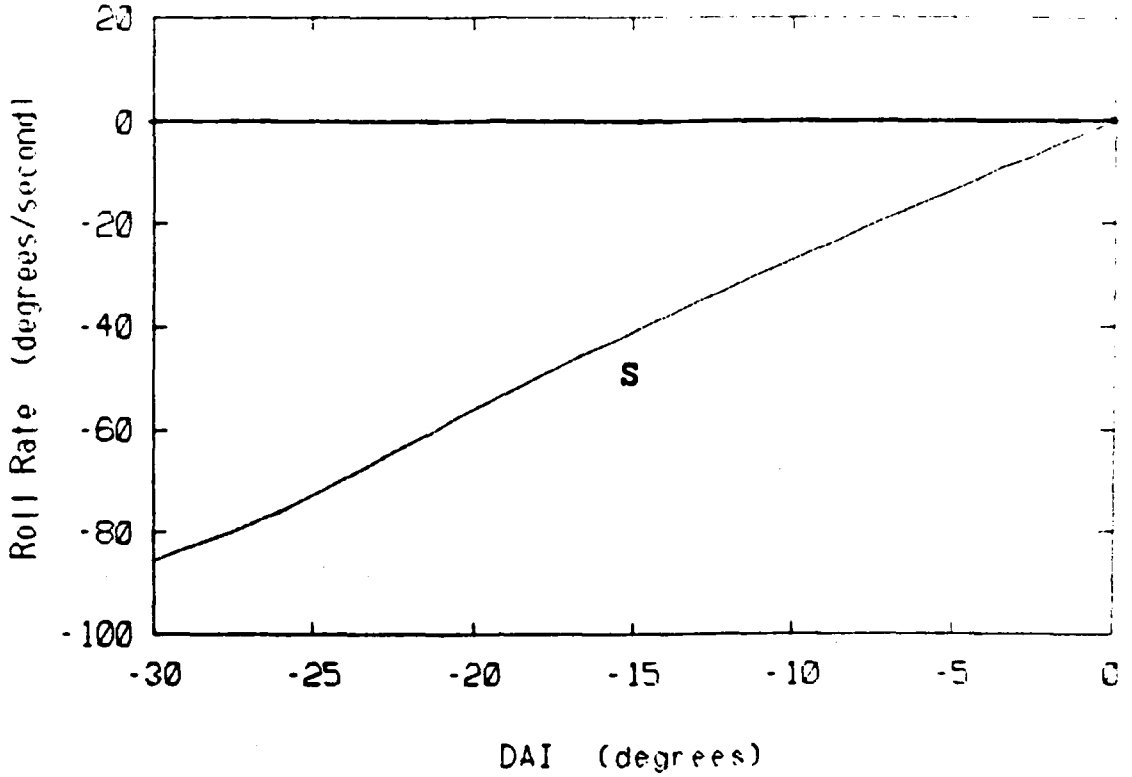

Fig. 7.4c: Roll Rate vs. Aileron

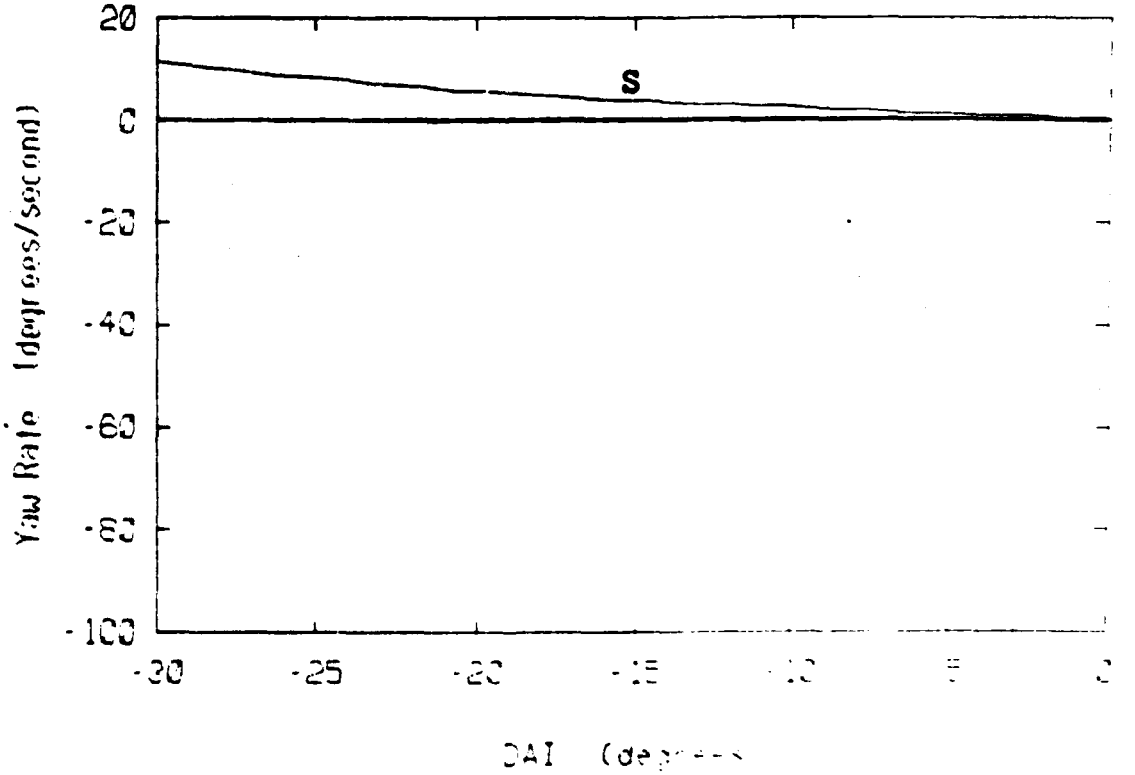

Fig. 7.4d: Yaw Rate vs. Aileron
V=500 f/s; g=0; DEL=5.31; DRU=0

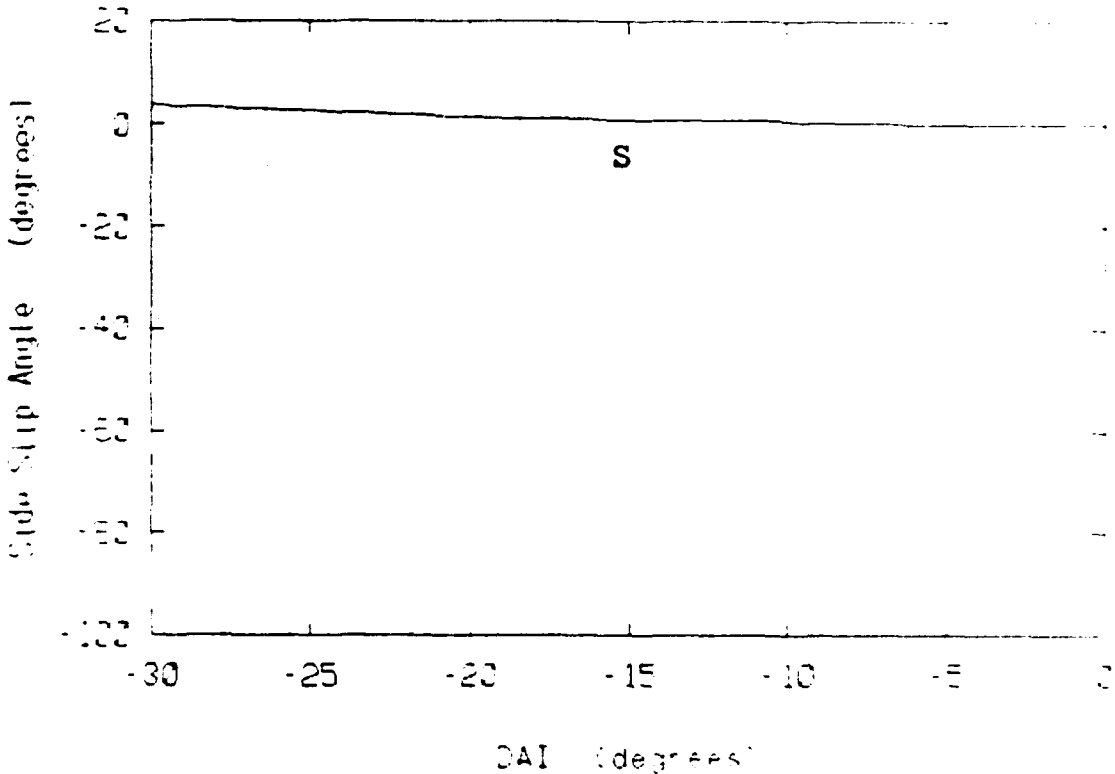

Fig. 7.4e: Side Slip Angle vs. Aileron

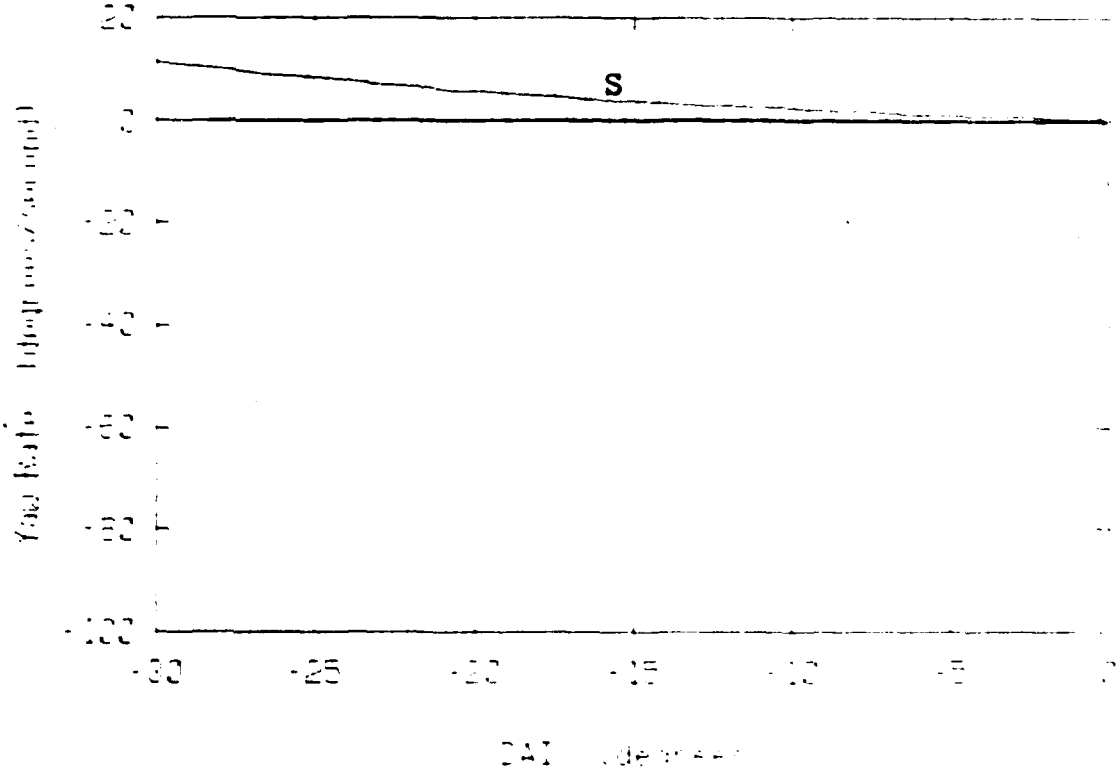

Fig. 7.4d: Yaw Rate vs. Aileron
V=500 f/s; g=0; DEL=5.31; DRU=0

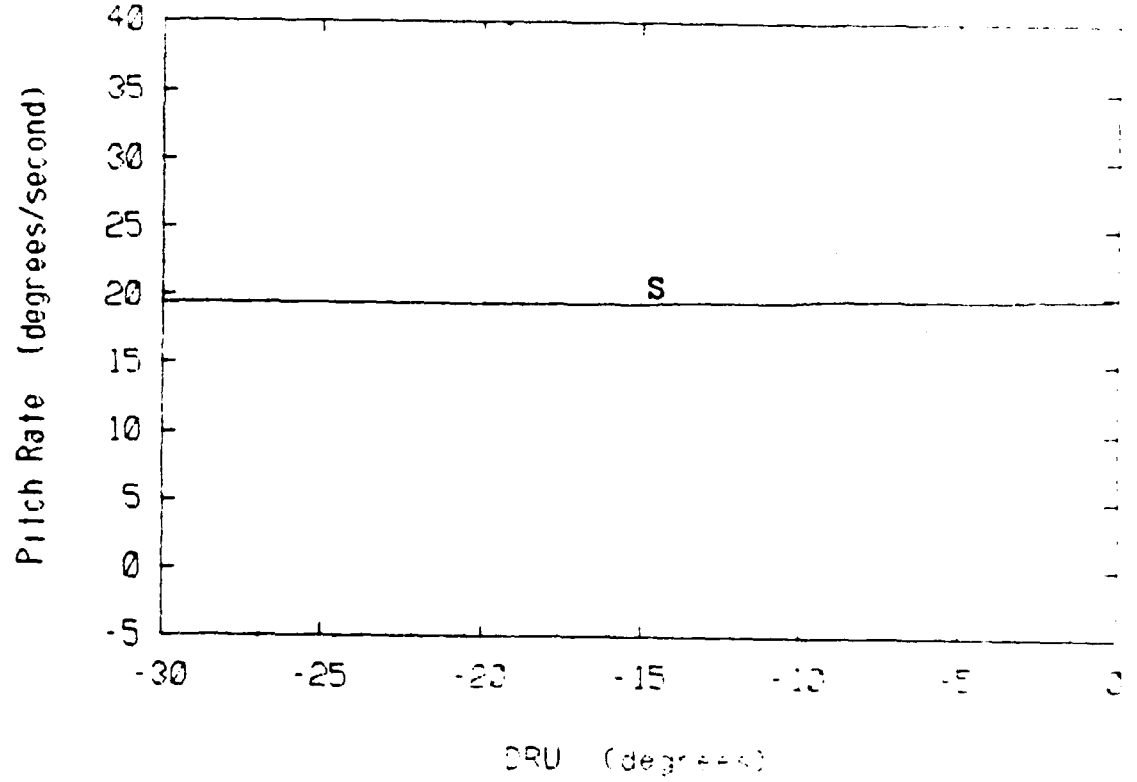

Fig. 7.5a: Pitch Rate vs. Rudder

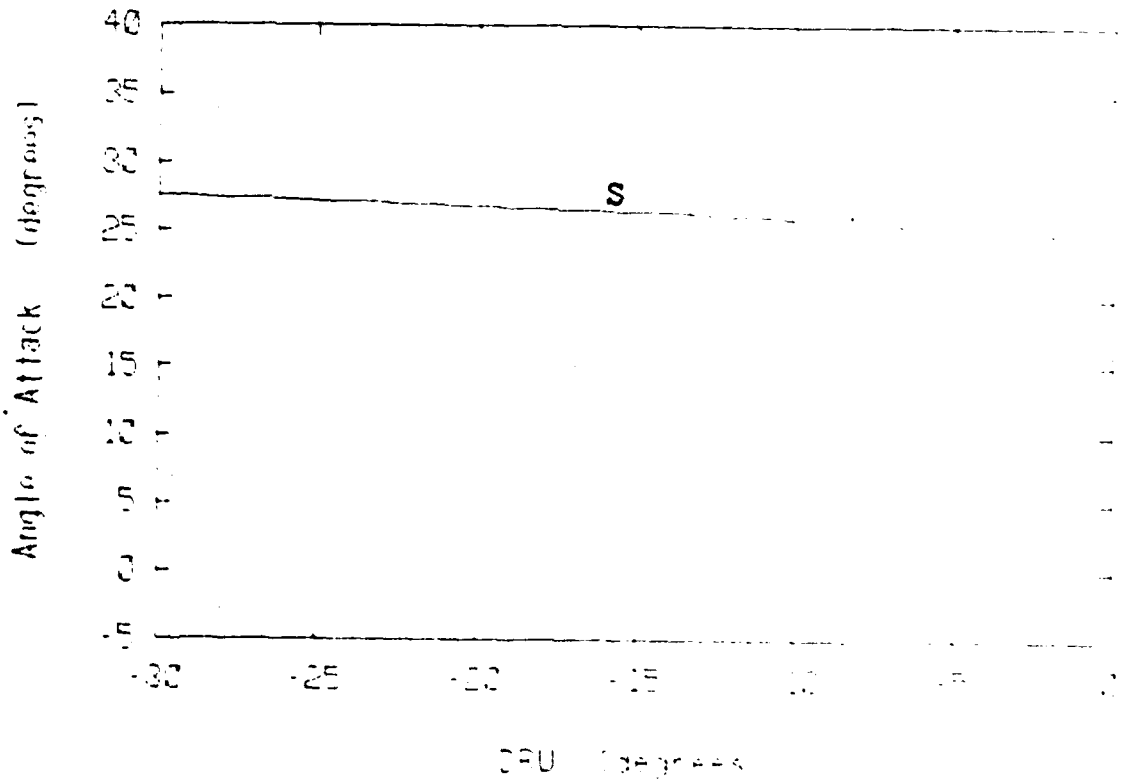

Fig. 7.5b: Angle of Attack vs. Rudder
V=500 f/s; g=0; DAI=-29.22; DEL=-10.16

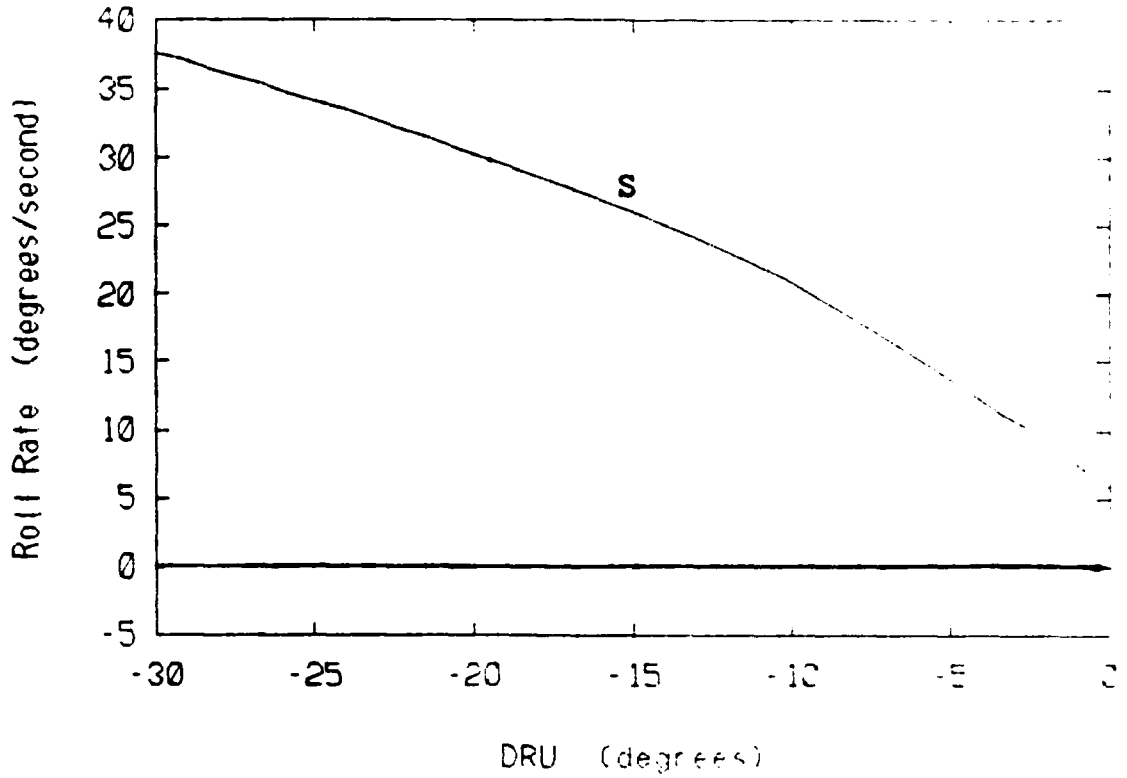

Fig.7.5c: Roll Rate vs. Rudder

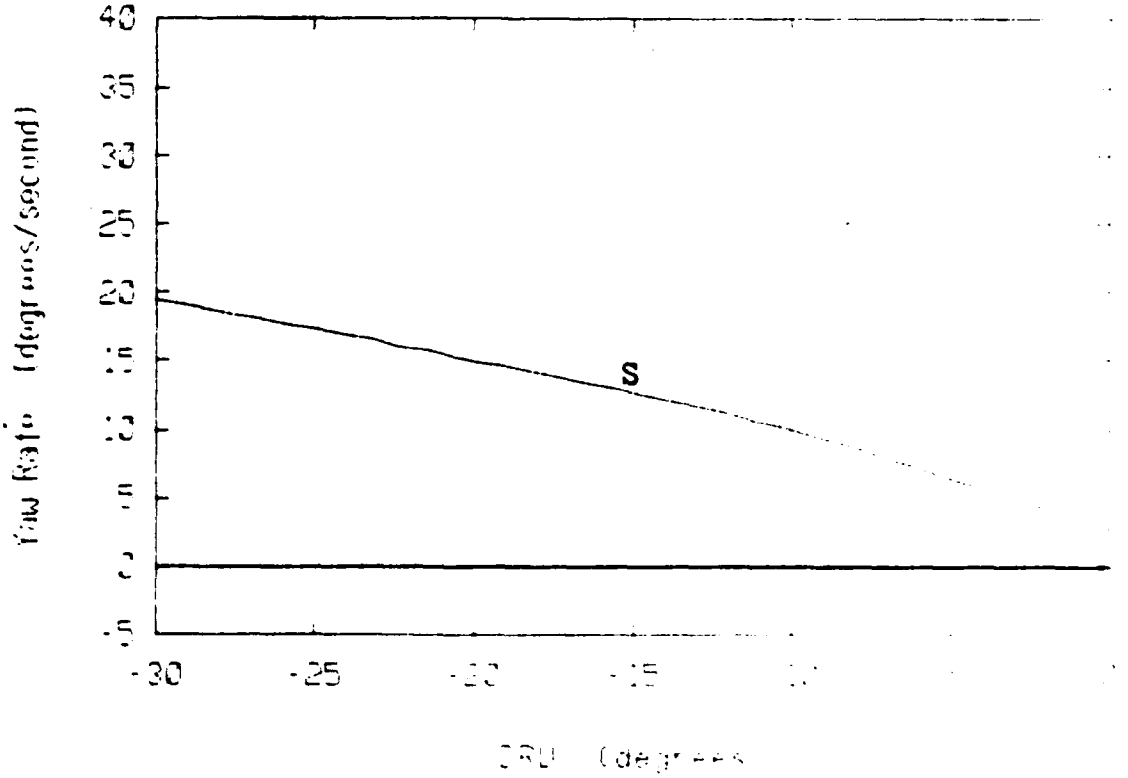

Fig. 7.5d: Yaw Rate vs. Rudder
V=500 f/s; g=0; DAI=-29.22; DEL=-10.16

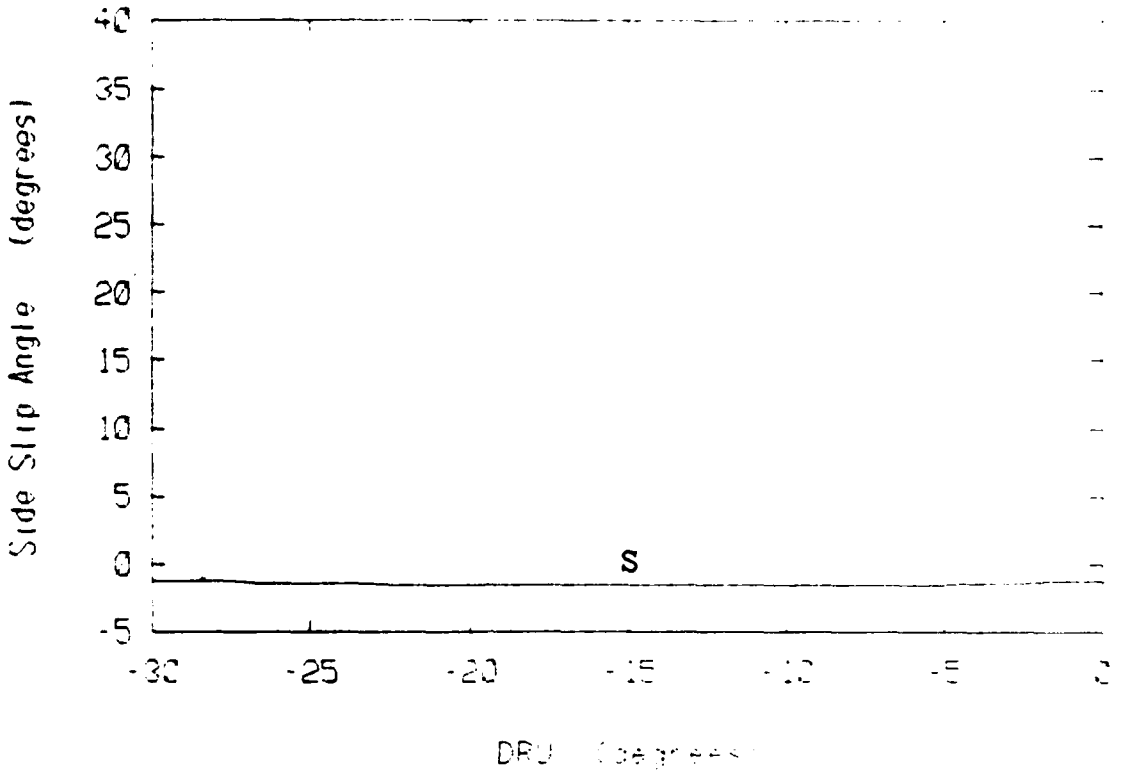

Fig. 7.5e: Side Slip Angle vs. Rudder

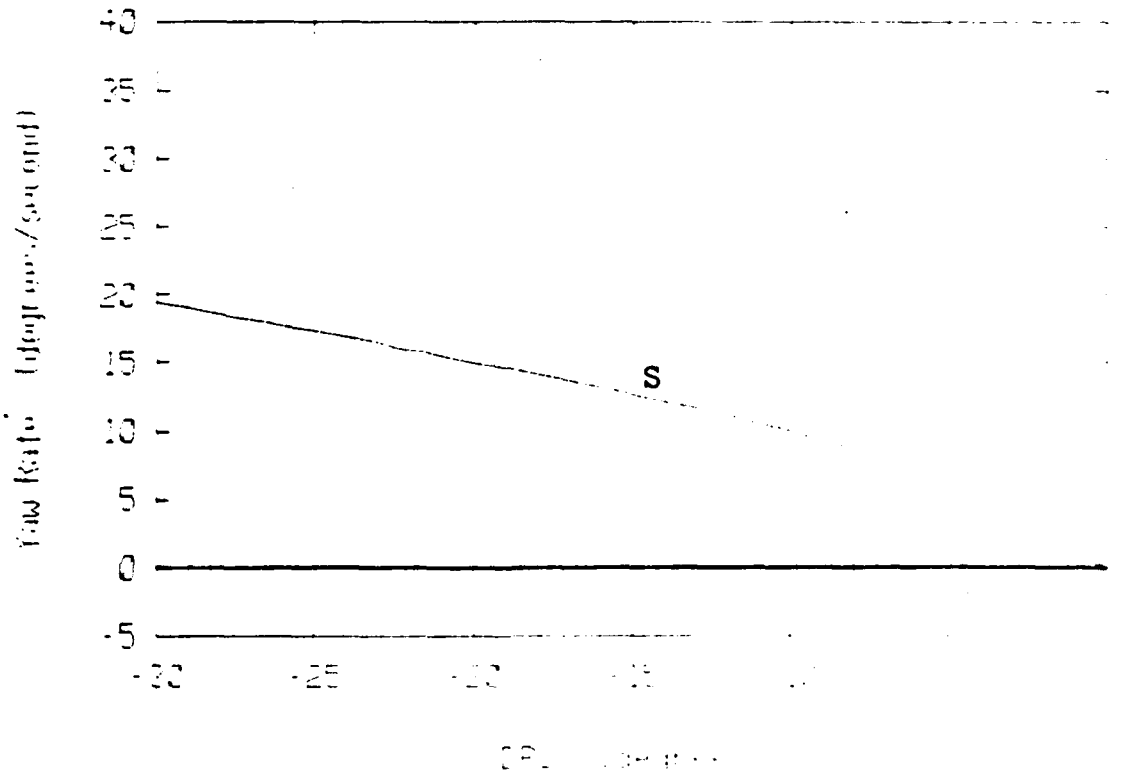

Fig. 7.5d: Yaw Rate vs. Rudder
V=500 f/s; g=0; DAI=-29.22; DEI=-10.16

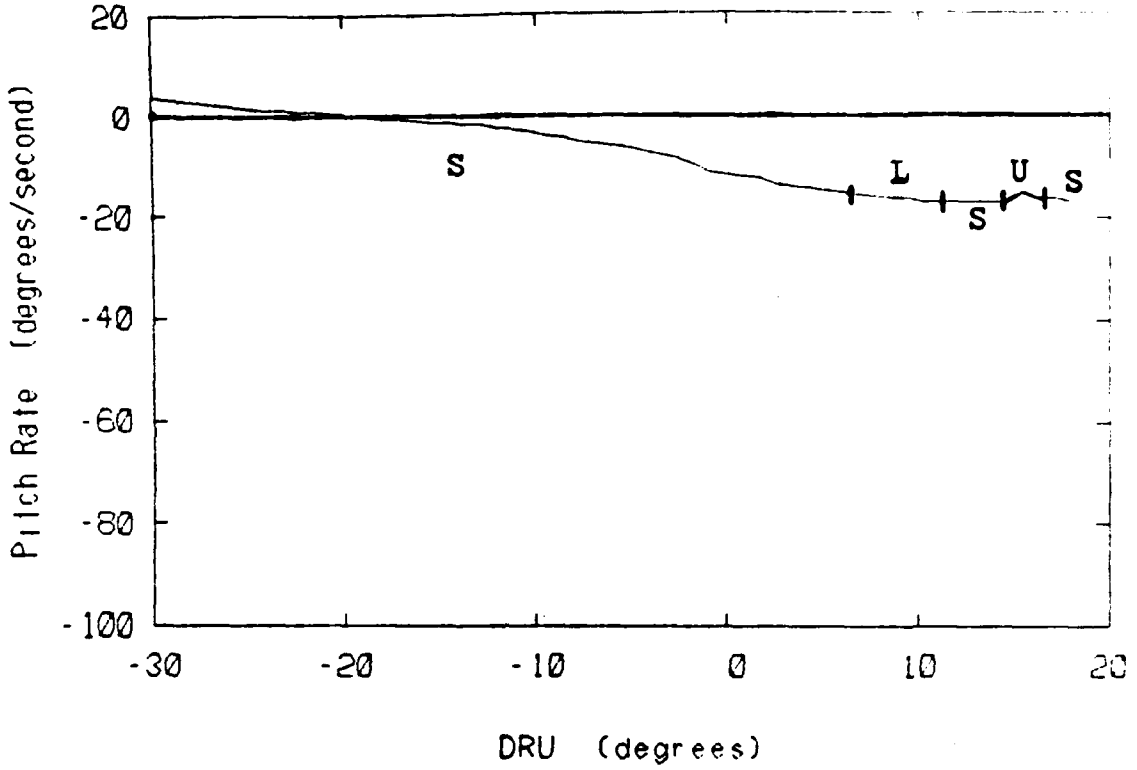

Fig. 7.6a: Pitch Rate vs. Rudder

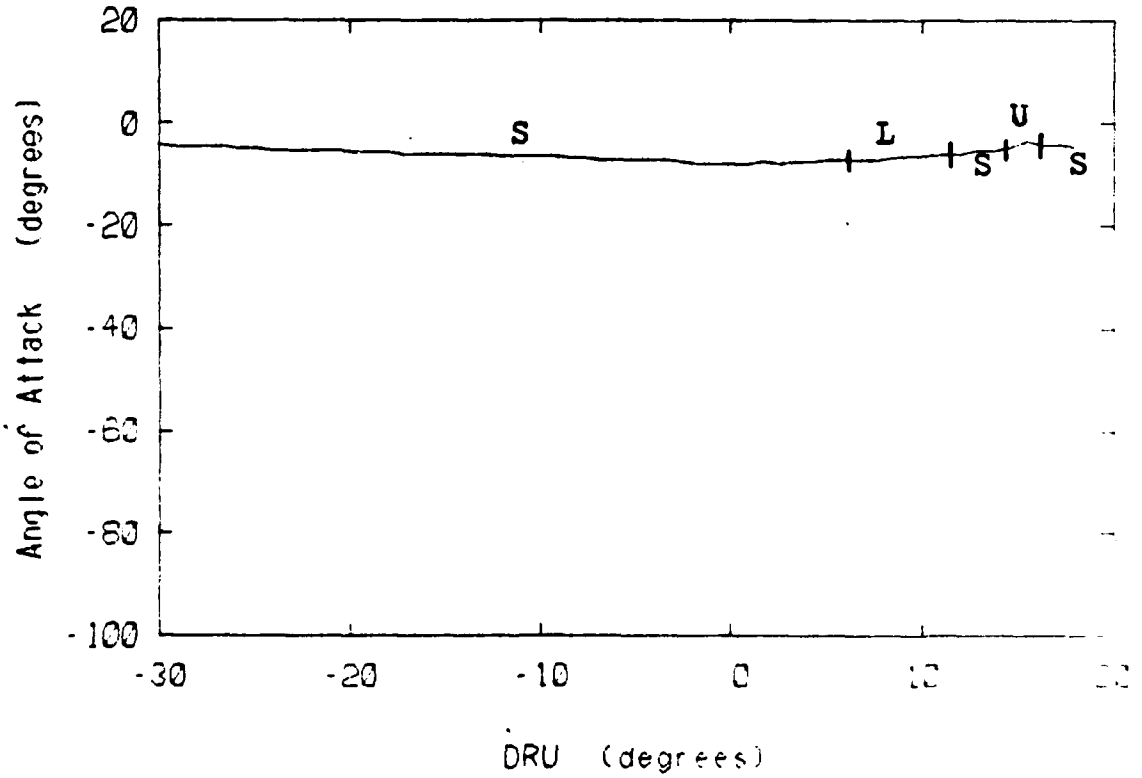

Fig. 7.6b: Angle of Attack vs. Rudder
V=500 f/s; g=0; DAI=-29.22; DEL=5.31

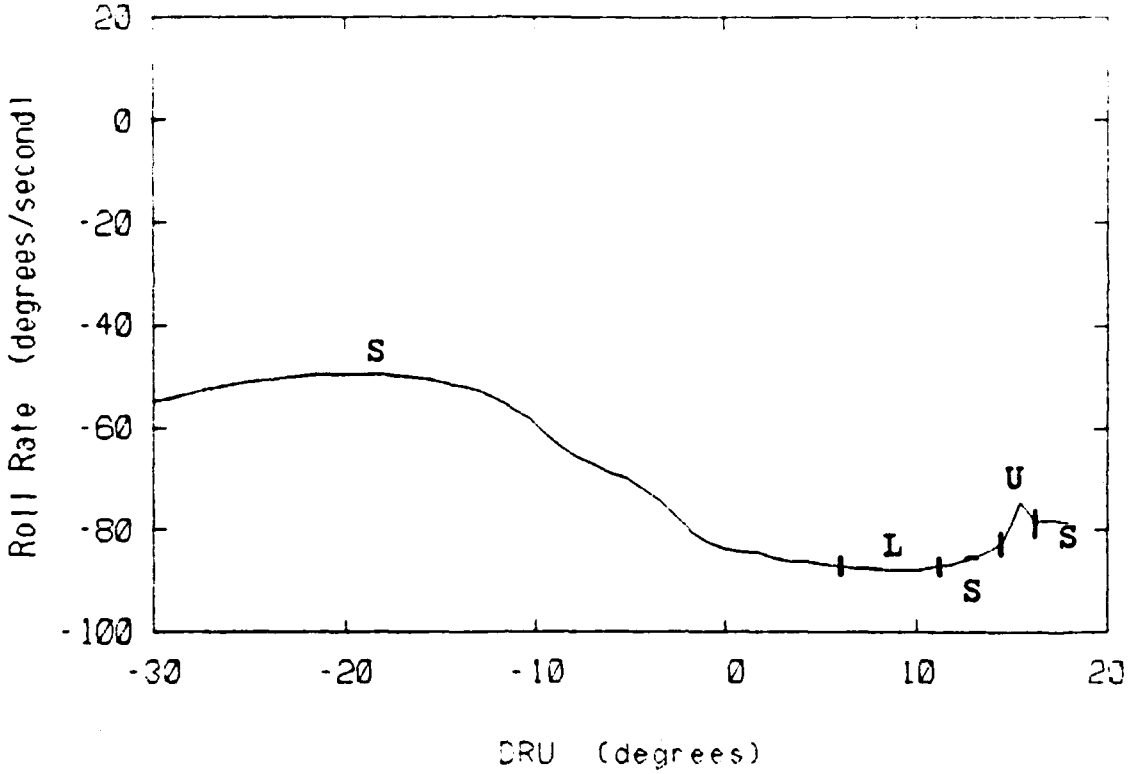

Fig. 7.6c: Roll Rate vs. Rudder

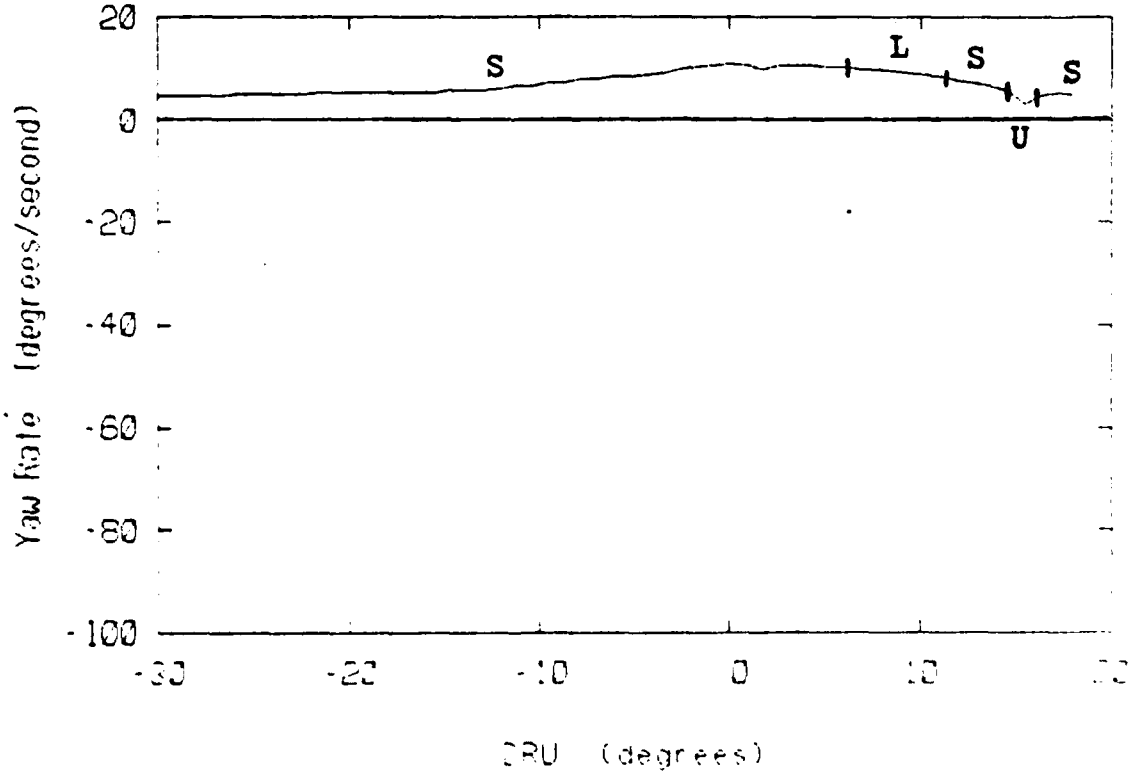

Fig. 7.6d: Yaw Rate vs. Rudder
V=500 f/s; g=0; DAI=-29.22; DEL= 5.31

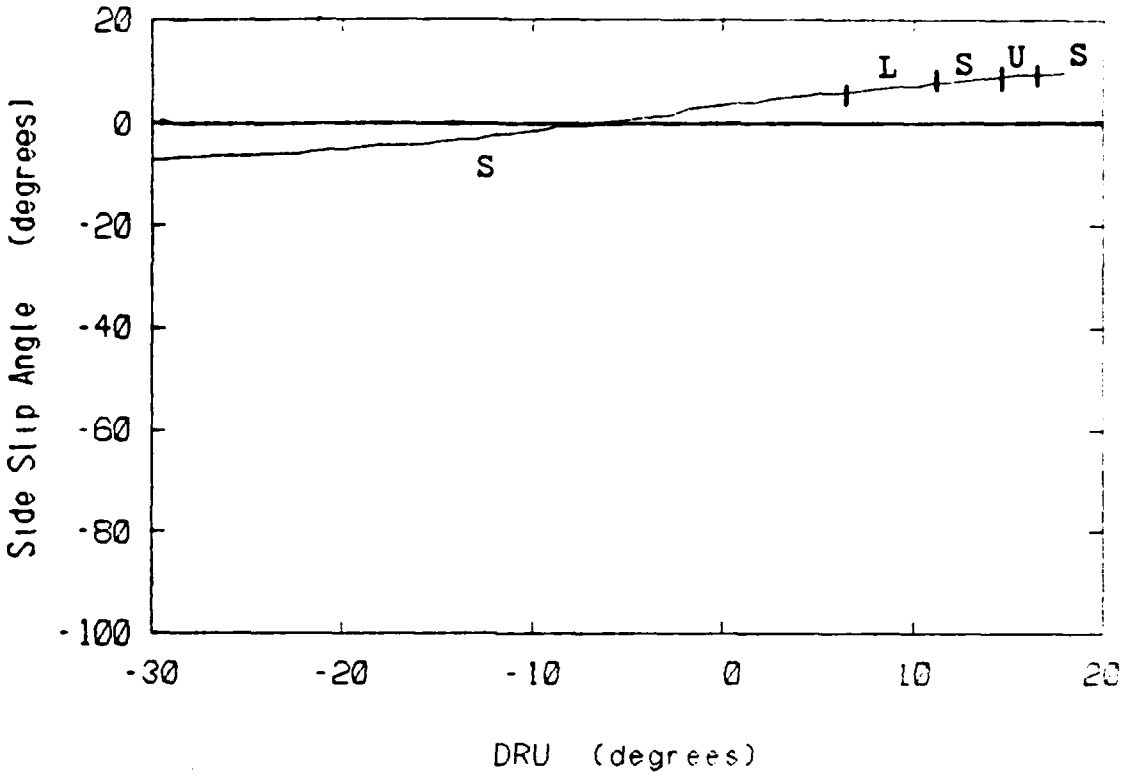

Fig. 7.6e: Side Slip Angle vs. Rudder

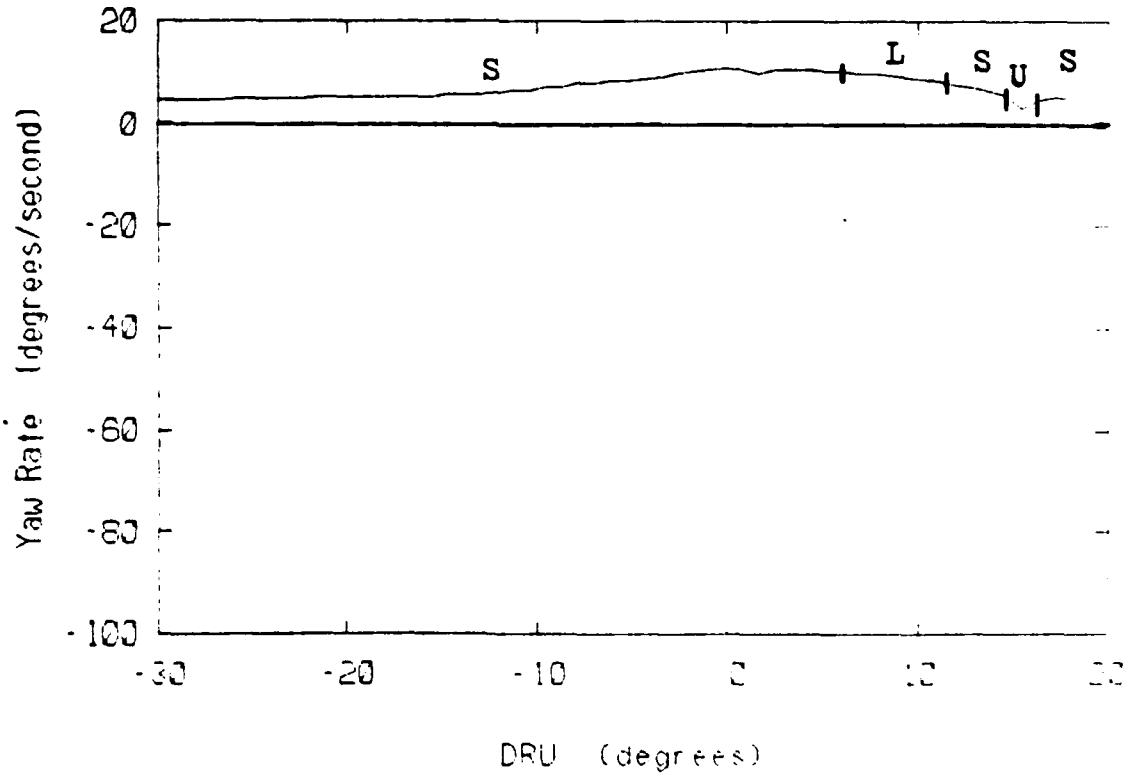

Fig. 7.6d: Yaw Rate vs. Rudder
V=500 f/s; g=0; DAI=-29.22; DEL=5.31

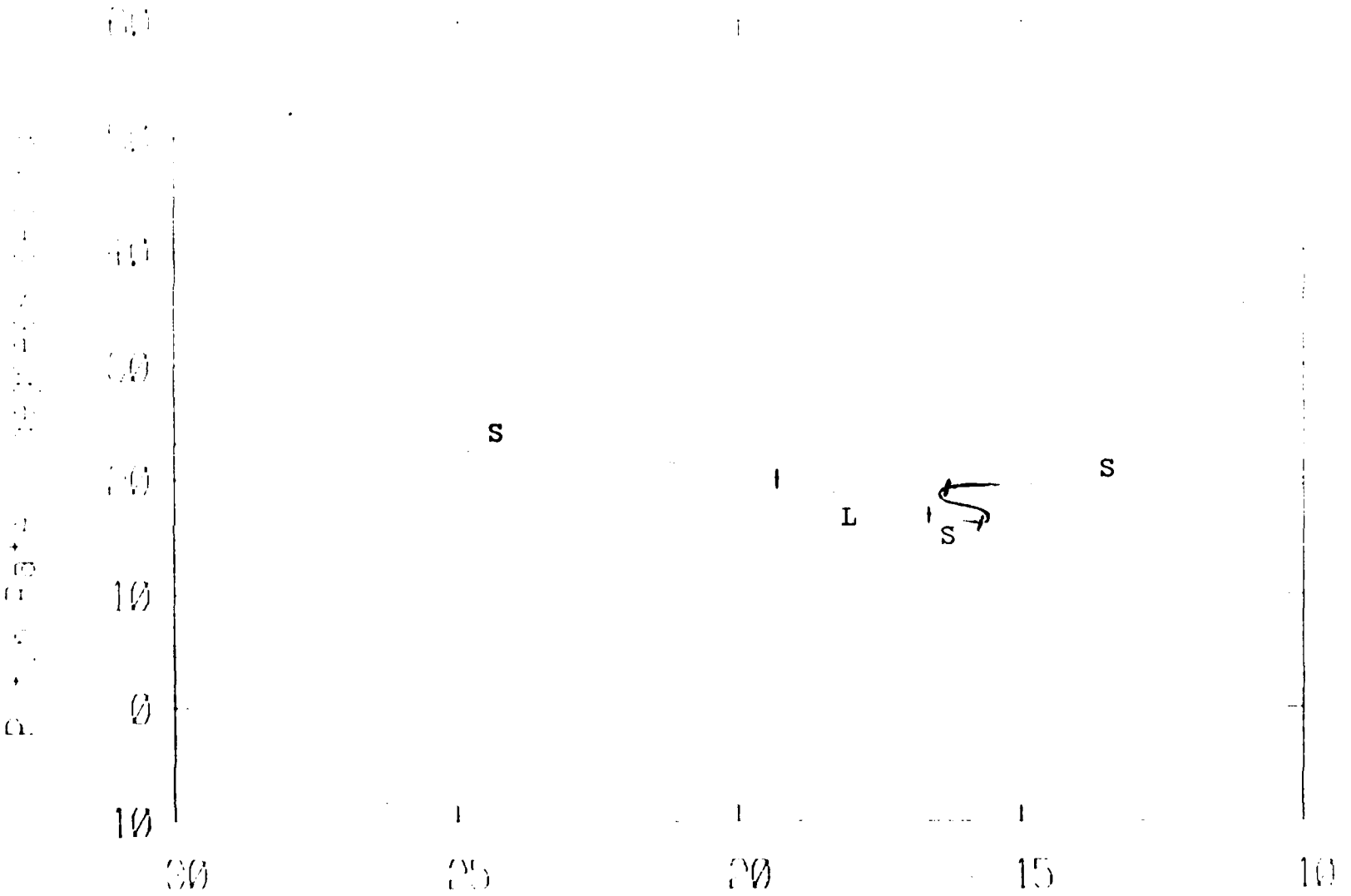

Fig. 7.7a: Pitch Rate vs. Stabilator
V=500 f/s; g=0; DAI=-29.22; DRU=-29.22

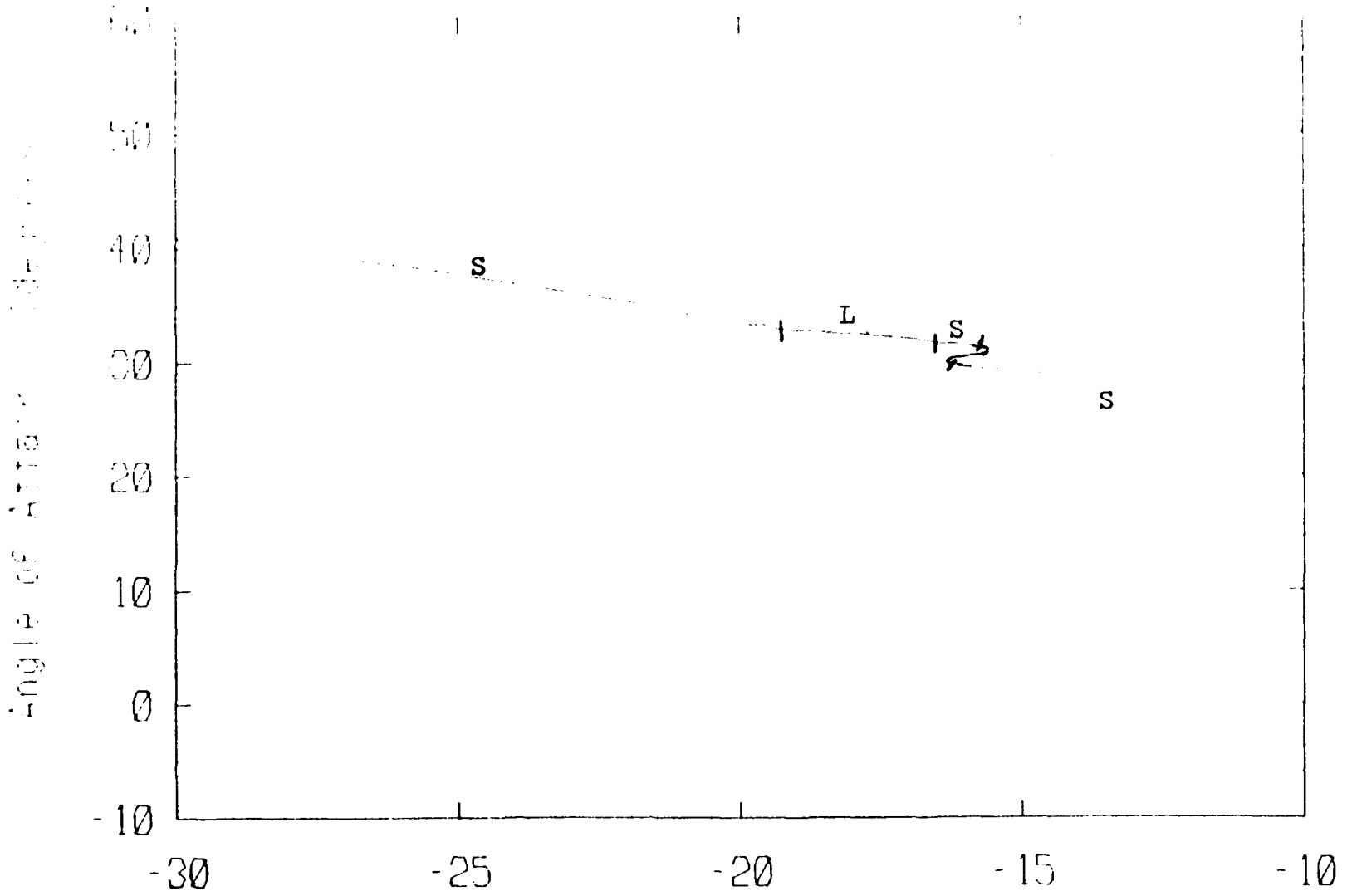

Fig. 7.7b; Angle of Attack vs. Stabilator
V=500 f/s; g=0; DAI=-29.22; DRU=-29.22

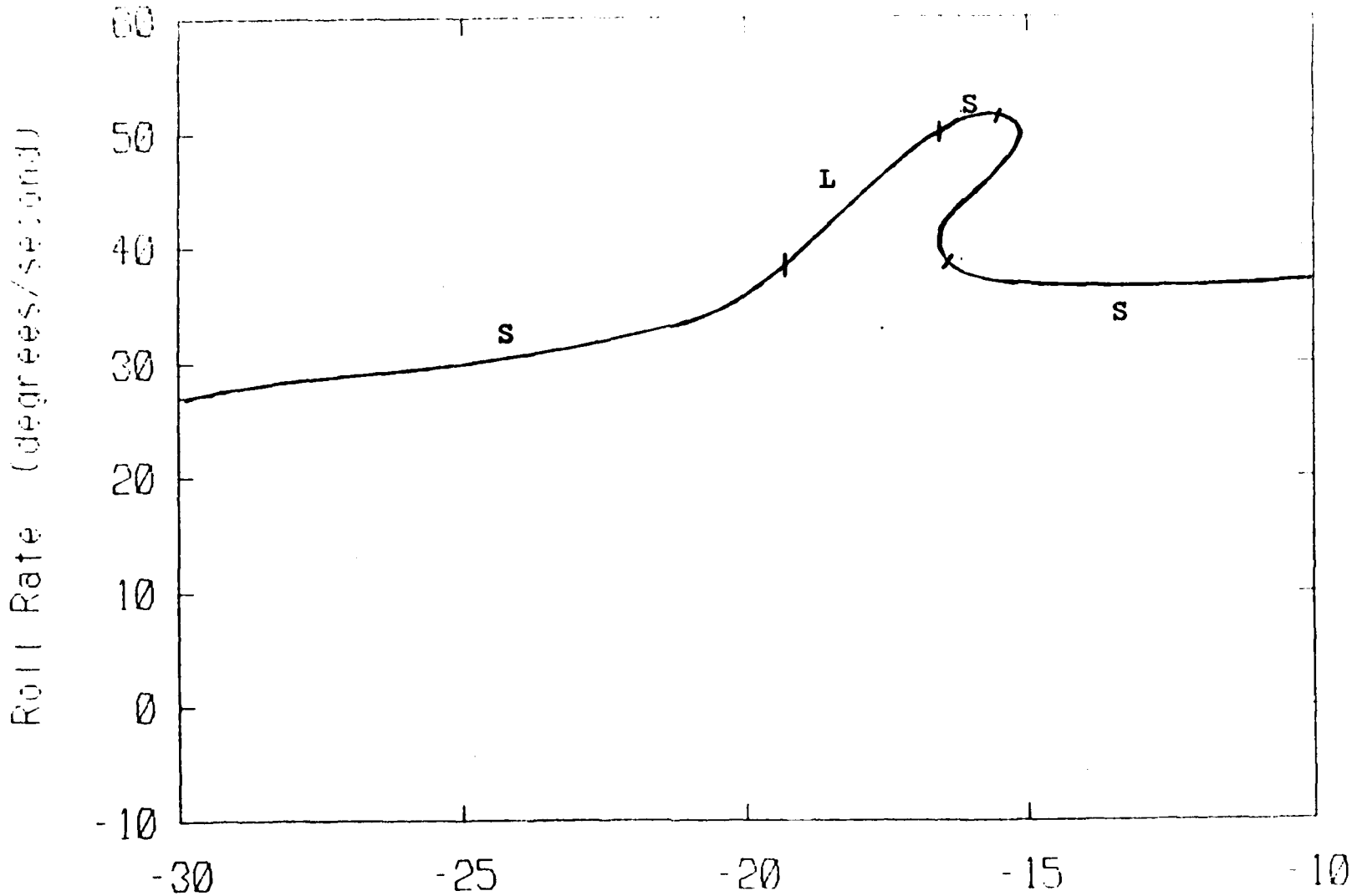

Fig. 7.7c: Roll Rate vs. Stabilator
V=500 f/s; g=0; DAI=-29.22; DRU=-29.22

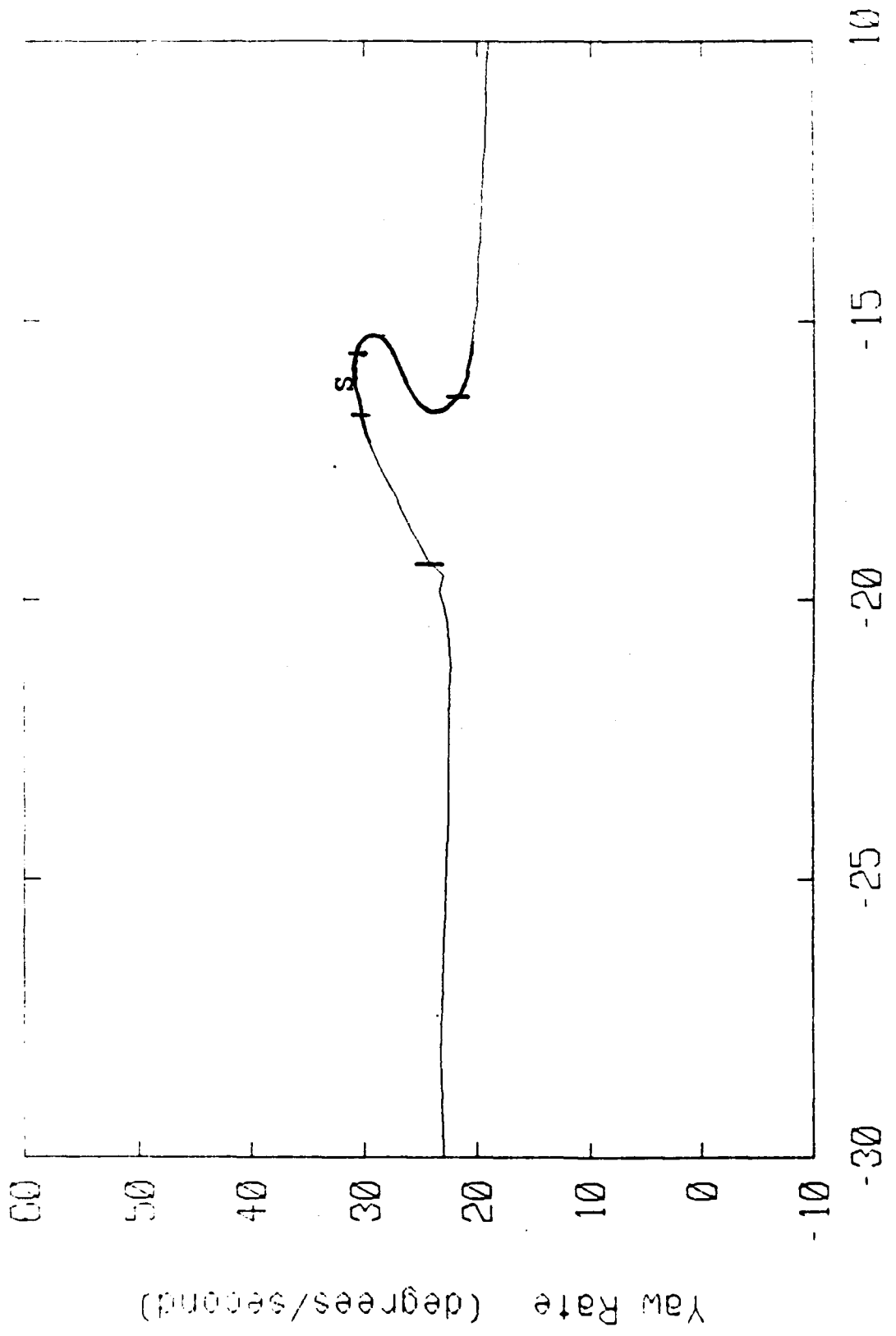

Fig. 7.7d: Yaw Rate vs. Stabilator
V=500 f/s; g=0, DAI=-29.22; DRU=-29.22

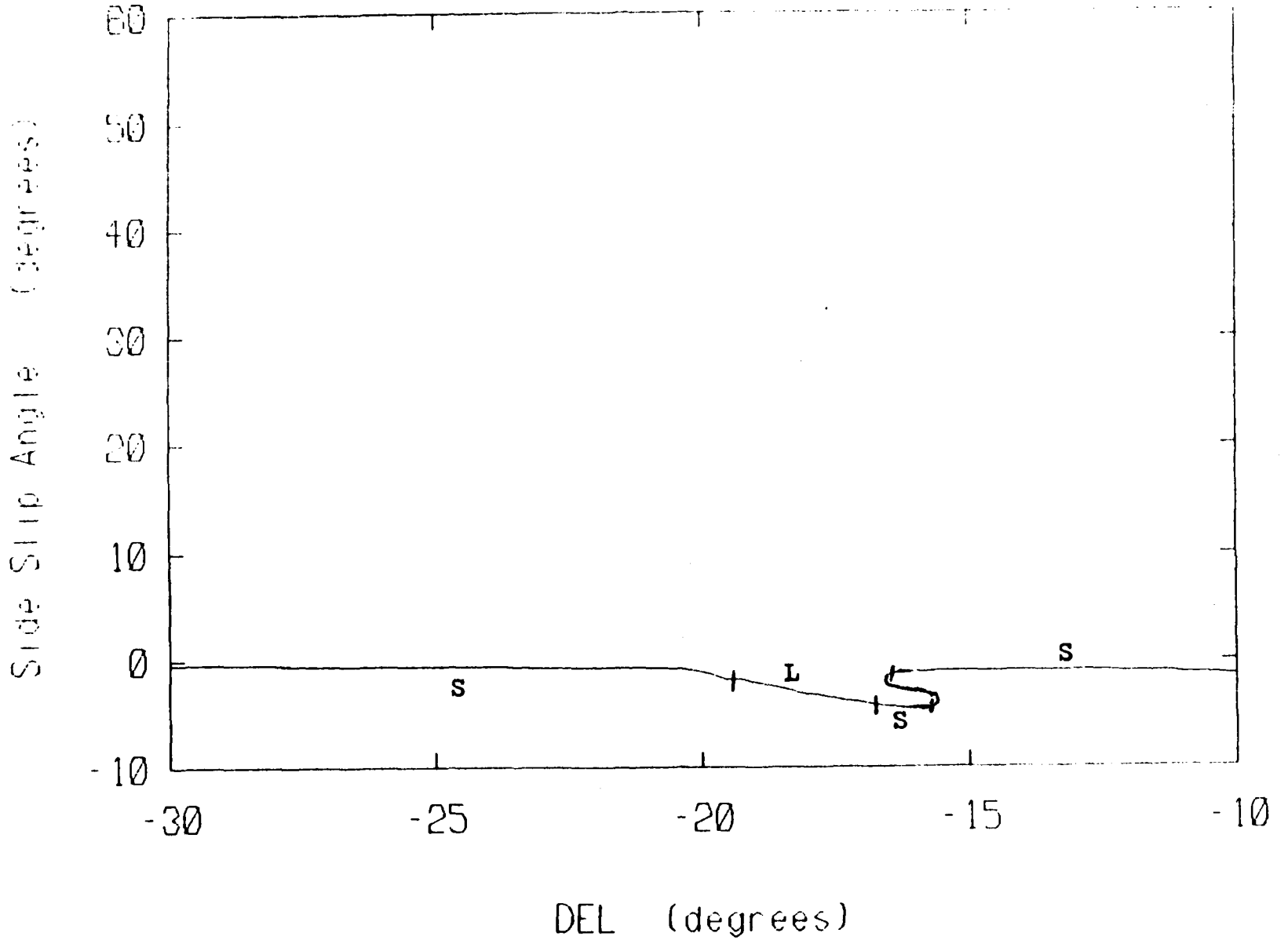

Fig. 7.7e: Side Slip Angle vs. Stabilator
V=500 f/s; g=0; DAI=-29.22; DEL=-29.22

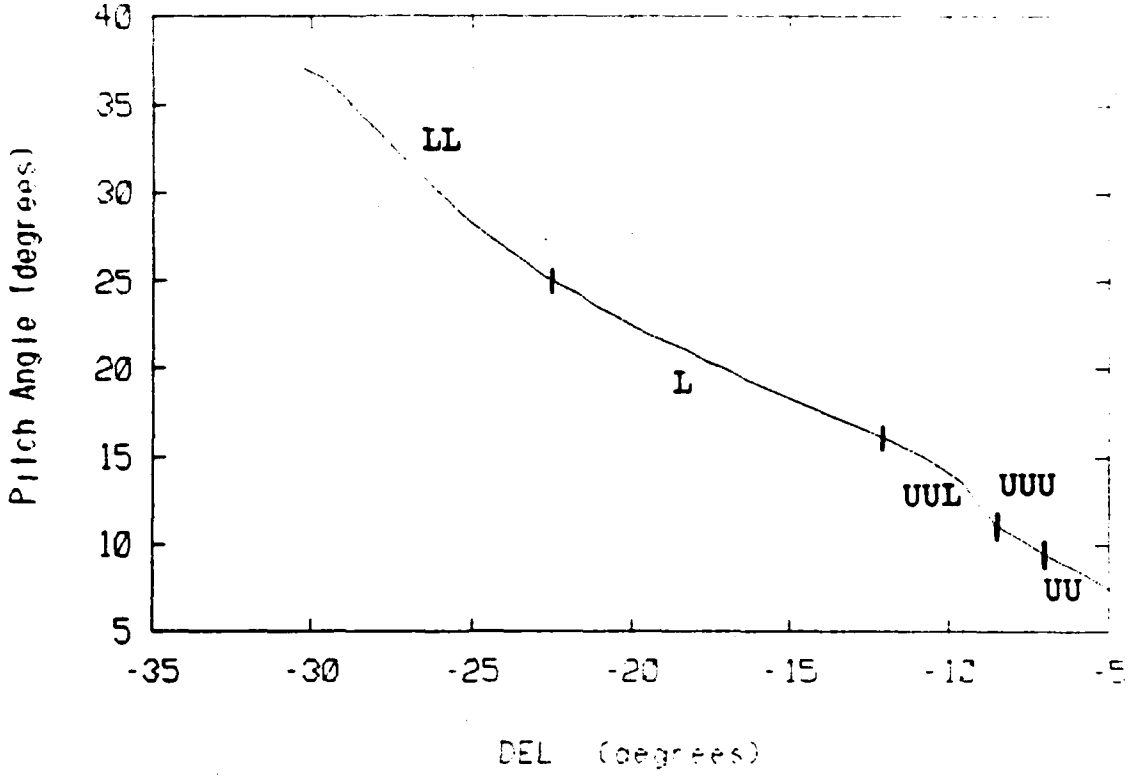

Fig. 7.8a: Pitch Angle vs. Stabilator

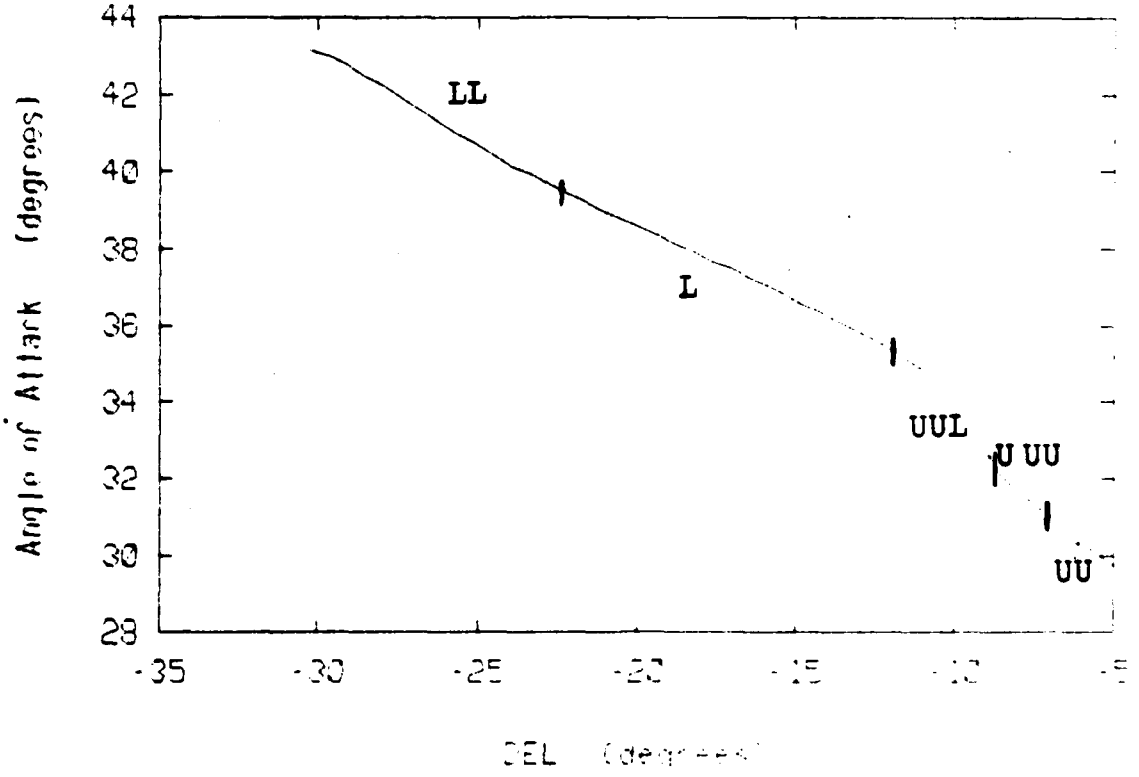

Fig. 7.8b: Angle of Attack vs. Stabilator
DAI=DRU=0

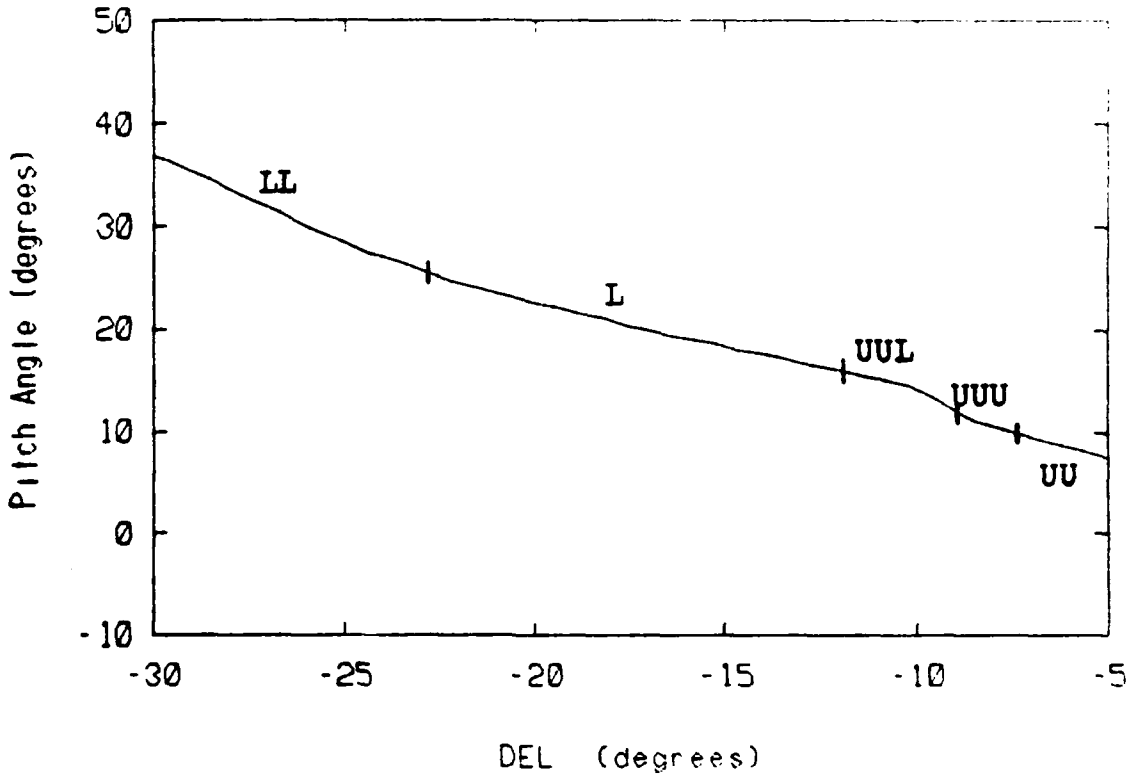

Fig. 7.8a: Pitch Angle vs. Stabilator

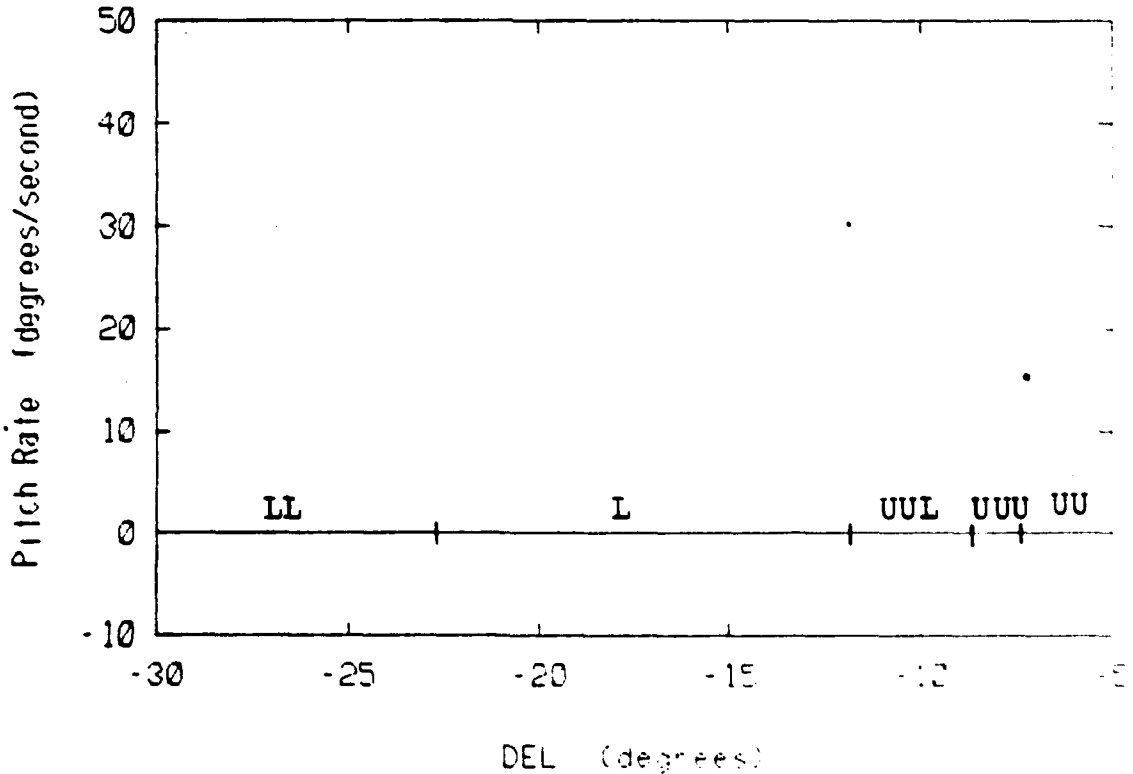

Fig. 7.8c: Pitch Rate vs. Stabilator
DAI=DRU=0

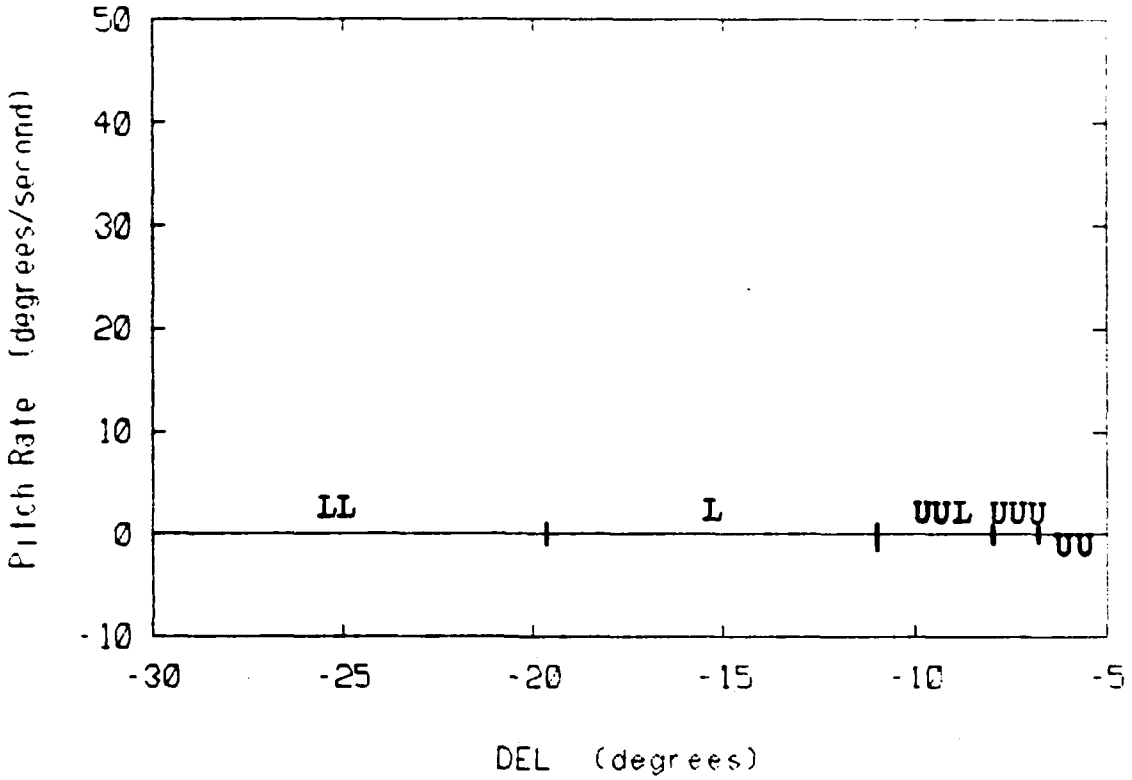

Fig. 7.8c: Pitch Rate vs. Stabilator

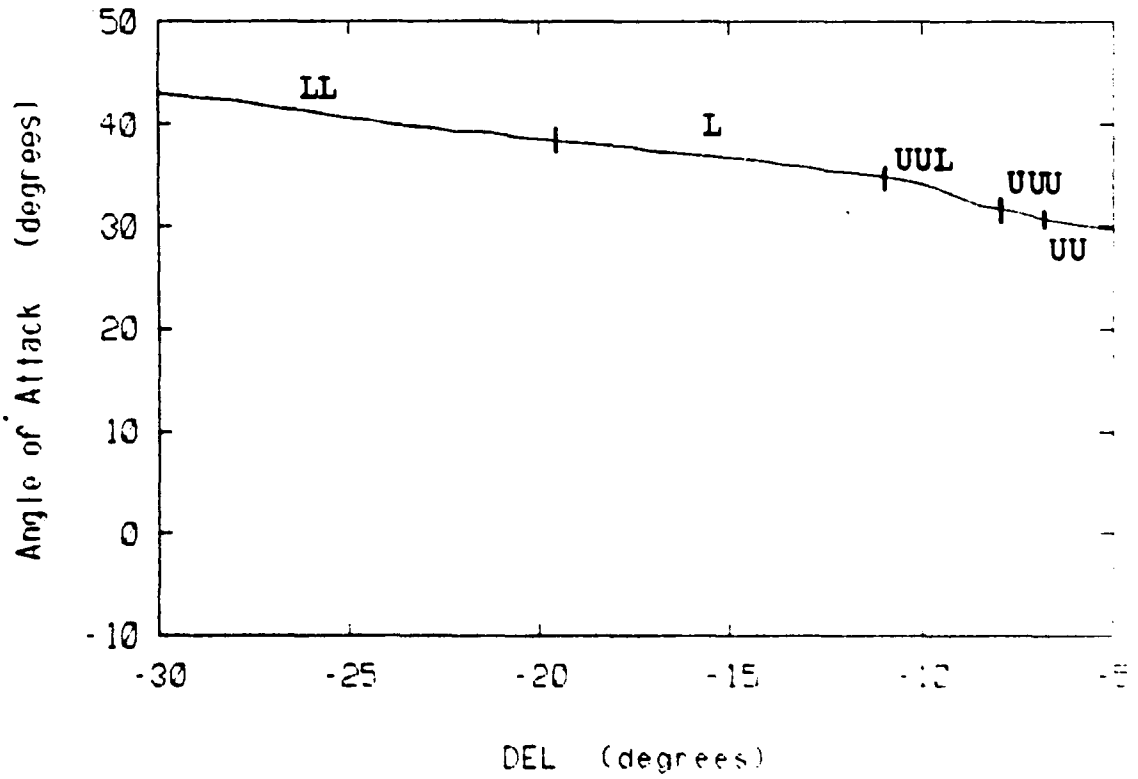

Fig. 7.8b: Angle of Attack vs. Stabilator
DAI=DRU=0

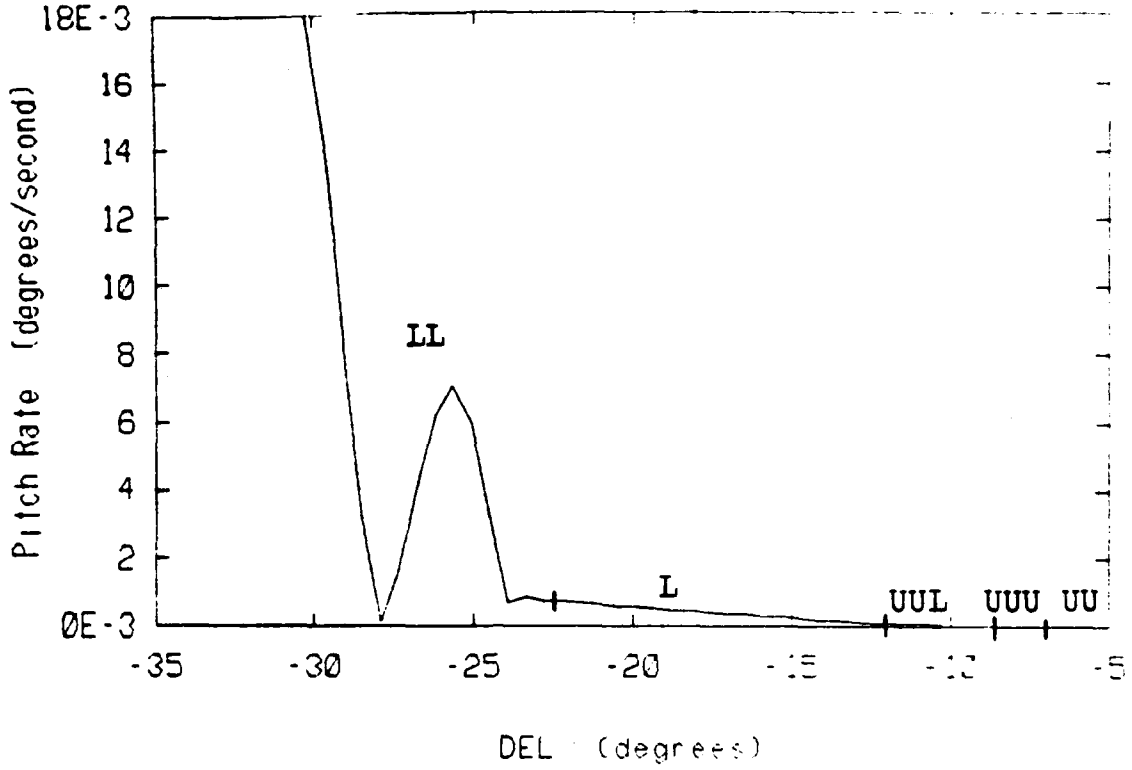

Fig. 7.8d: Amplified Pitch Rate vs. Stabilator

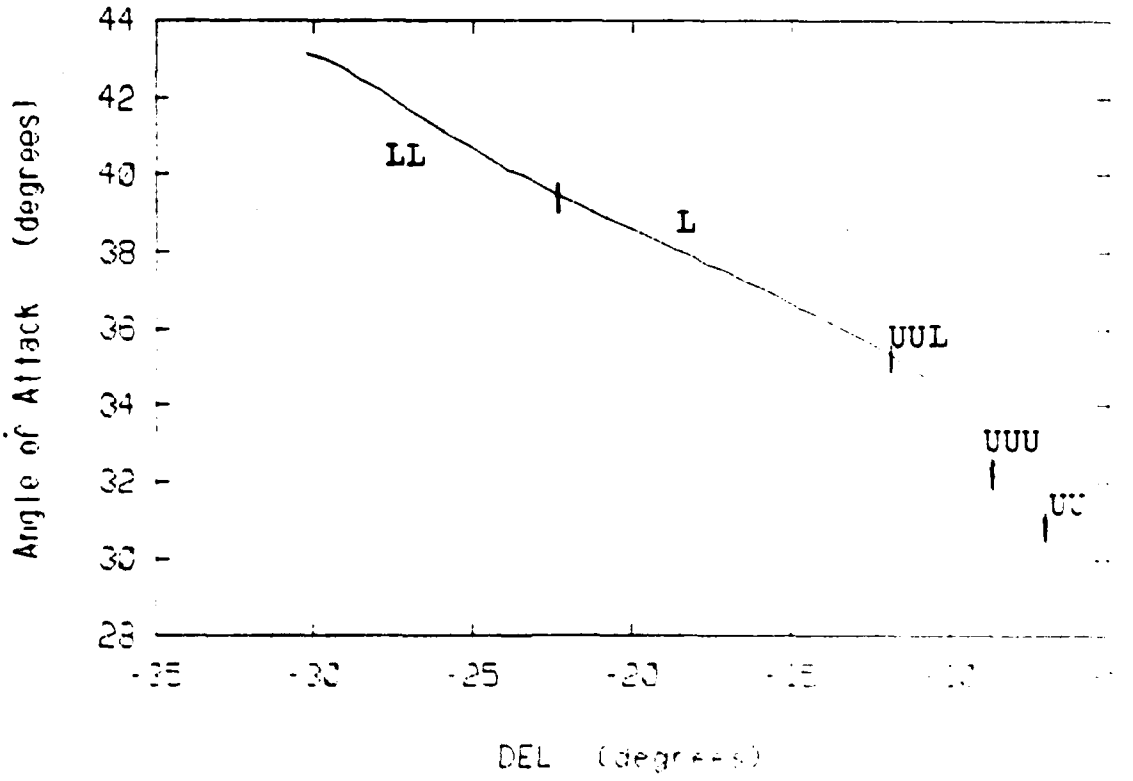

Fig. 7.8b: Angle of Attack vs. Stabilator
DAI=DRU=0

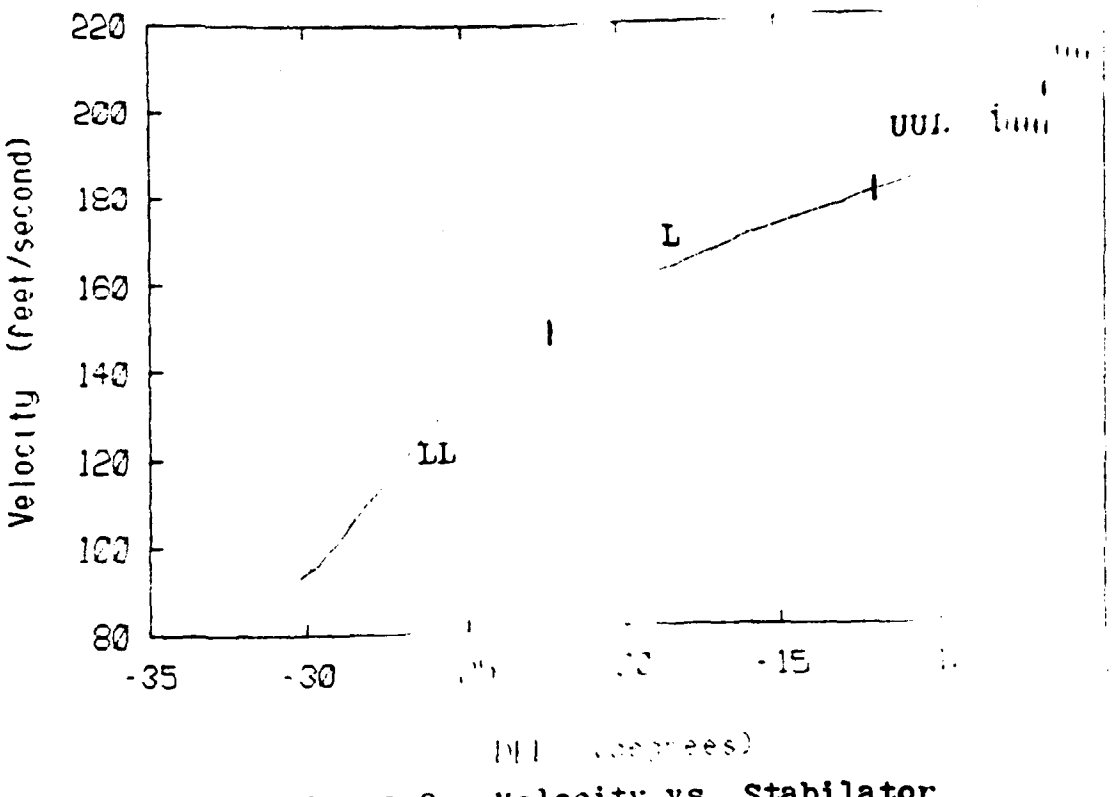

Fig. 7.8a: Velocity vs. Stabilator

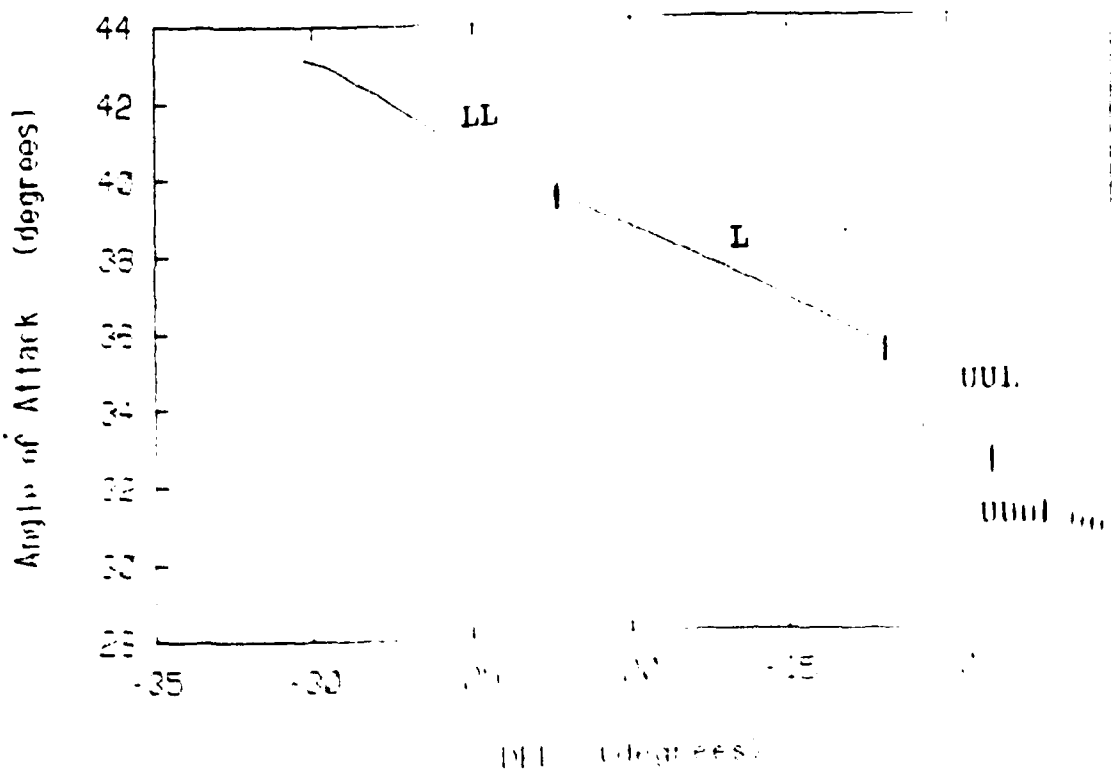

Fig. 7.8b: Angle of Attack vs. Stabilator
DAI=DRU=0

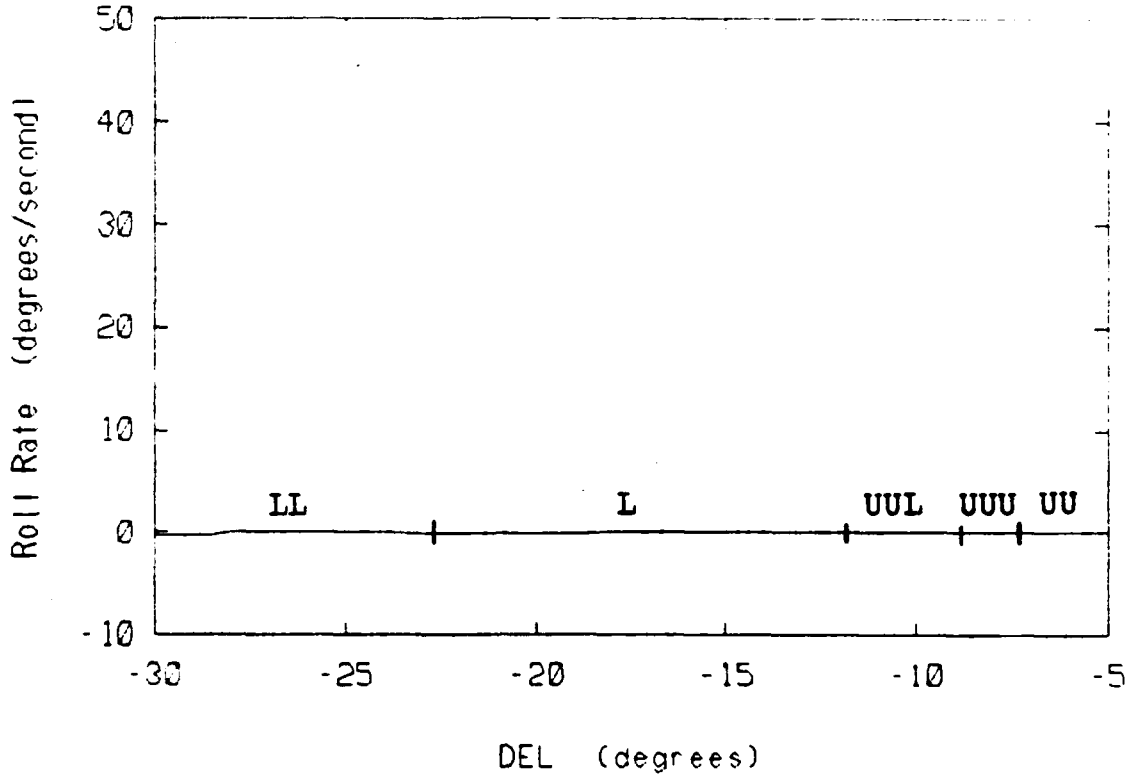

Fig. 7.8f: Roll Rate vs. Stabilator

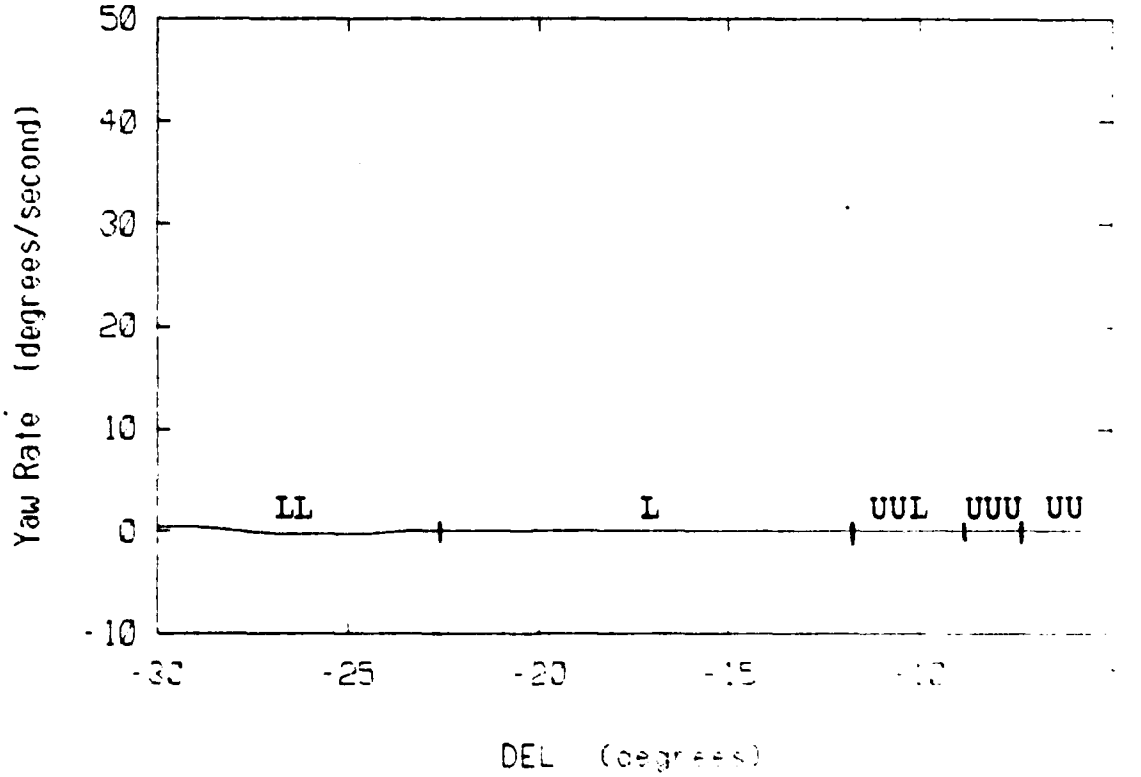

Fig. 7.8g: Yaw Rate vs. Stabilator
DAI=DRU=0

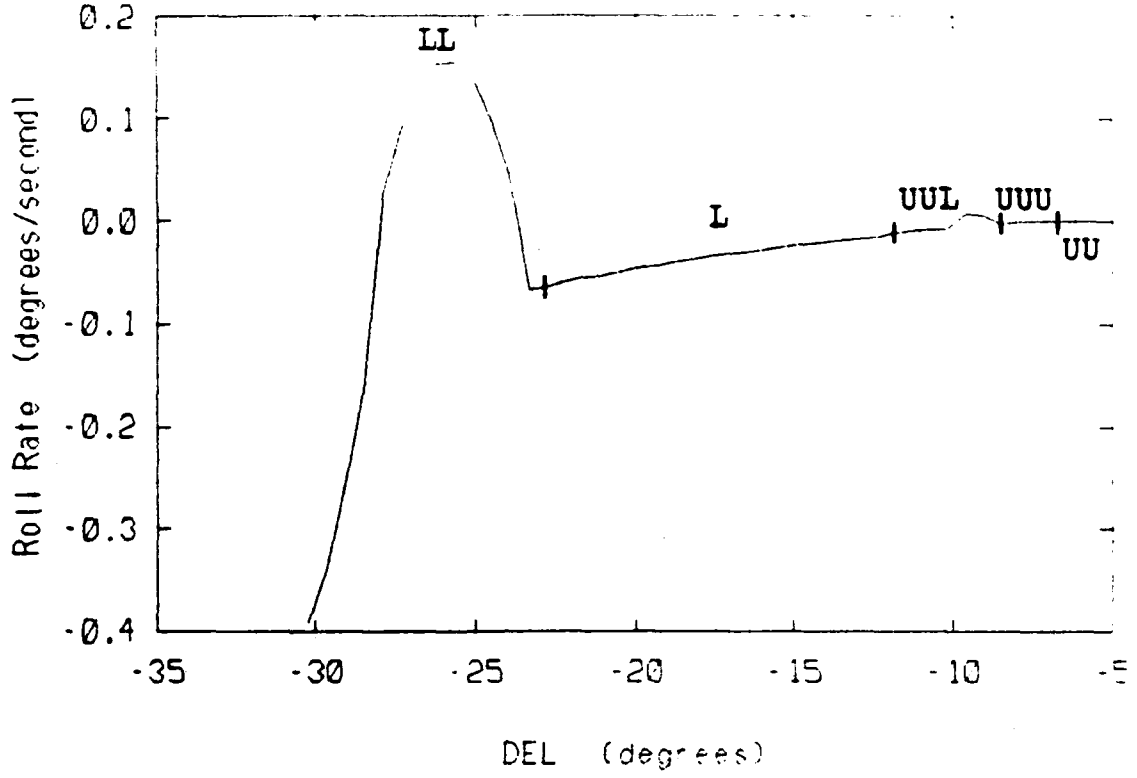

Fig. 7.8h: Amplified Roll Rate vs. Stabilator

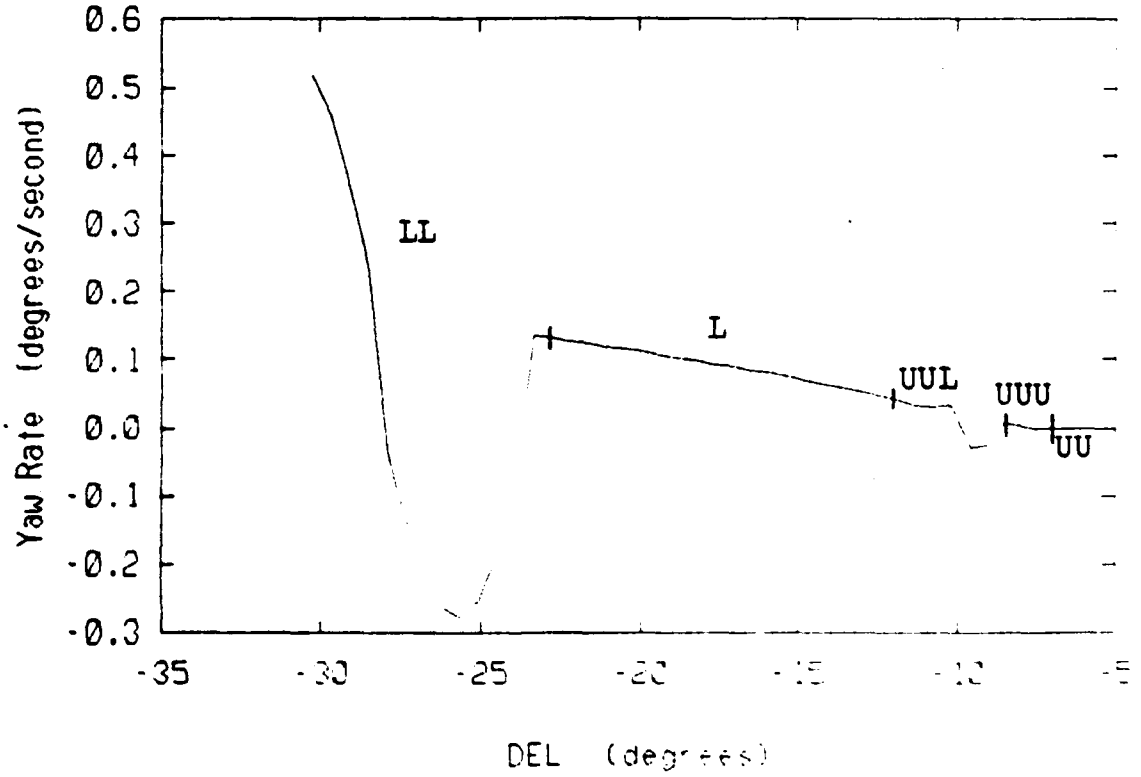

Fig. 7.8i: Amplified Yaw Rate vs. Stabilator
DAI=DRU=0

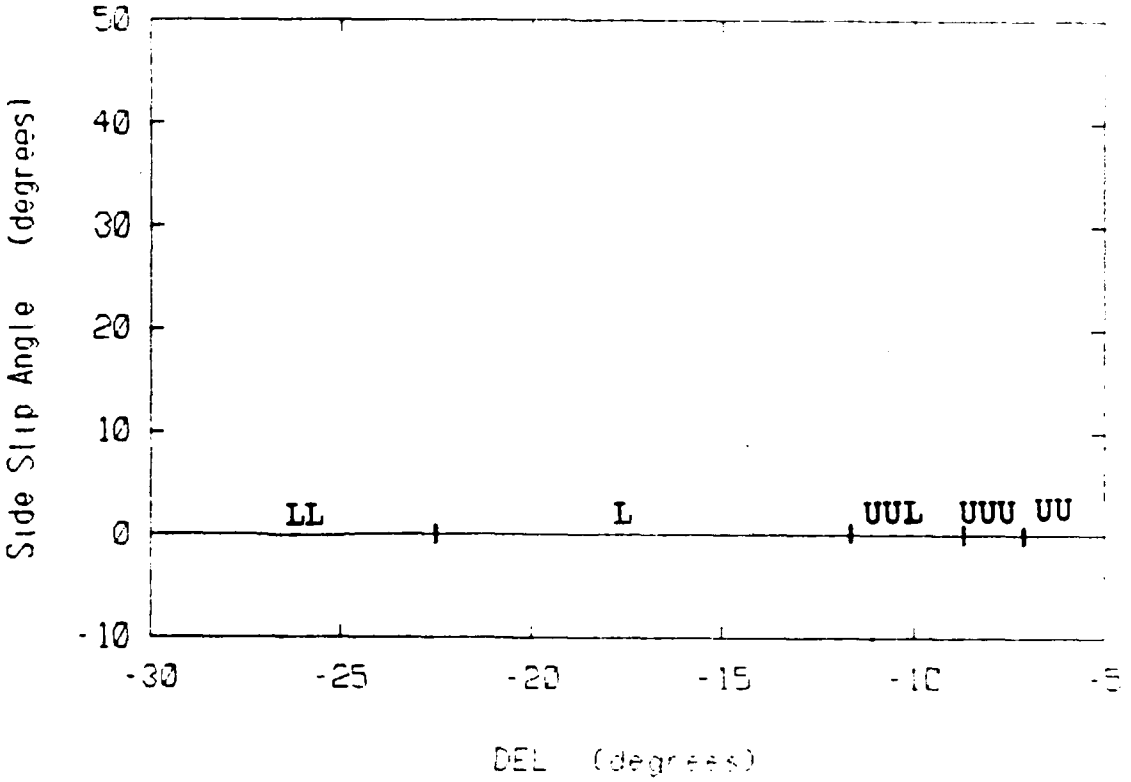

Fig. 7.8j: Side Slip Angle vs. Stabilator

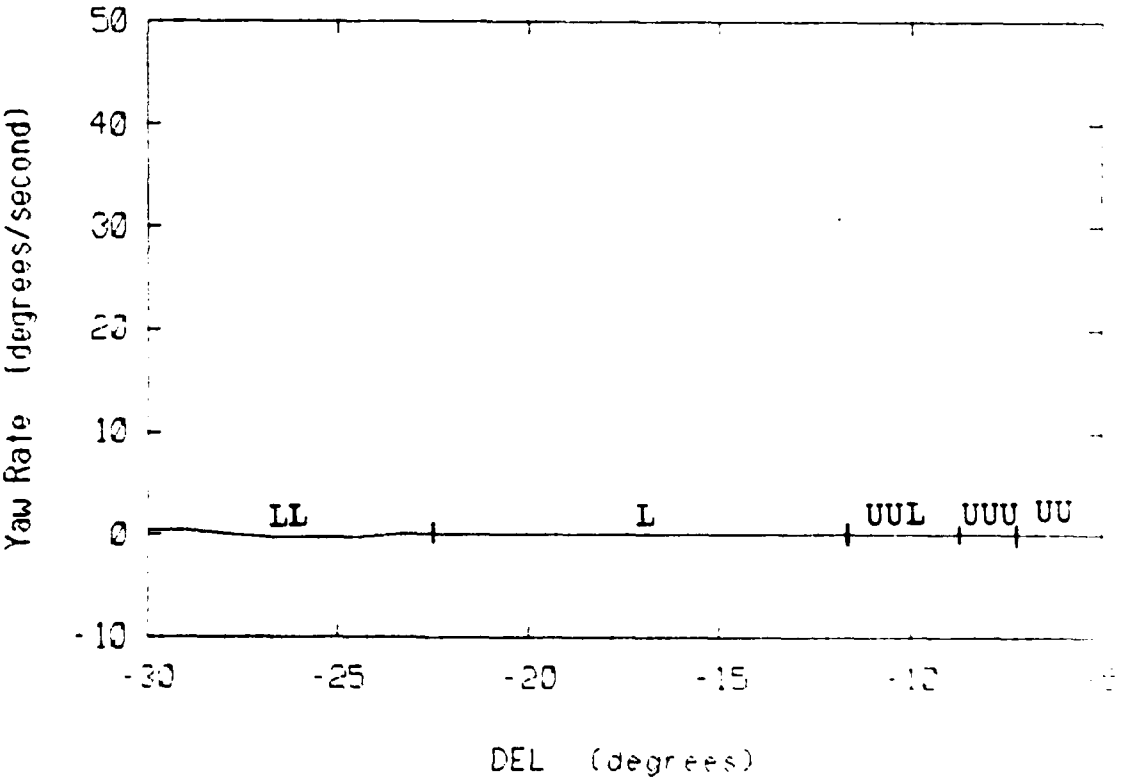

Fig. 7.8g: Yaw Rate vs. Stabilator
DAI=DRU=0

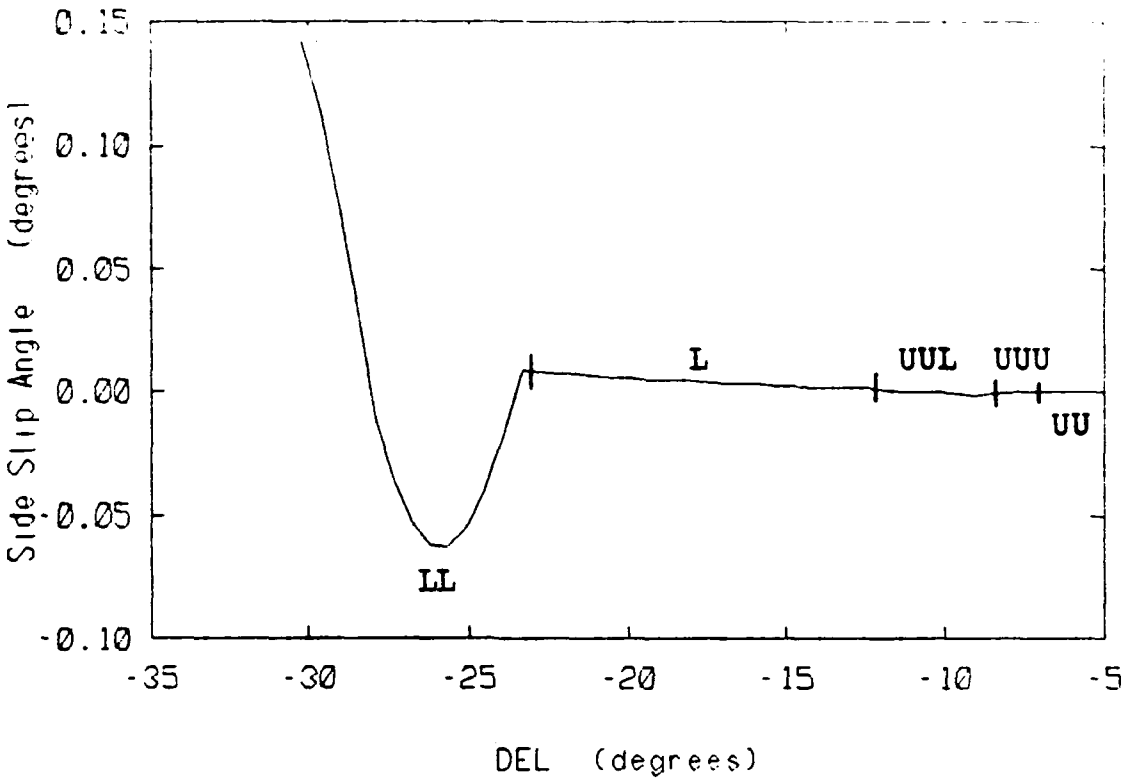

Fig. 7.8k: Amplified Side Slip Angle vs. Stabilator

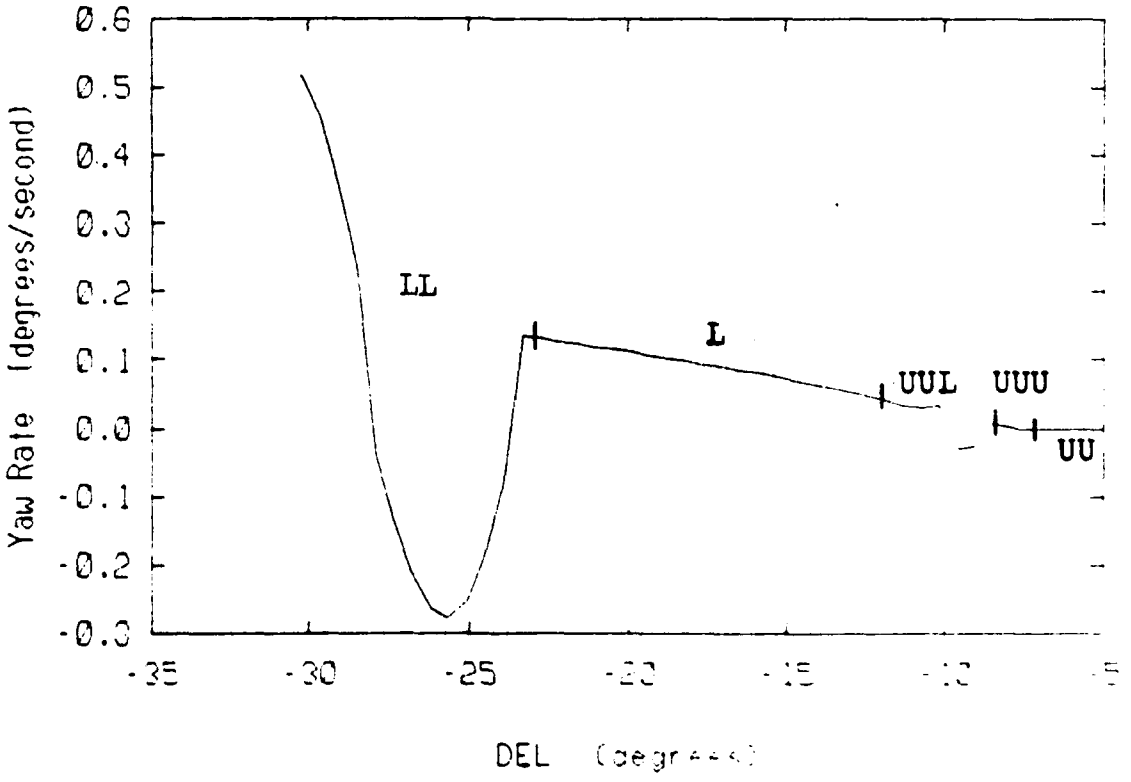

Fig. 7.8l: Amplified Yaw Rate vs. Stabilator
DAI=DRU=0

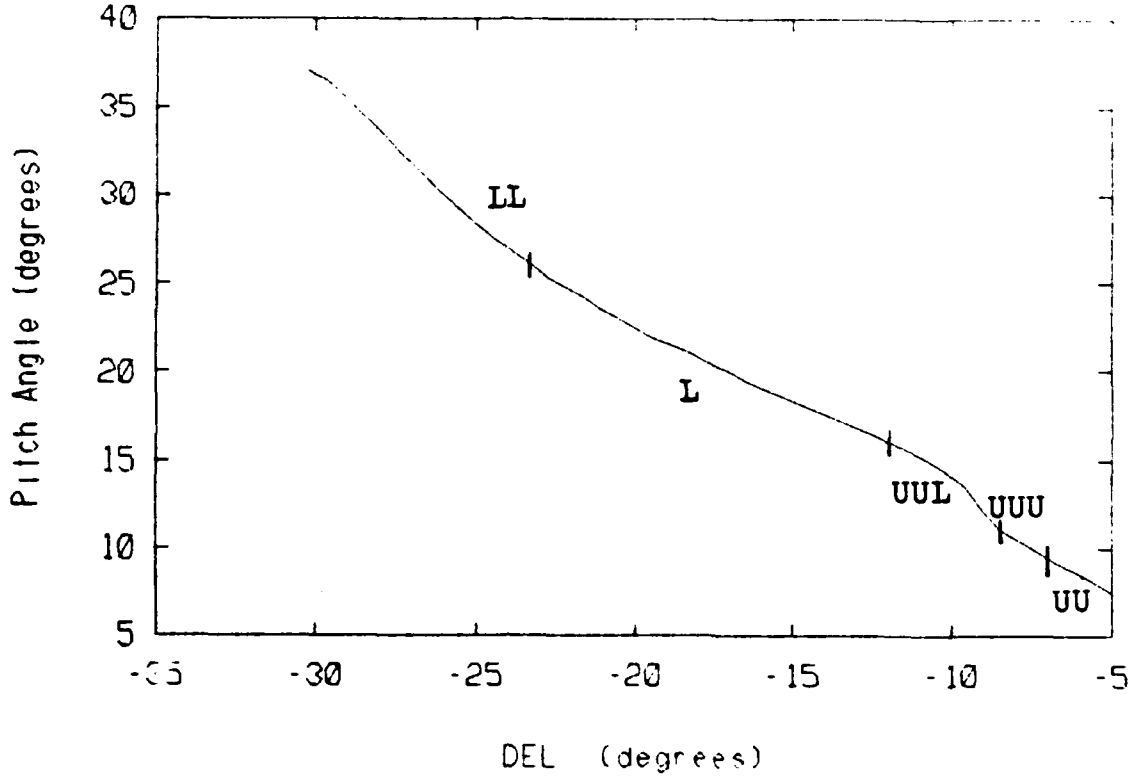

Fig. 7.8a: Pitch Angle vs. Stabilator

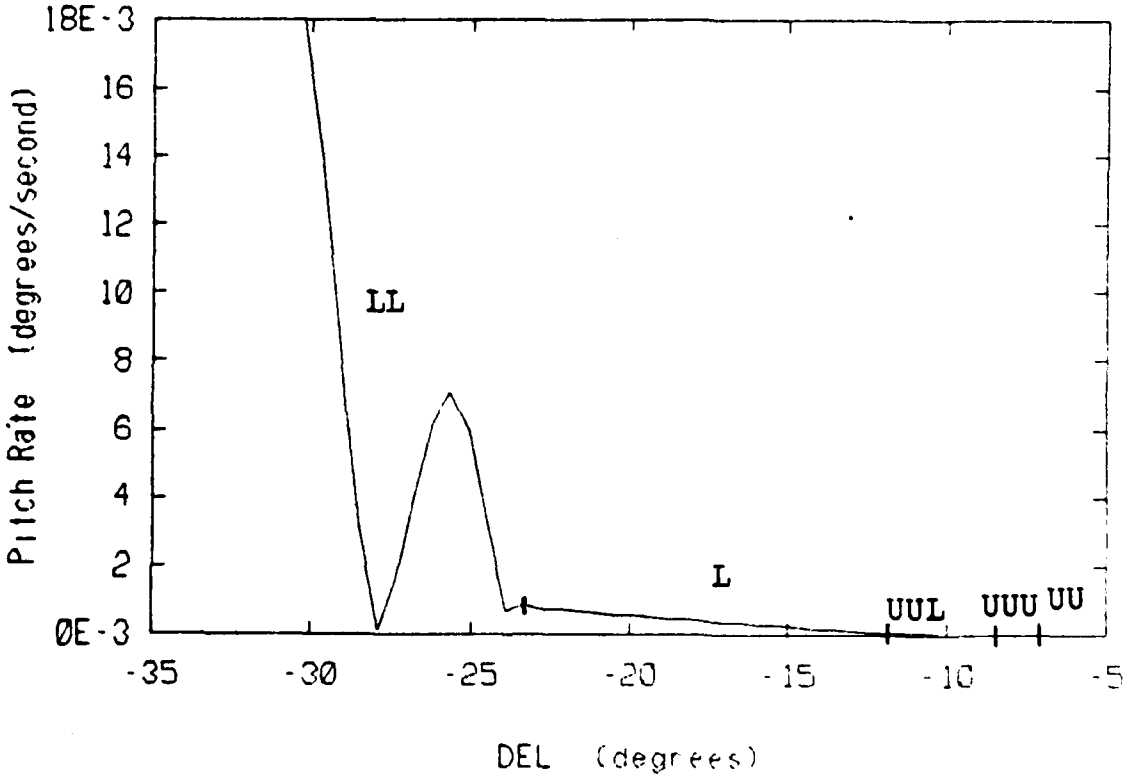

Fig. 7.8m: Amplified Pitch Rate vs. Stabilator
DAI=DRU=0

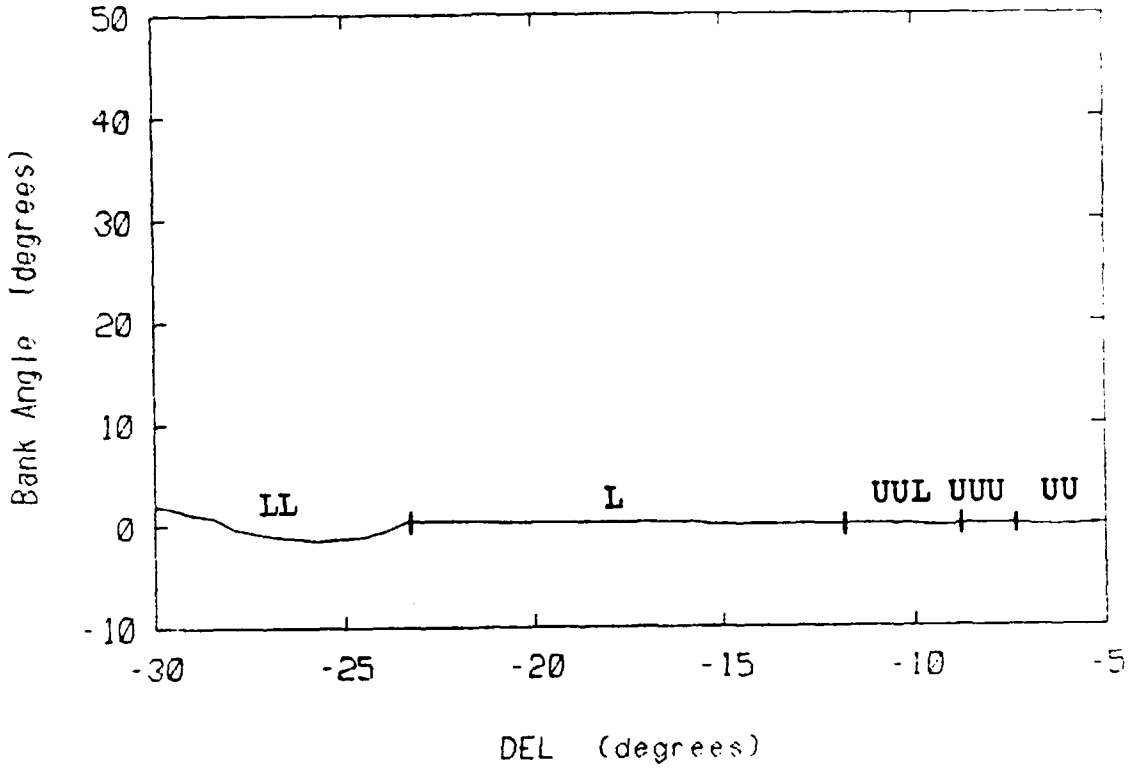

Fig. 7.8n: Bank Angle vs. Stabilator

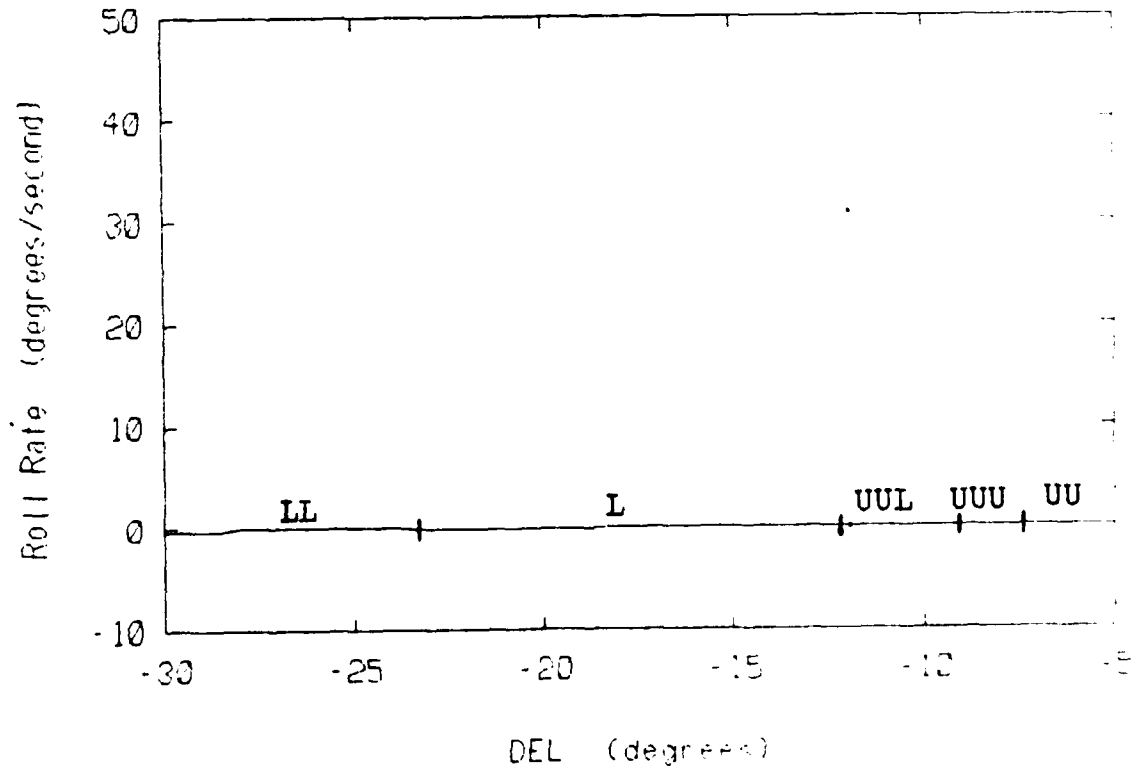

Fig. 7.8f: Roll Rate vs. Stabilator
DAI=DRU=0

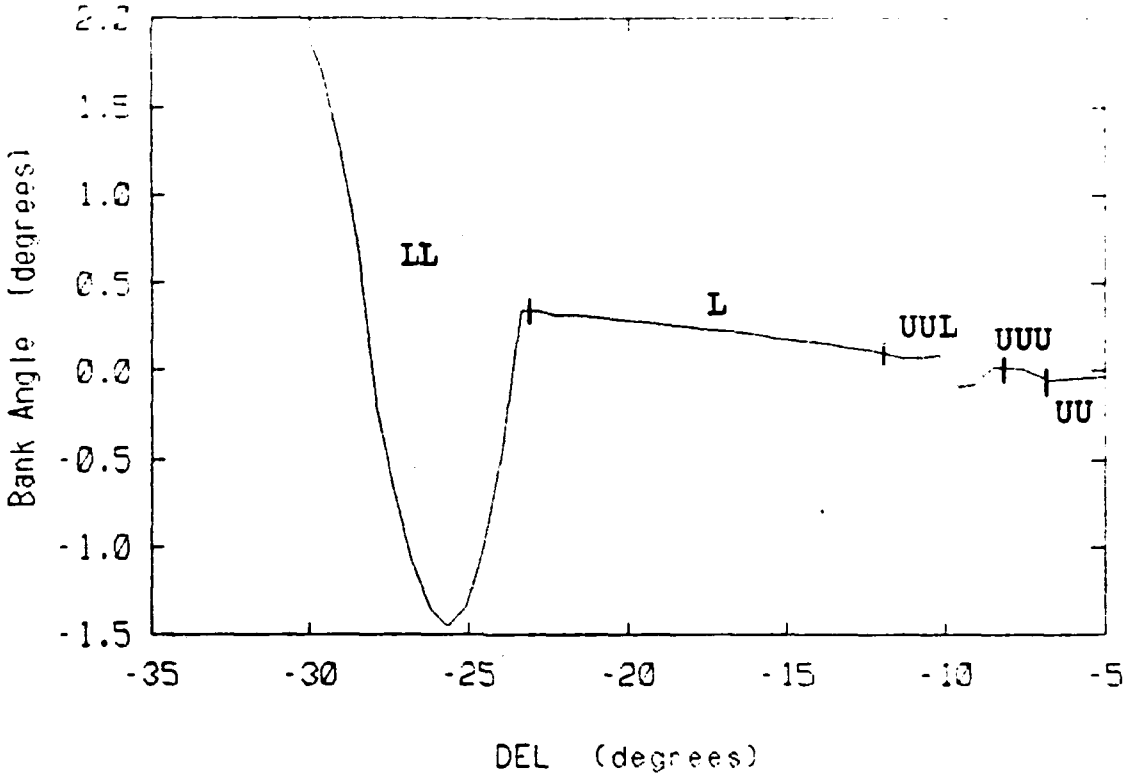

Fig. 7.8o: Amplified Bank Angle vs. Stabilator

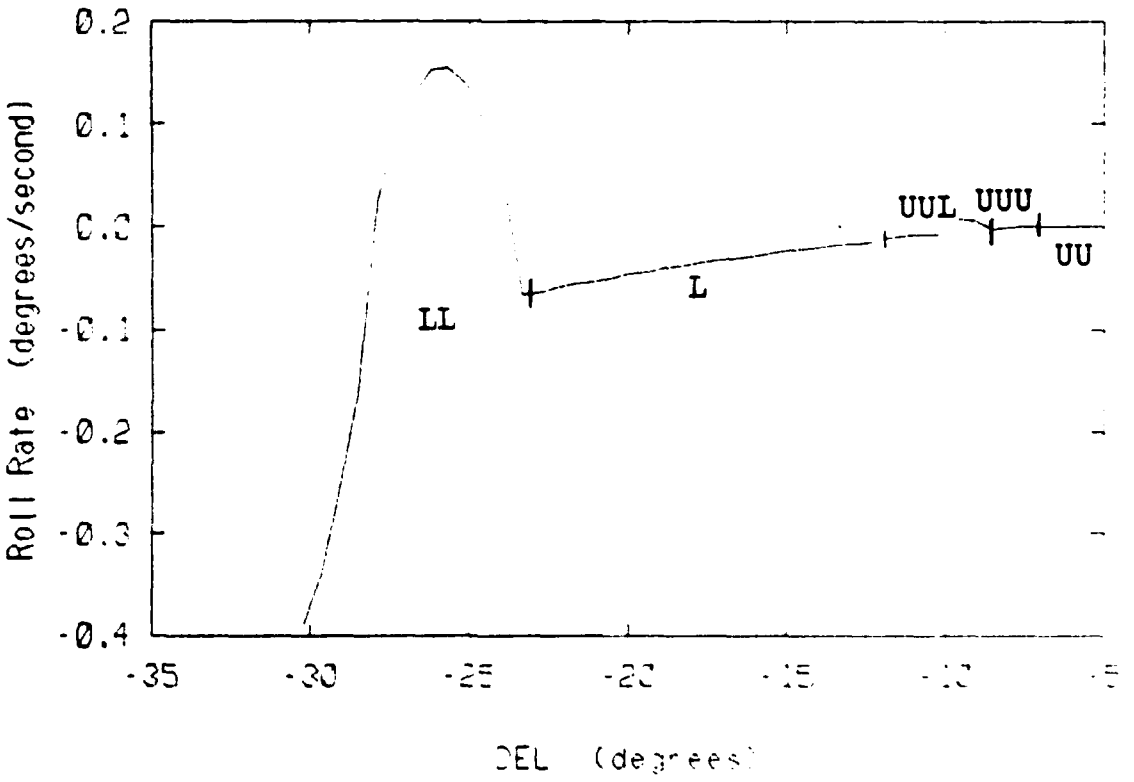

Fig. 7.8p: Amplified Roll Rate vs. Stabilator
DAI=DRU=0

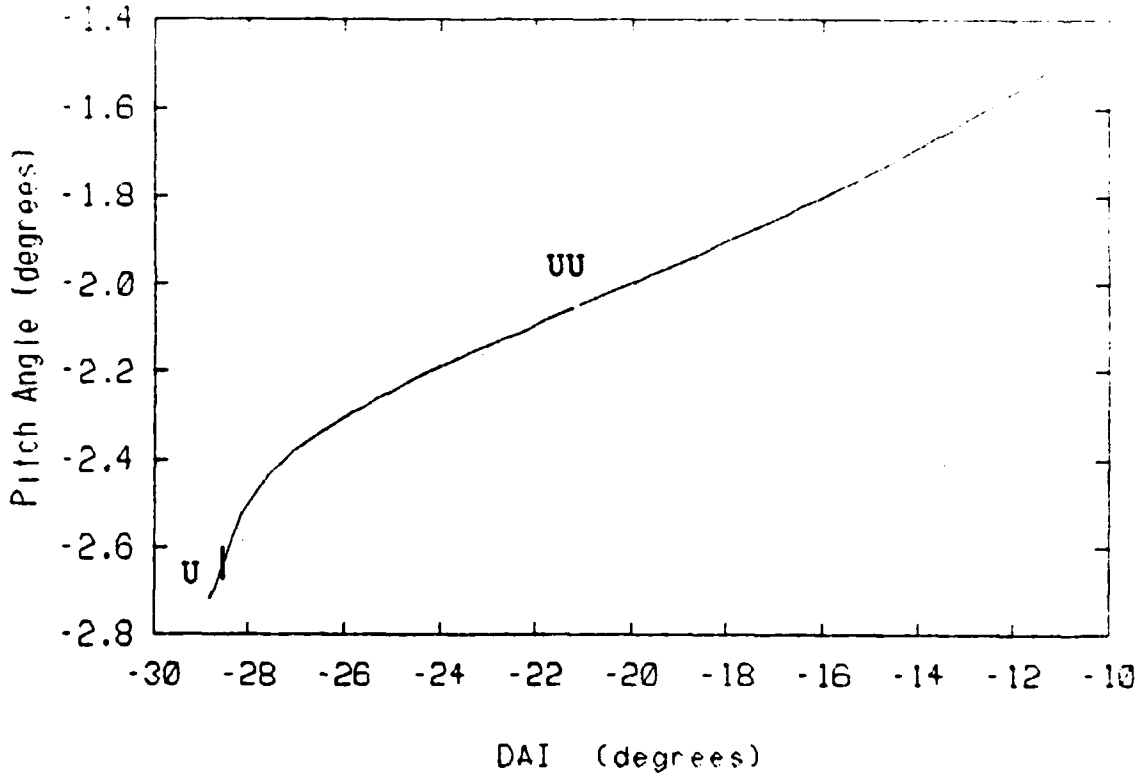

Fig. 7.9a: Pitch Angle vs. Aileron

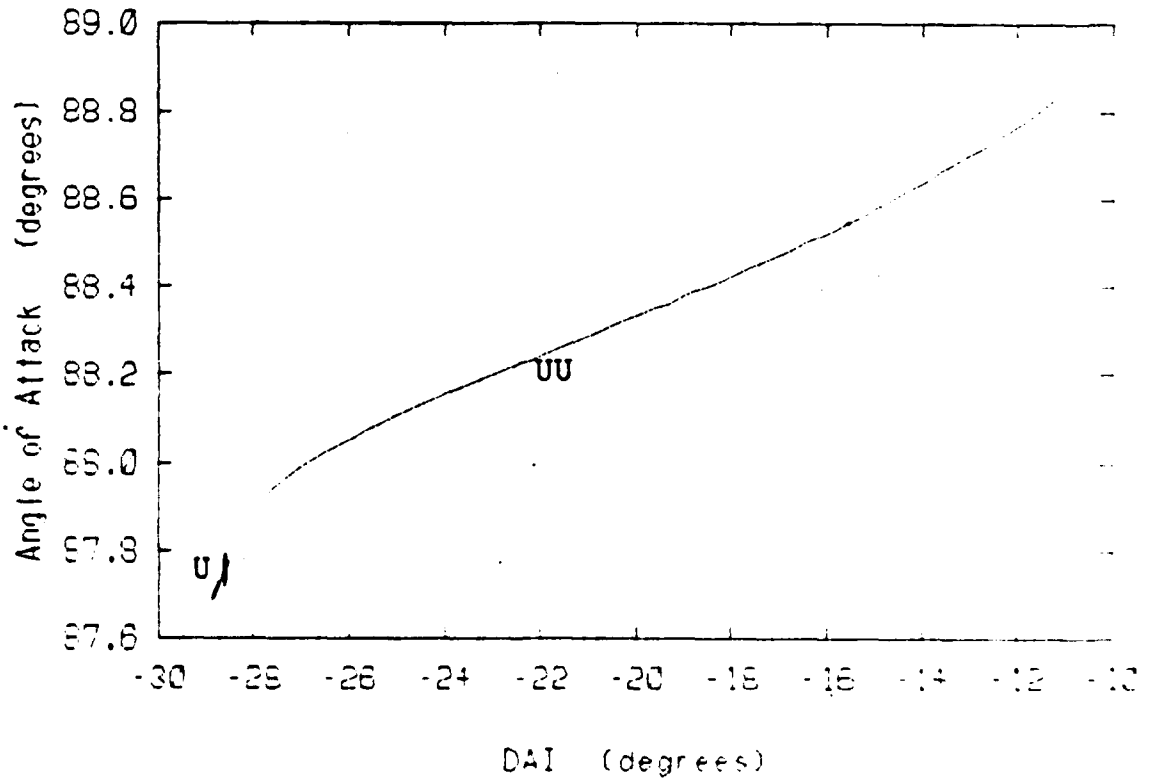

Fig. 7.9b: Angle of Attack vs. Aileron
DEL=-21.00; DRU=-24.46

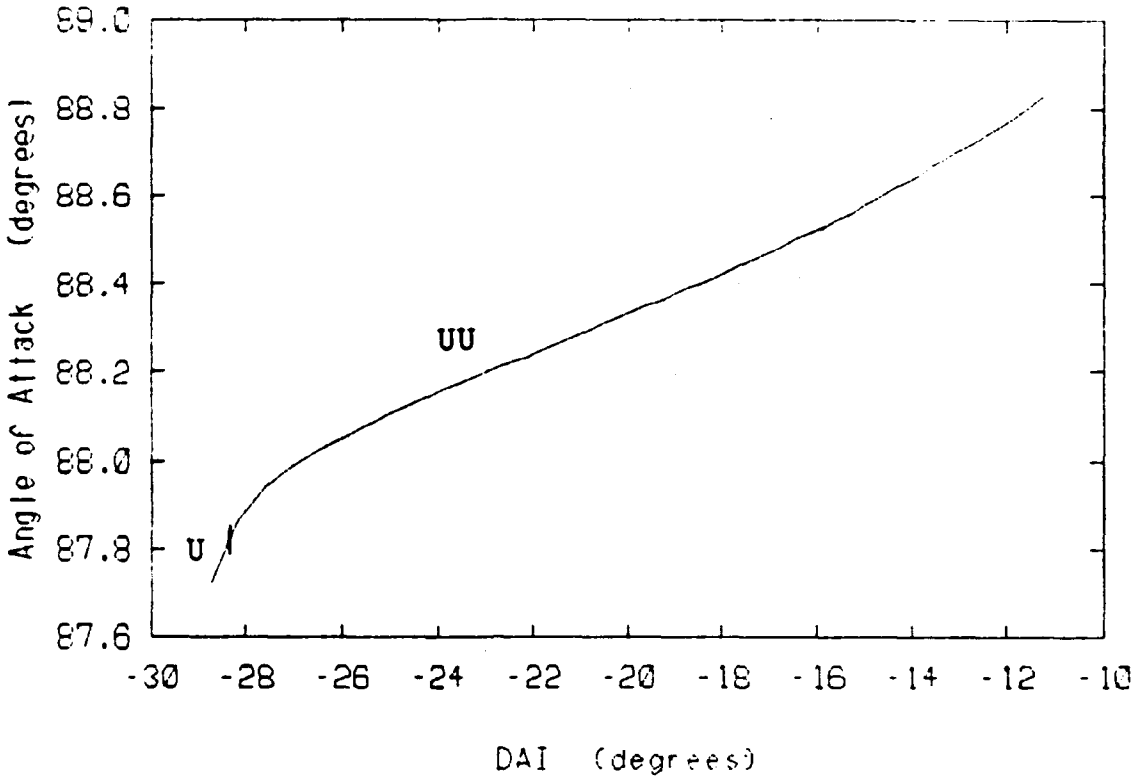

Fig. 7.9b: Angle of Attack vs. Aileron

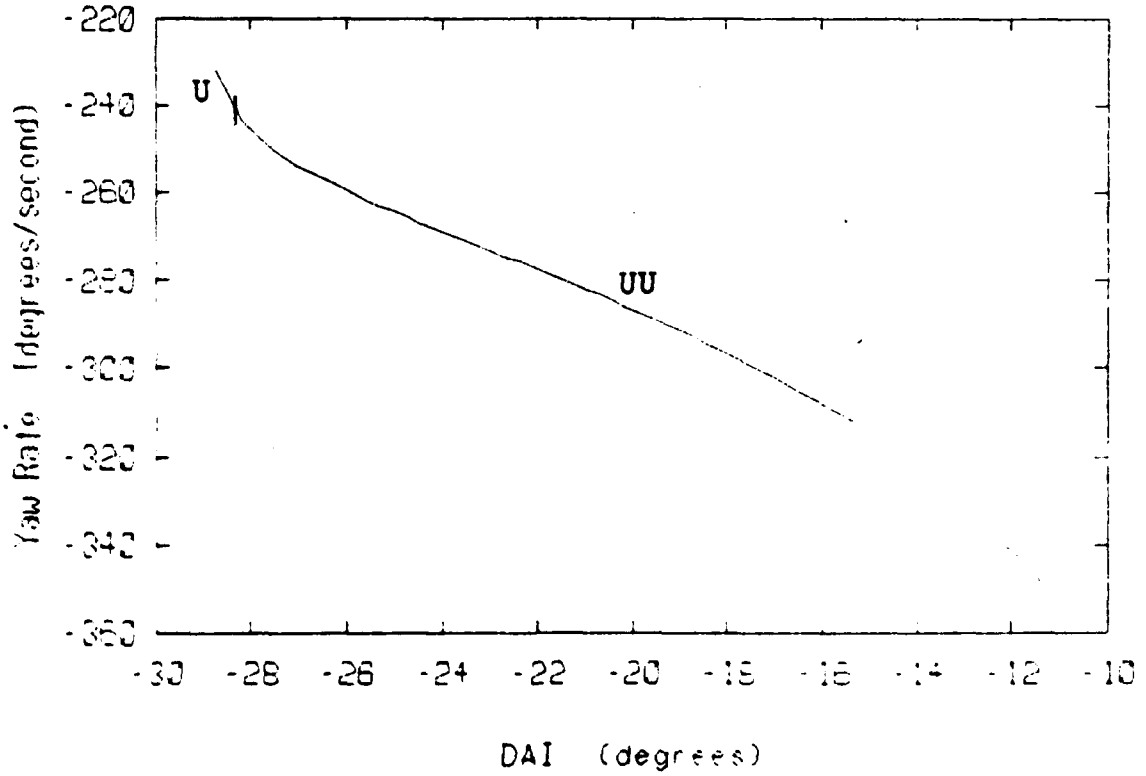

Fig. 7.9c: Yaw Rate vs. Aileron
DEL=-21.00; DRU=-24.46

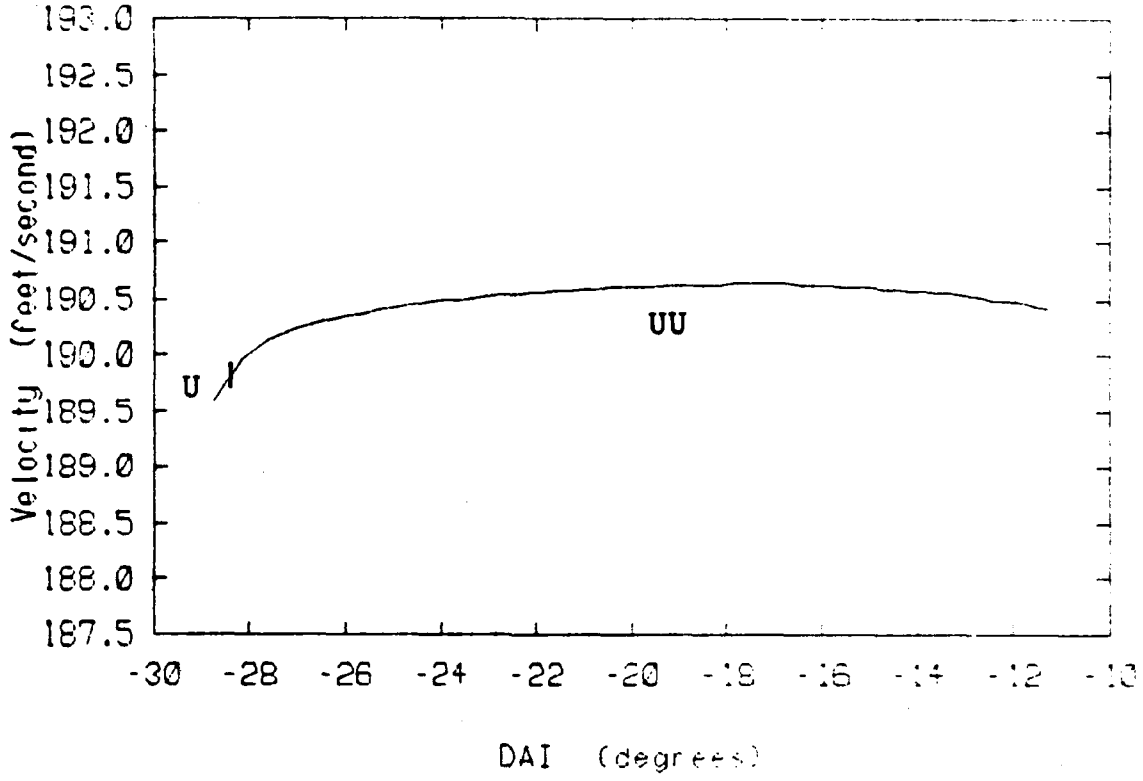

Fig. 7.9d: Velocity vs. Aileron

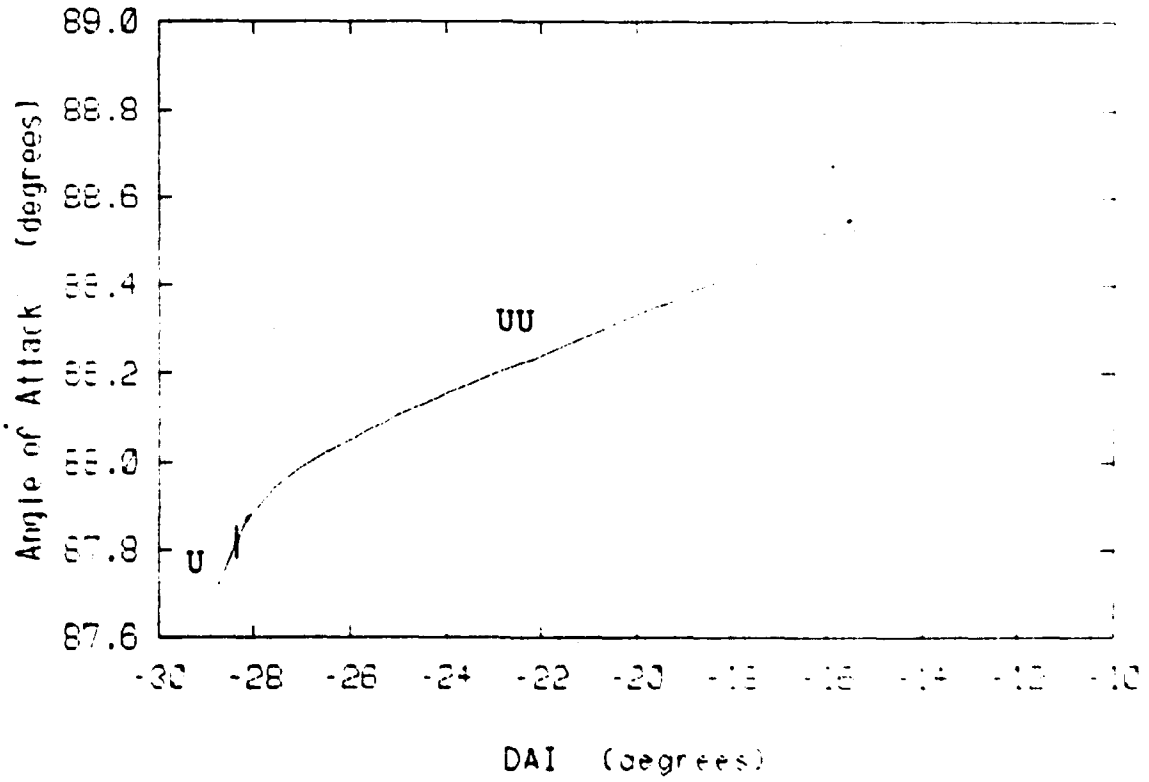

Fig. 7.9b: Angle of Attack vs. Aileron
DEL=-21.00; DRU=-24.46

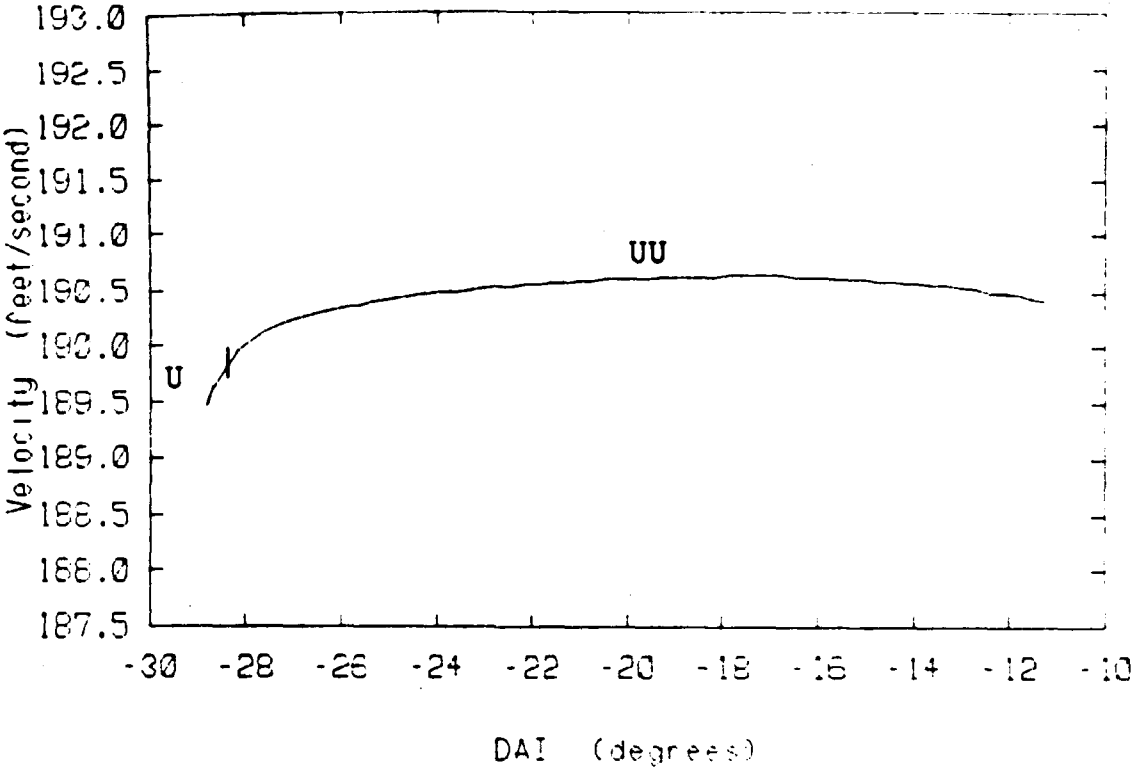

Fig. 7.9d: Velocity vs. Aileron

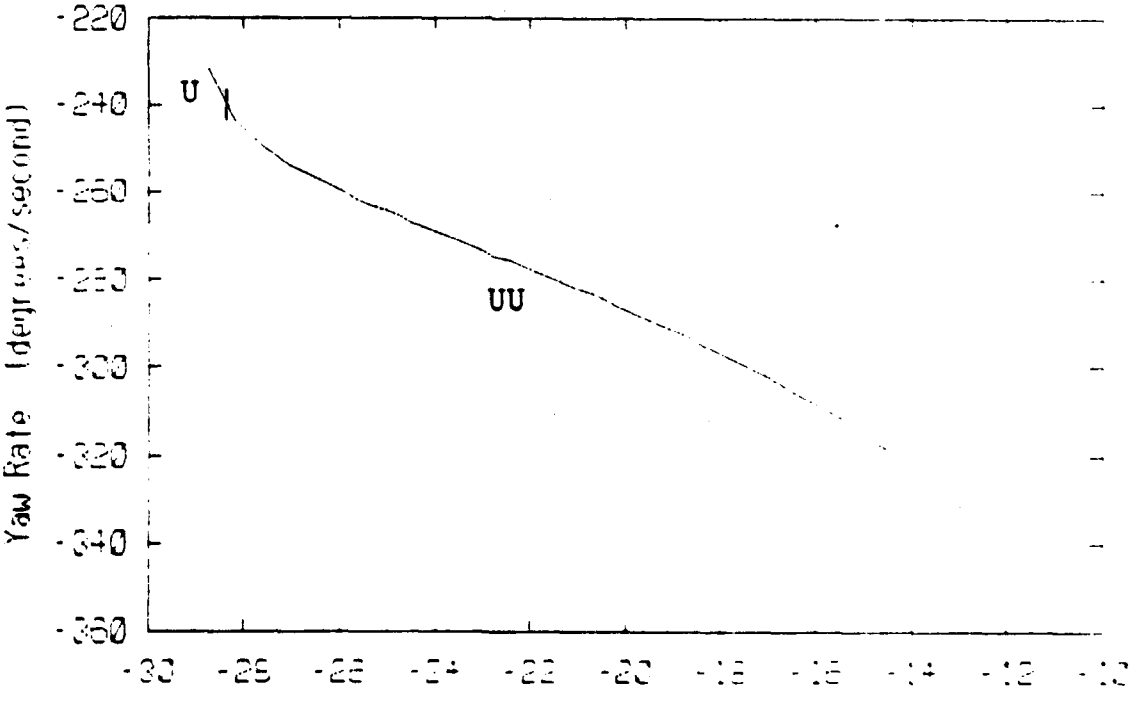

Fig. 7.9c: Yaw Rate vs. Aileron
DEL=-21.00; DRU=-24.46

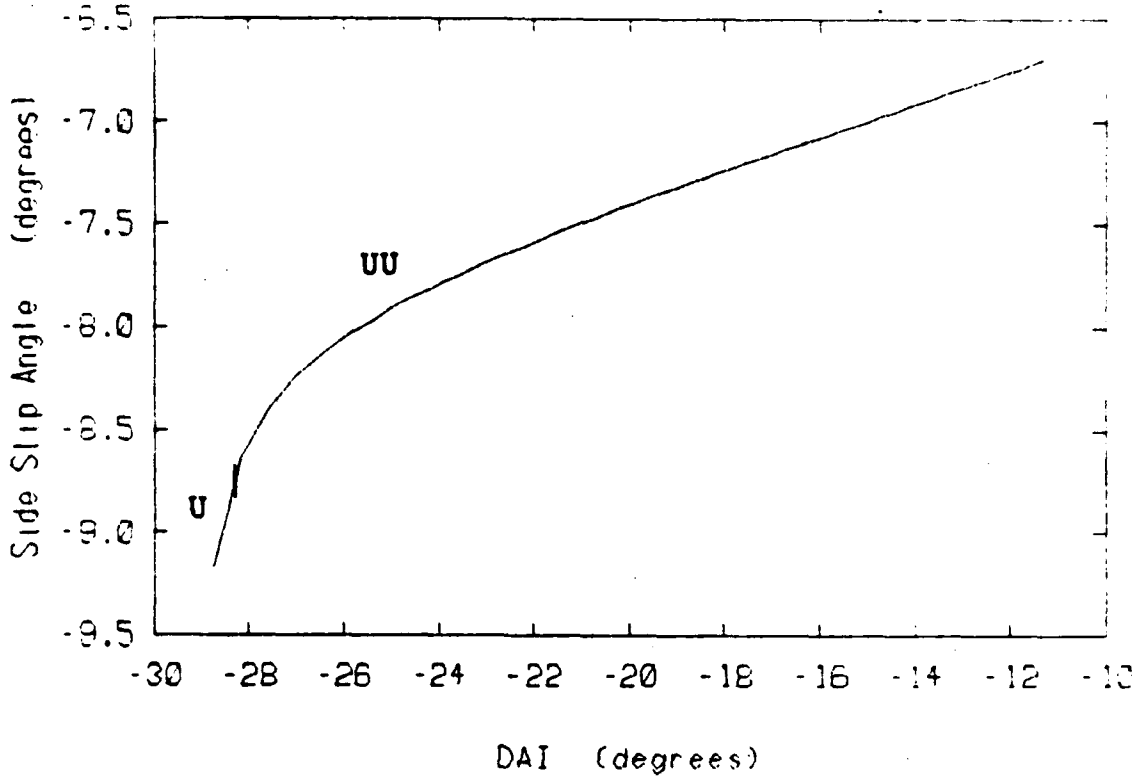

Fig. 7.9e: Side Slip Angle vs. Aileron

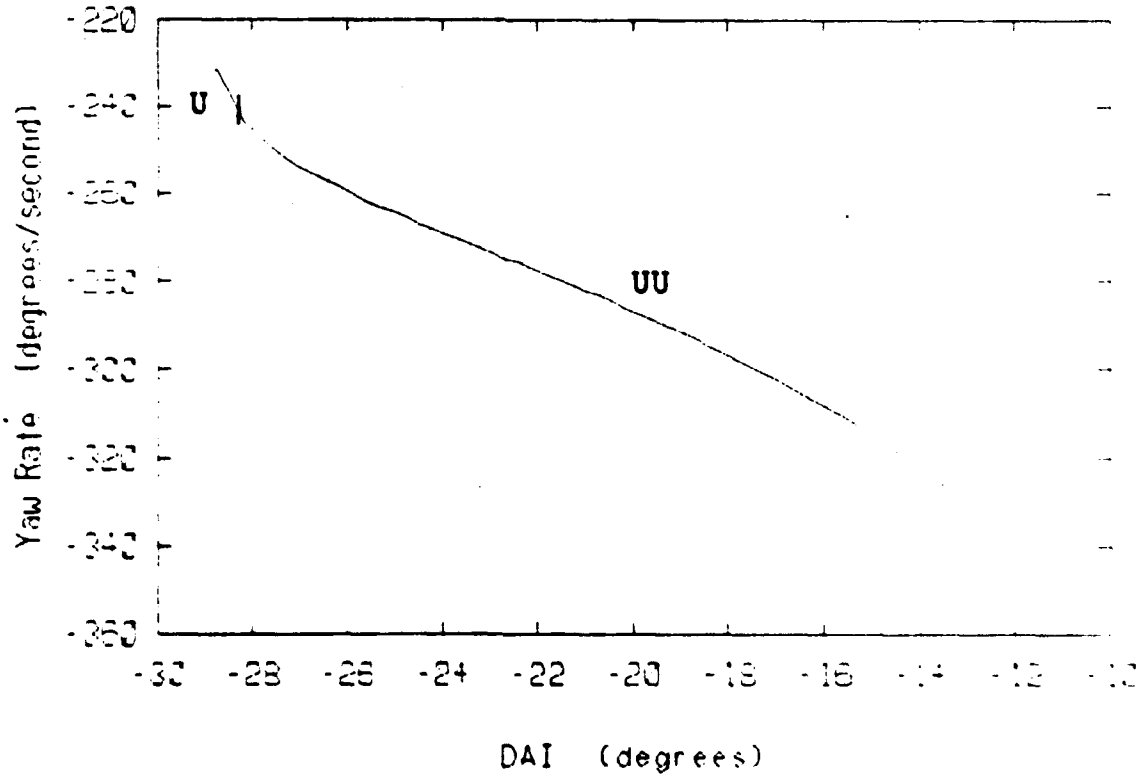

Fig. 7.9c: Yaw Rate vs. Aileron
DEL=-21.00; DRU=-24.46

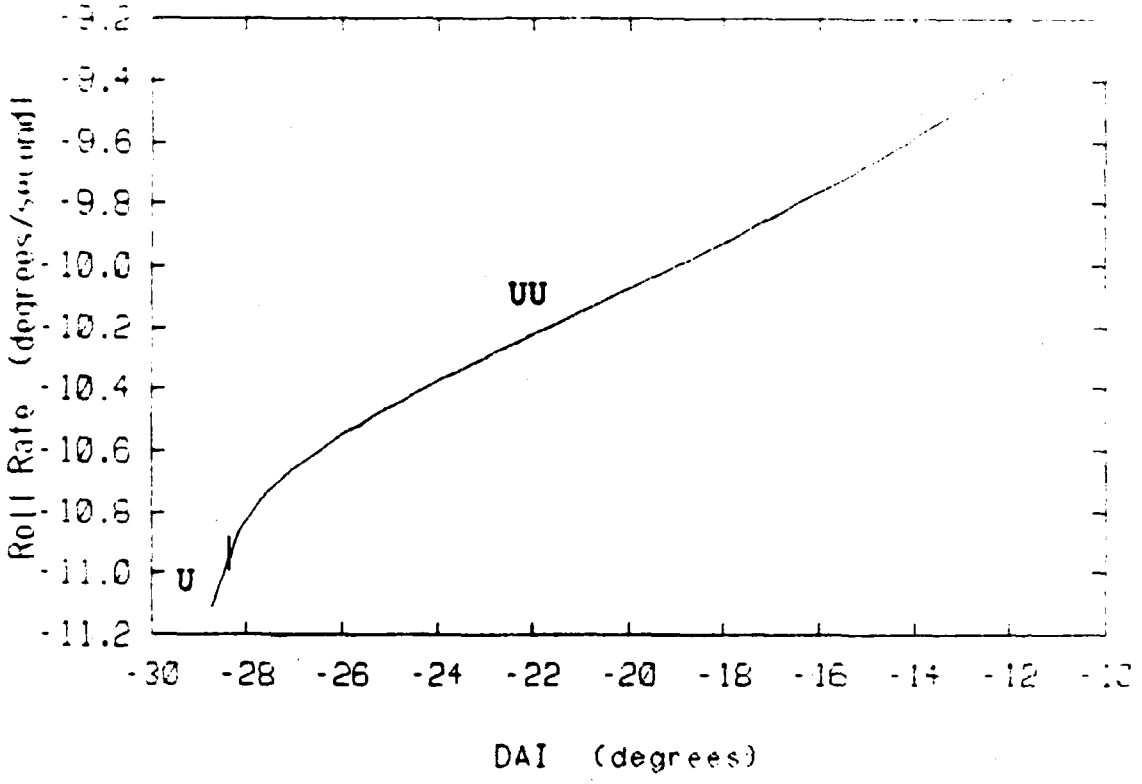

Fig. 7.9f: Roll Rate vs. Aileron

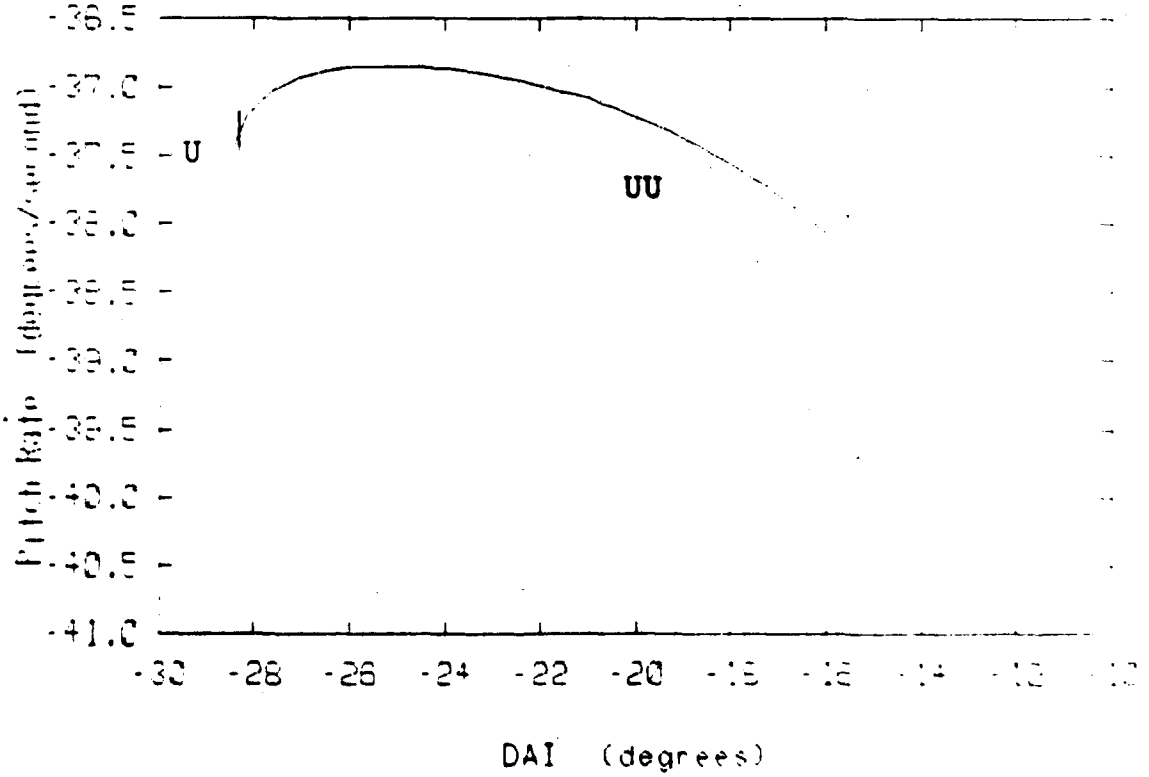

Fig. 7.9g: Pitch Rate vs. Aileron
DEL=-21.00; DRU=-24.46

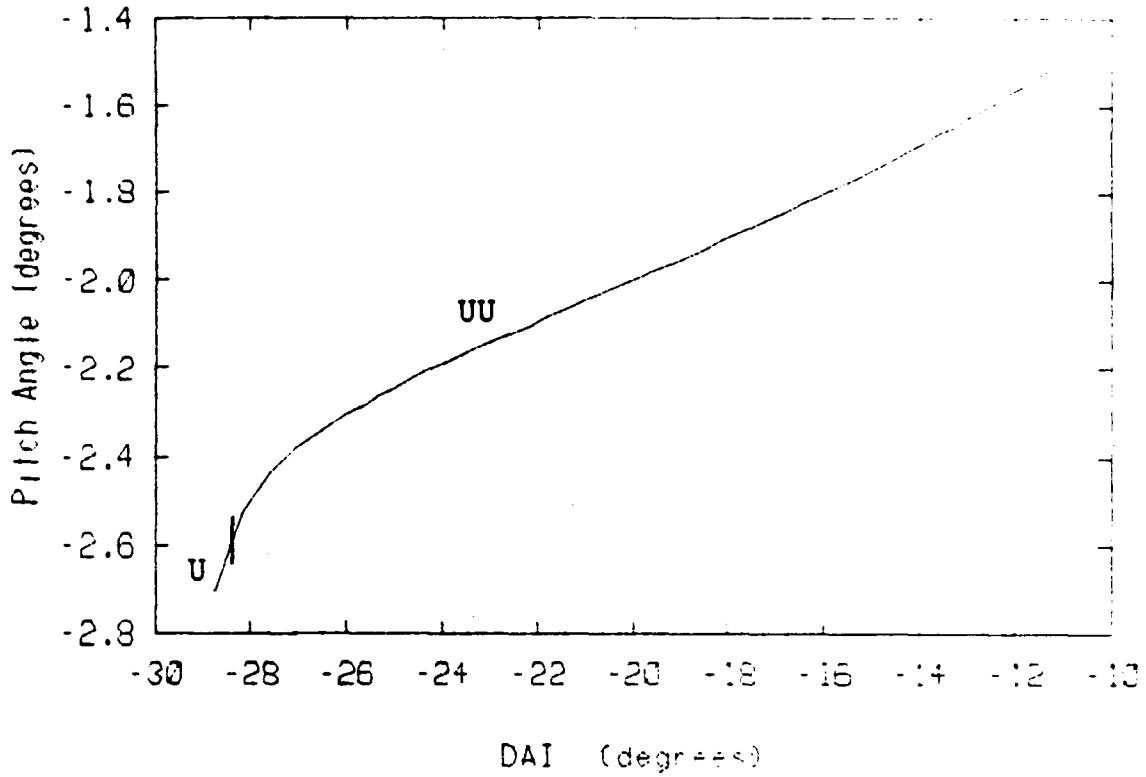

Fig. 7.9a: Pitch Angle vs. Aileron

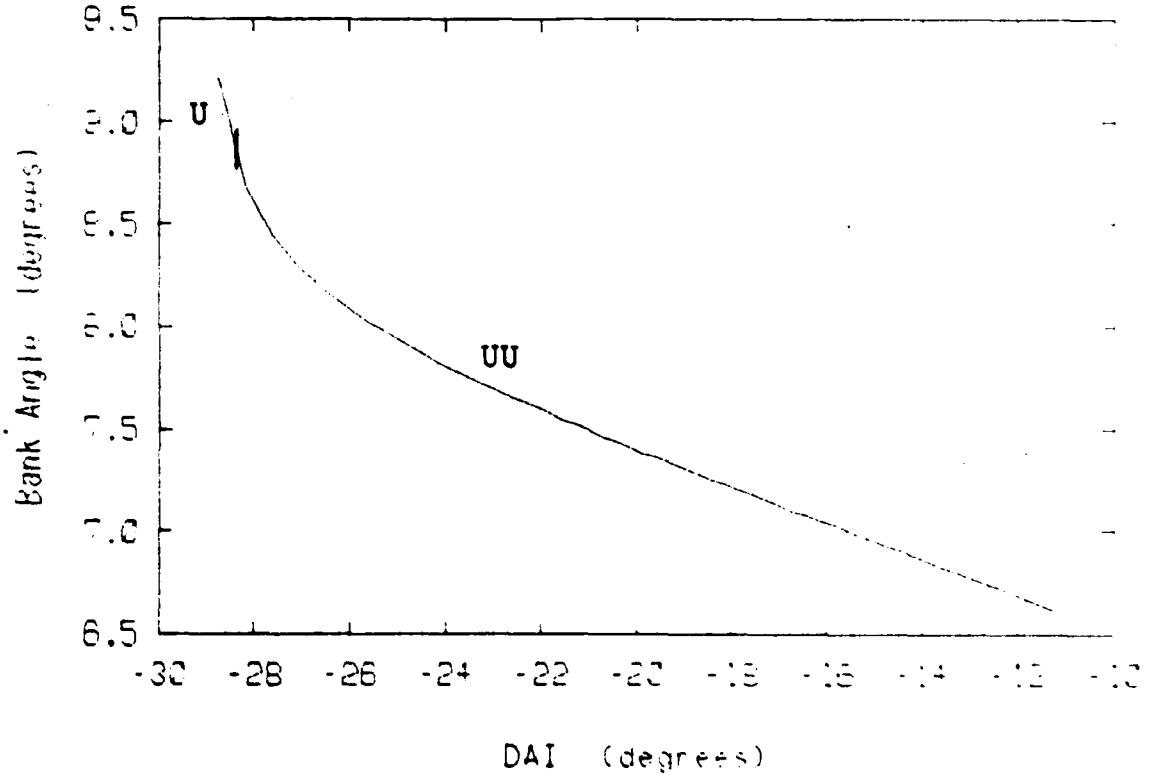

Fig. 7.9b: Bank Angle vs. Aileron
DEL=-21.00; DRU=-24.46

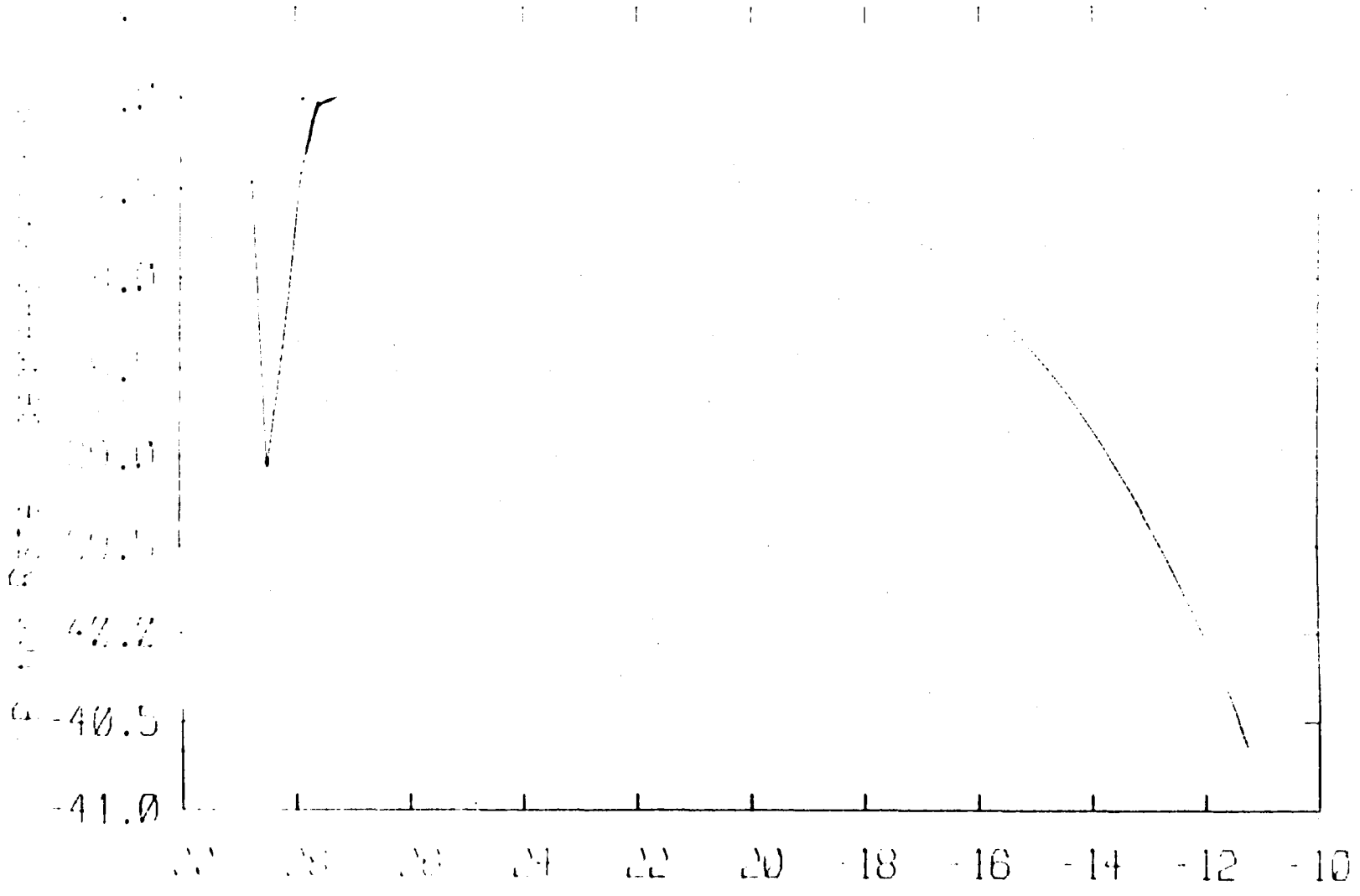

Fig. 7.9i: Enlarged Pitch Rate vs. Aileron
DEL=-21.00; DRU=-24.46

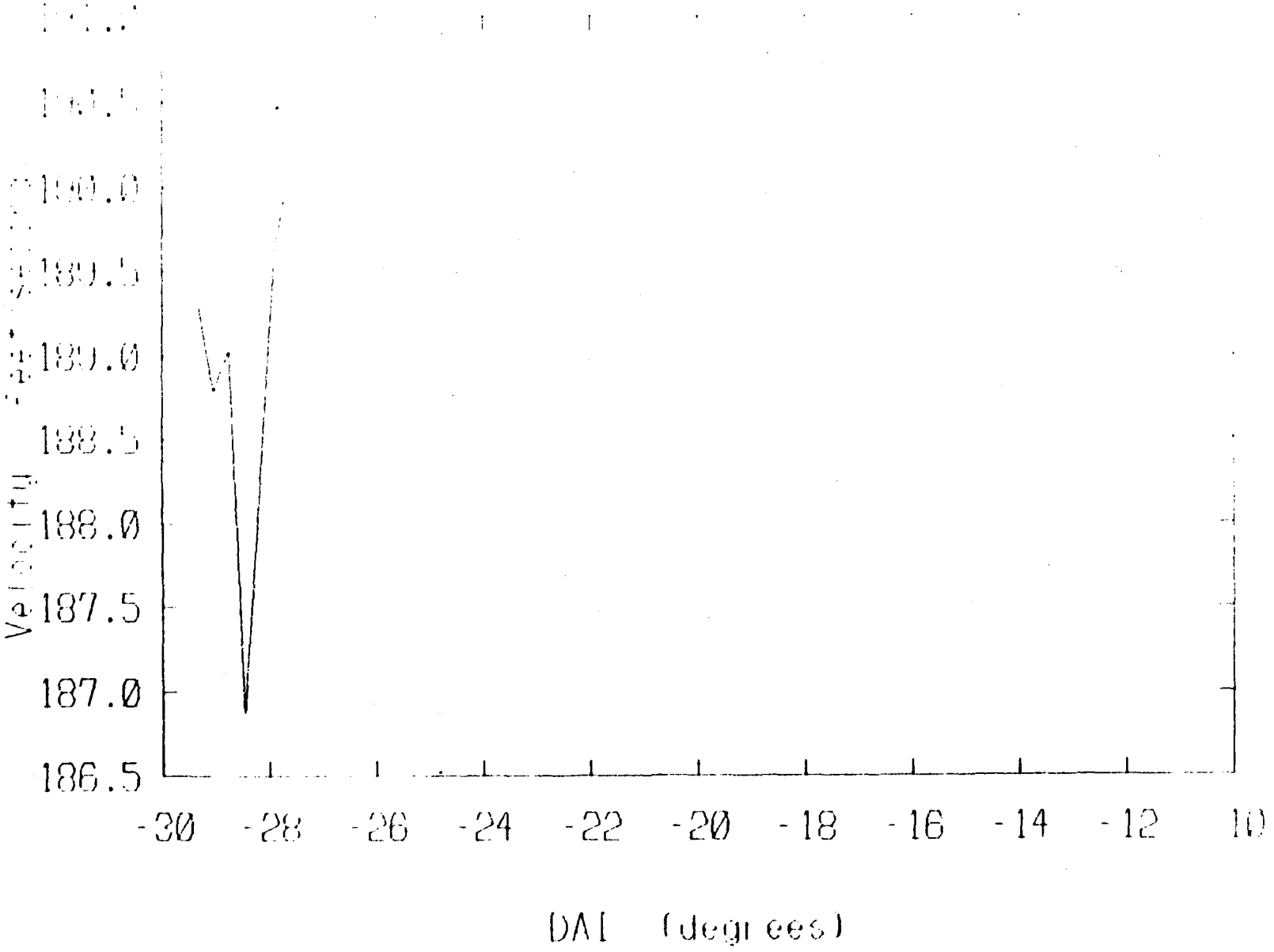

Fig. 7.9j: Enlarged Velocity vs. Aileron
DEL=-21.00; DRU=-24.46

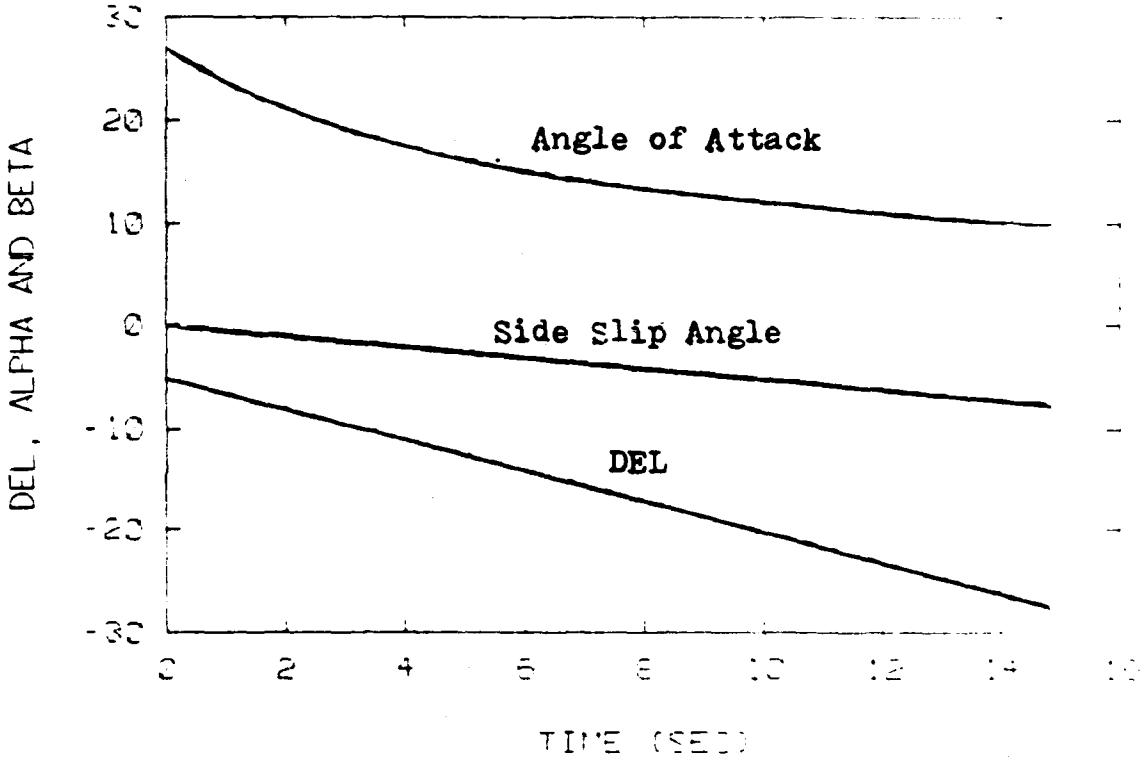

Fig. 7.10a; Time History
DAI=DRU=0

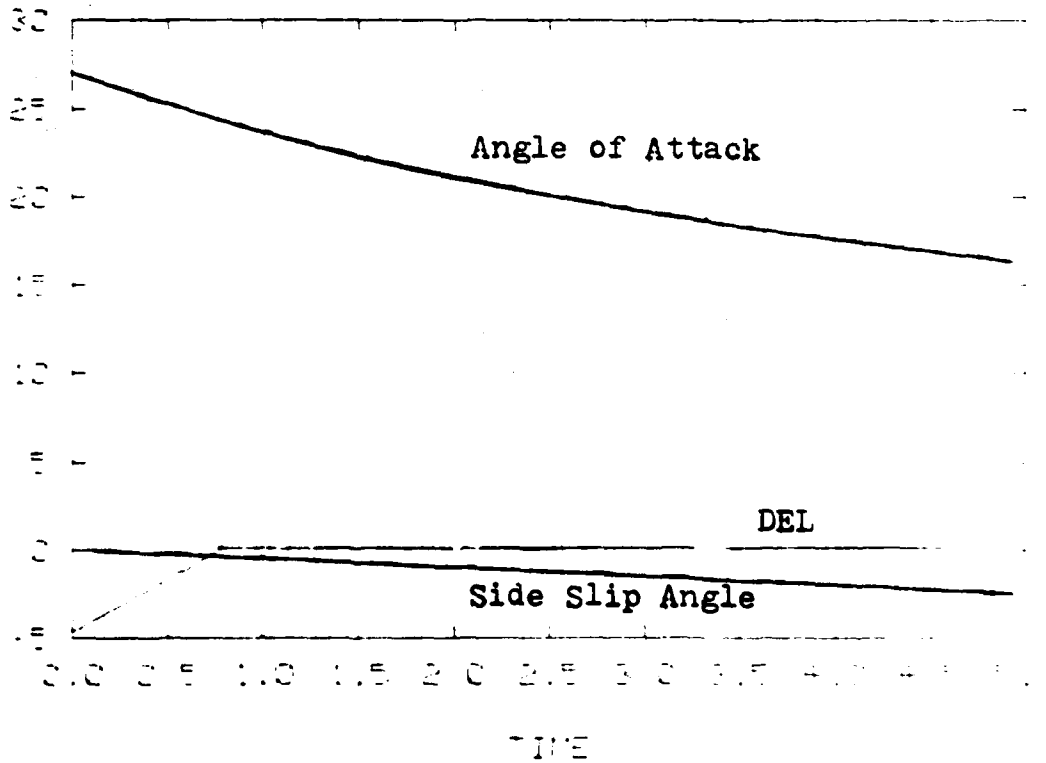

Fig. 7.11a; Time History
DAI=DRU=0

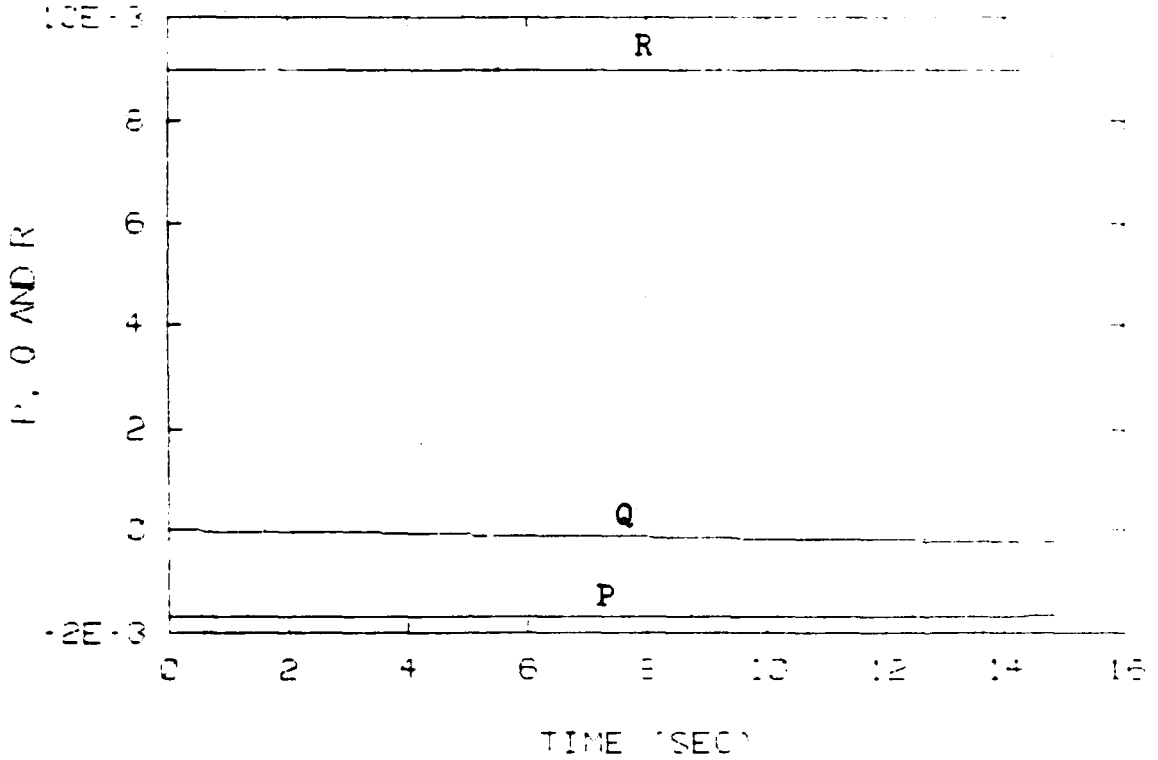

Fig. 7.10b: Time History (cont)
DAI=DRU=0

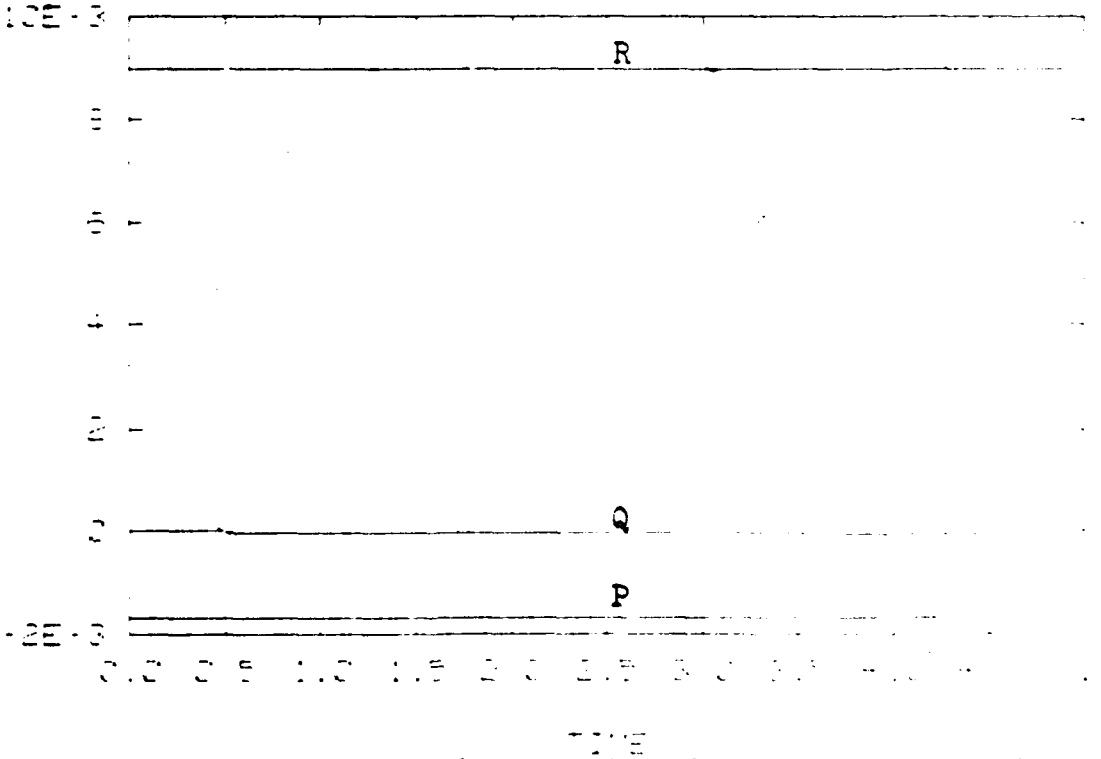

Fig. 7.11b: Time History (cont)
DAI=DRU=0

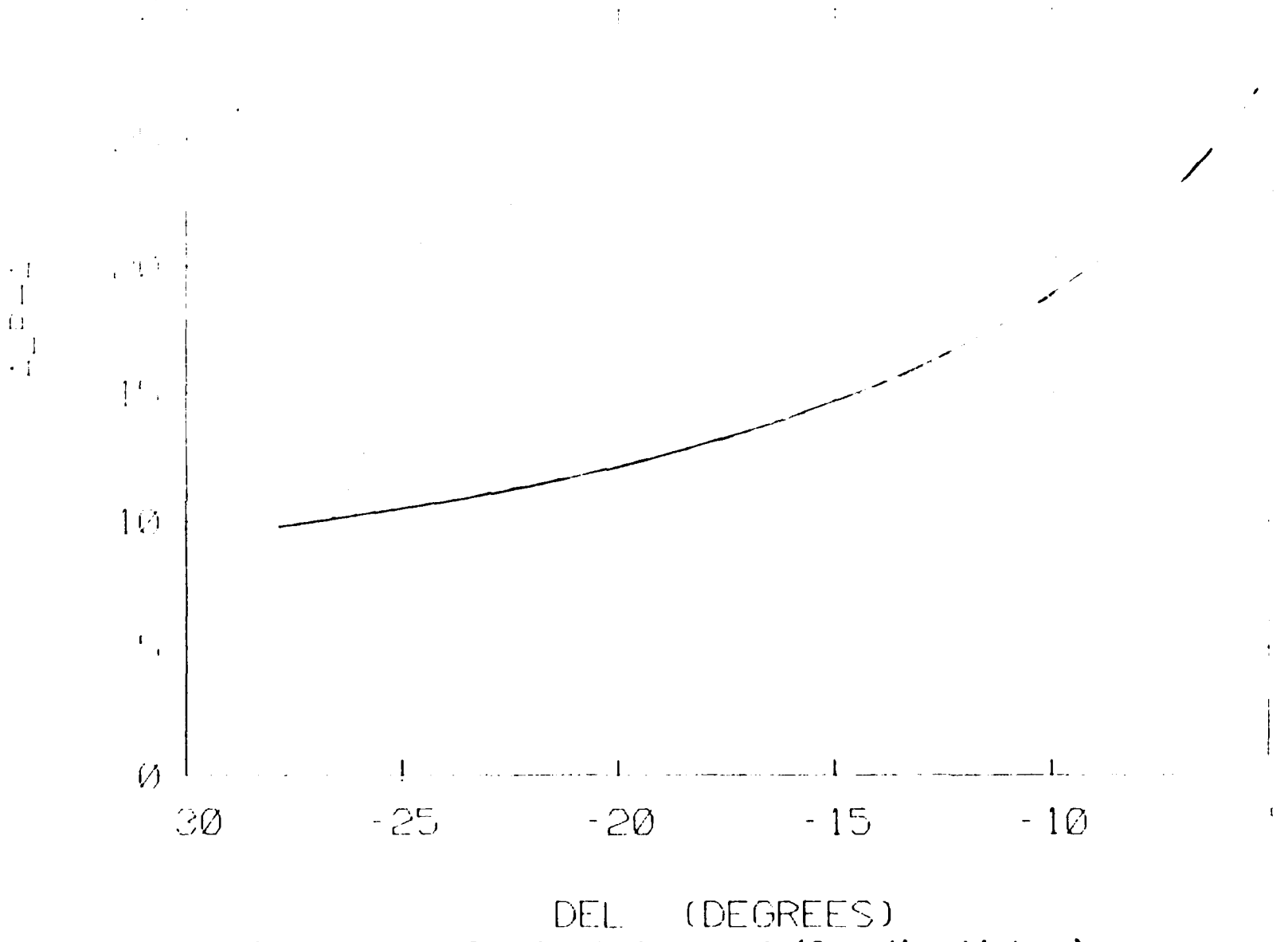

Fig. 7.10c: Angle of Attack vs. DEL (from time history)
DAL=DRU=0

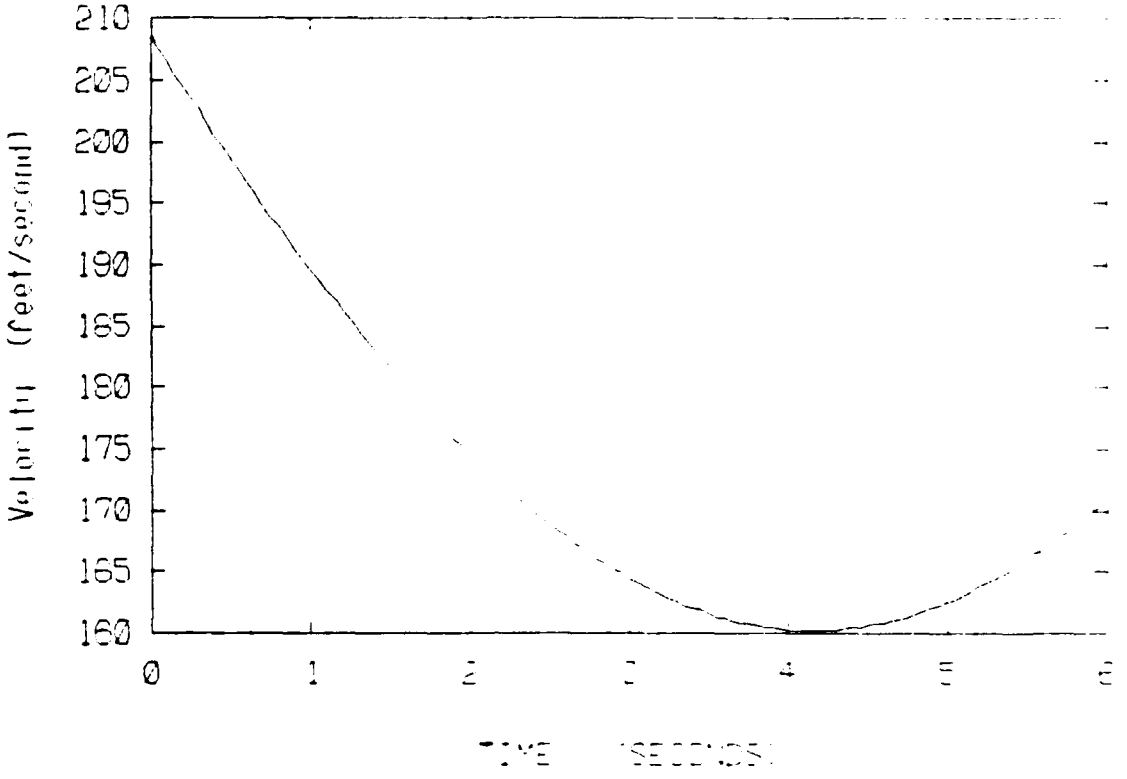

Fig. 7.12a: Velocity vs. Time

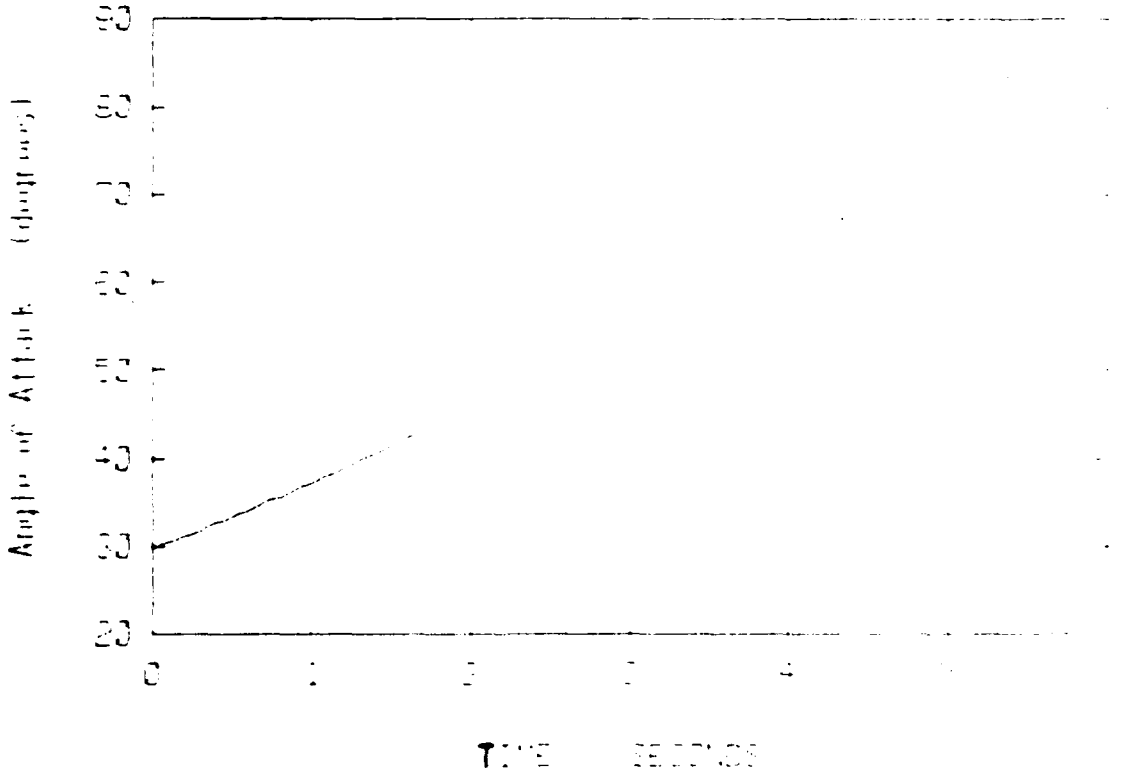

Fig. 7.12b: Angle of Attack vs. Time
DEL=-1.0; DRU=0; DAI=0; Thrust=0

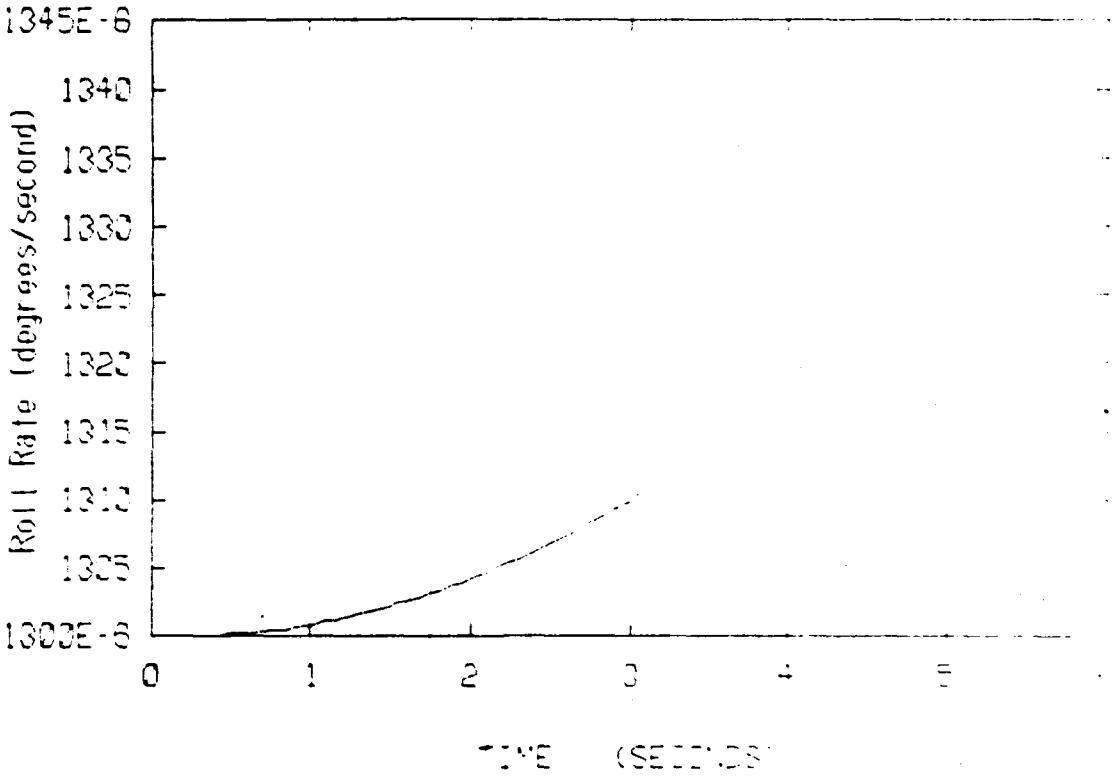

Fig. 7.12c: Roll Rate vs. Time

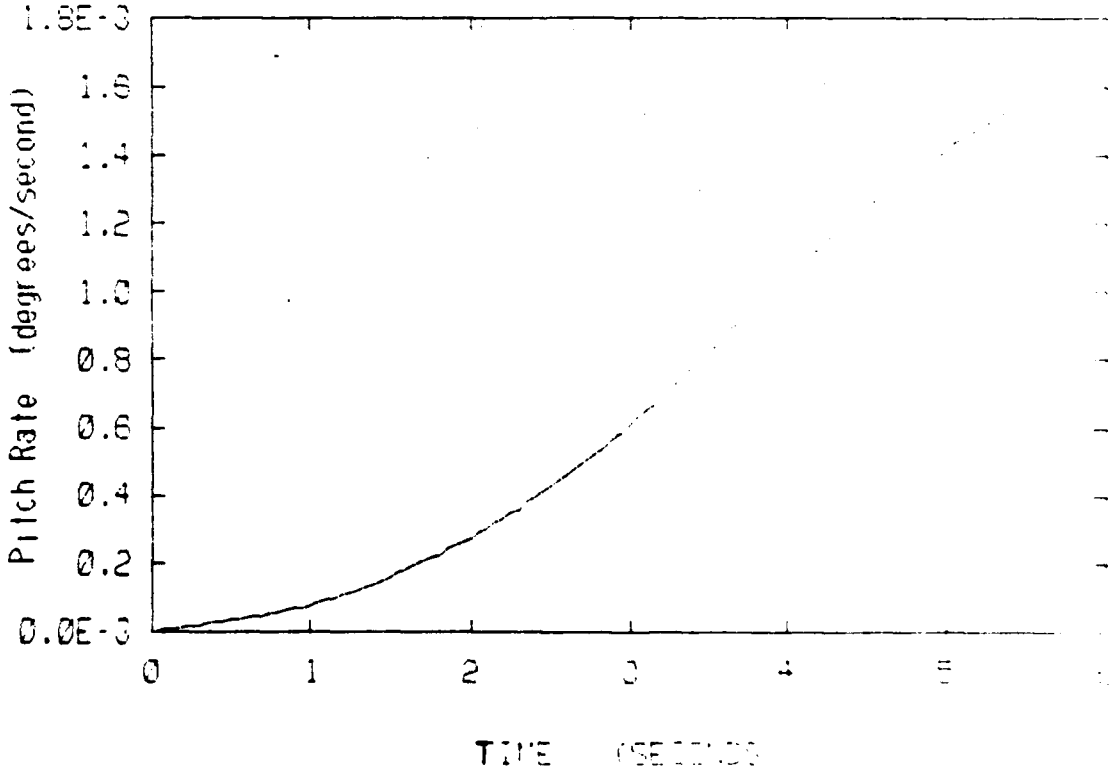

Fig. 7.12d: Pitch Rate vs. Time
DEL=-1.0; DAI=0; DRU=0; Thrust=0

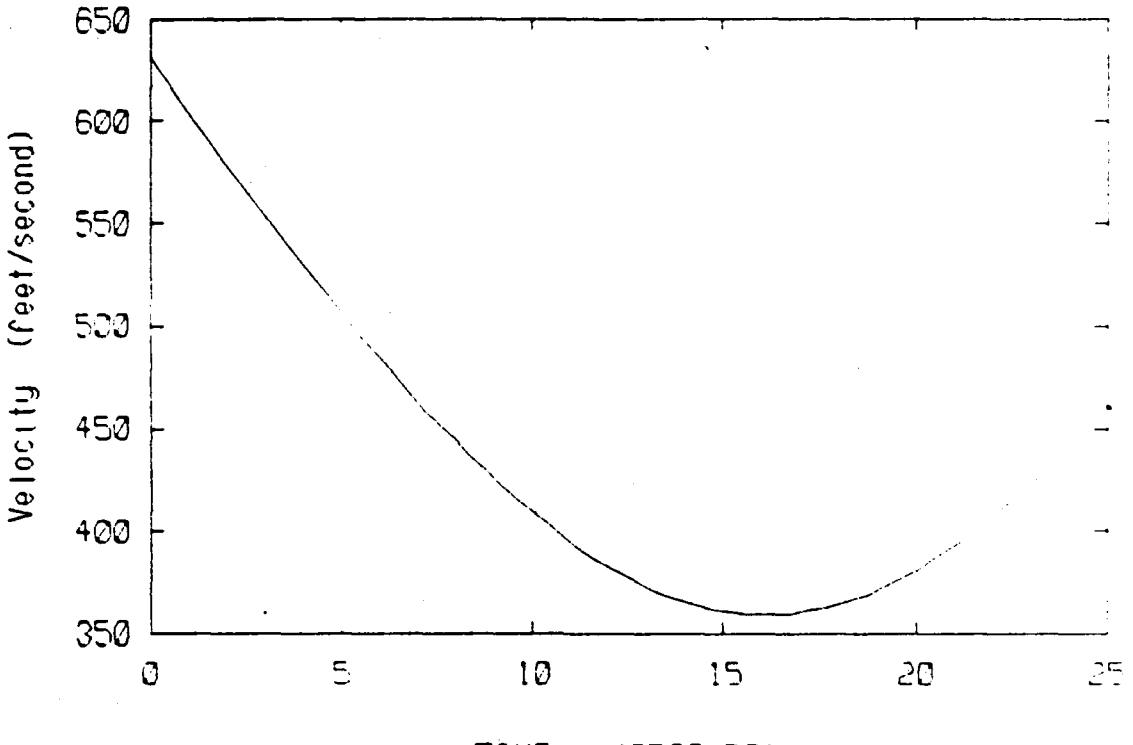

Fig. 7.13a: Velocity vs. Time
DEL=-1.0; DAI=0; DRU=0; Thrust=8500

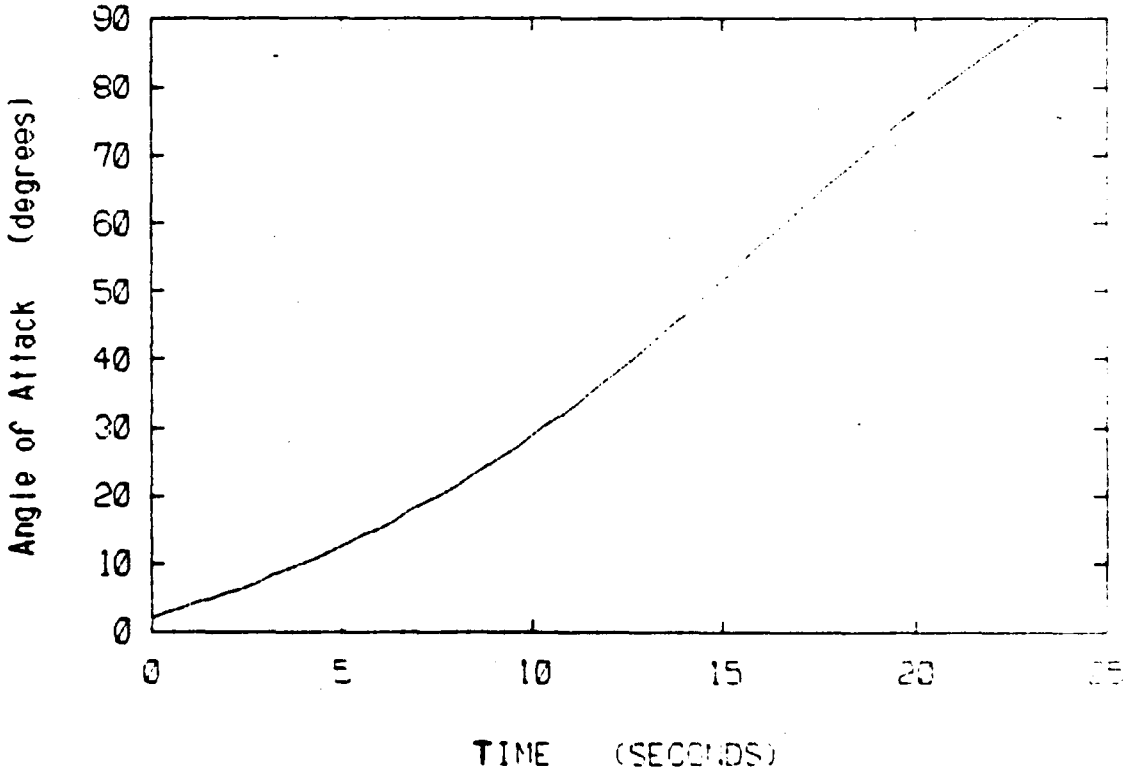

Fig. 7.13b: Angle of Attack vs. Time
DEL=-1.0; DAI=0; DRU=0; Thrust=8500